

Preparation of Hyperbranched Polymers by Controlled/ Living Polymerisations



**The University of
Nottingham**


Yu Zheng, M.Sc

**Thesis submitted to the University of Nottingham for
the degree of Doctor of Philosophy**

April 2010

Declaration

Except where specific reference has been made to other sources, the work presented in this thesis is the original work of the author. It has not been submitted, in whole, or in part, for any other degree or professional qualification.

Signed.....

Yu Zheng

Date.....**04/05/2010**

Acknowledgement

Foremost, I would like to express my sincere gratitude to my supervisor Prof. Steven. M. Howdle for his warm encouragement and thoughtful guidance during my Ph.D study and research. Without his guidance and inspiration, this work and thesis could not be successfully completed.

I am grateful to Dr Wenxin Wang, Dr Derek Irvine and Dr Kristofer Thurecht for all their professional advice and support to my research. I would also like to thank Professor Martyn Poliakoff for his invaluable advice. Also, I'd also like to thank Helen Carson who does an amazing work for our group.

I further express my thanks to all the staff and colleagues in the Clean Tech Group. Special thanks to Dr Jaouad El Harfi, Dr Jixin Yang, Dr Hongyun Tai, Dr Silvia Villarroya, Maria Gonzalez and Mark Guyler.

Finally, my deepest appreciation goes to my family who give me much love and warmth. Thanks to Katie for accompanying me during the toughest time. Thanks to the 'Brothers' in my house, Wenbo, Zifeng and Hongge. Thank you all for so much support, love and understanding.

Yu Zheng, April 2010

Abstract

This thesis describes the development of a novel route for preparation of hyperbranched polymers. The aim is to produce hyperbranched polymers via enhanced deactivation ATRP without crosslinking even at high conversion. Our strategy will be to use excess Cu(II) to control gelation, so called enhanced deactivation ATRP.

Chapter 1 provides a general introduction to the basic concepts of living polymerisation and dendritic polymers.

Chapter 2 covers the hyperbranched homopolymer prepared by enhanced deactivation ATRP. The hyperbranched poly(divinylbenzene) and poly(ethylene glycol dimethacrylate) are synthesised by enhanced deactivation ATRP in a concentrated system.

Chapter 3 focuses on the synthesis of hyperbranched copolymer via the enhanced deactivation ATRP. Also, the interesting potential applications, for example dye encapsulation and viscosity control are explored in this chapter.

Chapter 4 demonstrates two routes to prepare novel core-shell polymers. First, the hyperbranched polyDVB was used as a core to produce hyperbranched core-shell polymers. Second, a novel hyperbranched polymer which combines ring open polymerisation and RAFT technique was developed.

Chapter 5 summarises all the research presented in this thesis. Moreover, some possible research routes for the investigation in the future are listed in this part.

Abbreviations

v_{FRP}	Kinetics chain length in free radical polymerisation
v_{ATRP}	Kinetics chain length in atom transfer radical polymerisation
τ	Life-time of radicals in free radical polymerisation
τ'	Actual life-time of the radicals in atom transfer radical polymerisation
τ_{act}	Time span of activation in atom transfer radical polymerisation
τ_{deact}	Time span of deactivation in atom transfer radical polymerisation
ACP-RAFT	4,4-Azobis(4-cyanovaleric acid) RAFT
AFM	Atomic Force Microscopy
AGET	Activator Generated by Electron Transfer
AIBN	2,2'-Azo-bis-isobutyronitrile
ARGET	Activator Regenerated by Electron Transfer
ATRA	Atom Transfer Radical Addition
ATRP	Atom Transfer Radical Polymerisation
BOD	4,4-bioxepanyl-7,7-dione
Bpy	2,2'-bipyridine
CCTP	Cobalt Catalytic Transfer Polymerisation
$CDCl_3$	Deuterated chloroform
$CHCl_3$	Chloroform
C_{load}	Encapsulation ability of dyes
Conv.	Monomer Conversion
CR	Congo Red
CLRP	Controlled/Living Free Radical Polymerisation
$^{\circ}C$	Degrees Celsius
DB	Degree of Branching
DE-ATRP	Deactivation Enhanced ATRP
DLS	Dynamic Light Scattering
DMAEMA	2-Dimethylaminoethyl Methacrylate

DMF	<i>N,N</i> -dimethylformamide
dNbpy	4,4'-dinonyl-2,2'-bipyridine
DP _n	Degree of Polymerisation
DSC	Differential Scanning Calorimetry
DVB	Divinylbenzene
EGDMA	Ethylene glycol dimethacrylate
EVB	Ethylvinylbenzene
FRP	Free Radical Polymerisation
GTP	Group Transfer Polymerisation
GPC	Gel Permeation Chromatography
HBP	Hyperbranched Polymer
HMTETA	1,1,4,7,10,10-Hexamethyltriethylenetetramine
IFIRP	Initiator-Fragment Incorporation Radical Polymerisation
k_{act}	Activation rate in atom transfer radical polymerisation
k_{deact}	Deactivation rate in atom transfer radical polymerisation
K_{ATRP}	Equilibrium constant for atom transfer radical polymerisation
K_{BD}	Bond dissociation energy of the alkyl halide
K_{EA}	Electron affinity of the halogen
K_{ET}	Equilibrium constants for electron transfer of metal complexes
K_{X}	Equilibrium constant for the heterolytic cleavage of the $\text{Cu}^{\text{II}}\text{-X}$ bond
LRP	Living Free Radical Polymerisation
MALLS	Multi-Angle Laser Light Scattering
MBrAc	Methyl bromoacetate
MBriP	Methyl 2-bromoisobutyrate
MBrP	Methyl 2-bromopropionate
MCiP	Methyl 2-chloropropionate
MIP	Methyl 2-iodopropionate
Me ₄ -cyclam	1,4,8,11-tetramethyl-1,4,8,11-tetraazacyclotetradecane
Me ₆ -TREN	Tris[(2-dimethylamino)ethyl]amine

MeOH	Methanol
MMA	Methyl Methacrylate
M_n	Number Average Molecular Weight
MO	Methyl Orange
MW	Molecular Weight
M_w	Weight Average Molecular Weight
NMP	Nitroxide Mediated Polymerisation
NMR	Nuclear Magnetic Resonance
PCL	Poly(caprolactone)
PDI	Polydispersity Index
PDMAEMA	Poly(2-(diethylamino)ethyl methacrylate)
PDMS	Poly(dimethyl siloxane)
PDMS-ma	Poly(dimethyl siloxane) monomethacrylate
PE	Polyethylene
PEBr	1-Phenylethyl bromide
PMDETA	<i>N,N,N',N'',N'''</i> -pentamethyldiethylenetriamine
PMMA	Poly(methyl methacrylate)
PP	Polypropylene
PRE	Persistent radical effect
PS	Polystyrene
PSD	Particle Size Distribution
PVA	Poly(vinyl alcohol)
PVAc	Poly(vinyl acetate)
R	Free Radical Leaving Group on RAFT Agent
RAFT	Reversible Addition Fragmentation Chain Transfer
R_g	Gyration Radius
R_h	Hydrodynamic Radius
RI	Refractive Index
ROP	Ring-Opening Polymerisation

rpm	Rotations Per Minute
SCVP	Self-Condensation Vinyl Polymerisation
SEC	Size Exclusion Chromatography
SET	Single Electron Transfer
Sn(OCT) ₂	Tin (II) Ethyl Hexanoate/ Stannous octoate
SR&NI	Simultaneous Reverse and Normal Initiation
T _g	Glass Transition Temperature
THF	Tetrahydrofuran
TMEDA	<i>N,N,N,N</i> -tetramethylethylenediamine
tNtpy	4,4'-trinionyl-2,2'-6',2''-terpyridine
T _m	Melting Temperature
UV-vis	Ultraviolet-visible
wt %	Weight %
Z	Stabilising Group on RAFT Agent
ε-CL	ε-caprolactone

Table of Contents

CHAPTER ONE: INTRODUCTION

1.1 Polymers and Polymerisation	1
1.1.1 General	1
1.1.2 Free Radical Polymerisation	3
1.1.3 Controlled/ Living Free Radical Polymerisation	6
1.2 Atom Transfer Radical Polymerisation (ATRP)	14
1.2.1 Mechanism of Atom Transfer Radical Polymerisation	14
1.2.2 Mechanism of Electron Transfer	19
1.2.3 Kinetics and Components	21
1.2.4 Different ATRP Procedures	24
1.2.5 Monomers	28
1.2.6 Initiators	29
1.2.7 Transition Metal Catalysts	32
1.2.8 Ligands	33
1.2.9 Materials Made by ATRP	35
1.2.10 Deactivation Enhanced ATRP (DE-ATRP)	41
1.3 Reversible Addition Fragmentation Chain Transfer Polymerisation (RAFT)	49
1.4 Hyperbranched Polymers	53
1.4.1 Dendritic Polymers	53
1.4.2 Dendrimers	54
1.4.3 Random Hyperbranched Polymers	57
1.4.4 Previous Synthesis of Hyperbranched Polymers	58
1.5 An Overview of This Thesis	65
1.6 References	67

CHAPTER TWO: HOMOPOLYMERISATIONS OF DIVINYL MONOMERS

2.1 Mechanism	79
2.1.1 Previous Methods	79
2.1.2 Preparation of Hyperbranched Polymer via DE-ATRP Method	80
2.1.3 Deactivation Enhanced Strategy in Other Controlled/Living Polymerisations	88
2.2 Experimental	90
2.2.1 Materials	90
2.2.2 Polymerisation Procedure	92
2.2.3 Characterisation of Hyperbranched Polymers	95
2.3 Results and Discussion	97
2.3.1 Synthesis and Characterisation of Hyperbranched polyDVB	99
2.3.2 Synthesis and Characterisation of Hyperbranched polyEGDMA	127
2.4 Conclusion	140
2.5 References	141

CHAPTER THREE: HYPERBRANCHED COPOLYMERS

3.1 Introduction	144
3.1.1 Hyperbranched Copolymers	144
3.1.2 Hyperbranched Amphiphilic Copolymers	149
3.1.3 Hyperbranched Siloxane Copolymers	151
3.2 Experimental	155
3.2.1 Materials	155
3.2.2 Polymerisation Procedures	156
3.2.3 Characterisation Section	158
3.3 Results and Discussion	168

3.3.1 Poly(EGDMA- <i>co</i> -DMAEMA)	168
3.3.2 Encapsulation Study	179
3.3.3 Hyperbranched poly(DVB- <i>co</i> -PDMS _{ma})	192
3.4 Conclusion	208
3.5 References	209

CHAPTER FOUR: CORE-SHELL HYPERBRANCHED POLYMERS

4.1 Introduction	213
4.1.1 Core-Shell Star Polymers	213
4.1.2 Biodegradable Core-Shell Hyperbranched Materials	217
4.2 Experimental	220
4.3 Results and Discussion	224
4.3.1 Core-shell Hyperbranched poly(DVB _{core} - <i>co</i> -MMA _{shell})	224
4.3.1 Core-shell Hyperbranched poly(CL- <i>co</i> -BOD) _{core} -DMAEMA _{shell}	243
4.4 Conclusion	255
4.4 References	256

CHAPTER FIVE: CONCLUSION AND FUTURE WORK

5.1 Conclusion	259
5.1.1 Homopolymerisations of Divinyl Monomers	259
5.1.2 Hyperbranched Copolymers	260
5.1.3 Hyperbranched Core-Shell Polymers	261

5.2 Future work	261
5.2.1 More Experimental Work for DE-ATRP	261
5.2.2 Kinetic Modeling and Simulation of Deactivation Enhanced Polymerisation	262
5.2.3 Extension of Enhanced Deactivation Strategy for Other Living Polymerisation	262
5.2.4 Further Application Tests for Hyperbranched Polymers	263
5.2.5 Biodegradable Hyperbranched Core-Shell Polymer via Arm-First Route	264
5.3 References	266

CHAPTER ONE: INTRODUCTION

1.1 Polymers and polymerisations

1.1.1 General

The simplest definition of a polymer, also called macromolecule, is a molecule made of many repeating units. The number of repeating units can range from several hundreds to millions. Polymers as important functional and structural materials have accompanied human beings throughout history. Silk, protein and bamboo are all examples of natural macromolecules. With the development in organic chemistry, polymeric materials have become even more important in recent centuries. Man-made polymers are also very common in people's daily life. Many common polymers are composed of hydrocarbons, where carbon makes up the backbone of the molecule and hydrogen atoms are bonded along it. Besides carbon and hydrogen, elements such as oxygen, chlorine, fluorine, nitrogen, silicon, phosphorus, and sulfur can also be found in the molecular makeup of polymers. The first semi-synthetic polymer derived from a naturally occurring product is nitrocellulose, discovered by Braconnot in 1832. Named Xyloidine, it was prepared by the nitration of cellulose-containing wood fibres, forming an unstable explosive material. In mid-nineteenth century, people started to modify natural polymers for different purposes. For example, Charles Goodyear discovered vulcanised rubber in 1839. Later, the chemical building blocks of rubber and protein were established by scientists. In the early 20th century, the first recorded synthetic polymer Bakelite was fabricated by Leo Bakeland.^{1,2} Since then, a vast number of different polymers and synthetic methods have been developed, with applications being both diverse and widespread.

Over eighty years have elapsed since Staudinger's original papers on polymerisation, in which he first proposed the term 'macromolecules' to describe the very long

molecular chains he suggested were responsible for the unusual properties of natural and synthetic polymers.^{3, 4} Initially Staudinger was widely ridiculed, and his ideas only began to become universally accepted in the 1920s. Carothers was instrumental in this acceptance, providing definitive proof for the existence of macromolecules using a set of reactions that could only result in the synthesis of macromolecular chains. During this work Carothers classified either condensation and addition polymers, depending on the relationship between the chemical structures of the polymer and constituent monomer molecules.⁵⁻⁷ Condensation polymers are those in which the chemical structure of the repeat unit differs from that of the monomers due to the elimination of small molecules (such as water) during the polymerisation (1, Figure 1.1). Examples of this type of polymers, also known as step-growth polymers, include nylon. In contrast, addition or chain-growth polymers are those in which the chemical formulas of the polymer and monomers are isomeric (2, Figure 1.1).⁸ Examples of this type of polymers include polyethylene (PE) and polystyrene (PS). During a chain polymerisation, monomer units are added to the end of a growing polymer chain via an active centre (such as a radical, carbocation, carbanion, oxyanion, or organometallic complex). The general examples of step and addition polymerisations are shown in the following scheme (Figure 1.1).

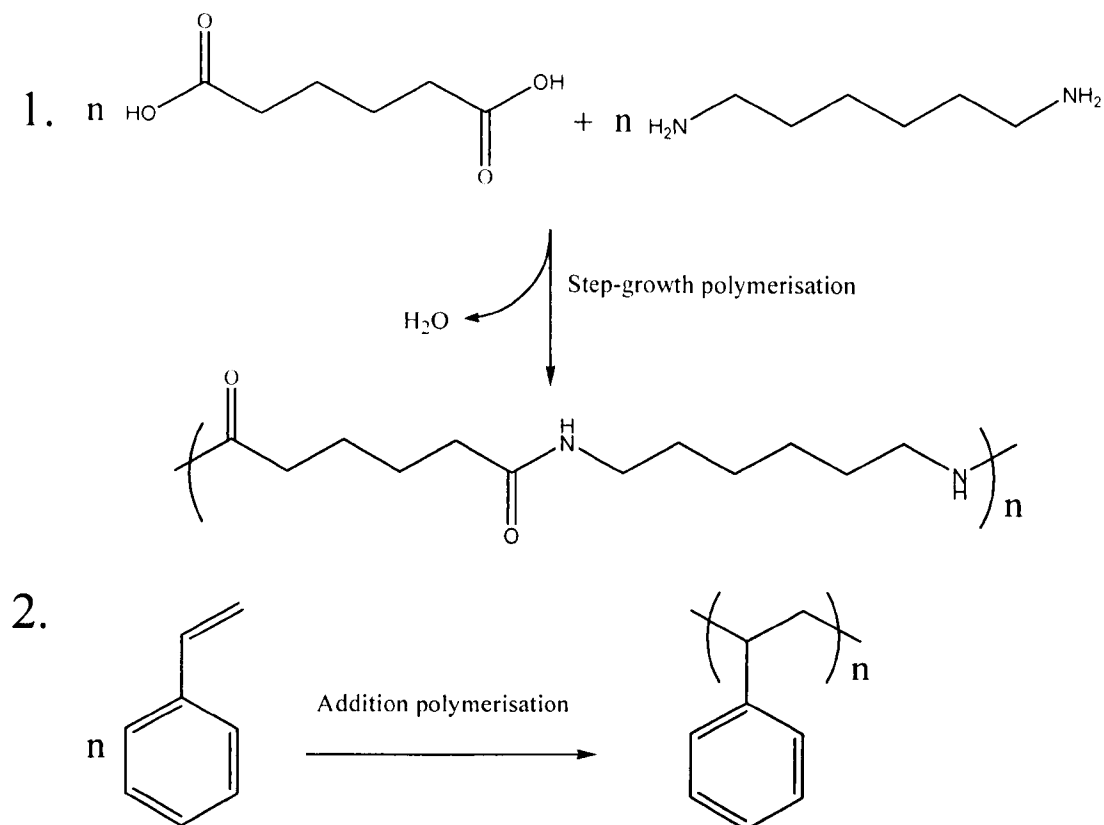


Figure 1.1 General examples of step and addition polymerisations: 1. step-growth polymerisation with the formation of nylon 6,6 via the condensation reaction; 2. an example of addition polymerisation with the synthesis of polystyrene using addition polymerisation.

1.1.2 Free Radical Polymerisation

Free radical polymerisation (FRP) is a type of polymerisation in which the reactive centre of the polymer chain consists of a radical.^{8,9} The whole process starts off with initiator decomposition and generates radicals.¹⁰ Then the polymerisation proceeds by the chain reaction addition of monomer units to the free radical ends of growing chains. Finally, two propagating species (growing free radicals) combine or disproportionate to terminate the chain growth and form polymer molecules. The FRP has been an important technological area widely used since 1940s. Now commercial polymers produced using FRP include polyethylene (PE), polystyrene (PS),¹¹⁻¹⁵ poly(vinyl chloride) (PVC), poly(vinyl acetate) (PVAc),¹⁶ poly(methyl

methacrylate) (PMMA),¹⁷ polypropylene (PP) and polyacrylonitrile (PAN). Figure 1.2 shows the chemical structures of these polymers.

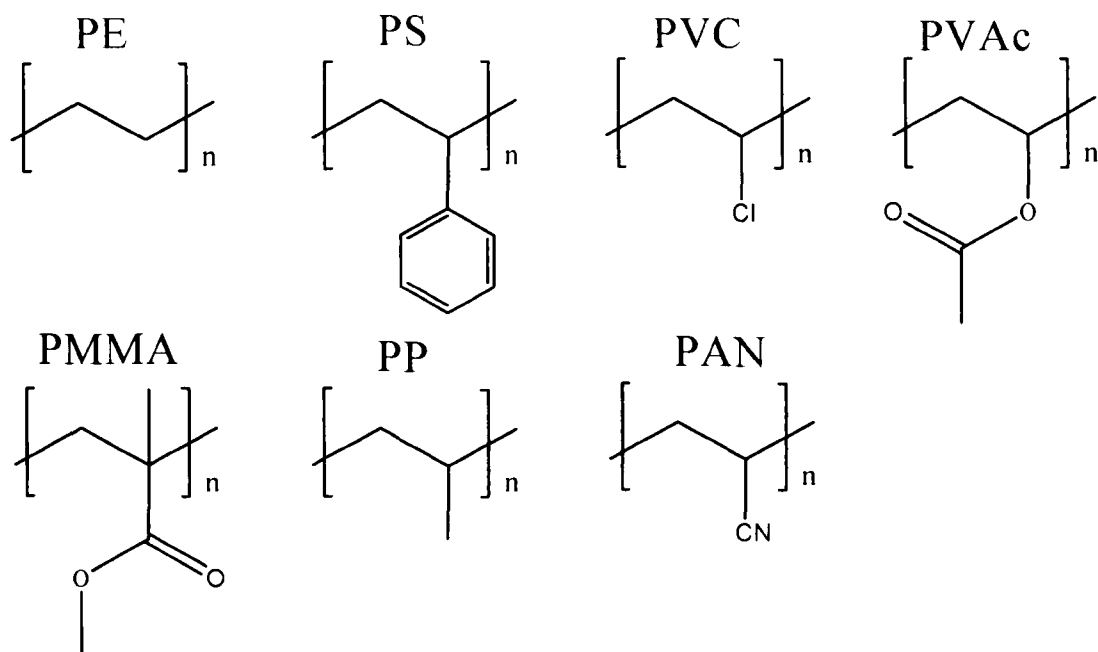


Figure 1.2 Common polymers produced commercially by free radical polymerisation (FRP).

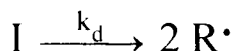
Free radical polymerisation consists of the elementary steps of initiation, propagation and termination.⁸

Initiation: The free radicals are generated by thermal or photochemical breakage of covalent bonds (Figure 1.3 A). These primary radicals add to the double bonds of monomer resulting in primary propagating radicals (Figure 1.3 B).

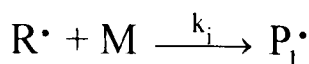
Propagation: After initiation, there is a succession of rapid propagation steps and these result in the formation of a growing polymer chain (P_n^\bullet) known as propagation (Figure 1.3 C).

Termination: termination refers to the bimolecular reaction of propagation radical species by combination or disproportionation. (Figure 1.3 D)

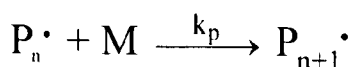
(A) Decomposition



(B) Initiation



(C) Propagation



(D) Termination

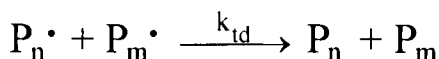
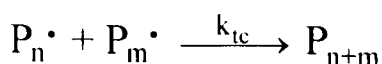


Figure 1.3 The mechanism of FRP: decomposition (A), initiation (B), propagation (C), and termination (D).

Initiation, propagation and termination rates can be summarised by kinetic treatment (Equation 1.1, 1.2 and 1.3), respectively, where R_i is the rate of initiation (Eq. 1.1), R_p is the rate of propagation (Eq. 1.2), R_t is the rate of termination (Eq. 1.3), and $k_t = k_{tc} + k_{td}$.

$$R_i = \frac{d[R^\bullet]}{dt} = 2 k_d f[I] \quad (\text{Eq. 1.1})$$

$$R_p = -\frac{d[M]}{dt} = k_p [P^\bullet][M] \quad (\text{Eq. 1.2})$$

$$R_t = \frac{d[P^\bullet]}{dt} = 2 k_t [P^\bullet]^2 \quad (\text{Eq. 1.3})$$

During a typical FRP, the rate of polymerisation can be derived from the kinetics (Eq. 1.4). R correlates the rate of polymerisation with the initiator $[I]$ and monomer $[M]$ concentration. Also, it correlates the kinetic rate coefficients f (normally in the range

of 0.3-0.8) is the efficiency of an initiator I which defined as $[P_1\bullet]/[R\bullet]$ (Figure 1.3). Since a proportion of primary radicals that are produced by the decomposition of initiator do not initiated with the monomer due to the ‘cage’ effect.¹⁸ k_d is the rate constant of initiator decomposition, k_p is the rate constant for propagation for a monomer M, and k_t is the rate constant for termination. This kinetics equation is successful in describing the experimental reality.

$$R_p = -\frac{d[M]}{dt} = k_p \left(\frac{k_d f[I]}{k_t} \right)^{1/2} [M] \quad (\text{Eq 1.4})$$

The main disadvantage of free radical polymerisation is the diffusion controlled termination reactions between growing radicals. Furthermore, the fast propagation rate is a key problem that needs to be solved. The typical lifetime of a propagation chain is very short before termination, typically is in the range of 1 second. During that time, approximately thousands monomers units are added to the generated radicals before termination. Thus, it is difficult to control molecular weight, polydispersity or add a new monomer to form special block polymer chain and end functionalities within 1 second. Normally, there are two methods in radical polymerisation that can provide polymers with lower molecular weights. The first method requires a large amount of initiator and may be accompanied by a significant increase of polymerisation rate and poor control. The other approach is based on transfer agents to provide polymer with controlled molecular weight and functionalities. However, the polydispersity cannot be well controlled in this way.

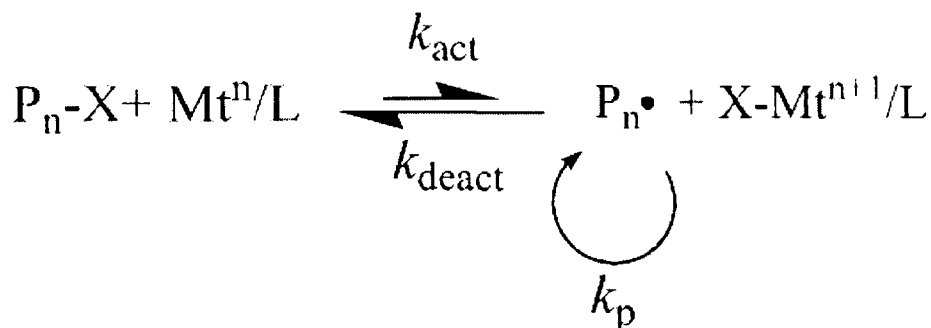
1.1.3 Controlled/Living Free Radical Polymerisations

Free radical polymerisation provides only poor control and has many limitations, for example, molecular weight, polydispersity, end functionality, chain architecture and composition.¹⁹⁻²¹ In a ‘living’ polymerisation, the polymers can be propagated for a long period with a predictable molecular weight. In addition, the irreversible termination or chain transfer effects are negligible in the reaction. Therefore, the

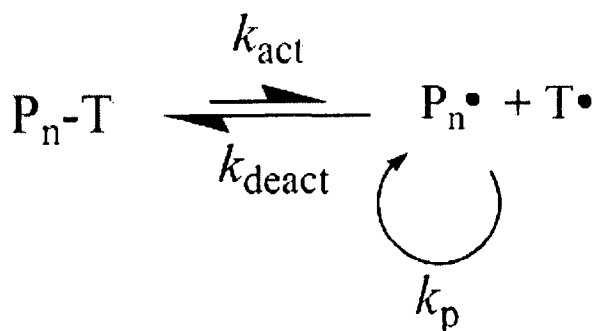
controlled/living radical polymerisation (CLRP) method becomes a very important commercial process for preparing high molecular weight polymer with narrow polydispersity. Since the first living free radical polymerisation was reported by Otsu in 1982^{22, 23} used a ‘iniferter’ agent (initiator-chain transfer agent-terminator, typically are compound containing C-S bonds), this kind of polymerisation attracts many scientists’ attention due to the expanding market for specialty materials prepared from a wide range of available monomers. Applications of these materials include coatings, adhesives, surfactants, dispersants, lubricants, gels, additives, thermoplastic elastomers, electronics, biomaterials etc. The concept of CLRP is to control the free radical polymerisation process via selecting conditions that allow dynamic equilibrium between a low concentration of active propagating chains and a large number of dormant chains. The dormant chains mean the chains are unable to propagate or terminate. Since the equilibrium is shifted towards dormant species, the concentration of propagating chains has decreased, and the termination become less significant compared to propagation. There are several CLRP processes based on this fundamental concept. The most important system is atom transfer radical polymerisation (ATRP),^{21, 24, 25} which is based on the fundamental work on ATRA.²⁶⁻²⁸ Also, another method named stable free radical polymerisation (SFRP)²⁹ which includes nitroxide mediated polymerisation (NMP).²⁰ A third method is the degenerative transfer (DT)^{30, 31} processes which includes reversible addition fragmentation transfer (RAFT).^{32, 33} All of these objectives are accomplished by formation of a dynamic equilibrium between the propagating radicals and dormant species.

The controlled process is achieved by: (1) extending the life of propagating chains (from <1s to >1 h); (2) enabling quantitative initiation which allowing the $R_i > R_p$ in the case for conventional radical polymerisation to $R_i < R_p$ for CLRP processes; (3) allowing the ratio of polymerised monomer to initiator ($DP_n = D[M]/[I]$) to control molecular weight, polydispersity, functionality, composition and topology. The equilibrium is formed by:

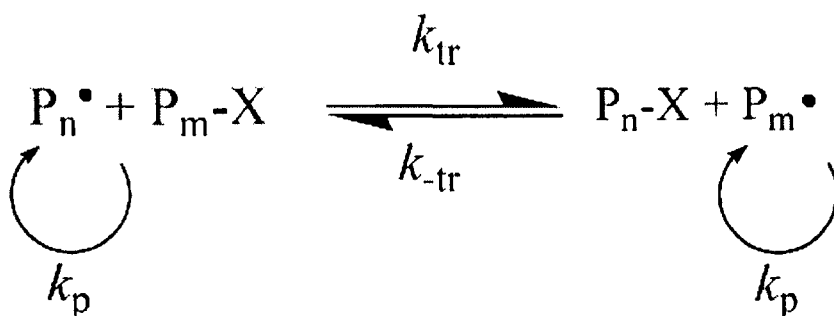
1) Reversible deactivation by atom transfer. e.g. ATRP.²¹



2) Reversible deactivation by coupling. e.g. nitroxide-mediated polymerisation (NMP).²⁰



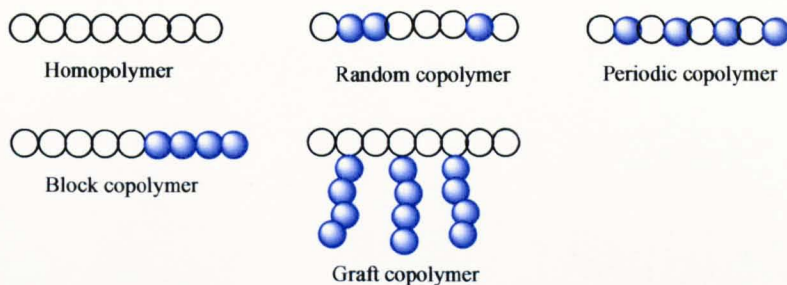
3) Degenerative transfer. e.g. Alkyl iodides, unsaturated polymethacrylates (CCT), dithioesters (RAFT).³⁴



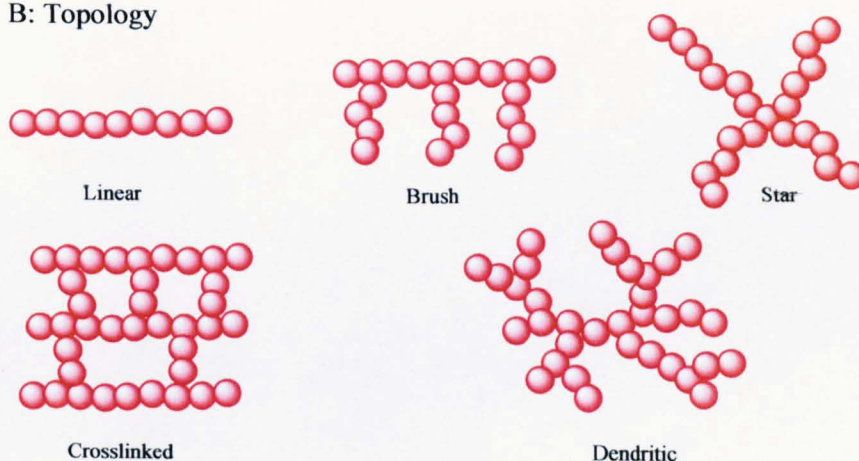
The CLRP can be used for the preparation of copolymers incorporating a broad range of commercial monomers forming materials with predetermined molecular weight and narrow distribution. The polymerisation process conditions are selected

so that the contributions of the chain termination processes are insignificant when compared to chain propagation. Thus, polymers with predetermined molecular weight, low polydispersity and specific functionality are achievable (Figure 1.4).

A: Composition



B: Topology



C: Functionality

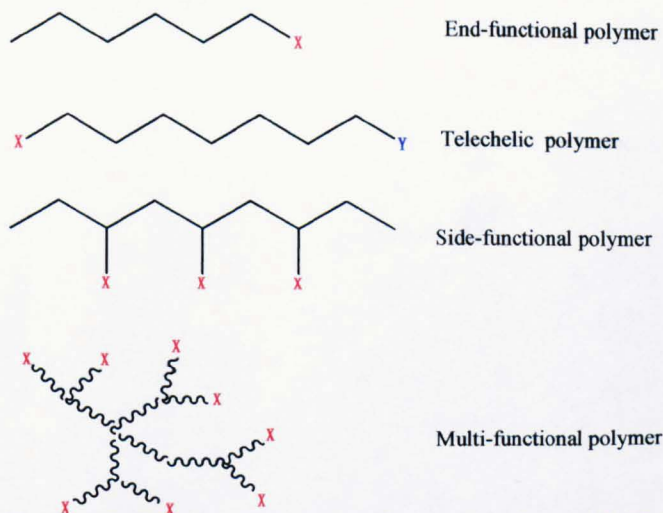


Figure 1.4 Controlled/living radical polymerisations (CLRP) can be used for the preparation of specific polymer with different composition (A), architecture (B) or functionality (C).

It is widely accepted that a controlled radical polymerisation process should display the following features. First, the first-order kinetics during the polymerisation, for instance, the polymerisation rate (R) which with respect to the monomer concentration ($[M]$) is a linear function of time (Eq. 1.5 and 1.6). This is due to the lack of termination, and thus the concentration of the active propagating species ($[P\bullet]$) is constant.

$$R = \frac{-d[M]}{dt} = k_p [P\bullet] [M] \quad (\text{Eq. 1.5})$$

$$\ln \frac{[M]_0}{[M]} = k_p [P\bullet] t = k_p^{\text{app}} [P\bullet] t \quad (\text{Eq. 1.6})$$

It can be seen from Figure 1.5 that the dependence of $\ln([M]_0/[M])$ on time is linear. This semi-logarithmic plot is very sensitive to the change of the concentration of the active propagating species. A constant $[P\bullet]$ is revealed by a straight line. However, this line could be curved in the experiments. In the case of slow initiation, an upward curvature indicates an increased $[P\bullet]$. On the other hand, a downward curvature suggests the decrease of $[P\bullet]$, which may due to the termination or some other side reactions. It should also be noted that the semi-logarithmic plot is not sensitive to chain transfer processes or slow exchange between different active species, since they do not affect the concentration of the active propagating species. However, the chain transfer processes could decrease the molecular weight of the polymers.

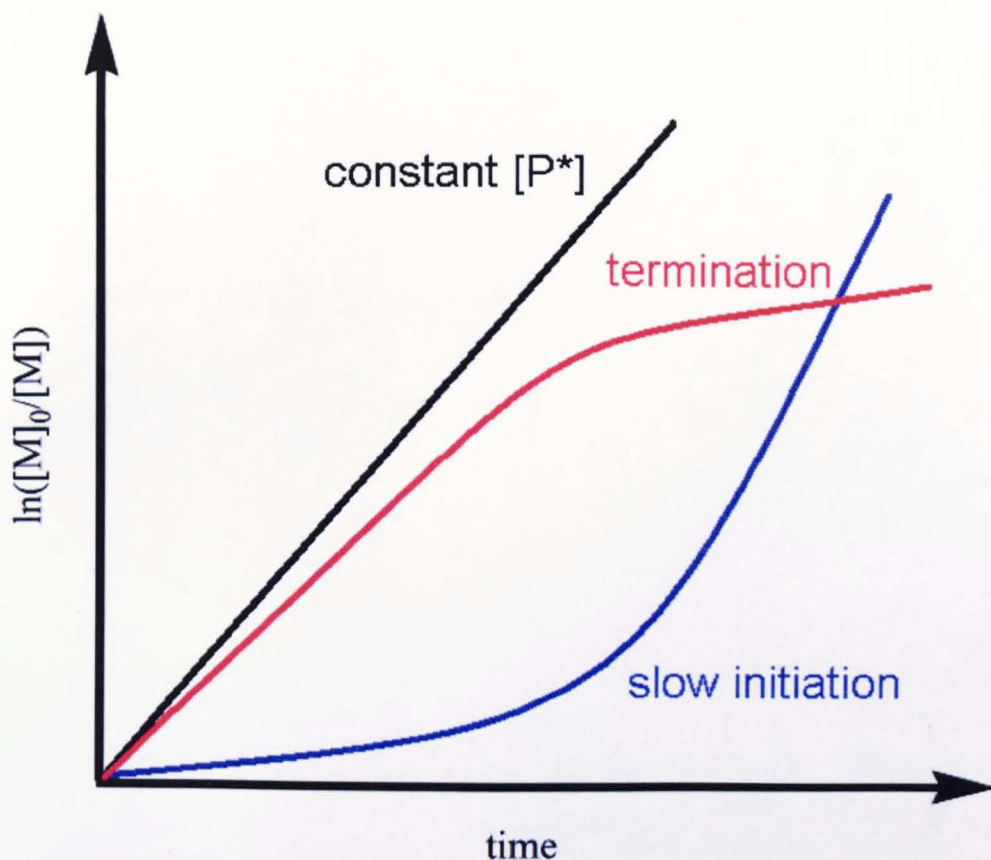


Figure 1.5 Illustration of the dependence of $\ln([M]_0/[M])$ on time. The scheme is redrawn from the original picture in the reference paper.²¹

Second, the living radical polymerisation should have predeterminable degree of polymerisation (DP). Thus, the number average molecular weight (M_n) is a linear function of monomer conversion (Eq. 1.7). This equation is not applicable to the RAFT reaction which the $DP = [M]_0/[RAFT]_0 \times \text{conversion}$.

$$DP = \frac{M_n}{M_0} = \frac{\Delta[M]}{[I]_0} = \frac{[M]_0}{[I]_0} \times \text{conversion} \quad (\text{Eq. 1.7})$$

This result comes from a constant number of chains throughout the polymerisation, which requires the following two conditions: (1) initiation should be sufficiently fast

so that nearly all the chains start to grow simultaneously; (2) no chain transfer occurs that increases the total number of chains.

The plot of conversion *versus* M_n (Figure 1.6) shows the ideal growth of molecular weights with conversion, as well as the effects of slow initiation, coupling and chain transfer on the molecular weight evolution.

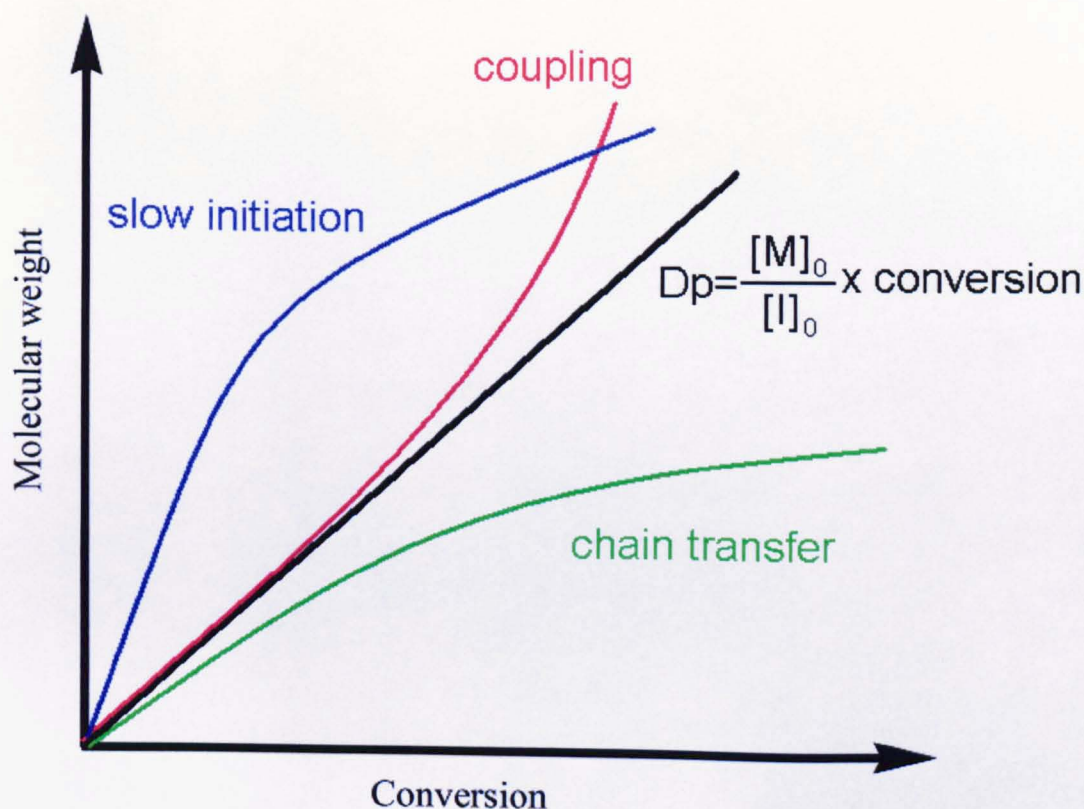


Figure 1.6 Illustration of the ideal growth of molecular weights with conversion, as well as the effects of slow initiation and chain transfer on the molecular weight evolution. The scheme is redrawn from the original picture in the original paper.²¹

Third, the controlled radical polymerisation should have low polydispersity. However, this is not easy to achieve because it requires the absence of chain transfer and termination, also ignores the effect from the rates of initiation and exchange. Substantial studies indicate that in order to obtain a polymer with a narrow

molecular weight distribution, the following requirements should be fulfilled.^{35, 36} (1)

The rate of initiation is competitive with the rate of propagation. This condition allows the simultaneous growth of all the polymer chains. The exchange between species of different reactivity is faster than propagation. This condition allows all the active chain termini are equally able to react with monomer for a uniform growth. There must be a negligible chain transfer or termination. The rate of depropagation is substantially lower than propagation. This guarantees that the polymerisation is irreversible. In addition, the system is homogeneous, and mixing is sufficiently fast. Therefore all active centres are introduced at the onset of the polymerisation. (2) The polydispersity should yield a Poisson distribution (Eq. 1.8),²¹ where X_w is the weight average degree of polymerisation, X_n is the number average degree of polymerisation, p is the conversion of monomers. According to the equation, polydispersity (M_w/M_n) decreases with increasing molecular weight. A polymerisation that satisfies all of the above requirements is expected to form a final polymer with a polydispersity less than 1.1 if X_n greater than 10.

$$X_n = \frac{1}{1-p}; X_w = \frac{1+p}{1-p}$$

$$\frac{M_w}{M_n} = \frac{X_w}{X_n} = 1 + \frac{X_n}{(X_n+1)^2} \cong 1 + \frac{1}{X_n} \quad (\text{Eq 1.8})$$

(3) The living free radical polymerisation should have long-lived polymer chains. This is a consequence of negligible chain transfer and termination. Therefore, all the chains retain their active centres after the full consumption of the monomers. Furthermore, this allows the propagation to resume after the introduction of additional monomer. This unique feature enables the preparation of block copolymers by sequential monomer addition.

The controlled/living free radical polymerisation is widely recognised as a powerful synthetic tool. Also, the polymers having uniform and predictable chain length are

readily available. Controlled/living polymerisation provides the best opportunity to control the variety properties of a target material. This can be achieved by control of the multitude of variations in composition, functionality and topology now attainable at molecular level.

The copolymers can have any desired topology through appropriate selection of the functional initiator. Furthermore, the CLRP allows the use of macroinitiators or macromonomers which are prepared by the previous polymerisations. Since the initiator sites or functionalities in the polymer allow the incorporation of a variety of functionalities and different polymer segments into the copolymers prepared by CLRP. Thus, many previously unattainable polymeric materials can be prepared. Numerous examples of gradient,³⁷ block³⁸ and graft³⁹ copolymers have been reported, as well as polymers with complex architectures, including polymer comb shaped brushes³⁹, stars⁴⁰ and hyperbranched polymers.⁴¹

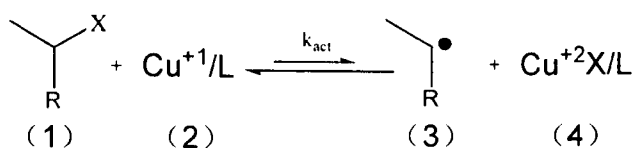
1.2 Atom Transfer Radical Polymerisation

1.2.1 Mechanism of Atom Transfer Radical Polymerisation

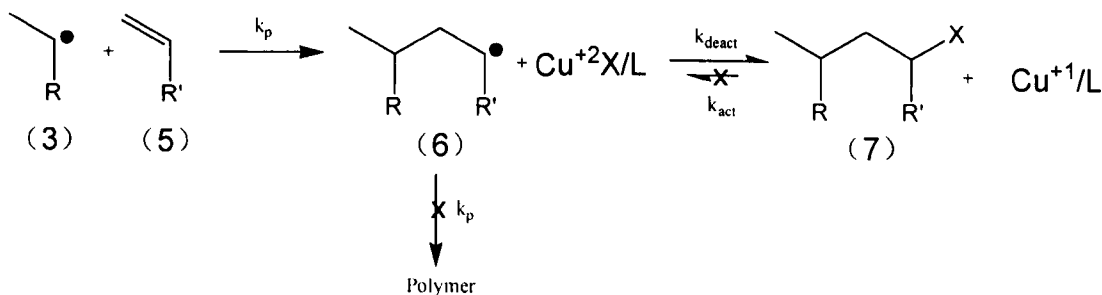
Free radical polymerisation is one of the most important processes for the preparation of a wide variety of homopolymers and copolymers. However, the main drawback of free radical polymerisation is the poor control over molecular weight and structure due to the unavoidable bimolecular termination. Thus, the development of a 'controlled/living' radical polymerisation route became an attractive goal in polymer chemistry. In the early of 1990s, several methods were found for controllable radical addition reaction.^{26,27} One of these reactions was promoted by a transition metal complex, so called atom transfer radical addition (ATRA).⁴²⁻⁴⁵ The catalyst acts as the halogen atom (X) carrier by way of a redox reaction between Cu^{I} and Cu^{II} . The general mechanism of ATRA is shown in Figure 1.7. Firstly, the halogen atom is transferred from an organic halide (1) to a transition metal complex (2) to generate a radical (3). Following this the radical is added to another

inter-molecular or intra-molecular (cyclisation) double bond (6), the halogen atom is transferred back from the transition metal (4) and forms the final product (7). At the same time, the Cu^{I} complex is reformed after the catalytic cycle. This reaction is widely used for cyclisation reactions in organic synthesis.^{42, 43} In this case, the termination reaction is ignored due to the relatively low concentration of free radicals. However, the deactivation rate (k_{deact}) is much higher than the activation rate ($k_{\text{act}} \approx 0$) due to the poor stability of newly formed radicals (6). Thus, the activation-deactivation cycle can only occur once in this reaction.

Initiation



Propagation



Termination

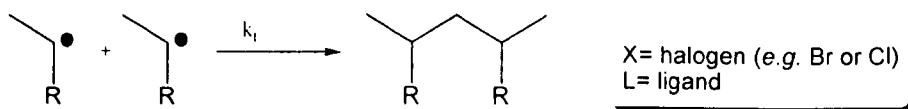


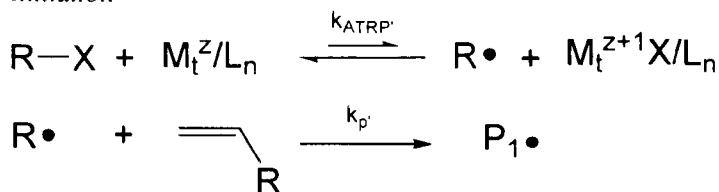
Figure 1.7 Proposed mechanism for copper catalyzed atom transfer radical addition (ATRA) reaction.

In 1995, the first proposed concept of atom transfer radical polymerisation (ATRP) was reported by Matyjaszewski^{24, 25, 46} (copper catalyst) and Sawamoto^{47, 48} (ruthenium catalyst) independently. They realised the huge potential of the ATRA reaction which could be essential extend to a 'controlled/living' free radical polymerisation. Based on the principles of ATRA reaction, ATRP comes from the

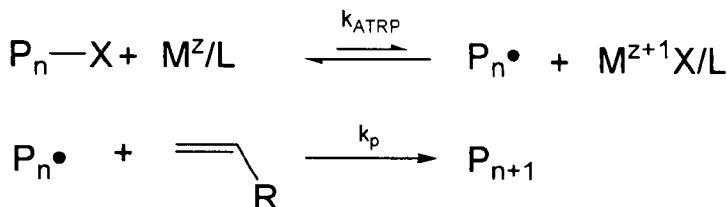
atom transfer step. However, in ATRP, the reaction condition of ATRA is modified to afford more stable radical species. Thus, the activation-deactivation cycles will repeat many times until all the monomers are consumed. ATRP has been developed by designing specific catalysts based on transition metal compounds and ligands.^{24, 25}

The general mechanism of ATRP is presented in Figure 1.8. In principle, ATRP is based on an inner sphere electron transfer process.²⁵ The reaction involves a reversible halogen transfer between an initiator, the dormant species, the propagating chain end and the transition metal complex. First, the halogen atom transfers from initiator ($R-X$) to a transition metal complex in a lower oxidation state (M^Z/L_n) resulting in the formation of a propagating radical ($R\bullet$) and the metal complex in its higher oxidation state with a coordinated halide ligand ($M^{Z+1}X/L_n$). The active radicals form at a rate constant of activation (k_{act}), subsequently propagate with a rate constant (k_p) and reversibly deactivate (k_{deact}). Termination reactions (k_t) can also occur in ATRP by radical coupling and disproportionation. However, the termination step is suppressed to a minimum in a well controlled ATRP. Since as the reaction progresses, the termination step is slowed down as a result of the persistent radical effect (PRE). The Cu^{II} are accumulated and radical concentration is decreased by PRE in ATRP. The concentration of radicals in ATRP remains quite low because the equilibrium is strongly shifted towards the dormant species ($k_{act} \ll k_{deact}$).

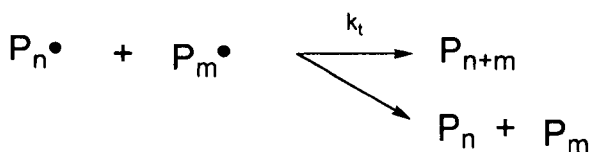
Initiation



Propagation



Termination



$$k_{ATRP} = k_{act}/k_{deact}$$

X=Cl or Br

M= transition metal

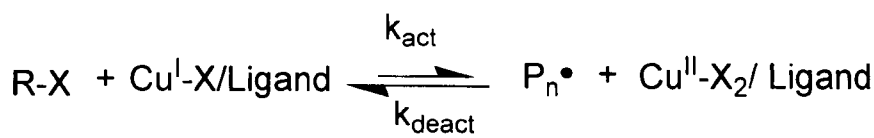
L=ligand

Figure 1.8 General mechanism of atom transfer radical polymerisation (ATRP) reaction.

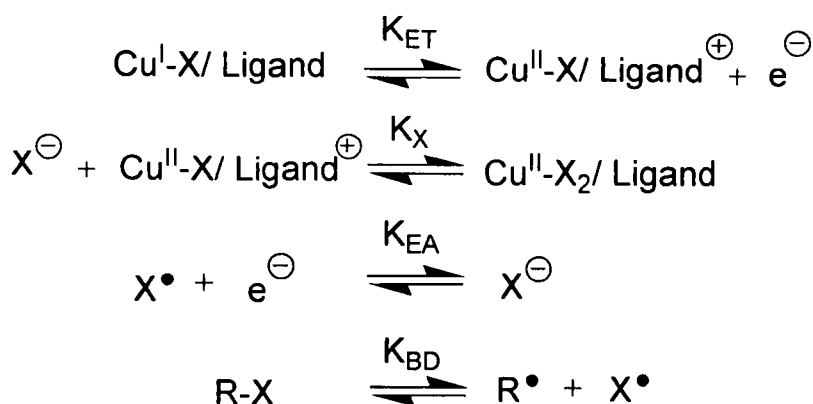
An overall mechanism for ATRP using copper complex is shown in Figure 1.9.^{49, 50} Consequently, the ATRP equilibrium can be expressed as a combination of four contributing reactions: the redox reaction of Cu^I , heterolytic cleavage of the $Cu^{II}-X$ bond, the redox of halogen atom (X) and homolysis of the alkyl halide (Figure 1.9). Thus, the constant of ATRP reaction (K_{ATRP}) can be written as the equilibrium constants for electron transfer of metal complexes (K_{ET}), the equilibrium constant for the heterolytic cleavage of the $Cu^{II}-X$ bond (K_X , also called halidophilicity), electron affinity of the halogen (K_{EA}) and bond dissociation energy of the alkyl halide (K_{BD}). Moreover, the scheme shows the ATRP equilibrium constant (K_{ATRP}) depends not only on the alkyl halide (R-X) and the activity of catalyst redox potential, but also on the halidophilicity of transition metal in the reaction. Therefore, the choice of

initiator, metal and ligand complex in ATRP can significantly influence the polymerisation rate and molecular weight control.

Overall equilibrium



Contributing reactions



$$K_{\text{ATRP}} = k_{\text{act}}/k_{\text{deact}} = K_{\text{ET}}K_{\text{X}}K_{\text{EA}}K_{\text{BD}}$$

Figure 1.9 The overall mechanism of ATRP by copper catalyst. The copper complex activates reversibly the dormant polymer chain via a halogen transfer reaction ($\text{X}=\text{Cl}$ or Br , and ligand= 2,2'-bipyridine).⁵⁰

There are two key requirements to obtain good control in ATRP. Firstly, the concentration of radicals should be much lower than free radical polymerisation leading to a termination step which can be ignored. Secondly, the initiation rate should be fast and the deactivation of polymerisation (k_{deact}) should be much higher than propagation rate (k_p). As a result, the molecular weights increase linearly with conversion and the polydispersity index is typical of a living process (*e.g.* $\text{PDI} < 1.5$). This allows for outstanding control over the chain topology (stars, combs, branched), composition and end functionalities for a wide range of monomers. In addition, ATRP does not require the low temperatures (*e.g.* $T < 0^\circ\text{C}$) that are often crucial for

anionic living polymerisation. This is especially important from an industrial perspective, since it is costly to maintain large scale reactions at such conditions. Although ATRP may be the most versatile system among the recently developed methods, there are some drawbacks to the use of ATRP. These disadvantages can have significant implications for its exploitation in polymer synthesis on a commercial scale. First of all, high molecular weights are often difficult to achieve. Furthermore, the metal catalyst which is used in most situations is normally toxic and needs to be removed from the final products. Moreover, ATRP typically requires a relatively high concentration of catalyst to ensure a rapid shift between activation and deactivation. This makes ATRP less attractive for industry because the transition metal catalysts and ligands are the most expensive components of this reaction. Recently, some approaches have been developed to overcome these problems. More details are discussed in the following section (see section 1.2.4).

1.2.2 Mechanism of Electron Transfer

The mechanism of ATRP was firstly described by Wang and Matyjaszewski in 1995,^{24, 25} since it was believed that the reaction was based on the principles of atom transfer radical addition (ATRA). This concept was widely accepted by polymer scientists. Typically, non-activated olefins such as vinyl chloride cannot be polymerised by ATRP. However, the controlled/living polymerisation of vinyl chloride was successfully conducted in a water/THF medium at room temperature in the presence of ‘nascent’ Cu^0 /ligand was reported by Percec in 2002.⁵¹ The mechanism was postulated to be single electron transfer (SET).⁵²⁻⁵⁶

The general mechanism of SET is shown in Figure 1.10.⁵⁵ The key in this polymerisation is the disproportionation step of Cu^I into Cu^0 and Cu^{II} . Firstly, Cu^0 and Cu^{II}X_2 /ligand are generated by the disproportionation reaction ($k_{\text{dis}} \approx 10^7$) of the Cu^I species. Secondly, the initiation or activation step (k_{act}) is mediated by the outer sphere electron transfer from the Cu^0 to the alkyl halide (electron-acceptor).

Thereafter, polymer chains grow by the addition of the free radicals to monomers with the rate constant of propagation (k_p). Moreover, radicals react reversibly with the Cu^{II} to reform the dormant species and Cu^{I} species. Finally, the Cu^{I} generated in above steps instantaneously disproportionates into Cu^{II} and Cu^0 species again. The termination step is suppressed into a minimum ratio in this process.

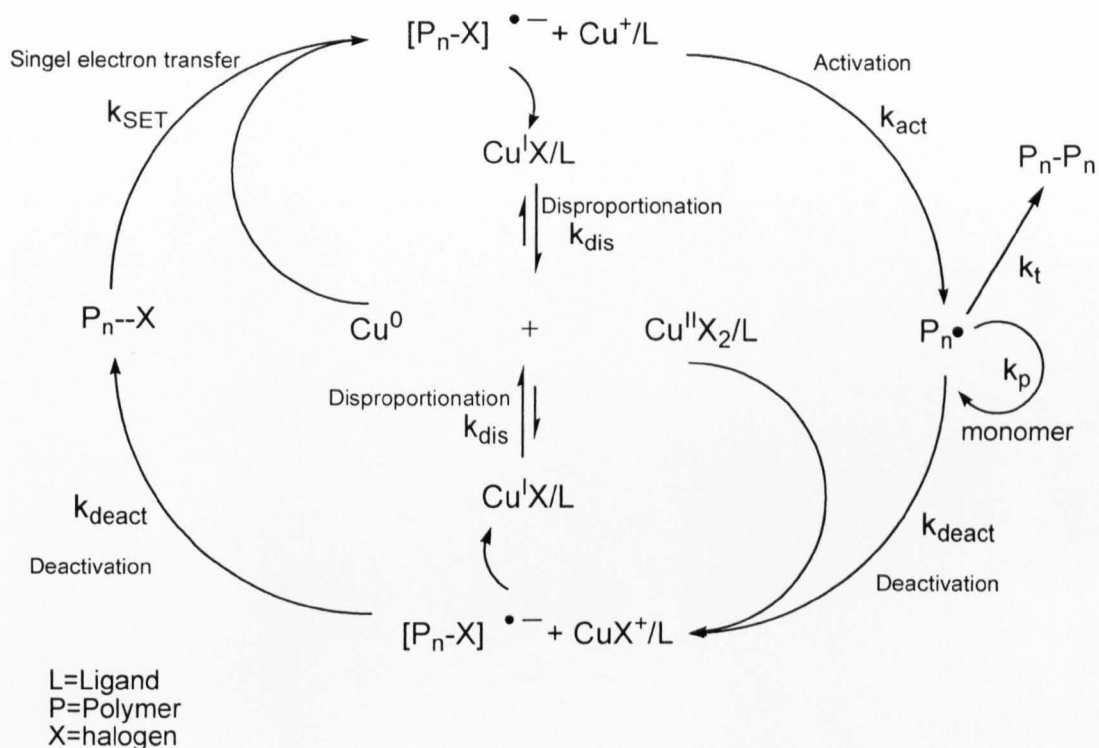
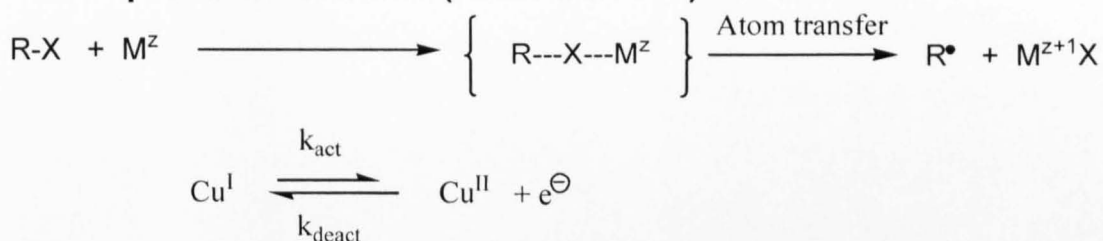


Figure 1.10 General mechanism of single electron transfer (SET) reaction.⁵⁵

The difference between ATRP and SET mechanisms are shown in Figure 1.11.⁵⁶ In both cases, the oxidation state of the metal was increased from M^z to M^{z+1} . In the inner sphere or atom transfer process, the metal approaches the halogen atom and forms a medium transition state (R-X-M^z), from which the halogen atom is transferred with one electron, leaving an alkyl radical behind. On the other hand, in the outer sphere or electron transfer process, the electron is transferred from the metal to the alkyl halide to produce a radical anion. Depending on the substrate and the nature of the monomer and initiator, these two mechanisms are used to describe the different reaction system. Percec suggested that the ATRP mechanism dominates

in the polymerisation of styrene, methacrylates, and acrylates, and is activated by Cu^{I} compounds. On the other hand, the outer sphere electron transfer mechanism operates rather than the atom transfer processes in the systems with electron-rich donors (Cu^0) and electron-poor acceptors (*e.g.* CHI_3 used as initiator). The argument about ATRP or SET mechanism is not over since there is no absolute proof for or against any of these possibilities. In this thesis, atom transfer was considered as the main mechanism of the reaction. Therefore, the following kinetics and calculations are all based on the atom transfer mechanism.

Inner sphere mechanism (Atom transfer)



Outer sphere mechanism (Single electron transfer)

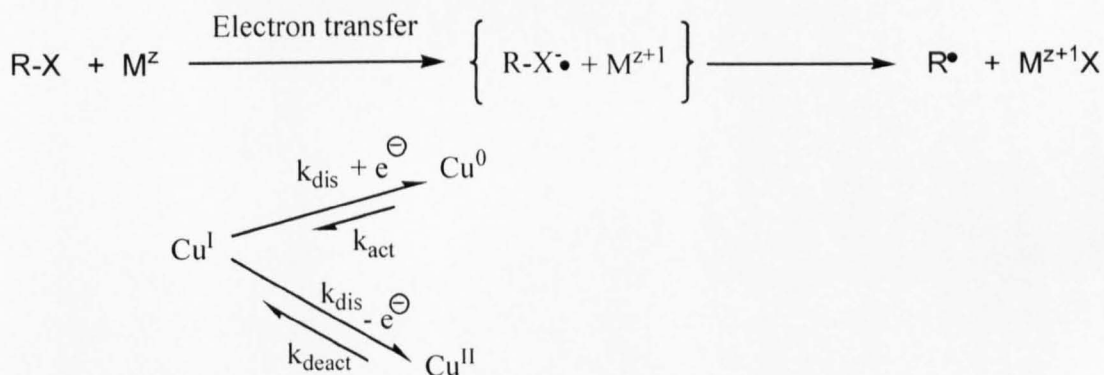


Figure 1.11 Comparison of ATRP and SET mechanism in the reaction of metal complex with alkyl halides.

1.2.3 Kinetics and components

As a multi-component system, ATRP is composed of a monomer, an initiator with a weak C-X bond and a transition metal complex catalyst. For a successful ATRP, other factors such as solvent and temperature must also be taken into consideration.

In the case of ATRP, the rates of both activation and deactivation must be rapid so that addition of monomer units in each cycle is controlled.²⁴ If this is not the case, the polymer chains are more likely to grow at different rates, leading to a broad molecular weight distribution. Also, the equilibrium must shift towards the deactivation reaction. Therefore, k_{deact} must be significantly higher than k_{act} in order to ensure a sufficiently low concentration of polymer radicals and minimise termination reactions.

Herein, the kinetics of ATRP is discussed for copper-mediated polymerisation. Linear semi-logarithmic plot of monomer conversion *versus* time indicates that the polymer radical concentration remains constant during the polymerisation, which implies a living character. This can be shown by considering the kinetic rate equation for ATRP. In the case of an ideal ATRP conditions (fast initiation and negligible termination), it allows that the polymerisation rate (R_p) is equal to the rate of consumption of monomer ($-d[M]/dt$), which is also equal to the propagation rate constant (k_p) (Eq. 1.9). Thus, the rate of polymerisation is affected by the concentration of polymer radicals ($[P^\bullet]$) and concentration of monomer ($[M]$).

$$R_p = \frac{-d[M]}{dt} = k_p [P^\bullet] [M] \quad (\text{Eq 1.9})$$

Moreover, the activation rate ($R_{\text{activation}}$), deactivation rate ($R_{\text{deactivation}}$) and propagation rate ($R_{\text{propagation}}$) of ATRP are given in Eq. 1.10, respectively. Thus, the polymerisation rate (R_p) can also be expressed as a function of $[Cu^I]$ and $[Cu^{II}]$, where k_p is the rate constants of propagation, K_{ATRP} is the equilibrium constant in ATRP ($K_{\text{ATRP}} = k_{\text{act}}/k_{\text{deact}}$), $[M]$ is the monomer concentration, $[I]_0$ is the initial concentration of initiators.

$$\begin{aligned}
 \text{activation rate } R_{\text{activation}} &= [\text{P-X}][\text{Cu}^{\text{I}}]k_{\text{act}} \\
 \text{propagation rate } R_{\text{propagation}} &= [\text{P}^{\bullet}][\text{M}]k_{\text{p}} \\
 \text{deactivation rate } R_{\text{deactivation}} &= [\text{P}^{\bullet}][\text{Cu}^{\text{II}}]k_{\text{deact}}
 \end{aligned}$$

$$\begin{aligned}
 R_{\text{p}} &= \frac{R_{\text{activation}}}{R_{\text{deactivation}}} \times R_{\text{propagation}} \\
 &= k_{\text{p}} K_{\text{ATRP}} [\text{M}][\text{I}]_0 \frac{[\text{Cu}^{\text{I}}]}{[\text{Cu}^{\text{II}}]}
 \end{aligned}$$

$$K_{\text{ATRP}} = k_{\text{act}}/k_{\text{deact}}; \quad [\text{P-X}] \cong [\text{I}]_0 \quad (\text{Eq. 1.10})$$

Furthermore, the number average degree of polymerisation (DP_n , Eq. 1.11) and molecular weights of the polymers in a well-controlled ATRP follow the ratio of the mass of the consumed monomer to the initial initiator concentration.

$$\text{DP}_n = \frac{[\text{M}]_0}{[\text{I}]_0} \times \text{conversion} \quad (\text{Eq. 1.11})$$

The molecular weight distribution or polydispersity index (PDI) refers to the polymer chain length distribution. In ATRP, the PDI (Eq. 1.12) relates to the concentrations of initiator ($[\text{I}]_0$) and deactivator ($[\text{Cu}^{\text{II}}]$), monomer conversion(c), the rate constants of propagation (k_{p}) and deactivation (k_{deact}) if the DP_n is higher enough ($1/\text{DP}_n \approx 0$).

$$\begin{aligned}
 \text{PDI} = \frac{M_w}{M_n} &= 1 + \frac{1}{\text{DP}_n} + \left(\frac{2-c}{c} \right) \left(\frac{k_{\text{p}}[\text{I}]_0}{k_{\text{deact}}[\text{Cu}^{\text{II}}]} \right) \\
 &\approx 1 + \left(\frac{2-c}{c} \right) \left(\frac{k_{\text{p}}[\text{I}]_0}{k_{\text{deact}}[\text{Cu}^{\text{II}}]} \right) \\
 \text{where } c &= \frac{[\text{M}]_0 - [\text{M}]}{[\text{M}]_0} \quad (\text{Eq. 1.12})
 \end{aligned}$$

An important factor in achieving control in an ATRP reaction is the persistent radical effect (PRE) described by Fisher.¹⁹ During the activation step of ATRP, transient organic radicals $[\text{R}^{\bullet}]$ and persistent radicals (oxidised transition metal catalyst) are

formed in equal quantities. However, in the early stages of ATRP reaction, a small number of the transient radicals are removed from the equilibrium by termination. This step leaves an excess of persistent radicals relative to transient radicals for the rest of the polymerisation. Therefore, this effect excess increases the probability of polymer radical deactivation, thereby reducing the probability of irreversible termination reaction.

1.2.4 Different ATRP Procedures

Recently, several different ATRP procedures were developed to cover the shortages in ATRP reaction, especially at industry scale. These ATRP procedures were conducted by the different conditions for initiation step. The advantage and disadvantages of each method were discussed as below.

Firstly, the procedure for the normal initiation ATRP starts by an alkyl halide (R-X, initiator), transition metal catalyst in a lower oxidation ($\text{Cu}^{\text{I}}/\text{Ligand}$) and monomers (Figure 1.12). The normal initiation ATRP procedure is the first procedure which developed in 1995.^{24, 25} The degree of polymerisation and polydispersity can be predicted by Eq. 1.11 and Eq. 1.12. As mentioned before, the concentration of metal and ligands is relative high which is the main shortage for the industry scale requirement. Moreover, the metal catalyst which at a lower oxidation (*e.g.* Cu^{I}) is sensitive to the air.

Normal Initiation ATRP

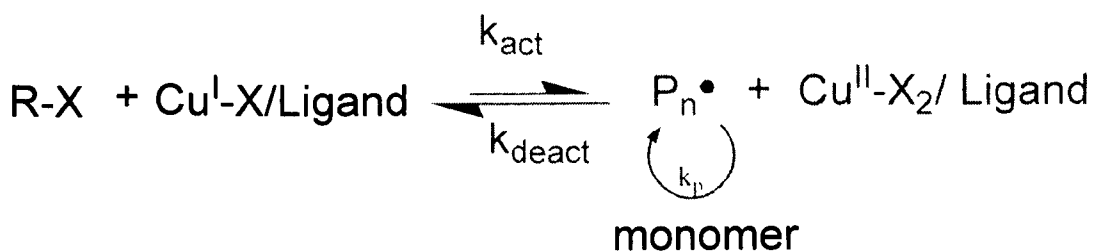


Figure 1.12 General mechanism of normal initiation ATRP reaction by copper catalyst. The alkyl halide initiator (R-X), metal complex in a lower oxidation state ($\text{Cu}^{\text{I}}/\text{Ligand}$) and monomer were added into reaction initially.

Secondly, the reverse ATRP was also developed in 1995.^{46, 57} In the reverse ATRP, the alkyl halide initiator was replaced by conventional free radical initiator (*e.g.* AIBN) (Figure 1.13). Furthermore, the transition metal complexes in the higher oxidation state (*e.g.* Cu^{II}) were added to the reaction at beginning. After the radicals generated by the thermal decomposition of initiator, the dormant polymer chain and Cu^{I} are formed immediately by the deactivation reaction of active chain and Cu^{II} . The degree of polymerisation can be calculated by Eq. 1.13, where $[\text{M}]$ is concentration of monomer, $[\text{I-I}]$ is the concentration of conventional initiator, f is the initiation efficiency. In reverse ATRP, the reaction starts with Cu^{II} which is not sensitive to air. However, the initiator terminal (I) remaining on the polymer chain (I-P-X) is the main disadvantage in this reaction. Moreover, the architecture of final polymer chain was limited to linear. In addition, the polydispersity is relative higher than normal ATRP.

Reverse ATRP

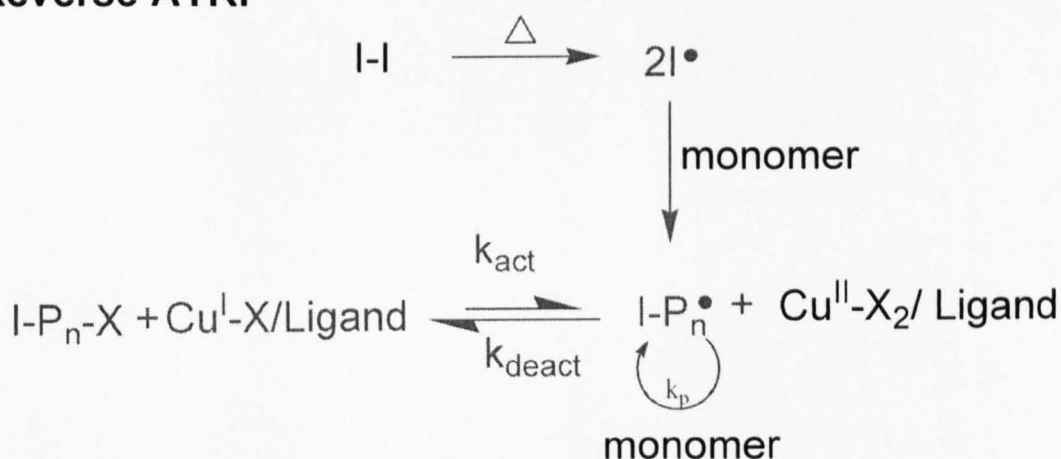


Figure 1.13 General mechanism of reverse ATRP reaction by copper catalyst. The conventional initiator (I-I), metal complex in the higher oxidation state ($\text{Cu}^{\text{II}}/\text{Ligand}$) and monomer were added at the beginning of reaction.

Reverse ATRP

$$\text{DP}_n = \frac{[\text{M}]_0}{2 \times f \times [\text{I-I}]_0} \times \text{conversion} \quad (\text{Eq 1.13})$$

Thirdly, the modified procedure called simultaneous reverse and normal initiation ATRP (SR&NI) was developed in 2001 to cover the shortage in reverse ATRP.⁵⁸ SR&NI ATRP use a dual initiation system comprised of conventional initiators (e.g. AIBN) and alkyl halide (R-X) and the metal complex in higher oxidation state (Cu^{II}) (Figure 1.14). Once the radicals formed by conventional initiator (I-I), the metal in higher oxidation state was reduced to the activator state by the deactivation reaction. On the other hand, the most of the polymer chains are initiated by the alkyl halide via normal ATRP initiation mechanism. The degree of polymerisation can be calculated by Eq. 1.14, where $[\text{M}]$ is the concentration of monomer, $[\text{R-X}]$ is the concentration of alkyl halide, $[\text{I-I}]$ is the concentration of conventional initiator, f is the initiation efficiency. In SR&NI ATRP, the metal complex was added to the reaction in stable oxidation state and the most chain ends of the polymers were from the alkyl halide initiator. This procedure has also successfully adapted in miniemulsion systems.^{59, 60} However, some homopolymer chains were formed directed from the AIBN initiator which are unexpected in the block copolymerisation.

SR&NI ATRP

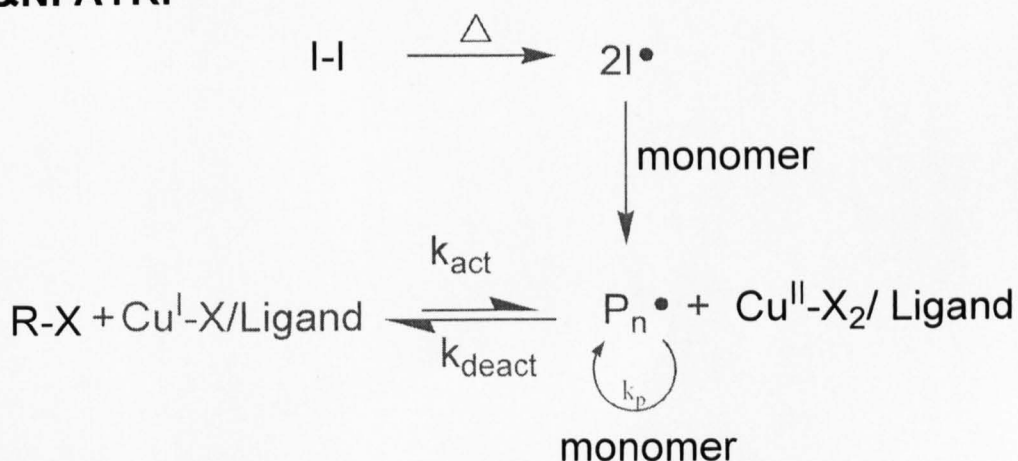


Figure 1.14 General mechanism of SR&NI ATRP reaction by copper catalyst. The conventional initiator (I-I), alkyl halide (R-X), metal complex in the higher oxidation state ($\text{Cu}^{\text{II}}/\text{Ligand}$) and monomers were added at the beginning of reaction.

SR&NI ATRP

$$DP_n = \frac{[M]_0}{[R-X]_0 + 2 \times f \times [I-I]_0} \times \text{conversion} \quad (\text{Eq 1.14})$$

The activator generated by electron transfer ATRP (AGET) procedure was developed in 2005 to overcome the disadvantage in SR&NI procedure.^{61, 62} In AGET technique, the activator (Cu^{I}) is generated from the higher oxidation state transition metal complex (Cu^{II}) by reducing agent (Figure 1.15). Thereafter, the alkyl halide initiators are activated by Cu^{I} and generated radicals. Thus, no polymers are initiated by AIBN as in the SR&NI ATRP. The molecular weight of polymer chain can be calculated as the same as normal ATRP (Eq. 1.11). Many reducing agents could be used in AGET, such as tin(II) 2-ethylhexanoate, glucose and ascorbic acid which are all approved by food and drug administration (FDA). Thus, the AGET includes all the outstanding advantages, such as stable catalyst system, without conventional initiator end-group, good control over molecular weight and polydispersity.

AGET ATRP

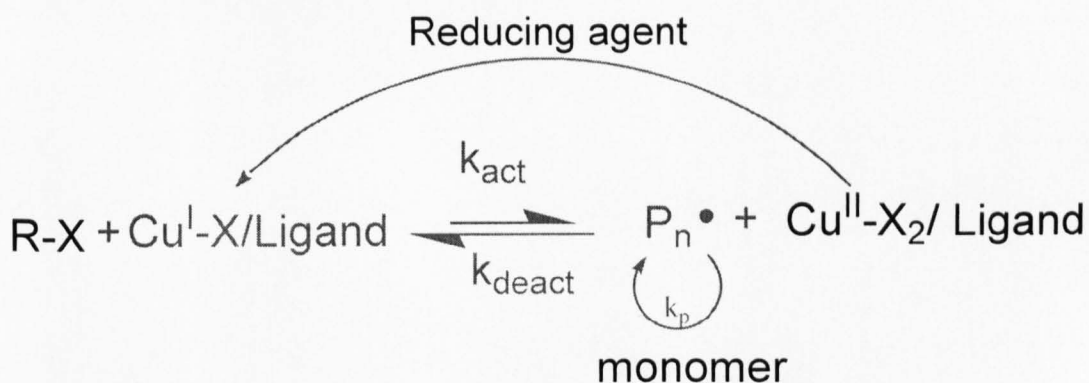


Figure 1.15 General mechanism of AGET ATRP reaction by copper catalyst. The alkyl halide (R-X), metal complex in the higher oxidation state ($\text{Cu}^{\text{II}}/\text{Ligand}$), reducing agent and monomer were added at the beginning of reaction.

For the industrial requirement, the polymerisation should be conducted under the acceptable polymerisation rate and polydispersity in the presence of very low

metal/ligand concentration. Thus, the activator regenerated by electron transfer ATRP (ARGET) procedure was developed in 2006^{63, 64} as an extension of the concept of AGET ATRP to reduce the amount of metal complex catalyst in the polymerisation. Generally, there are two conditions are modified in the ARGET ATRP. Firstly, it shows that the polymerisation rate of ATRP depends on the K_{ATRP} ($k_{\text{act}}/k_{\text{deact}}$) and ratio of the Cu^{I} to Cu^{II} in Eq. 1.10. Thus, the absolute concentration of Cu^{I} and Cu^{II} can be reduced to quite low level without influence on the polymerisation rate. Moreover, the ligands with very high activity (K_{ATRP} is extremely high, *e.g.* Me_6TREN) are used in this reaction. Thus, the requirement of Cu^{I} was decreased since the K_{ATRP} increased significantly. However, the ATRP equilibrium was shifted to the deactivation direction gradually by the PRE effect¹⁹ and termination reaction. The concentration of Cu^{II} in the reaction is increased along reaction time. Therefore, if the amount of Cu^{I} is reduced to the very low level, the polymerisation will be retarded by the unavoidable irreversible termination or other side reaction. Secondly, large excess amounts of reducing agent were added into the reaction to keep the ratio of Cu^{I} to Cu^{II} at a necessary level. Furthermore, the excess reducing agent can help to remove the oxygen and radical inhibitors. In the ARGET ATRP, the concentration of initial added Cu^{II} complex can be reduced to the ppm level with the excess reducing agent. Hence, the ARGET ATRP exhibits the great potential in industry.

1.2.5 Monomers

A variety of monomers have been reported successfully polymerised using ATRP: styrenes,^{65, 66} acrylates,⁶⁷ methacrylates,⁶⁸⁻⁷¹ acrylamides⁷² and acrylonitrile⁷³⁻⁷⁶ (Figure 1.16). Moreover, multi-functional monomers have also been used to prepare branched polymers.⁴¹ Even under the same conditions using the same catalyst or system, each monomer has its own unique equilibrium constant ($k_{\text{ATRP}} = k_{\text{act}}/k_{\text{deact}}$). The suitability of a monomer for ATRP strongly depends on k_{ATRP} as non-polar monomers tend to give highly unstable radicals. Some monomers lack appropriate

substituent groups to stabilise the active radical and are subsequently difficult to polymerise using ATRP. In recent years, some encouraging progress has been made in the cases of vinyl chloride and vinyl acetate.^{77, 78} A successful catalyst for these monomers would require a sufficiently negative reduction potential. However, this may then cause reduction of radicals or induce coordination polymerisation instead.

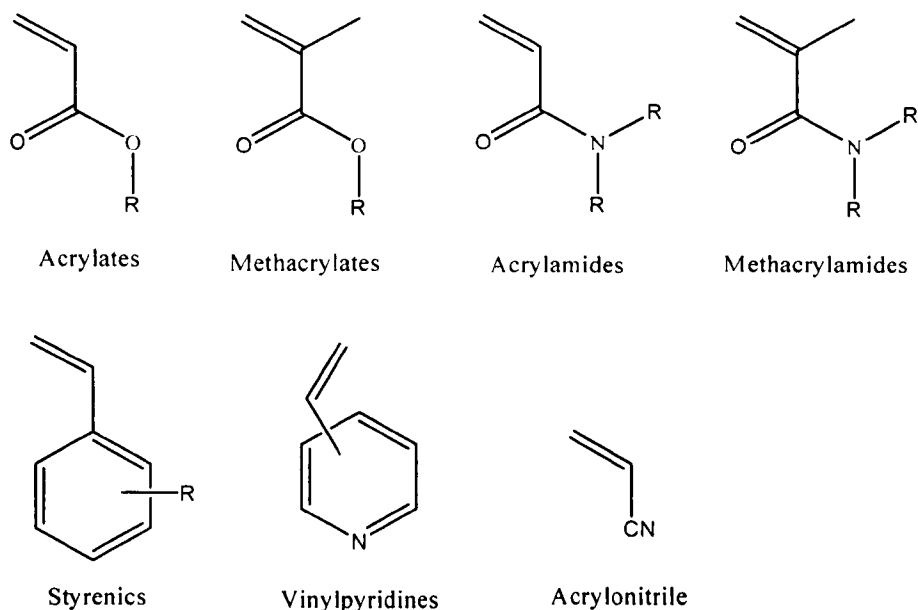


Figure 1.16 Monomer classes that have been polymerised successfully using ATRP, including styrenics, acrylates, methacrylates, acrylamides, methacrylamides, vinylpyridine and acrylonitrile.

1.2.6 Initiators

The main role of the initiator is to determine the number of growing polymer chains. In ATRP, alkyl halides ($R-X$) are typically used as initiators.²¹ Initiation should be fast and quantitative with a good initiator with suitable group R . Furthermore, the rate of initiation is determined by the choice of catalyst. The activation rates (k_{act}) of some typical initiators in ATRP are shown in Figure 1.14.⁷⁹ The initiator with higher k_{act} value has the higher initiation rate in ATRP. General, there are three factors can affect the k_{act} of the initiators.

Firstly, the leaving halide groups can affect the activation rate of initiator. To obtain well-defined polymers with narrow molecular weight distribution, the halide group

should rapid exchange between the growing chain and transition metal complex. The activity of the alkyl halides follow decreases in the order $R-I > R-Br > R-Cl$. Since the carbon-iodine bond is much weaker than the carbon-bromine bond or carbon-chloride bond. Thus, the k_{act} value of MIP (5.3) is much higher than the MBrP (0.33) and MCIP (0.015) (Figure 1.17). Moreover, the activation rate also depends on the bond energy of halide to the metal species.

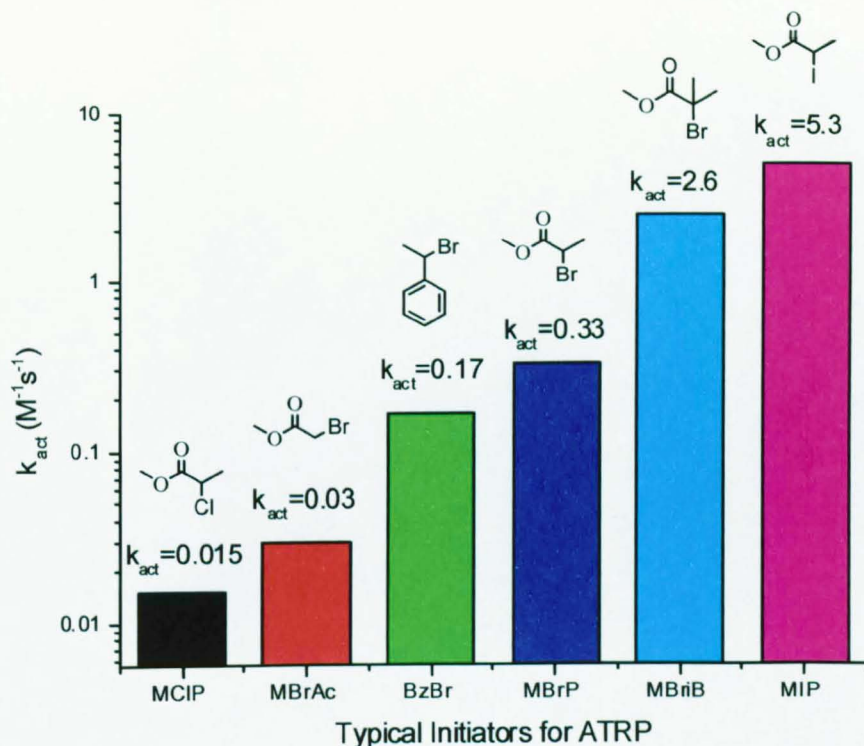


Figure 1.17 ATRP activation rate constants for various initiators by CuX/PMDETA in acetonitrile at 35 °C. MCIP= methyl 2-chloropropionate; MBrAc= Methyl bromoacetate; PEBr=1-phenylethyl bromide; MBrP=methyl 2-bromopropionate; MBriB= methyl 2-bromoisobutyrate; MIP=methyl 2-iodopropionate. The rate constants values were taken from references.⁷⁹

Secondly, substituent group in the initiator molecule influences the resulting radical stability, with the relative stability increasing in the following order: $CN > C(O)R > C(O)OR > Ph > Cl > CH_3$. Therefore, the k_{act} value of MBrP (0.33) is higher than the BzBr (0.17) (Figure 1.17).

Last, the activation rate for primary, secondary and tertiary alkyl halides follows the

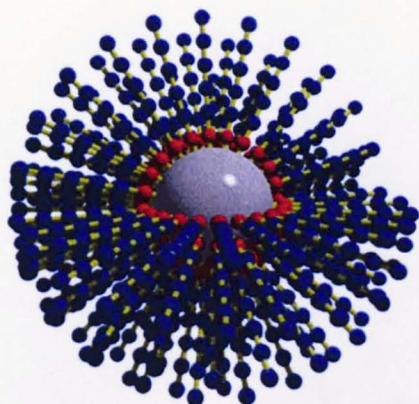
order tertiary > secondary > primary alkyl halides. The order of the activation rate is consistent with the stability of the generated radical. Thus, the k_{act} of MBriB (2.6) is higher than MBrP (0.33) and MBrAc (0.03).

There are also some other factors that can determine the initiator choice. For instance, an appropriate initiator can provide a useful end-group to determine the degree of polymerisation (DP_n) or molecular weight by NMR spectroscopy or titration. Additionally, a mono-functional or bi-functional initiator can provide initiator sites for the preparation of special architectures.

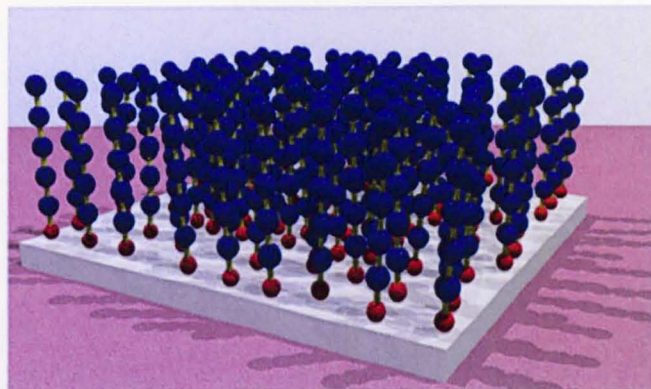
An alternative choice to a normal ATRP initiator is a macro-initiator which is prepared by chemical modification of polymer chains. This approach gives a convenient method for the synthesis of block copolymers. In addition, it results in lower polydispersity compared to block copolymers prepared using sequential monomer addition. It is especially useful if one block cannot be synthesised via ATRP, or if suitable ATRP conditions cannot be found for the synthesis of both blocks. In addition, graft copolymers are often prepared using a multifunctional monomer. In principal, any suitable functional polymer can be used to prepare an ATRP macro-initiator.

The synthesis of organic and inorganic hybrid materials is an area of growing interest. Scientists try to grow polymer on the surface of inorganic materials. CLRP has been demonstrated to be suitable for the preparation of organic and inorganic hybrid materials with varying structural complexity on different dimensions. ATRP has been research for this purpose as inorganic particles and substrates can be easily functionalised with initiating alkyl halides. Also, block copolymers can be synthesised with segments attaching to the surface functionality. This technique called surface-initiated ATRP which involves the chemical modification of surface is developing to achieve this purpose. In this case, ATRP has been conducted from the initiation sites on a range of surfaces (Figure 1.18).⁸⁰ These kinds of materials have

been called polymer brushes because of their unique appearance. Polymer brushes have been formed by ‘grafting from’ or ‘grafting to’ inorganic particles⁸¹⁻⁸⁵ and flat surfaces.^{86, 87} The applications of this kind of materials include surfactants, elastomers, magnetic materials, sensors, reinforced ultra-thin films, bio-responsive materials and patterned surfaces.



Spherical Particles



Flat Surfaces

Figure 1.18 ATRP initiated from surface which can form spherical particles or flat brushes.⁸⁰

1.2.7 Transition Metal Catalysts

The most important component of ATRP is the transition metal catalyst because it is the key to determine the atom transfer equilibrium and the dynamics between the dormant and active species. There are some critical factors that can determine an efficient transition metal catalyst. Firstly, the metal must have two readily available oxidation states separated by one electron. Secondly, the metal centre should have suitable attraction toward a halogen. Also, the ligand must complex with the metal strongly. Finally, the position and dynamics of the ATRP equilibrium should be appropriate for the chosen system.

There are a number of transition metal complexes that have been reported for ATRP. In this thesis, copper complex is used as the catalyst in the following chapters. Since the copper catalysts are superior in ATRP in terms of versatility and cost. Styrenes, (meth)acrylate esters and amides, and acrylonitrile have been successfully polymerised using copper-mediated ATRP.^{25, 46} The first copper-based ATRP system was reported in 1995.

1.2.8 Ligands

In ATRP, the main role of the ligand is to make the transition metal salt soluble in the organic solvent. Also, the ligand should be able to adjust the redox potential and halogen attracting ability of the metal centre to form a complex for the atom transfer step. The choice of ligand significantly influences the effective of the metal catalyst. Ligands used in the copper and iron based ATRP are usually nitrogen-based.^{88, 89} Some of common nitrogen-based ligands are shown in Figure 1.19. The activation rates (k_{act}) of these ligands indicate their activity in ATRP reaction. Moreover, ligands based on phosphorus, sulfur and oxygen have been reported, but they are less effective due to poor binding constants and electronic effects.

The activities of copper complexes strongly depend on the ligand structures. Firstly, ligands have a higher number of coordination sites which increase catalytic activity. Therefore, the activities of ligand follow the order as tetradentate > tridentate > bidentate with the similar structure. For example, the k_{act} of tNtpy (4,4'-trinyonyl-2,2'-6',2''-terpyridine, $k_{act}=8.2$) is much higher than dNbpy (4,4'-dinonyl-2,2'-bipyridine, $k_{act}=0.6$). However, the PMDETA (1,1,4,7,7-pentamethyldiethylenetriamine, $k_{act}=2.7$) is an exception which is more active than HMTETA (1,1,4,7,10,10-Hexamethyltriethylenetetramine, $k_{act}=0.14$).

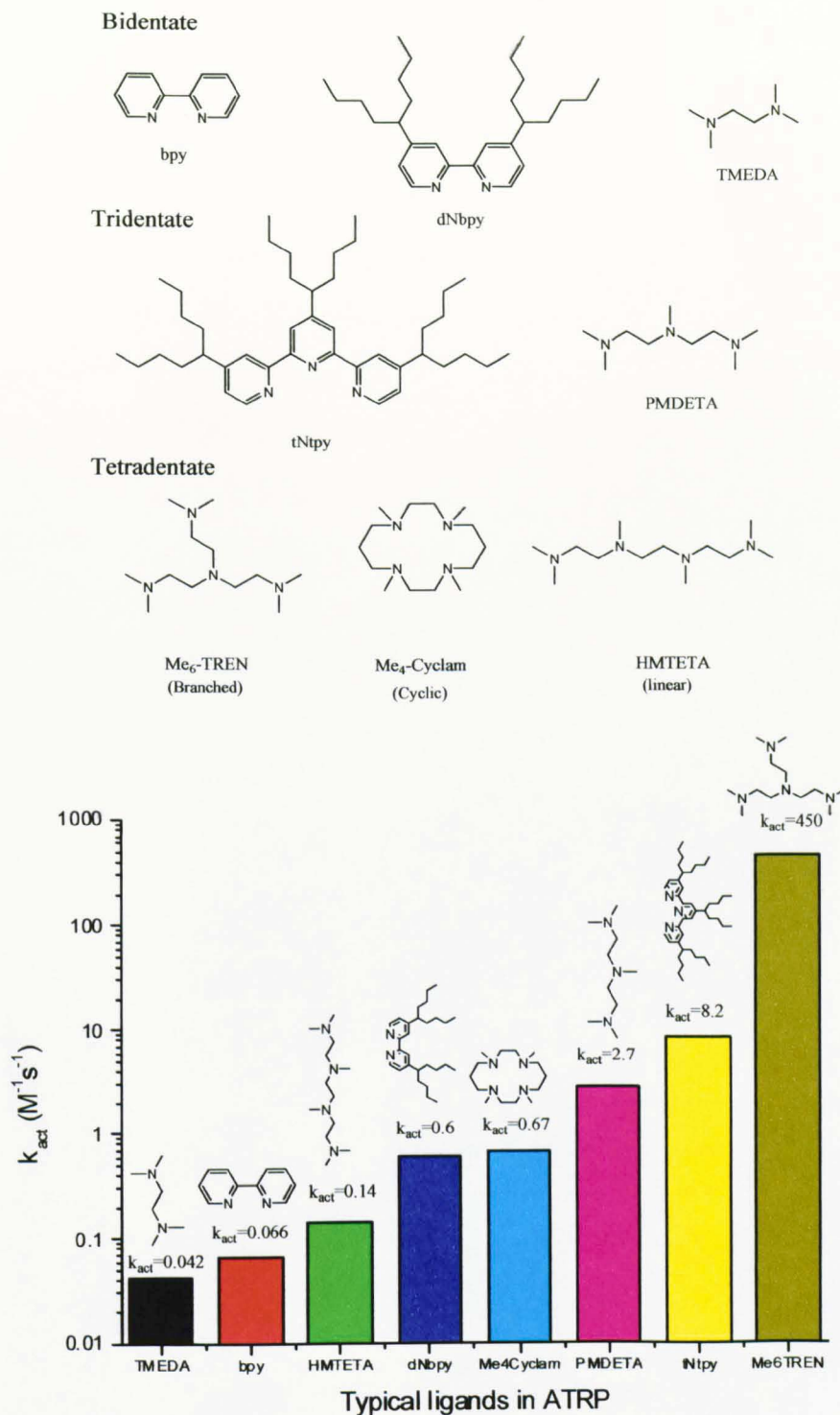


Figure 1.19 ATRP activation rate constants for various ligands using $[EtBr]_0=1$ mM and $[Cu^I Br/L]_0=20$ mM in acetonitrile at 35 °C. The rate constants values were taken from references.⁹⁰

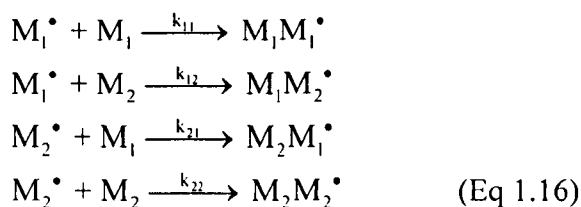
Secondly, the long alkyl groups on the pyridine ring improve the solubility of the Bpy ligands in non-polar solvent and also increases the activation rate. Thus, the k_{act}

of dNbpy ($k_{\text{act}}=0.6$) is higher than Bpy (2,2-bipyridine, $k_{\text{act}}=0.066$). Thirdly, the activity of tetradenate ligand with different molecular shape decreases in the following order, branched structure>cyclic structure>linear. Thus, the activity of Me₆-TREN (tris[(2-dimethylamino)ethyl]amine, $k_{\text{act}}=450$) is much higher than Me₄-cyclam (1,4,8,11-tetramethyl-1,4,8,11-tetraazacyclotetradecane, $k_{\text{act}}=0.67$) and HMTEMA ($k_{\text{act}}=0.14$). The different structure of the molecules may lead to significantly changes in their activities. Last, it seems that pyridine based ligands generate more active catalyst than aliphatic amines (eg. Bpy>TMEDA (*N,N,N,N*-tetramethylethylenediamine), tNtpy>PMDETA). In this thesis, the Bpy and HMTEMA were chosen as ligand in ATRP reaction since the Bpy is one of the most commonly used ligands in the copper catalyst ATRP. Also, HMTETA can provide higher activation rate in the relative slow ATRP reactions (e.g. the copolymerisation of divinylbenzene and siloxane monomer in Chapter 3).

1.2.9 Materials Made by ATRP

A. Polymer with different composition

Conventional radical polymerisation has been used for many years to synthesise different statistical copolymers. This is due to the different reactivity ratios for the various monomers. In a copolymerisation of two monomers (M_1 and M_2), there are four different reactions that can take place at the propagating radical with their reaction rate constants (Eq.1.16).



Consequently, the reactivity ratio of M_1 (r_1) and M_2 (r_2) can be defined as Eq. 1.17:

$$r_1 = \frac{k_{11}}{k_{12}} \quad r_2 = \frac{k_{22}}{k_{21}} \quad (\text{Eq 1.17})$$

However, conventional radical polymerisation is inefficient in the formation of block copolymers because of the very short lifetime of the growing chain and the slow initiation process. ATRP and other CLRP methods have many advantages over conventional radical polymerisation. First, each chain in ATRP keeps growing from the very early to the final stage of polymerisation. All the chains are initiated early in ATRP and remain active over the reaction. Thus, after the different comonomers feed into the polymerisation, the comonomers with different reactivity will continue to be incorporated into the polymer chain. The different relative concentrations of monomers will change the composition and this is reflected along all chains. This leads to the formation of a new class of polymers, gradient copolymers³⁷ (Figure 1.20). In the extreme case of very different reactivity ratios, this may lead to block copolymers. At the end of the reaction, the cumulative compositions of the conventional and controlled reactions should be the same. However, a variety of compositions will be observed between the chains in the conventional case, while in ATRP all chains will have a similar monomer sequence and composition. Such gradient copolymers are expected to have properties unlike other copolymers (block or random), making them good candidates for applications such as blend compatibilisers and pressure sensitive adhesives.

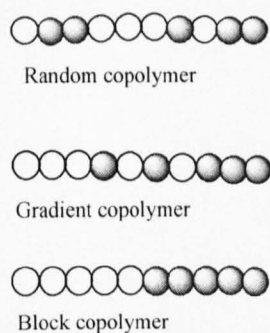


Figure 1.20 Schematic representation of random, gradient and block copolymers.

Block copolymers can be generated from a macroinitiator synthesised either by ATRP or by other CLRP. In all living radical polymerisation techniques, ATRP was the first one to provide a variety of block copolymers from monomers polymerised by a free-radical mechanism. The polymers prepared by ATRP have an activated

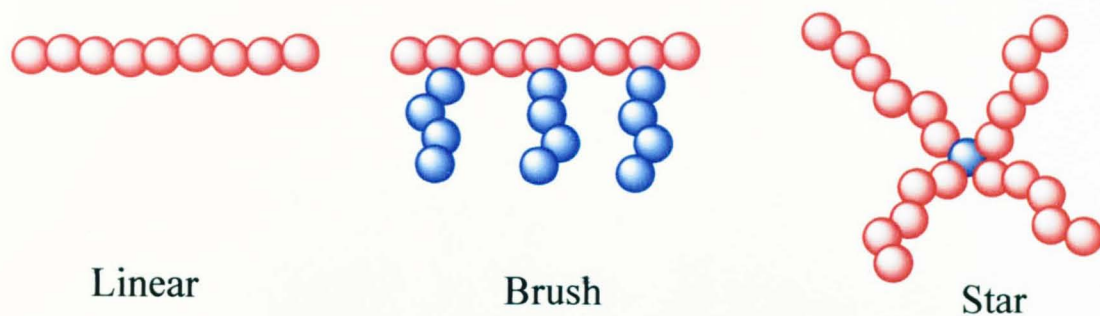
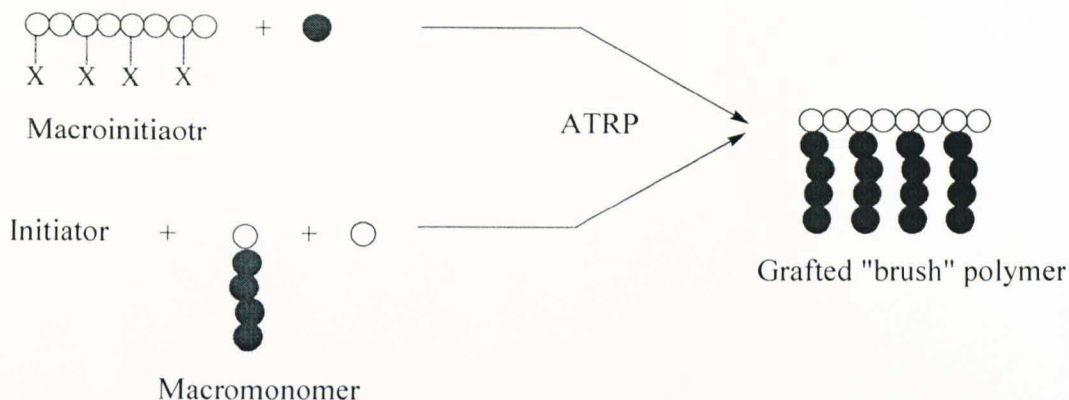


Figure 1.22 Scheme of different architectures from the polymer synthesised by ATRP method.

The field of densely grafted copolymers (also called brush polymers) has received growing attention in recent years because these materials contain a grafted chain at each repeat unit on the polymer backbone. As a result, the macromolecules have a more elongated conformation. In the case of ATRP, the synthesis of graft/brush copolymers can be normally accomplished through two routes: Firstly, ‘grafting from’ reactions⁹⁴⁻⁹⁹ which utilise polymerisation of grafts from a macroinitiator with pendant functionalities (Figure 1.23 A). Secondly, ‘grafting through’ processes^{100, 101} which operate by homo- or copolymerisation of a macromonomer (Figure 1.23 B). In the ‘graft from’ route, the grafted polymer can be obtained without the excessive purification of unreacted chains which is normally required in the ‘graft through’ method. However, the ‘graft through’ route can provide better control over the side chain (*e.g.* MW and PDI). These two methods have been used in conjunction with ATRP in the design of graft copolymers. Also, these two routes can provide a variety of copolymers if different backbones or side chain monomers are chosen. Furthermore, graft polymers can be attached to a surface by being grown solely from a functional initiator molecule on the surface (Figure 1.18).^{81-85, 87}

(A) "Graft from" process



(B) "Graft through" process

Figure 1.23 Mechanism of graft polymer which prepared by ATRP. (A): 'Graft from' process which utilises polymerisation of grafts from a macroinitiator with pendant functionality. (B): 'Graft through' route which operates by homo- or copolymerisation of a macromonomer.

Another interesting shape of polymer is the star-like polymer. The use of multi-functional initiators to synthesise star polymers was recognised shortly after the development of ATRP. Typically, there are two routes to prepare star polymers. First, in a so-called 'core-first' method, multifunctional initiators with three, four, six, and eight halide groups were used to prepare star polymers with methacrylates or styrene (Figure 1.24 A).¹⁰²⁻¹⁰⁶ Second, the other way so-called 'arm-first' approach has also been demonstrated. In this case, linear polymers were first prepared by ATRP (Figure 1.24 B).¹⁰⁷⁻¹⁰⁹ Then, the resulting polymers were subsequently allowed to react with a cross-linking reagent such as divinyl benzene to form cross-linked cores.

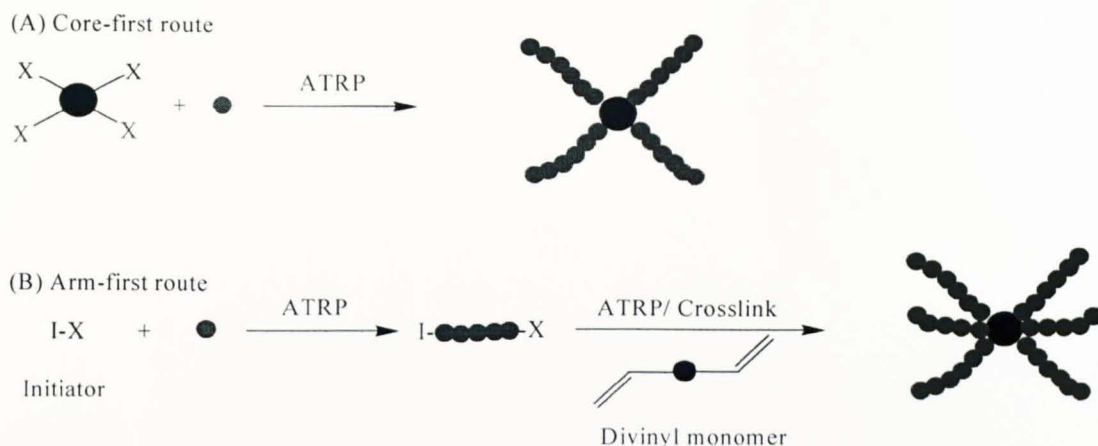


Figure 1.24 Functional star-like polymers by the ‘core first’ approach and ‘arm-first’ approach.

C. Polymer with different functionalities

Functionalities are important aspects of polymers because they provide many different properties to the polymer chain.¹¹⁰ In ATRP, the functionalities on the polymer chain are included functional monomers,¹¹¹⁻¹¹³ initiator fragments^{114, 115} and end groups.¹¹⁶⁻¹²¹ Firstly, a functionalised monomer may directly provide the different properties to the material through pendant functional groups (hydrophilicity, polarity or metal complexation). Secondly, the R-X (X=halogen) bond in the initiator will break during the initiation process and the generated radicals can react with alkenes. The R-end of initiator is incorporated into the polymer chain and provides a number of functional groups tolerant to ATRP catalysts and radicals. Attachment of initiator fragments to organic or inorganic surfaces can be used as a means to modify the surface. Furthermore, the activated alkyl halides can be incorporated to the chain ends by other routes and possible to prepare further block copolymers. Last but not least, the terminal halogen can also be displaced by nucleophilic substitution, free-radical chemistry or electrophilic addition catalysed by Lewis acids.

1.2.10 Deactivation Enhanced ATRP

Deactivation Enhanced ATRP (DE-ATRP) was conducted in the presence of initial added deactivator species.^{122, 123} In the system of copper-mediated ATRP, Cu^{II} was added to change the equilibrium of reaction, since the added Cu^{II} pushes the equilibrium to deactivation direction and hence the deactivation rate ($R_{\text{deact}} = k_{\text{deact}}[\text{Cu}^{\text{II}}][\text{P}^\bullet]$) will be increased significantly. The kinetics of various ATRP system, including normal ATRP and ATRP with initially added Cu^{II} (DE-ATRP) were modelled by Matyjaszewski^{122, 124} and Fischer¹⁹. The kinetics calculations help to better understand the evolution of all species in the reactions. In this part, kinetic analysis was applied to the conventional free radical polymerisation (FRP), normal ATRP and DE-ATRP to reveal the difference between these three reactions. The concentration of radicals ($[\text{P}^\bullet]$), instantaneous kinetic chain length (ν), average life-time of the radicals (τ) and the time span of activation (τ_{act}) and deactivation (τ_{deact}) periods are investigated under the same conditions (*e.g.* $[\text{M}]_0$, $[\text{I}]_0$, $[\text{Cu}^{\text{I}}]$, solvent and temperature are the same) in FRP, ATRP and DE-ATRP reactions. The chain transfer and other side reactions were excluded from the kinetics studies in this part.

Kinetic study of FRP

In the FRP, the polymerisation of styrene was analysed by the parameters listed in Table 1.1. The concentration of radicals ($[\text{P}^\bullet]$) in the reaction can be calculated as Eq. 1.18, since the quasi-steady-state of radicals was reached when the initiator decomposition rate (R_{dc}) was equal to the termination rate (R_{t}).

$$R_{\text{dc}} = R_{\text{t}}$$

$$2fk_{\text{d}}[\text{I}] = 2k_{\text{t}}[\text{P}^\bullet]^2$$

$$[\text{P}^\bullet] = \left(\frac{fk_{\text{d}}[\text{I}]}{k_{\text{t}}} \right)^{\frac{1}{2}} = \left(\frac{0.8 \times 3.9 \times 10^{-4} \text{ s}^{-1} \times 0.025 \text{ M}}{5 \times 10^7 \text{ M}^{-1} \text{ s}^{-1}} \right)^{\frac{1}{2}} = 3.95 \times 10^{-7} \text{ M} \quad (\text{Eq. 1.18})$$

Table 1.1 Parameters and reaction conditions of free radical polymerisation of styrene by using AIBN as initiator. T=90 °C, [M]=5.0 M; [I]=0.025 M. The rate constants values were taken from references.¹²⁵⁻¹²⁸

Reaction step	Rate constant	Value
Initiation	decomposition rate (k_{dc})	$3.9 \times 10^{-4} \text{ s}^{-1}$
	decomposition efficiency (f)	0.8
Propagation	propagation rate (k_p)	$900 \text{ M}^{-1} \text{ s}^{-1}$
Termination	combination rate (k_{tc})	$1 \times 10^8 \text{ M}^{-1} \text{ s}^{-1}$
	disproportion (k_{td})	$1 \times 10^7 \text{ M}^{-1} \text{ s}^{-1}$
	overall termination (k_t)	$5 \times 10^7 \text{ M}^{-1} \text{ s}^{-1}$

The kinetic chain length (ν) is given by Eq. 1.19.

$$\nu = \frac{R_p}{R_i} = \frac{k_p[M][P^*]}{2k_t[P^*]^2} = \frac{900 \text{ M}^{-1} \text{ s}^{-1} \times 5 \text{ M}}{2 \times 5 \times 10^7 \text{ M}^{-1} \text{ s}^{-1} \times 3.95 \times 10^{-7} \text{ M}} = 114 \quad (\text{Eq. 1.19})$$

Moreover, the average life time of radicals (τ_{FRP}) in free radical polymerisation is determined by Eq. 1.20.

$$\tau_{FRP} = \frac{[P^*]}{R_i} = \frac{[P^*]}{2k_t[P^*]^2} = \frac{1}{2 \times 5 \times 10^7 \text{ M}^{-1} \text{ s}^{-1} \times 3.95 \times 10^{-7} \text{ M}} = 0.025 \text{ s} \quad (\text{Eq. 1.20})$$

Kinetics study of normal ATRP

In normal ATRP, the initiators are activated by Cu^{I} to produce a radical and Cu^{II} species when the reaction starts. Therefore, the concentrations of both Cu^{II} and $[\text{P}^*]$ increase linearly with the same rate. When R_{act} ($R_{\text{act}} = [\text{Cu}^{\text{I}}][\text{I}]k_{\text{act}}$) reaches the value of R_{deact} ($R_{\text{deact}} = [\text{Cu}^{\text{II}}][\text{P}^*]k_{\text{deact}}$), the reaction enters the quasi-equilibrium stage. During this quasi-steady-state stage, the deactivation is the major process for radical consumption ($R_{\text{deact}} \gg R_i$). In this calculation, the quasi-equilibrium is the only stage considered for comparison purpose. The polymerisation of styrene was analysed by

the parameters listed in Table 1.2.

Table 1.2 Parameters and reaction conditions of normal ATRP of styrene by using PEBr (1-phenylethyl bromide) as initiator. $[M]_0/[I]_0/[Cu^I]_0/[Cu^{II}]_0/[L]_0 = 200/1/1/1$, $I = \text{PEBr}$, $L = \text{PMDETA}$ (N,N,N',N',N''-pentamethyldiethyl enetriamine, $[M]_0 = 5 \text{ M}$; $[I]_0 = 0.025 \text{ M}$, $T = 90^\circ \text{C}$. The rate constants values were taken from references.^{79, 90, 129, 130}

Reaction step	Rate constant	Value ($\text{M}^{-1} \text{s}^{-1}$)
Initiation	activation rate (k_{act})	0.79
	deactivation rate (k_{deact})	8.4×10^6
Propagation	propagation rate (k_p)	900
	activation rate (k_{act})	0.79
	deactivation (k_{deact})	8.4×10^6
Termination	termination rate for small molecules (k_{t0})	2.5×10^9
	termination rate for polymer units (k_t)	5×10^7

The reaction time of the equilibrium can be calculated by the Eq. 1.21^{19, 124}. The result indicates the quasi-equilibrium was reached at 0.74 s after the reaction started.

$$t_{\text{equilibrium}} = \frac{\sqrt{6k_{t0}} K_{\text{ATRP}}}{k_{\text{act}}^{3/2} [I]_0} = \frac{\sqrt{6 \times 2.5 \times 10^9} \times \frac{0.79}{8.4 \times 10^6}}{0.79^{3/2} \times 0.025} = 0.74 \text{ s} \quad (\text{Eq. 1.21})$$

During the quasi-equilibrium stage, the R_{act} is equal to R_{deact} . Thus, the $[\text{Cu}^{II}]$ and $[\text{P}\cdot]$ were calculated assuming the equilibrium was established. The values are calculated by the Eq. 1.22 and Eq. 1.23.¹²⁴

$$\begin{aligned}
 [\text{Cu}^{\text{II}}]_{\text{equilibrium}} &= k_{\text{act}} [\text{Cu}^{\text{I}}]_0 [\text{I}]_0 t \\
 &= 0.79 \text{ M}^{-1}\text{s}^{-1} \times 0.025 \text{ M} \times 0.025 \text{ M} \times 0.74 \text{ s} = 3.65 \times 10^{-4} \text{ M} \quad (\text{Eq. 1.22})
 \end{aligned}$$

$$R_{\text{act}} = R_{\text{deact}}$$

$$k_{\text{act}} [\text{I}][\text{Cu}^{\text{I}}] = k_{\text{deact}} [\text{P}^*][\text{Cu}^{\text{II}}]$$

$$[\text{P}^*]_{\text{ATRP}} = \frac{k_{\text{act}}}{k_{\text{deact}}} [\text{I}]_0 \frac{[\text{Cu}^{\text{I}}]}{[\text{Cu}^{\text{II}}]} = \frac{0.79}{8.4 \times 10^6} \times 0.025 \times \frac{0.025 - 3.65 \times 10^{-4}}{3.65 \times 10^{-4}} \text{ M} = 1.5 \times 10^{-7} \text{ M} \quad (\text{Eq. 1.23})$$

For ATRP, the instantaneous kinetic chain length is defined as the average number of monomer units added to the propagating radical during each activation-deactivation cycle. From the calculation (Eq. 1.24), it shows there are average 1.47 monomer units added onto the propagating centre during each activation-deactivation cycle.

$$v_{\text{ATRP}} = \frac{R_p}{R_{\text{deact}}} = \frac{k_p [\text{M}][\text{P}^*]}{k_{\text{deact}} [\text{P}^*][\text{Cu}^{\text{II}}]} = \frac{900 \text{ M}^{-1}\text{s}^{-1} \times 5 \text{ M}}{8.4 \times 10^6 \text{ M}^{-1}\text{s}^{-1} \times 3.65 \times 10^{-4} \text{ M}} = 1.47 \quad (\text{Eq. 1.24})$$

The radical life-time (τ_{ATRP}) was calculated Eq. 1.25. The life-time of radical is extended to 0.06 s due to the relative lower radical concentration.

$$\tau_{\text{ATRP}} = \frac{[\text{P}^*]}{R_i} = \frac{[\text{P}^*]}{2k_i [\text{P}^*]^2} = \frac{1}{2 \times 5 \times 10^7 \text{ M}^{-1}\text{s}^{-1} \times 1.6 \times 10^{-7} \text{ M}} = 0.06 \text{ s} \quad (\text{Eq. 1.25})$$

Moreover, the time span of deactivation ($\tau_{\text{deact(ATRP)}}$) and activation ($\tau_{\text{act(ATRP)}}$) periods were calculated to be $3.3 \times 10^{-4} \text{ s}$ (Eq. 1.26) and 51.5 s (Eq. 1.27), respectively. This indicates that the dormant species is activated every 50.6 s and then deactivated after $3.3 \times 10^{-4} \text{ s}$.

$$\tau_{\text{deact(ATRP)}} = \frac{[\text{P}^*]}{R_{\text{deact}}} = \frac{[\text{P}^*]}{k_{\text{deact}} [\text{P}^*][\text{Cu}^{\text{II}}]} = \frac{1}{8.4 \times 10^6 \text{ M}^{-1}\text{s}^{-1} \times 3.65 \times 10^{-4} \text{ M}} = 3.3 \times 10^{-4} \text{ s} \quad (\text{Eq. 1.26})$$

$$\tau_{\text{act(ATRP)}} = \frac{[\text{P}^*]}{R_{\text{act}}} = \frac{[\text{P}^*]}{k_{\text{act}} [\text{P}^*][\text{Cu}^{\text{I}}]} = \frac{1}{0.79 \text{ M}^{-1}\text{s}^{-1} \times 0.0246 \text{ M}} = 51.5 \text{ s} \quad (\text{Eq. 1.27})$$

Last, the actual life-time of the radicals in normal ATRP is 2.3×10^5 seconds (2.3 days) which include the activation-deactivation cycles from the calculation (Eq. 1.28).

$$\tau'_{\text{ATRP}} = \frac{\tau_{\text{ATRP}}}{\tau_{\text{deact}}} \tau_{\text{act}} = \frac{1.3 \text{ s}}{3.3 \times 10^{-4} \text{ s}} \times 51.5 \text{ s} = 2.3 \times 10^5 \text{ s} \approx 2.3 \text{ days} \quad (\text{Eq. 1.28})$$

Kinetics study of DE-ATRP

In the presence of initially added Cu^{II} , the kinetics of DE-ATRP is quite different from normal ATRP. The polymerisation reached the quasi-steady-state at the very beginning of reaction. The PRE effect (see page 23-24) is ignored in this process. The concentrations of almost all species were constant during the polymerisation.^{123, 124} In this analysis, 30% Cu^{II} (*versus* Cu^{I}) was initially added to the system. The polymerisation of styrene was calculated by the parameters listed in Table 1.3.

Table 1.3 Parameters and reaction conditions of DE-ATRP of styrene by using PEBr as initiator. $[\text{M}]_0/[\text{I}]_0/[\text{Cu}^{\text{I}}]_0/[\text{Cu}^{\text{II}}]_0/[\text{L}]_0=200/1/1/0.3/1.3$, $\text{I}=\text{PEBr}$, $\text{L}=\text{PMDETA}$, $[\text{M}]_0=5 \text{ M}$; $[\text{I}]_0=0.025 \text{ M}$, $T=90^\circ\text{C}$. The rate constants values were taken from references.^{79, 90, 122, 129, 130}

Reaction step	Rate constant	Value ($\text{M}^{-1}\text{s}^{-1}$)
Initiation	activation rate (k_{act})	0.79
	deactivation rate (k_{deact})	8.4×10^6
Propagation	propagation rate (k_{p})	900
	activation rate (k_{act})	0.79
	deactivation (k_{deact})	8.4×10^6
Termination	termination rate	5×10^7
	for polymer units (k_{t})	

The concentration of radicals can be calculated as Eq. 1.29. The result ($7.84 \times 10^{-9} \text{ M}$) is much lower than previous calculation in FRP and ATRP.

$$[P^*]_{\text{ED-ATRP}} = \frac{k_{\text{act}}}{k_{\text{deact}}} [I]_0 \frac{[Cu^I]}{[Cu^{II}]} = \frac{0.79}{8.4 \times 10^6} \times 0.025 \times \frac{0.025}{0.0075} \text{ M} = 7.84 \times 10^{-9} \text{ M} \quad (\text{Eq. 1.29})$$

For DE-ATRP, the instantaneous kinetic chain length is defined the same as the ATRP. This assures that all the radicals are activated and propagate at the same rate. Therefore, the average number of monomer units added at one activation step calculated from Eq. 1.30 was 0.07. This value was much smaller than in a typical FRP ($v_{\text{FRP}}=114$) and normal ATRP ($v_{\text{ATRP}}=1.47$). This means only one monomer unit is added to the radical chain end after 14 cycles of activation and deactivation in DE-ATRP.

$$v_{\text{ED-ATRP}} = \frac{R_p}{R_{\text{deact}}} = \frac{k_p [M][P^*]}{k_{\text{deact}} [P^*][Cu^{II}]} = \frac{900 \text{ M}^{-1}\text{s}^{-1} \times 5 \text{ M}}{8.4 \times 10^6 \text{ M}^{-1}\text{s}^{-1} \times 0.0075 \text{ M}} = 0.07 \quad (\text{Eq. 1.30})$$

The radical life-time ($\tau_{\text{DE-ATRP}}$) can be calculated to be 1.3 s from Eq. 1.31 which is 52 times longer than the conventional free radical polymerisation (0.025 s), due to the quite lower radical concentration.

$$\tau_{\text{ED-ATRP}} = \frac{[P^*]}{R_t} = \frac{[P^*]}{2k_t [P^*]^2} = \frac{1}{2 \times 5 \times 10^7 \text{ M}^{-1}\text{s}^{-1} \times 7.84 \times 10^{-9} \text{ M}} = 1.3 \text{ s} \quad (\text{Eq. 1.31})$$

In addition, the time span of deactivation ($\tau_{\text{deact(DE-ATRP)}}$) and activation ($\tau_{\text{act(DE-ATRP)}}$) periods were calculated to be 1.6×10^{-5} s (Eq. 1.32) and 50.6 s (Eq. 1.33), respectively. This indicates that the dormant species is activated every 50.6 seconds and then fast deactivated after only 1.6×10^{-5} seconds.

$$\tau_{\text{deact(ED-ATRP)}} = \frac{[P^*]}{R_{\text{deact}}} = \frac{[P^*]}{k_{\text{deact}} [P^*][Cu^{II}]} = \frac{1}{8.4 \times 10^6 \text{ M}^{-1}\text{s}^{-1} \times 0.0075 \text{ M}} = 1.6 \times 10^{-5} \text{ s} \quad (\text{Eq. 1.32})$$

$$\tau_{act(ED-ATRP)} = \frac{[P^*]}{R_{act}} = \frac{[P^*]}{k_{act}[P^*][Cu^I]} = \frac{1}{0.79 M^{-1} s^{-1} \times 0.025 M} = 50.6 \text{ s} \quad (\text{Eq. 1.33})$$

As a result, the actual life-time of the radicals was extended to 4.1×10^6 seconds (47.6 days) in DE-ATRP reaction which includes numerous activation-deactivation cycles (Eq. 1.34).

$$\tau'_{ED-ATRP} = \frac{\tau_{ED-ATRP}}{\tau_{deact}} \tau_{act} = \frac{1.3 \text{ s}}{1.6 \times 10^{-5} \text{ s}} \times 50.6 \text{ s} = 4.1 \times 10^6 \text{ s} \approx 47.6 \text{ days} \quad (\text{Eq. 1.34})$$

All of the above results are summarised in Table 1.4. Firstly, the concentration of radicals ($[P^*]$) in DE-ATRP is much lower than FRP and normal ATRP. Thus, the chance of bimolecular termination is suppressed significantly. The life time of radical (τ) in DE-ATRP is extended longer than FRP and ATRP. Secondly, the instantaneous kinetic chain length (ν) of DE-ATRP is much lower than FRP and ATRP, since the time span of deactivation (τ_{deact}) is quite shorter in DE-ATRP. Therefore, the propagating radical is only allowed add very few monomer units (ν_{ATRP}) during each activation-deactivation cycle. Last, the actual life-time of the radicals (τ') was increased to 4.1×10^6 seconds (47.6 days) in DE-ATRP. This result shows the great potential importance for the better control of ATRP reactions by DE-ATRP.

Table 1.4 The Summary results of kinetics calculation in the polymerisation of styrene by free radical polymerisation, ATRP and DE-ATRP reaction (Eq. 1.13-Eq. 1.29). FRP reaction conditions: T=90 °C, $[M]_0/[I]_0=200/1$ $[M]=5.0$ M; $[I]=0.025$ M, I=AIBN. ATRP reaction conditions: T=90 °C, $[M]_0/[I]_0/[Cu^I]_0/[Cu^{II}]_0/[L]_0=200/1/1/1$, $[M]_0=5$ M; $[I]_0=0.025$ M, I=PEBr, L=PMDETA. DE-ATRP reaction conditions: T=90 °C, $[M]_0/[I]_0/[Cu^I]_0/[Cu^{II}]_0/[L]_0=200/1/1/0.3/1.3$, I=PEBr, L=PMDETA; $[M]_0=5$ M, $[I]_0=0.025$ M.

	Concentration of radicals	Kinetic chain length (FRP)	Kinetic chain length (ATRP) ^a	Life-time of radicals	Time span of deactivation	Time span of activation	Actual life-time of the radicals in ATRP
	$[P\bullet]$	ν_{FRP}	ν_{ATRP} or $\nu_{DE-ATRP}$	τ	τ_{deact}	τ_{act}	τ'
	(M)			(s)	(s)	(s)	(s)
FRP	3.95×10^{-7}	114		0.025			
ATRP	1.6×10^{-7}		1.47	0.06	3.3×10^{-4}	51.5	2×10^5
DE-ATRP	7.84×10^{-9}		0.07	1.3	1.6×10^{-5}	50.6	4.1×10^6

a. For ATRP, the instantaneous kinetic chain length is defined as the average number of monomer units added to the propagating free radical during each activation-deactivation cycle.

1.3 Reversible Addition Fragmentation Chain Transfer Polymerisation (RAFT)

The process of chain transfer in free radical polymerisation is used to moderate the molecular weight of polymers and introduce functionality at the ends of polymer chains. However, the chain transfer can only occur once by normal chain transfer agent. Thus, slow initiation and changes of concentration of chain transfer agent during the polymerisation can influence the control of molecular weight. In the late 1980s, scientists developed a new technique called reversible addition fragmentation chain transfer polymerisation (RAFT) to cover these drawbacks of traditional chain transfer polymerisation. RAFT polymerisation is performed by adding a quantity of appropriate RAFT agent to a radical polymerisation and yields polymer with controlled weight and polydispersity.^{32, 131} The mechanism was envisaged to operate by reversible addition-fragmentation chain transfer and represented a new process for achieving living polymerisation.^{33, 34} The mediating compounds employed in all RAFT polymerisations are called RAFT agents, which are in the form of thio-containing compounds such as: thiocarbonates, thiocarbamates or dithioesters (Figure 1.25) all of which have been successfully applied for controlled CLRP.

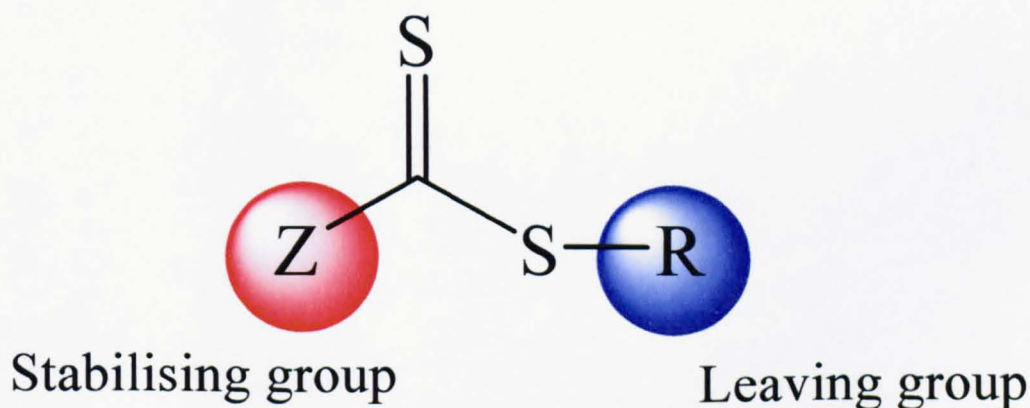


Figure 1.25 General structure for a dithioester based RAFT agent with the leaving group (R), allowing re-initiation, and the stabilising group (Z).³⁴

There are four classes of RAFT agent, depending on the Z group: (1) dithioesters¹³²

(Z= aryl or alkyl), (2) trithiocarbonates¹³³ (Z= substituted sulfur), (3) dithiocarbonates¹³⁴⁻¹³⁶ (xanthates) (Z= substituted oxygen) and dithiocarbamates (Z= substituted nitrogen). The mechanism for the RAFT process is shown in following scheme (Figure 1.26).¹³⁷

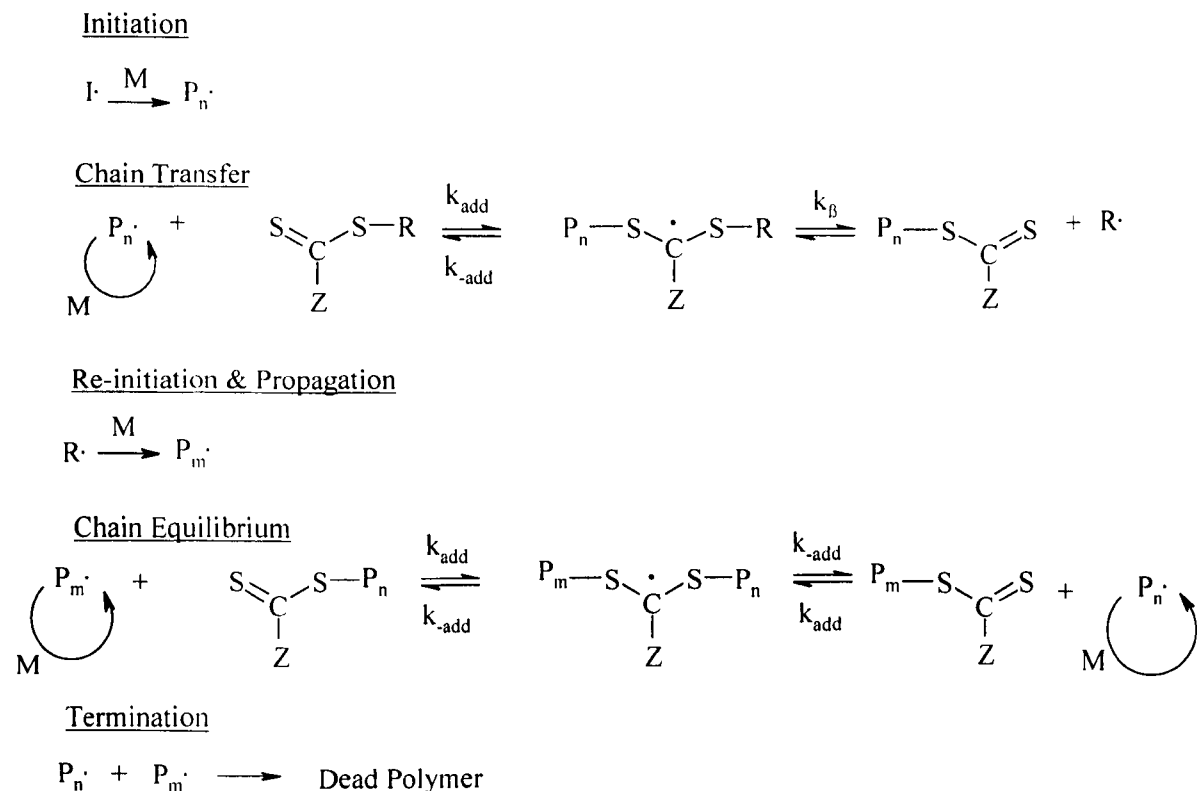


Figure 1.26 The mechanism of reversible addition fragmentation chain transfer (RAFT) polymerisation. The scheme is redrawn from the original picture in the reference paper.¹³⁷

The formation of the primary polymer chains with monomer (M) through initiation to produce the primary polymer radicals (Initiation). After the initiator generated radicals, the radicals should initiate RAFT agent within a short time. Upon first contact with the RAFT agent, chain transfer occurs leading to addition of the polymer radical and fragmentation of the R group (leaving group). This leads to further monomer initiation by the released radical R. The most important part of the RAFT mechanism is the chain equilibrium step where the process cycles through producing propagating radicals and the dormant species (chain equilibrium). The

instance of termination is kept low by the presence of excess RAFT agent. Typically, a radical inducing species is required, for example, an azo or peroxide based initiator. In all cases, the addition rate constants to the mediating species should be significantly higher than the propagation rate constant. This is the key factor for controlling the polymerisation.

After the monomers were consumed, the final polymers are capped with the fragment of RAFT agent (Figure 1.27). The other chain end is the R group from the RAFT agent or a fragment from the initiator. To produce only one form of polymer product, an initiator is required with a fragmented form which is identical to the R group or exceptionally low initiator concentrations must be used. Once a polymer has been formed through the RAFT process, additional monomer can be introduced and block copolymerisation occurs. This demonstrates the living nature of the RAFT method. One drawback of the formation of block copolymers through the RAFT process is the production of unwanted homopolymer in low concentrations.

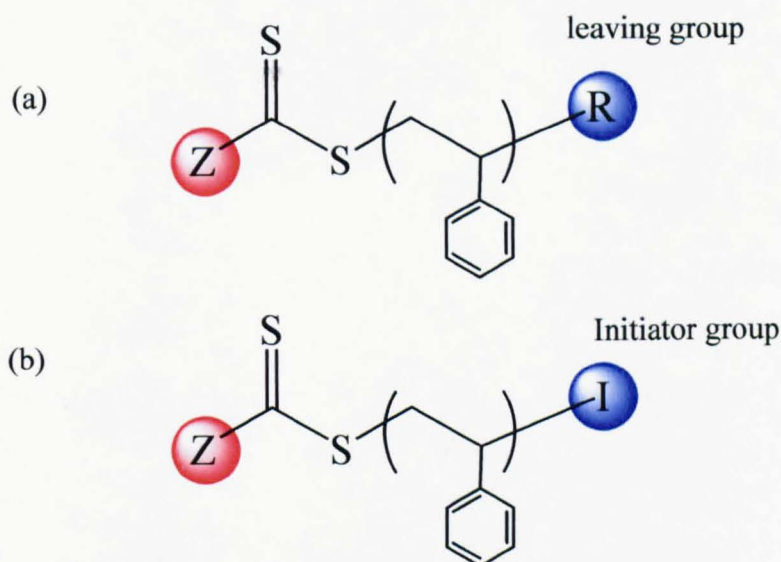


Figure 1.27 Schematic of the final polymer (polystyrene) structures formed through the RAFT process. The polymer in both examples is capped with the dithioester moiety. The other chain end is formed from initiation and hence is either a) the leaving group from the RAFT agent or b) the primary initiator fragment.

One characteristic of polymers produced by RAFT processes is that they are usually coloured (normally pink or yellow) due to the RAFT agent end-group, which is also a major disadvantage for industrial requirement. Researchers have developed some methods to remove the colour of polymer including the application of primary and secondary amines (aminolysis) to produce thiol terminated polymers, heat or the reaction with tri-*n*-butylstannane, removing the mediating group and transforming it into terminal hydrogen.^{138, 139} Recently, Perrier *et al.* proposed a novel method of chain functionalisation (concomitant with dithioester removal), by using an excess of initiator to promote termination by capping the growing polymer chain with an initiator fragment.¹⁴⁰ As many initiators can be synthesised and are commercially available, the polymer chains can be capped with a wealth of different functionalities to produce polymers with special properties.

1.4 Hyperbranched Polymers

1.4.1 Dendritic Polymers

Recently, the dendritic topology has been recognised as a fourth major class of macromolecular architecture.¹⁴¹⁻¹⁴³ The signature for such a distinction is the unique property manifested by this class of polymer. The unique three-dimensional structure of these materials makes them attractive for many new applications ranging from drug delivery to nano-building blocks.¹⁴⁴⁻¹⁵³ The origins of three-dimensional of dendritic branching concepts (infinite network theory) were introduced by Flory in 1950s.¹⁵⁴ Numerous synthetic strategies have been reported for the preparation of these materials, which have led to a broad range of dendritic structures. Presently, this architectural class consists of three dendritic subclasses, namely: (a) hyperbranched polymers,^{144, 149, 155, 156} (b) dendrigraft polymers¹⁵⁷⁻¹⁵⁹ and (c) dendrons¹⁶⁰⁻¹⁶³/dendrimers.^{147, 153, 164, 165} (Figure 1.28)

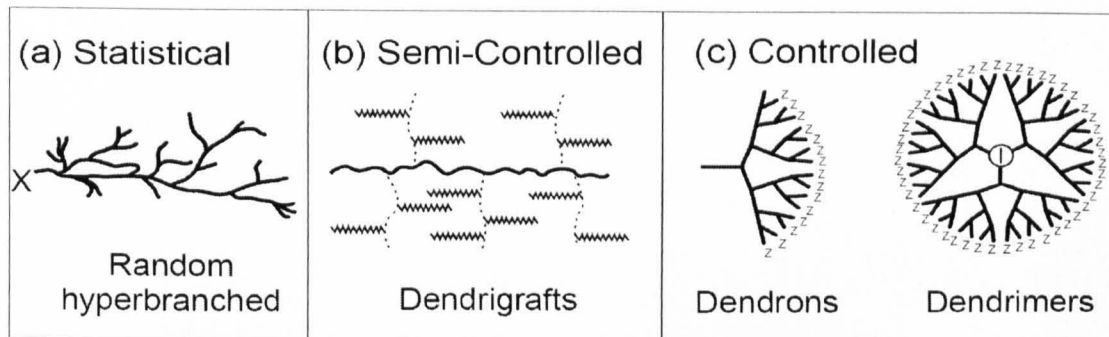


Figure 1.28 Dendritic subclasses derived from branches (a) random hyperbranched, (b)dendrigrafts and (c) dendrons/dendrimers.

All dendritic polymers are open covalent assemblies of branch cells. The respective subclasses and the level of structure control are defined by the propagation methodology used to produce these structures, as well as by the branch cell construction parameters. The dendrimers and dendrons are organised into a very symmetrical and monodispersed array. As shown in above (Figure 1.29), the dendrimers or dendrons arrays of branch cells usually connect to some molecular reference core. Thus, they ideally organise into a highly controlled core-shell type structure ($M_w/M_n = 1.01-1.1$).

On the other hand, random hyperbranched polymers are defined as irregular polydispersed assemblies. In the case of random hyperbranched polymers, these branch cell arrays may be very non-ideal and possess highly polydispersity (e.g. $M_w/M_n = 2-10$). Dendrigraft polymers reside between these two extremes of structure control, frequently manifesting rather narrow polydispersity of $M_w/M_n = 1.1-1.5$ depending on the synthesis route used to generate them.

1.4.2 Dendrimers

As described above, dendrimers are the dendritic polymers with very symmetric and nearly perfect architectures. Degree of branching (DB) is a very important parameter

to distinct the dendrimer and hyperbranched polymers. The degree of branching for dendritic polymer is defined as the ratio of branched, terminal, and linear units in the polymer (Eq. 1.35)^{166, 167} by Fréchet. For an ideal dendritic macromolecule structure (e.g. dendrimer), the DB should be equal to 1 (Figure 1.30 A). The DB of hyperbranched polymer should be between 0 and 1 (Figure 1.30 B). However, the DB value is higher than 0 even in the fully linear polymer by this term (Figure 1.30 C).

$$DB_{\text{Fréchet}} = \frac{\sum \text{dendritic units} + \sum \text{terminal units}}{\sum \text{dendritic units} + \sum \text{terminal units} + \sum \text{linear units}} \quad (\text{Eq.1.35})$$

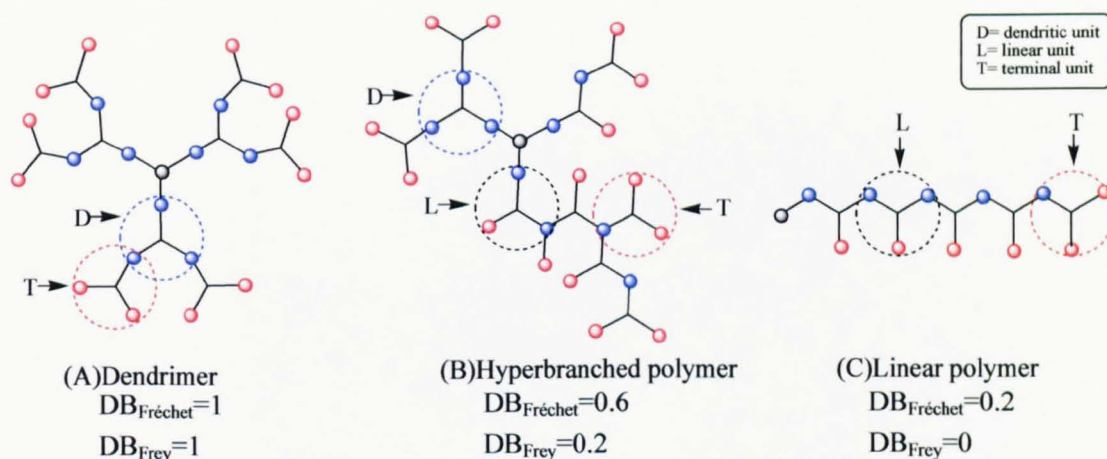


Figure 1.30 Scheme of the different units in the dendrimer, hyperbranched polymer and linear polymer. The different degrees of branching values were given by two different definitions ($DB_{\text{Fr chet}}$ and DB_{Frey}).

Therefore, a modified equation was introduced for the calculation of DB by Frey¹⁶⁸ and Yan¹⁶⁹. The DB_{Frey} is defined as the ratio of the number of growth directions (r) to the maximum possible number of growth directions (r_m) (Eq. 1.36). Thus, the DB_{Frey} of dendrimer is still 1 (Figure 1.30 A), and this value is decreased to 0 for the linear polymer (Figure 1.30 C). The definition of DB_{Frey} is used to calculate the degree of branching in the following chapters of this thesis (Chapter 2, 3 and 4).

$$DB_{\text{Frey}} = \frac{r}{r_m} = \frac{2 \times \sum \text{dendritic units}}{2 \times \sum \text{dendritic units} + \sum \text{linear units}} \quad (\text{Eq.1.36})$$

Typically, dendrimers were synthesised via two different step-by-step processes: ‘Divergent’ and ‘Convergent’ approach. The divergent route afforded the first family of well-characterised dendrimers. The divergent methodology based on acrylate monomers was discovered in 1970s and developed in the Dow laboratories during the period of 1979–1985 (Figure 1.31 A).^{154, 164, 165, 170-172} In this method, the dendrimer grows outward from a central core step by step. This route covers the problem of low yields, purity or purification encountered by Vögtle in the ‘cascade’ synthesis route.¹⁷³ Normally, the Poly(amido amine) (PAMAM) dendrimer with molecular weights ranging from several hundreds to over one million Daltons were prepared at high yields.¹⁶⁴ This methodology was so successful that today it is still the most common commercial route to dendrimer products. However, the numerous synthesis and purification steps in this reaction have limited the application of this method.

The other methodology so-called ‘convergent’ for dendrimer synthesis was developed in the period 1988–1989 by Fréchet and Hawker at Cornell University (Figure 1.31 B).¹⁷⁴⁻¹⁷⁷ The convergent growth approach was first demonstrated with poly(ether) dendrimers. Globular macromolecules with outstanding controlled growth, structure and functionality were prepared via this route. Instead of growing ‘outward’ from core in divergent route, the convergent growth starts at the periphery of the molecules. Then, these building blocks (dendrons) proceed ‘inward’ and are coupled to a branching monomer at the ‘focal point’. This allows a significant reduction in the amount of reagents and the purification at each step of growth. More importantly, the convergent growth allows control over functionality at specified locations of the growing macromolecule. Furthermore, it provides access to numerous novel architectures through the attachment of dendrons to different cores. This has led to novel dendrimers consisting of different blocks, chemically distinct

layers or functionalities. Finally, this method provides the opportunity to prepare hybrid linear-dendritic macromolecules and ‘dendronised’ macromolecules.^{160, 162}

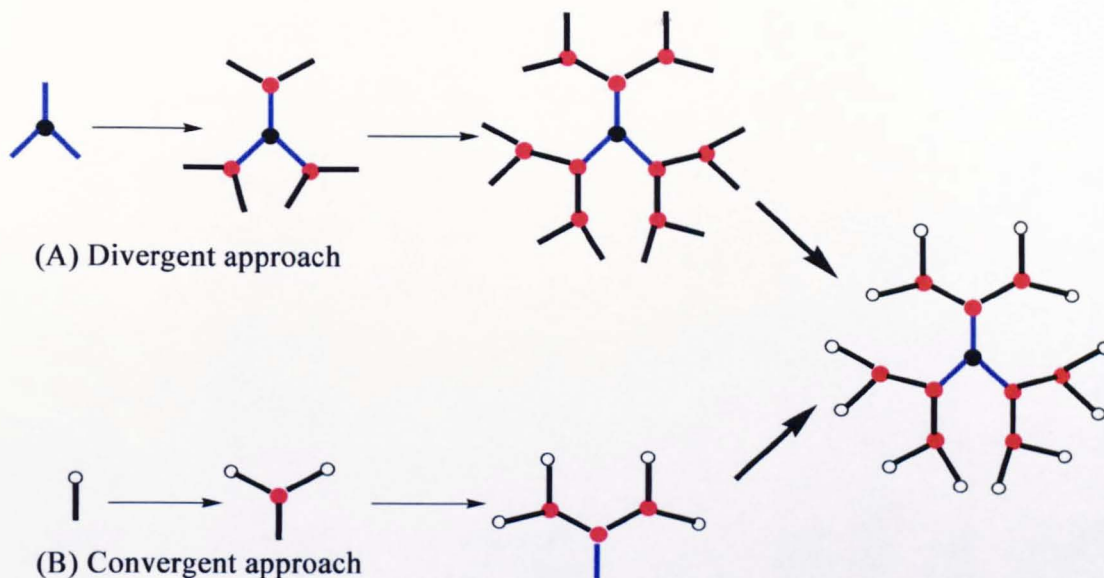


Figure 1.31 Representation of dendrimer growth by the divergent (A) and convergent (B) methods.

1.4.3 Random Hyperbranched Polymers

Dendritic polymers have unique properties because of their physical properties and many branches leading to many functional end groups. Functional dendritic polymers have emerged as a research area with huge potential.^{155, 156, 178-180}

Unfortunately, dendrimers are only accessible through tedious, solvent-intensive and multi-step synthesis routes. Thus, practical applications for dendrimers have been limited due to the difficulties with their synthesis. By contrast, hyperbranched polymers which are essentially less structurally defined dendrimers, may be synthesised more easily and effectively.^{144, 148, 181-185} Flory was the first to report a statistical study for the polymerisation and the infinite network formation of multifunctional monomer. Later, the first examples of ‘random hyperbranched’ polymers were introduced by Odian/Tomalia¹⁸⁶ and Webster/ Kim^{182, 183} in 1980s. This type of polymer was obtained by condensation polymerisation of AB_x-type

monomers and a name coined internally in DuPont as ‘hyperbranched polymers’.

Since then, polymer chemists have explored numerous routes to these statistically hyperbranched macromolecular structures. In theory, all the polymerisation reactions can be utilised for the synthesis of hyperbranched polymers. However, some reactions are practically more suitable than others. Currently, hyperbranched polymers are typically prepared by: (1) one-pot polymerisation of AB_x monomers or macromonomers involving polycondensation (step growth), (2) self-condensing vinyl polymerisation of AB^* monomer (step-chain growth) or (3) living radical copolymerisation of multifunctional monomer and linear monomer (chain growth).

1.4.4 Previous Synthesis of Hyperbranched Polymers

The scope of this part is to examine the utilised polymerisation synthetic routes to hyperbranched polymers. This section is divided into three main parts: (1) hyperbranched polymers by polycondensation;^{150-152, 182, 183, 186, 187} (2) self-condensing vinyl polymerisation (SCVP)^{188, 189} and (3) controlled free radical polymerisation strategies to hyperbranched polymers.^{41, 190-195}

(1) Polycondensation methods

As polycondensation is the traditional way to prepare dendritic polymer. The step-growth polymerisation of AB_x -monomers become the first and most intensively studied route to hyperbranched polymers.^{196, 197} The one-pot polymerisation of AB_2 -monomers (Figure 1.32) offers no control over molecular weight, and consequently, gives rise to highly polydispersed polymers. A number of AB_2 -monomers which are commercially available were chosen for step-growth polymerisations. There is now a wide variety of hyperbranched condensation polymers and examples have been reported in the literature. Typically, the degrees of branching of these polymers are in the range of 0.5-0.6.^{166, 167, 185}

A typical condensation procedure involves a one-step reaction. First of all, the monomer, catalyst and initiator are mixed and heated to the required reaction temperature. During the reaction, low molar mass polymers are formed throughout the reaction and have to be removed to achieve high conversion. This is most often done by using a flow of inert gas or by reducing the pressure of the reaction. The resulting polymer is generally precipitated by anti-solvent and does not need any other special purification process.

In the case of highly functional monomers, unwanted side reactions normally lead to the occurrence of gelation. For example, in the reaction of an AB_x -system which the functional A should be preferred to react with functional B, even very low levels of A-A or B-B reaction can lead to gelation at low conversion.

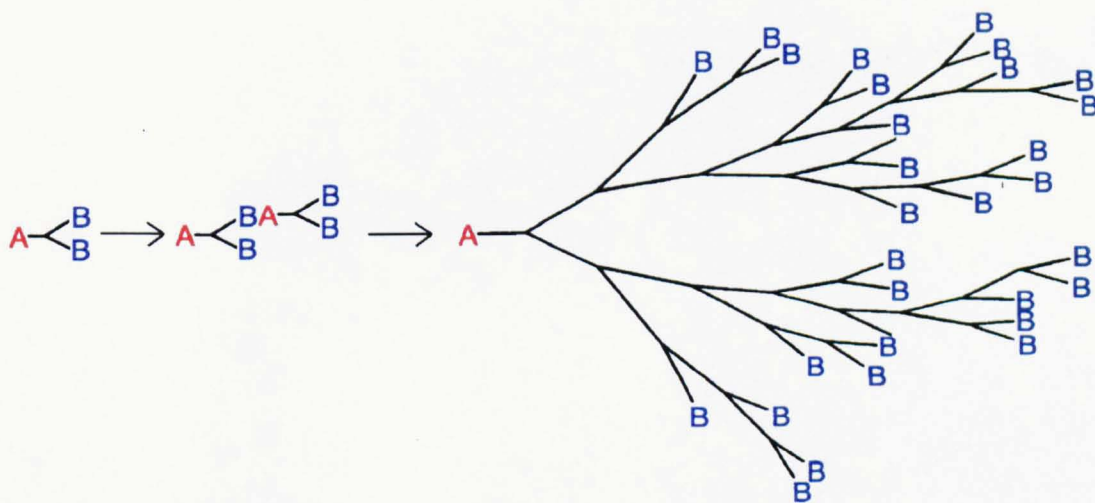


Figure 1.32 Hyperbranched polymer prepared by AB_2 type monomer.

To cover the disadvantages of A-B type monomer, the addition of a 'core' molecule B_x ($x > 2$) was explored (Figure 1.33). This route is not only for a better control over molar mass, but also for controlling the resulting polymer shape.^{155, 198-200} Furthermore, polymerisation of AB_x monomers with core molecules (B_x) can also increase the branched degree of the hyperbranched polymer. It was suggested that

copolymerisation of AB_2 and B_3 -type monomers, for instance, 2,2-bis(methylol)propionic acid (bis-MPA) and tris(methylol)propane (TMP), could give better geometrical control in the hyperbranched polymer synthesis (Figure 1.33).¹⁹⁷ In this reaction, the degree of branching is increased up to 0.8 which confirmed by the ^1H and ^{13}C NMR spectroscopy.^{196, 197} Furthermore, the copolymerisation of the AB_2 and B_x molecules allows for the control of the molecular weight of the hyperbranched polymers.

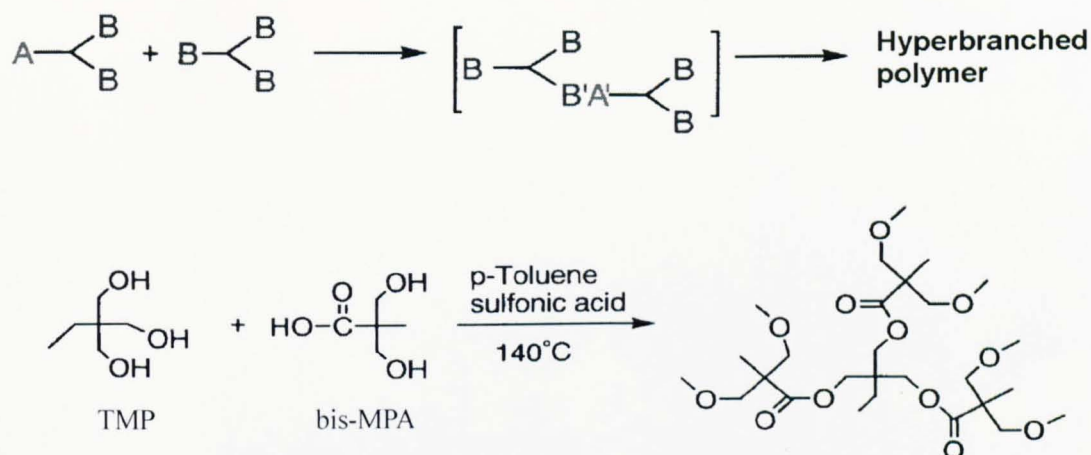


Figure 1.33 Hyperbranched polymer prepared by AB_2 and B_3 type monomer.

Typically, the shortcoming of the hyperbranched polymers prepared by polycondensation is their sensitivity towards hydrolysis. This feature might restrict the application of these hyperbranched polymers. Thus, some hyperbranched polymers are synthesised via substitution or ring opening reactions that provide more hydrolytically stable polymers.

(2) Self-condensing vinyl polymerisation (SCVP) strategies

Apart from the traditional polycondensation method, scientists attempt to prepare hyperbranched polymer from vinyl monomer. Recently, the discovery of 'self-condensing vinyl polymerisation' (SCVP) by Fréchet in 1995 made it possible to use vinyl monomers for synthesis of hyperbranched structures.^{169, 188, 189} In this

approach, a vinyl monomer of the general structure AB is used, where A is a vinyl group and B is a functional group which can be converted to an initiating group B* by an external stimulus. The polymerisation is initiated by addition of B* to an A group, which produces a dimer possessing one double bond and two active sites, B*. This reaction assumed the reactivities of A* and B* are similar. Thus, both of the initiating B* group and the newly created propagating cation can react with the vinyl group of another molecule (monomer or polymer) in the same way. These events eventually lead to a hyperbranched polymer (Figure 1.34).

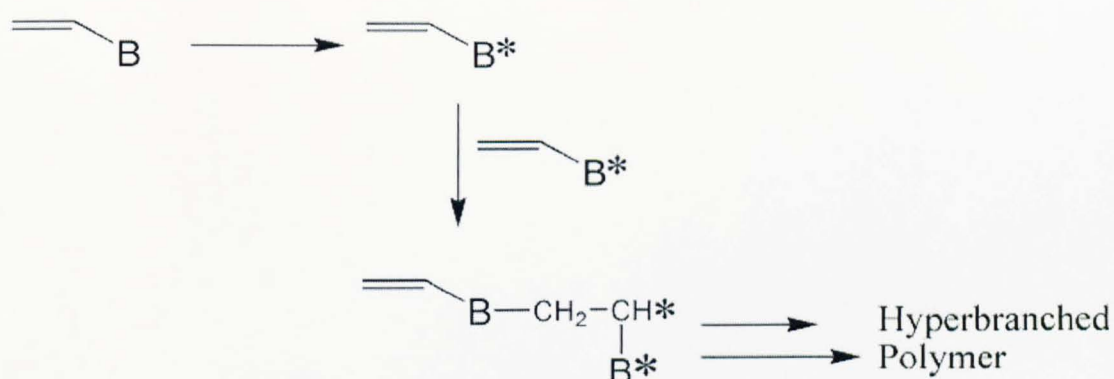


Figure 1.34 Schematic representation of the self-condensing vinyl polymerisation (SCVP) of an AB* monomer to give a hyperbranched vinyl polymer.

This kind of AB* monomer which also named ‘inimer’ combines the features of an initiator and a monomer. Figure 1.30 shows the three examples of such inimer molecules: (1) activation can occur by removing the chlorine to either form a cation¹⁸⁸ (Figure 1.30 A) or a radical¹⁹⁵ (Figure 1.30 B); (2) the silylketene acetal group can be activated by nucleophilic catalysts to initiate group transfer polymerisation (Figure 1.30 C).^{185, 201} The two different reactivity of propagating group (A*) and initiating group (B*) have strong effect on the polydispersity and branching degree of polymers in SCVP method. Typically, the polydispersity of hyperbranched polymer formed by SCVP is in the range of 3-6.^{188, 189} However, it should taking into consideration that the published results depended on the GPC

calibration with linear standards which is inappropriate for highly branched sample. Furthermore, a modified definition of degree of branching in SCVP is given by Yan and Müller¹⁶⁹ (Eq. 1.37). Theoretically, the DB of hyperbranched polymer by SCVP is lower than the polycondensation of AB₂ type monomer.

$$DB_{SCVP} = \frac{2 \times (\text{number of branched units})}{(\text{total number of units}) - 1} \quad (\text{Eq.1.37})$$

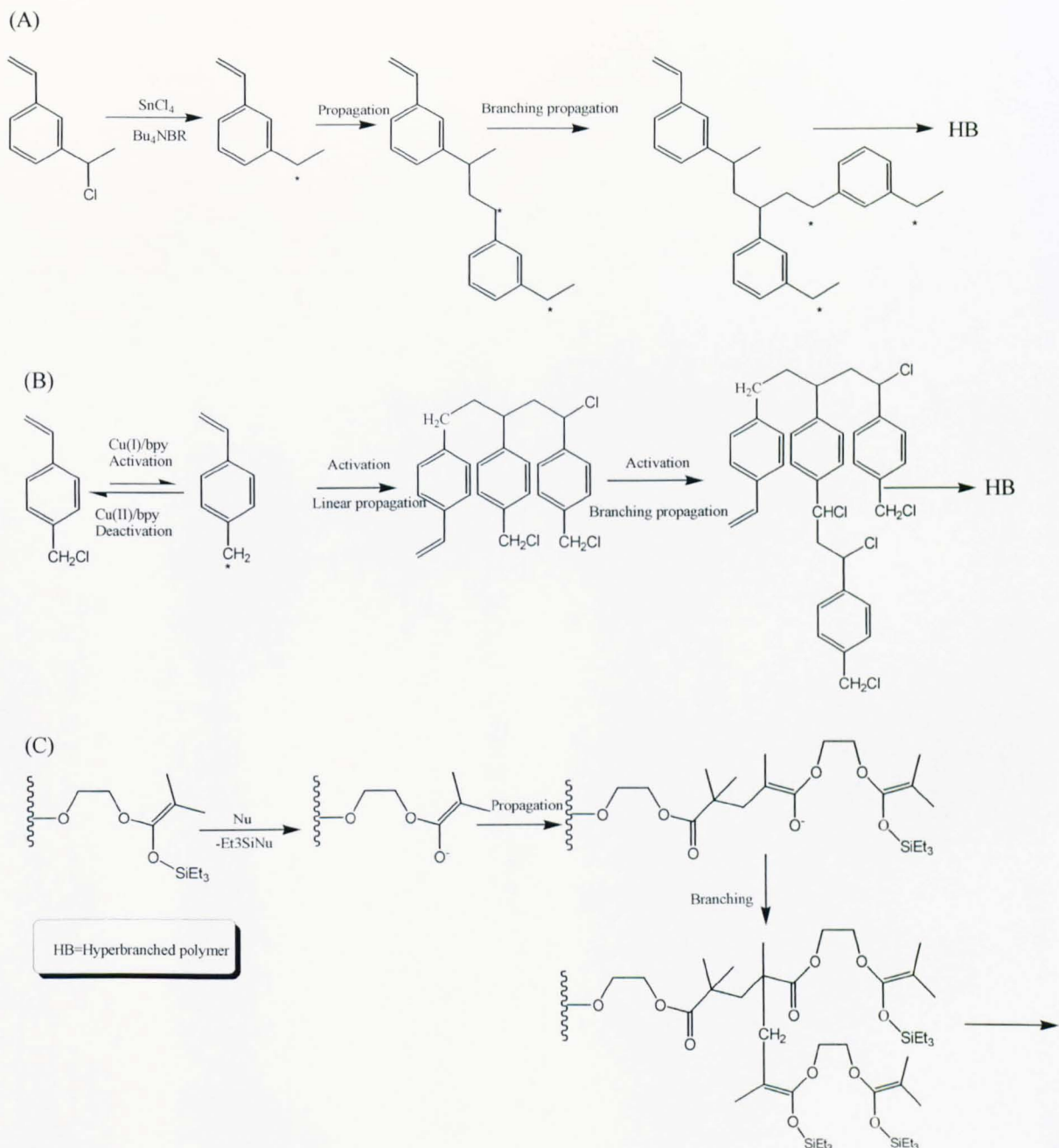


Figure 1.35 Examples of AB* monomers.

Last, the mechanism of SCVP method limits the choice of monomer. Normally, only a few inimers with specific structures can be used in this method. Furthermore, the strict conditions and requirements of SCVP obstruct the promotion of this method on the industry scale.

(3) Controlled/living free radical polymerisation

Recently, chemists have explored preparing hyperbranched polymers from commercial available monomer and conditions. Multifunctional vinyl monomers (MFM) were used as a branched point to yield highly branching structures. However, multifunctional vinyl monomers generally lead to crosslinked or gelled polymer networks in a free-radical polymerisation even in low concentrations and yields. It was found that branched polymers are precursors to crosslinked gels in this approach. Thus, researchers used a suitable free radical transfer agent to provide a practical and highly convenient synthesis of branched vinyl polymers.

From 1999, Sherrington and co-workers recently developed a facile and generic synthetic methodology (the ‘Strathclyde methodology’, Figure 1.36) for the high yielding synthesis of branched vinyl polymers using conventional free radical polymerisation.^{193, 202-204}

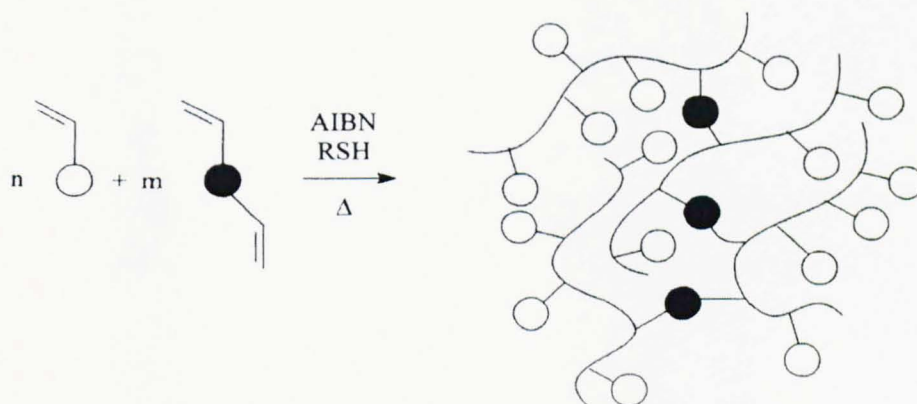


Figure 1.36 Synthesis of branched vinyl polymer using a balance of multifunctional monomer and radical transfer agent (Strathclyde method).

This methodology involves the simple free radical copolymerisation of a vinyl

monomer with a difunctional (or multifunctional) comonomer. Cross-linking and network formation was inhibited by use of appropriate levels of a stoichiometric free radical chain transfer agent, such as a thiol. However, it requires use of an organic solvent which dilutes the whole reaction medium and contributes to the inhibition of cross-linking. Furthermore, it was reported that low concentration of multifunctional vinyl comonomers (typically lower than 15%), and a limited molar ratio of branching monomer to initiator of ≤ 1 were required to ensure soluble hyperbranched materials without crosslinking. When this ratio exceeds 1, it will lead to an insoluble cross-linked material or microgel product. Therefore, the final result is that the copolymers produced had only a low degree of branching. Since then, the synthesis of low molecular weight dendrimer-like oligomers has also been reported using a similar strategy involving a catalytic chain transfer species.¹⁹⁰ However, there is little control over molecular weight and branch structure through this strategy. Following the same strategy, Perrier adopted a similar procedure using reversible addition fragmentation chain transfer (RAFT) to prepare copolymers with a low degree of branching.¹⁹²

In 2002, Guan explored a new concept of controlling polymer topology by direct polymerisation of commercial monomers using transition-metal catalysts.¹⁹⁰ Instead of designing new monomers, he attempted to achieve new polymer topologies by controlling the assembly of divinyl monomers through catalysis. In this approach, hyperbranched polymers were synthesised by direct free radical polymerisation of commercially available divinyl monomers such as ethylene glycol dimethacrylate (EGDMA) by controlling the competition between propagation and chain transfer. In this study, a cobalt chain transfer catalyst (CCTC) was used to control the propagation of free radical polymerisation of the divinyl monomer. The mechanism demonstrates that the cobalt catalyst was used to control the polyEGDMA branching topology by regulating the competition between propagation and chain transfer (Figure 1.37).

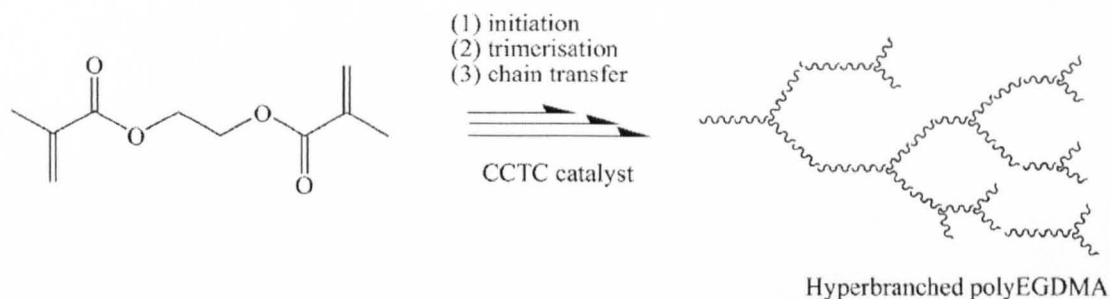


Figure 1.37 Synthesis of the hyperbranched polyEGDMA by CCTC method. In this route, hyperbranched polymer were synthesised by direct free radical polymerisation of commercially available divinyl monomers by controlling the competition between propagation and chain transfer using a chain transfer catalyst.

In 2003, Sato has reported a new class of radical polymerisation that can be termed initiator-fragment incorporation radical polymerisation (IFIRP) in which the initiator fragments are incorporated as a main constituent in the resulting polymer.¹⁹⁴ The copolymerisation of divinylbenzene (DVB) and ethylstyrene (EtSt) was carried out at 80 °C in benzene with dimethyl 2,2-azobisisobutyrate (MAIB) at high concentrations as initiator. Furthermore, this approach is in the presence of methyl benzyloxyiminoacetate (MBOIA) acts which as a retarder. The resulting polymer contained a comparable amount of a 1-methoxycarbonyl-1-methylethyl group as a fragment of MAIB to that of DVB.

1.5 A Overview of This Thesis

Now, developing new synthetic routes to dendritic polymeric materials by commodity monomers with controlled architecture is highly desirable. The work in this thesis focuses primarily on the controlled/living polymerisation of divinyl monomer to provide hyperbranched polymer. The aim is to produce hyperbranched polymers via enhanced deactivation ATRP without crosslinking even at high conversion. The strategy will be to use excess Cu(II) to control gelation, so called enhanced deactivation ATRP.

In this thesis, the homopolymerisation of two kinds of divinyl monomers

(divinylbenzene and ethylene glycol dimethacrylate) will be examined. The hyperbranched polyDVB and polyEGDMA are produced by deactivation enhanced ATRP in concentrated system. Furthermore, the DE-ATRP affects the polymerisation kinetics and pushes the gel point as high yield (Chapter 2).

This research will be extended to investigate the copolymerisation of divinyl monomer and other functional monomers. For instance, amphiphilic hyperbranched polymer (polyEGDMA-*co*-DMAEMA) and hyperbranched siloxane polymer (polyDVB-*co*-PDMS_{ma}) will be prepared by enhanced deactivation ATRP. Also, the interesting potential applications, for example dye encapsulation and viscosity control will be explored (Chapter 3).

Finally, the hyperbranched polyDVB will be used as a core and attempt to produce hyperbranched core-shell polymers. This material (polyDVB_{core}-*co*-MMA_{shell}) consists of a dense branched core and opened linear arms. Furthermore, another novel biodegradable hyperbranched polymer (polyCL-*co*-BOD_{core}-DMAEMA_{shell}) will be prepared by combining ring open polymerisation and RAFT technique (Chapter 4).

1.6 Reference

1. Baekeland, L. H. *Journal of Industrial and Engineering Chemistry-Us* **1909**, 1, 545-549.
2. Baekeland, L. H. *Journal of Industrial and Engineering Chemistry-Us* **1909**, 1, 149-161.
3. Staudinger, H. *Berichte Der Deutschen Chemischen Gesellschaft* **1920**, 53, 1073-1085.
4. Staudinger, H. *Berichte Der Deutschen Chemischen Gesellschaft* **1924**, 57, 1203-1208.
5. Carothers, W. H.; Arvin, J. A.; Dorough, G. L. *Journal of the American Chemical Society* **1930**, 52, 3292-3300.
6. Carothers, W. H.; Dorough, G. L. *Journal of the American Chemical Society* **1930**, 52, 711-721.
7. Carothers, W. H.; van Natta, F. J. *Journal of the American Chemical Society* **1930**, 52, 314-326.
8. Flory, P. J. *Journal of the American Chemical Society* **1937**, 59, 241-253.
9. Burnett, G. M. *Quarterly Reviews* **1950**, 4, (3), 292-326.
10. Engel, P. S. *Chemical Reviews* **1980**, 80, (2), 99-150.
11. Matheson, M. S.; Auer, E. E.; Bevilacqua, E. B.; Hart, E. J. *Journal of the American Chemical Society* **1951**, 73, (4), 1700-1706.
12. Mayo, F. R.; Gregg, R. A.; Matheson, M. S. *Journal of the American Chemical Society* **1951**, 73, (4), 1691-1700.
13. Smith, W. V. *Journal of the American Chemical Society* **1948**, 70, (11), 3695-3702.
14. Mayo, F. R. *Journal of the American Chemical Society* **1948**, 70, (11), 3689-3694.
15. Walling, C.; Briggs, E. R.; Mayo, F. R. *Journal of the American Chemical Society* **1946**, 68, (7), 1145-1149.
16. Matheson, M. S.; Auer, E. E.; Bevilacqua, E. B.; Hart, E. J. *Journal of the American Chemical Society* **1949**, 71, (8), 2610-2617.

17. Bamford, C. H.; Dewar, M. J. S. *Proceedings of the Royal Society of London Series a-Mathematical and Physical Sciences* **1949**, 197, (1050), 356-373.
18. Matyjaszewski, K.; P.Davis, T., *Handbook of radical polymerization*. John Wiley and Sons, Inc.: Hoboken, 2002.
19. Fischer, H. *Chemical Reviews* **2001**, 101, (12), 3581-3610.
20. Hawker, C. J.; Bosman, A. W.; Harth, E. *Chemical Reviews* **2001**, 101, (12), 3661-3688.
21. Matyjaszewski, K.; Xia, J. H. *Chemical Reviews* **2001**, 101, (9), 2921-2990.
22. Otsu, T. *Journal of Polymer Science, Part A-Polymer Chemistry* **2000**, 38, (12), 2121-2136.
23. Otsu, T.; Yoshida, M. *Makromolekulare Chemie-Rapid Communications* **1982**, 3, (2), 127-132.
24. Wang, J. S.; Matyjaszewski, K. *Macromolecules* **1995**, 28, (23), 7901-7910.
25. Wang, J. S.; Matyjaszewski, K. *Journal of the American Chemical Society* **1995**, 117, (20), 5614-5615.
26. Curran, D. P. *Synthesis-Stuttgart* **1988**, (7), 489-513.
27. Curran, D. P. *Synthesis-Stuttgart* **1988**, (6), 417-439.
28. Kharasch, M. S.; Jensen, E. V.; Urry, W. H. *Science* **1945**, 102, (2640), 128-128.
29. Georges, M. K.; Veregin, R. P. N.; Kazmaier, P. M.; Hamer, G. K. *Macromolecules* **1993**, 26, (11), 2987-2988.
30. Gaynor, S. G.; Wang, J. S.; Matyjaszewski, K. *Macromolecules* **1995**, 28, (24), 8051-8056.
31. Matyjaszewski, K.; Gaynor, S.; Wang, J. S. *Macromolecules* **1995**, 28, (6), 2093-2095.
32. Chiefari, J.; Chong, Y. K.; Ercole, F.; Krstina, J.; Jeffery, J.; Le, T. P. T.; Mayadunne, R. T. A.; Meijs, G. F.; Moad, C. L.; Moad, G.; Rizzardo, E.; Thang, S. H. *Macromolecules* **1998**, 31, (16), 5559-5562.
33. Moad, G.; Chiefari, J.; Chong, Y. K.; Krstina, J.; Mayadunne, R. T. A.; Postma, A.; Rizzardo, E.; Thang, S. H. *Polymer International* **2000**, 49, (9), 993-1001.

34. Goto, A.; Sato, K.; Tsujii, Y.; Fukuda, T.; Moad, G.; Rizzardo, E.; Thang, S. H. *Macromolecules* **2001**, 34, (3), 402-408.
35. Coleman, B. D.; Fox, T. G. *Journal of the American Chemical Society* **1963**, 85, (9), 1241-1244.
36. Patten, T. E.; Xia, J. H.; Abernathy, T.; Matyjaszewski, K. *Science* **1996**, 272, (5263), 866-868.
37. Matyjaszewski, K.; Ziegler, M. J.; Arehart, S. V.; Greszta, D.; Pakula, T. *Journal of Physical Organic Chemistry* **2000**, 13, (12), 775-786.
38. Davis, K. A.; Matyjaszewski, K., Statistical, gradient, block, and graft copolymers by controlled/living radical polymerizations. In *Statistical, Gradient, Block and Graft Copolymers by Controlled/Living Radical Polymerizations*, 2002; Vol. 159, pp 1-169.
39. Beers, K. L.; Gaynor, S. G.; Matyjaszewski, K.; Sheiko, S. S.; Möller, M. *Macromolecules* **1998**, 31, (26), 9413-9415.
40. Matyjaszewski, K. *Polymer International* **2003**, 52, (10), 1559-1565.
41. Matyjaszewski, K.; Gaynor, S. G.; Kulfan, A.; Podwika, M. *Macromolecules* **1997**, 30, (17), 5192-5194.
42. Nagashima, H.; Ozaki, N.; Ishii, M.; Seki, K.; Washiyama, M.; Itoh, K. *Journal of Organic Chemistry* **1993**, 58, (2), 464-470.
43. Nagashima, H.; Wakamatsu, H.; Ozaki, N.; Ishii, T.; Watanabe, M.; Tajima, T.; Itoh, K. *Journal of Organic Chemistry* **1992**, 57, (6), 1682-1689.
44. Seijas, J. A.; Vazquezato, M. P.; Castedo, L.; Estevez, R. J.; Onega, M. G.; Ruiz, M. *Tetrahedron* **1992**, 48, (9), 1637-1642.
45. Udding, J. H.; Tuijp, C. J. M.; Hiemstra, H.; Speckamp, W. N. *Tetrahedron* **1994**, 50, (6), 1907-1918.
46. Wang, J. S.; Matyjaszewski, K. *Macromolecules* **1995**, 28, (22), 7572-7573.
47. Kotani, Y.; Kato, M.; Kamigaito, M.; Sawamoto, M. *Macromolecules* **1996**, 29, (22), 6979-6982.
48. Kato, M.; Kamigaito, M.; Sawamoto, M.; Higashimura, T. *Macromolecules* **1995**, 28, (5), 1721-1723.

49. Tsarevsky, N. V.; Braunecker, W. A.; Vacca, A.; Gans, P.; Matyjaszewski, K. *Macromolecular Symposia* **2007**, 248, 60-70.
50. Tsarevsky, N. V.; Braunecker, W. A.; Matyjaszewski, K. *Journal of Organometallic Chemistry* **2007**, 692, (15), 3212-3222.
51. Percec, V.; Popov, A. V.; Ramirez-Castillo, E.; Monteiro, M.; Barboiu, B.; Weichold, O.; Asandei, A. D.; Mitchell, C. M. *Journal of the American Chemical Society* **2002**, 124, (18), 4940-4941.
52. Rosen, B. M.; Percec, V. *Journal of Polymer Science, Part A-Polymer Chemistry* **2008**, 46, (16), 5663-5697.
53. Lligadas, G.; Rosen, B. M.; Monteiro, M. J.; Percec, V. *Macromolecules* **2008**, 41, (22), 8360-8364.
54. Lligadas, G.; Rosen, B. M.; Bell, C. A.; Monteiro, M. J.; Percec, V. *Macromolecules* **2008**, 41, (22), 8365-8371.
55. Percec, V.; Guliashvili, T.; Ladislaw, J. S.; Wistrand, A.; Stjerndahl, A.; Sienkowska, M. J.; Monteiro, M. J.; Sahoo, S. *Journal of the American Chemical Society* **2006**, 128, (43), 14156-14165.
56. Percec, V.; Popov, A. V.; Ramirez-Castillo, E.; Weichold, O. *Journal of Polymer Science, Part A-Polymer Chemistry* **2003**, 41, (21), 3283-3299.
57. Xia, J. H.; Matyjaszewski, K. *Macromolecules* **1997**, 30, (25), 7692-7696.
58. Gromada, J.; Matyjaszewski, K. *Macromolecules* **2001**, 34, (22), 7664-7671.
59. Li, M.; Min, K.; Matyjaszewski, K. *Macromolecules* **2004**, 37, (6), 2106-2112.
60. Li, M.; Jahed, N. M.; Min, K.; Matyjaszewski, K. *Macromolecules* **2004**, 37, (7), 2434-2441.
61. Min, K.; Gao, H. F.; Matyjaszewski, K. *Journal of the American Chemical Society* **2005**, 127, (11), 3825-3830.
62. Jakubowski, W.; Matyjaszewski, K. *Macromolecules* **2005**, 38, (10), 4139-4146.
63. Jakubowski, W.; Min, K.; Matyjaszewski, K. *Macromolecules* **2006**, 39, (1), 39-45.
64. Jakubowski, W.; Matyjaszewski, K. *Angewandte Chemie-International Edition* **2006**, 45, (27), 4482-4486.

65. Kotani, Y.; Kamigaito, M.; Sawamoto, M. *Macromolecules* **1999**, 32, (20), 6877-6880.
66. Percec, V.; Barboiu, B. *Macromolecules* **1995**, 28, (23), 7970-7972.
67. Davis, K. A.; Paik, H. J.; Matyjaszewski, K. *Macromolecules* **1999**, 32, (6), 1767-1776.
68. Grimaud, T.; Matyjaszewski, K. *Macromolecules* **1997**, 30, (7), 2216-2218.
69. Haddleton, D. M.; Waterson, C.; Derrick, P. J.; Jasieczek, C. B.; Shooter, A. J. *Chemical Communications* **1997**, (7), 683-684.
70. Haddleton, D. M.; Jasieczek, C. B.; Hannon, M. J.; Shooter, A. J. *Macromolecules* **1997**, 30, (7), 2190-2193.
71. Wang, J. L.; Grimaud, T.; Matyjaszewski, K. *Macromolecules* **1997**, 30, (21), 6507-6512.
72. Huang, X.; Wirth, M. J. *Macromolecules* **1999**, 32, (5), 1694-1696.
73. Matyjaszewski, K.; Jo, S. M.; Paik, H. J.; Shipp, D. A. *Macromolecules* **1999**, 32, (20), 6431-6438.
74. Jo, S. M.; Paik, H. J.; Matyjaszewski, K. *Abstracts of Papers of the American Chemical Society* **1997**, 213, 325-POLY.
75. Jo, S. M.; Paik, H. J.; Matyjaszewski, K. *Abstracts of Papers of the American Chemical Society* **1997**, 213, 326-POLY.
76. Matyjaszewski, K.; Jo, S. M.; Paik, H. J.; Gaynor, S. G. *Macromolecules* **1997**, 30, (20), 6398-6400.
77. Asandei, A. D.; Percec, V. *Journal of Polymer Science, Part A-Polymer Chemistry* **2001**, 39, (19), 3392-3418.
78. Wakioka, M.; Baek, K. Y.; Ando, T.; Kamigaito, M.; Sawamoto, M. *Macromolecules* **2002**, 35, (2), 330-333.
79. Tang, W.; Matyjaszewski, K. *Macromolecules* **2007**, 40, (6), 1858-1863.
80. <http://www.chem.cmu.edu/groups/maty/about/research/07.html>.
81. Liu, T. Q.; Jia, S.; Kowalewski, T.; Matyjaszewski, K.; Casado-Portilla, R.; Belmont, J. *Langmuir* **2003**, 19, (16), 6342-6345.
82. Pyun, J.; Jia, S. J.; Kowalewski, T.; Patterson, G. D.; Matyjaszewski, K.

Macromolecules **2003**, 36, (14), 5094-5104.

83. Pyun, J.; Matyjaszewski, K. *Macromolecules* **2000**, 33, (1), 217-220.

84. Pyun, J.; Matyjaszewski, K.; Kowalewski, T.; Savin, D.; Patterson, G.; Kickelbick, G.; Huesing, N. *Journal of the American Chemical Society* **2001**, 123, (38), 9445-9446.

85. Savin, D. A.; Pyun, J.; Patterson, G. D.; Kowalewski, T.; Matyjaszewski, K. *Journal of Polymer Science, Part B-Polymer Physics* **2002**, 40, (23), 2667-2676.

86. Chen, X. Y.; Randall, D. P.; Perruchot, C.; Watts, J. F.; Patten, T. E.; von Werne, T.; Armes, S. P. *Journal of Colloid and Interface Science* **2003**, 257, (1), 56-64.

87. von Werne, T. A.; Germack, D. S.; Hagberg, E. C.; Sheares, V. V.; Hawker, C. J.; Carter, K. R. *Journal of the American Chemical Society* **2003**, 125, (13), 3831-3838.

88. Matyjaszewski, K.; Xia, J. H.; Zhang, X. *Abstracts of Papers of the American Chemical Society* **1999**, 217, U439-U439.

89. Matyjaszewski, K.; Wei, M. L.; Xia, J. H.; McDermott, N. E. *Macromolecules* **1997**, 30, (26), 8161-8164.

90. Tang, W.; Matyjaszewski, K. *Macromolecules* **2006**, 39, (15), 4953-4959.

91. Granel, C.; Dubois, P.; Jerome, R.; Teyssie, P. *Macromolecules* **1996**, 29, (27), 8576-8582.

92. Duxbury, C. J.; Wang, W. X.; de Geus, M.; Heise, A.; Howdle, S. M. *Journal of the American Chemical Society* **2005**, 127, (8), 2384-2385.

93. Shipp, D. A.; Wang, J. L.; Matyjaszewski, K. *Macromolecules* **1998**, 31, (23), 8005-8008.

94. Borner, H. G.; Beers, K.; Matyjaszewski, K.; Sheiko, S. S.; Möller, M. *Macromolecules* **2001**, 34, (13), 4375-4383.

95. Hong, S. C.; Pakula, T.; Matyjaszewski, K. *Macromolecular Chemistry and Physics* **2001**, 202, (17), 3392-3402.

96. Hong, S. C.; Pakula, T.; Matyjaszewski, K. *Abstracts of Papers of the American Chemical Society* **2001**, 221, U421-U421.

97. Matyjaszewski, K.; Teodorescu, M.; Miller, P. J.; Peterson, M. L. *Journal of*

Polymer Science, Part A-Polymer Chemistry **2000**, 38, (13), 2440-2448.

98. Fonagy, T.; Ivan, B.; Szesztay, M. *Macromolecular Rapid Communications* **1998**, 19, (9), 479-483.

99. Paik, H. J.; Gaynor, S. G.; Matyjaszewski, K. *Macromolecular Rapid Communications* **1998**, 19, (1), 47-52.

100. Roos, S. G.; Müller, A. H. E.; Matyjaszewski, K. *Macromolecules* **1999**, 32, (25), 8331-8335.

101. Yamada, K.; Miyazaki, M.; Ohno, K.; Fukuda, T.; Minoda, M. *Macromolecules* **1999**, 32, (2), 290-293.

102. Percec, V.; Barboiu, B.; Bera, T. K.; van der Sluis, M.; Grubbs, R. B.; Frechét, J. M. J. *Journal of Polymer Science, Part A-Polymer Chemistry* **2000**, 38, 4776-4791.

103. Matyjaszewski, K.; Miller, P. J.; Pyun, J.; Kickelbick, G.; Diamanti, S. *Macromolecules* **1999**, 32, (20), 6526-6535.

104. Kasko, A. M.; Heintz, A. M.; Pugh, C. *Macromolecules* **1998**, 31, (2), 256-271.

105. Matyjaszewski, K.; Miller, P. J.; Fossum, E.; Nakagawa, Y. *Applied Organometallic Chemistry* **1998**, 12, (10-11), 667-673.

106. Ueda, J.; Matsuyama, M.; Kamigaito, M.; Sawamoto, M. *Macromolecules* **1998**, 31, (3), 557-562.

107. Xia, J. H.; Zhang, X.; Matyjaszewski, K. *Macromolecules* **1999**, 32, (13), 4482-4484.

108. Zhang, X.; Xia, J. H.; Matyjaszewski, K. *Macromolecules* **2000**, 33, (7), 2340-2345.

109. Asgarzadeh, F.; Ourdouillie, P.; Beyou, E.; Chaumont, P. *Macromolecules* **1999**, 32, (21), 6996-7002.

110. Coessens, V.; Pyun, J.; Miller, P. J.; Gaynor, S. G.; Matyjaszewski, K. *Macromolecular Rapid Communications* **2000**, 21, (2), 103-109.

111. Coca, S.; Jasieczek, C. B.; Beers, K. L.; Matyjaszewski, K. *Journal of Polymer Science, Part A-Polymer Chemistry* **1998**, 36, (9), 1417-1424.

112. Muhlebach, A.; Gaynor, S. G.; Matyjaszewski, K. *Macromolecules* **1998**, 31, (18), 6046-6052.
113. Qiu, J.; Matyjaszewski, K. *Macromolecules* **1997**, 30, (19), 5643-5648.
114. Zhang, X.; Matyjaszewski, K. *Macromolecules* **1999**, 32, (22), 7349-7353.
115. Haddleton, D. M.; Heming, A. M.; Kukulj, D.; Duncalf, D. J.; Shooter, A. J. *Macromolecules* **1998**, 31, (6), 2016-2018.
116. Coessens, V.; Matyjaszewski, K. *Macromolecular Rapid Communications* **1999**, 20, (2), 66-70.
117. Coessens, V.; Matyjaszewski, K. *Macromolecular Rapid Communications* **1999**, 20, (3), 127-134.
118. Coessens, V.; Matyjaszewski, K. *Journal of Macromolecular Science-Pure and Applied Chemistry* **1999**, A36, (5-6), 653-666.
119. Coessens, V.; Matyjaszewski, K. *Journal of Macromolecular Science-Pure and Applied Chemistry* **1999**, A36, (5-6), 667-679.
120. Coessens, V.; Matyjaszewski, K. *Journal of Macromolecular Science-Pure and Applied Chemistry* **1999**, A36, (5-6), 811-826.
121. Coessens, V.; Nakagawa, Y.; Matyjaszewski, K. *Polymer Bulletin* **1998**, 40, (2-3), 135-142.
122. Matyjaszewski, K.; Nanda, A. K.; Tang, W. *Macromolecules* **2005**, 38, (5), 2015-2018.
123. Zhang, H. Q.; Klumperman, B.; Ming, W. H.; Fischer, H.; van der Linde, R. *Macromolecules* **2001**, 34, (18), 6169-6173.
124. Tang, W.; Matyjaszewski, K. *Macromolecular Theory and Simulations* **2008**, 17, (7-8), 359-375.
125. Barner-Kowollik, C.; Buback, M.; Egorov, M.; Fukuda, T.; Goto, A.; Olaj, O. F.; Russell, G. T.; Vana, P.; Yamada, B.; Zetterlund, P. B. *Progress in Polymer Science* **2005**, 30, (6), 605-643.
126. Beuermann, S.; Buback, M. *Progress in Polymer Science* **2002**, 27, (2), 191-254.
127. Fischer, H.; Radom, L. *Angewandte Chemie-International Edition* **2001**, 40,

(8), 1340-1371.

128. Fischer, H.; Paul, H. *Accounts of Chemical Research* **1987**, 20, (5), 200-206.

129. Tang, W.; Tsarevsky, N. V.; Matyjaszewski, K. *Journal of the American Chemical Society* **2006**, 128, (5), 1598-1604.

130. Tang, W.; Nanda, A. K.; Matyjaszewski, K. *Macromolecular Chemistry and Physics* **2005**, 206, (12), 1171-1177.

131. Moad, G.; Rizzardo, E.; Thang, S. H. *Australian Journal of Chemistry* **2005**, 58, (6), 379-410.

132. Chong, Y. K.; Le, T. P. T.; Moad, G.; Rizzardo, E.; Thang, S. H. *Macromolecules* **1999**, 32, (6), 2071-2074.

133. Mayadunne, R. T. A.; Rizzardo, E.; Chiefari, J.; Krstina, J.; Moad, G.; Postma, A.; Thang, S. H. *Macromolecules* **2000**, 33, (2), 243-245.

134. Mayadunne, R. T. A.; Rizzardo, E.; Chiefari, J.; Chong, Y. K.; Moad, G.; Thang, S. H. *Macromolecules* **1999**, 32, (21), 6977-6980.

135. Chong, Y. K.; Krstina, J.; Le, T. P. T.; Moad, G.; Postma, A.; Rizzardo, E.; Thang, S. H. *Macromolecules* **2003**, 36, (7), 2256-2272.

136. Chiefari, J.; Mayadunne, R. T. A.; Moad, C. L.; Moad, G.; Rizzardo, E.; Postma, A.; Skidmore, M. A.; Thang, S. H. *Macromolecules* **2003**, 36, (7), 2273-2283.

137. Perrier, S.; Takolpuckdee, P. *Journal of Polymer Science, Part A-Polymer Chemistry* **2005**, 43, (22), 5347-5393.

138. Chong, B.; Moad, G.; Rizzardo, E.; Skidmore, M.; Thang, S. H. *Australian Journal of Chemistry* **2006**, 59, (10), 755-762.

139. Postma, A. D., T. P.; Moad, G.; O'Shea, M. S. *Macromolecules* **2005**, 38, (13), 5371-5374.

140. Perrier, S.; Takolpuckdee, P.; Mars, C. A. *Macromolecules* **2005**, 38, (6), 2033-2036.

141. Tomalia, D. A.; Baker, H.; Dewald, J.; Hall, M.; Kallos, G.; Martin, S.; Roeck, J.; Ryder, J.; Smith, P. *Polymer Journal* **1985**, 17, (1), 117-132.

142. Tomalia, D. A.; Brothers, H. M.; Piehler, L. T. *Abstracts of Papers of the American Chemical Society* **1995**, 210, 39-PMSE.
143. Tomalia, D. A.; Frechét, J. M. J. *Journal of Polymer Science, Part A-Polymer Chemistry* **2002**, 40, (16), 2719-2728.
144. Kim, Y. H. *Journal of Polymer Science, Part A-Polymer Chemistry* **1998**, 36, (11), 1685-1698.
145. Archut, A.; Vögtle, F. *Chemical Society Reviews* **1998**, 27, (4), 233-240.
146. Fischer, M.; Vögtle, F. *Angewandte Chemie-International Edition* **1999**, 38, (7), 885-905.
147. Frechét, J. M. J. *Science* **1994**, 263, (5154), 1710-1715.
148. Inoue, K. *Progress in Polymer Science* **2000**, 25, (4), 453-571.
149. Jikei, M.; Kakimoto, M. *Progress in Polymer Science* **2001**, 26, (8), 1233-1285.
150. Newkome, G. R.; Baker, G. R.; Saunders, M. J.; Russo, P. S.; Gupta, V. K.; Yao, Z. Q.; Miller, J. E.; Bouillion, K. *Journal of the Chemical Society-Chemical Communications* **1986**, (10), 752-753.
151. Newkome, G. R.; Yao, Z. Q.; Baker, G. R.; Gupta, V. K. *Journal of Organic Chemistry* **1985**, 50, (11), 2003-2004.
152. Newkome, G. R.; Yao, Z. Q.; Baker, G. R.; Gupta, V. K.; Russo, P. S.; Saunders, M. J. *Journal of the American Chemical Society* **1986**, 108, (4), 849-850.
153. Aulenta, F.; Hayes, W.; Rannard, S. *European Polymer Journal* **2003**, 39, (9), 1741-1771.
154. Flory, P. J. *Journal of the American Chemical Society* **1952**, 74, (11), 2718-2723.
155. Hult, A.; Johansson, M.; Malmström, E., Hyperbranched polymers. In *Branched Polymers* 1999; Vol. 143, pp 1-34.
156. Yates, C. R.; Hayes, W. *European Polymer Journal* **2004**, 40, (7), 1257-1281.
157. Gauthier, M.; Möller, M. *Macromolecules* **1991**, 24, (16), 4548-4553.
158. Teertstra, S. J.; Gauthier, M. *Progress in Polymer Science* **2004**, 29, (4),

277-327.

159. Tomalia, D. A.; Hedstrand, D. M.; Ferritto, M. S. *Macromolecules* **1991**, 24, (6), 1435-1438.
160. Emrick, T.; Hayes, W.; Frechét, J. M. J. *Journal of Polymer Science, Part A-Polymer Chemistry* **1999**, 37, (20), 3748-3755.
161. Gitsov, I.; Frechét, J. M. J. *Journal of the American Chemical Society* **1996**, 118, (15), 3785-3786.
162. Gitsov, I.; Wooley, K. L.; Hawker, C. J.; Ivanova, P. T.; Frechét, J. M. J. *Macromolecules* **1993**, 26, (21), 5621-5627.
163. Leduc, M. R.; Hayes, W.; Frechét, J. M. J. *Journal of Polymer Science, Part A-Polymer Chemistry* **1998**, 36, (1), 1-10.
164. Tomalia, D. A. *Macromolecular Symposia* **1996**, 101, 243-255.
165. Tomalia, D. A.; Baker, H.; Dewald, J.; Hall, M.; Kallos, G.; Martin, S.; Roeck, J.; Ryder, J.; Smith, P. *Macromolecules* **1986**, 19, (9), 2466-2468.
166. Hawker, C. J.; Lee, R.; Frechét, J. M. J. *Journal of the American Chemical Society* **1991**, 113, (12), 4583-4588.
167. Turner, S. R.; Voit, B. I.; Mourey, T. H. *Macromolecules* **1993**, 26, (17), 4617-4623.
168. Holter, D.; Burgath, A.; Frey, H. *Acta Polymerica* **1997**, 48, (1-2), 30-35.
169. Yan, D. Y.; Müller, A. H. E.; Matyjaszewski, K. *Macromolecules* **1997**, 30, (23), 7024-7033.
170. Tomalia, D. A. *Advanced Materials* **1994**, 6, (7-8), 529-539.
171. Tomalia, D. A.; Hall, M.; Hedstrand, D. M. *Journal of the American Chemical Society* **1987**, 109, (5), 1601-1603.
172. Tomalia, D. A.; Naylor, A. M.; Goddard, W. A. *Angewandte Chemie-International Edition in English* **1990**, 29, (2), 138-175.
173. Buhleier, E.; Wehner, W.; Vögtle, F. *Synthesis-Stuttgart* **1978**, (2), 155-158.
174. Hawker, C. J.; Frechét, J. M. J. *Journal of the Chemical Society-Chemical Communications* **1990**, (15), 1010-1013.
175. Hawker, C. J.; Frechét, J. M. J. *Macromolecules* **1990**, 23, (21), 4726-4729.

176. Hawker, C. J.; Frechét, J. M. J. *Journal of the American Chemical Society* **1990**, 112, (21), 7638-7647.
177. Wooley, K. L.; Hawker, C. J.; Frechét, J. M. J. *Journal of the American Chemical Society* **1991**, 113, (11), 4252-4261.
178. Hecht, S.; Frechét, J. M. J. *Angewandte Chemie-International Edition* **2001**, 40, (1), 74-91.
179. Stiriba, S. E.; Frey, H.; Haag, R. *Angewandte Chemie-International Edition* **2002**, 41, (8), 1329-1334.
180. Stiriba, S. E.; Kautz, H.; Frey, H. *Journal of the American Chemical Society* **2002**, 124, (33), 9698-9699.
181. Frechét, J. M. J.; Hawker, C. J.; Gitsov, I.; Leon, J. W. *Journal of Macromolecular Science-Pure and Applied Chemistry* **1996**, A33, (10), 1399-1425.
182. Kim, Y. H.; Webster, O. W. *Macromolecules* **1992**, 25, (21), 5561-5572.
183. Kim, Y. H.; Webster, O. W. *Journal of the American Chemical Society* **1990**, 112, (11), 4592-4593.
184. Uhrich, K. E.; Hawker, C. J.; Frechét, J. M. J.; Turner, S. R. *Macromolecules* **1992**, 25, (18), 4583-4587.
185. Voit, B. *Journal of Polymer Science, Part A-Polymer Chemistry* **2000**, 38, (14), 2505-2525.
186. Gunatillake, P. A.; Odian, G.; Tomalia, D. A. *Macromolecules* **1988**, 21, (6), 1556-1562.
187. Jikei, M.; Chon, S. H.; Kakimoto, M.; Kawauchi, S.; Imase, T.; Watanabe, J. *Macromolecules* **1999**, 32, (6), 2061-2064.
188. Frechét, J. M. J.; Henmi, M.; Gitsov, I.; Aoshima, S.; Leduc, M. R.; Grubbs, R. B. *Science* **1995**, 269, (5227), 1080-1083.
189. Müller, A. H. E.; Yan, D. Y.; Wulkow, M. *Macromolecules* **1997**, 30, (23), 7015-7023.
190. Guan, Z. *Journal of the American Chemical Society* **2002**, 124, (20), 5616-5617.
191. Li, Y. T.; Armes, S. P. *Macromolecules* **2005**, 38, (12), 5002-5009.

192. Liu, B. L.; Kazlauciunas, A.; Guthrie, J. T.; Perrier, S. *Macromolecules* **2005**, 38, (6), 2131-2136.
193. O'Brien, N.; McKee, A.; Sherrington, D. C.; Slark, A. T.; Titterton, A. *Polymer* **2000**, 41, (15), 6027-6031.
194. Sato, T.; Sato, N.; Seno, M.; Hirano, T. *Journal of Polymer Science, Part A-Polymer Chemistry* **2003**, 41, (19), 3038-3047.
195. Gaynor, S. G.; Edelman, S.; Matyjaszewski, K. *Macromolecules* **1996**, 29, (3), 1079-1081.
196. Malmström, E.; Hult, A. *Macromolecules* **1996**, 29, (4), 1222-1228.
197. Malmström, E.; Johansson, M.; Hult, A. *Macromolecules* **1995**, 28, (5), 1698-1703.
198. Frey, H.; Lach, C.; Lorenz, K. *Advanced Materials* **1998**, 10, (4), 279-293.
199. Kricheldorf, H. R.; Bolender, O.; Wollheim, T. *Macromolecules* **1999**, 32, (12), 3878-3882.
200. Kricheldorf, H. R.; Zang, Q. Z.; Schwarz, G. *Polymer* **1982**, 23, (12), 1821-1829.
201. Sakamoto, K.; Aimiya, T.; Kira, M. *Chemistry Letters* **1997**, (12), 1245-1246.
202. Isaure, F.; Cormack, P. A. G.; Graham, S.; Sherrington, D. C.; Armes, S. P.; Butun, V. *Chemical Communications* **2004**, (9), 1138-1139.
203. Slark, A. T.; Sherrington, D. C.; Titterton, A.; Martin, I. K. *Journal of Materials Chemistry* **2003**, 13, (11), 2711-2720.
204. Costello, P. A.; Martin, I. K.; Slark, A. T.; Sherrington, D. C.; Titterton, A. *Polymer* **2002**, 43, (2), 245-254.

CHAPTER TWO:

HOMOPOLYMERISATIONS OF DIVINYLMONOMERS

2.1 Mechanism

2.1.1 Previous Methods

Free radical copolymerisation of only small amounts of mono-vinyl monomer and multi-vinyl monomer usually leads to gelation.¹ Sherrington² and Guan³ report the polymerisation of divinyl monomers as the branching species. Gelation is avoided by the usage of thiol compound or catalytic chain transfer (CCT) species. Sato has also reported a chain termination controlled free radical polymerisation route which named initiator-fragment incorporation radical polymerisation to suppress the gelation in the reaction(IFIRP).⁴ Sherrington claimed the 'Strathclyde method' which showed that the gelation can be eliminated if the ratio of divinyl monomer to primary linear chain is less than unity.² When this ratio exceeds 1, only an insoluble cross-linked network or microgel was produced. However, well control of the molecular weight and branched structure of the polymers cannot be provided by chain transfer method because of their non-living nature. Recently, the 'Strathclyde' approach was extended to controlled/living polymerisation such as ATRP or RAFT polymerisation. The copolymerisation of methyl methacrylate (MMA) and ethylene glycol dimethacrylate (EGDMA) using Cu-based ATRP were reported,⁵ and low concentrations of multifunctional vinyl monomer are found to be essential. In a recent study, Perrier reported a similar procedure which used RAFT polymerisation.⁶ The final result in all of these cases is that the copolymers produced are predominantly formed from monovinyl monomer and only contain a low degree of branching (*e.g.* 10-15%).

Hence, there is a dilemma in the case of preparation of hyperbranched polymer via controlled/living free radical polymerisation. Hyperbranched polymers are expected to be prepared with high branching degrees. However, the high ratio of divinyl monomer easily

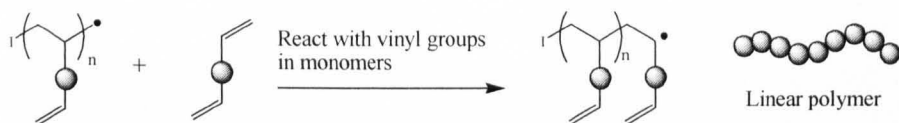
leads the polymer to a cross-linked gel. Consequently, the ratio of divinyl monomers has to be kept low to a percentage of up to approximately 15% in order to prevent crosslink. Developing new synthetic routes to such polymeric materials is of great interest. Also, a method that can directly polymerise existing commercial monomers to form dendritic materials with controlled architecture will be highly desirable. Can a synthesis route be developed to prepare hyperbranched polymer with all following advantages: easy polymerisation route, high branched degrees and also without cross-links? This chapter will investigate the homopolymerisations of divinyl monomers via deactivation enhanced ATRP (DE-ATRP) to see if it is possible.

2.1.2 Preparation of Hyperbranched Polymer via DE-ATRP

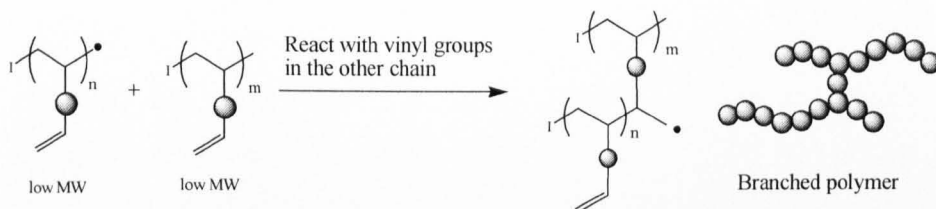
Method

In the homopolymerisation of divinyl monomers, there are four possible growth processes in the reaction (Figure 2.1). Firstly, the monomers are added onto the propagating centre by linear growth (A, Figure 2.1). The free radical was reacted with the vinyl groups in the monomers during this process. Secondly, the propagating centre could react with the vinyl groups in another polymer chain to form a branching point (B, Figure 2.1). Thirdly, the free radical can react with the pendant vinyl groups belonging to the same polymer chain to form a cyclic or intramolecular cross-linking (C, Figure 2.1). Finally, the gelation is formed between the high molecular weight polymer chains by intermolecular crosslinking (D, Figure 2.1). A small fraction of the units might form an 'infinite' network, while the other polymer units yield comparatively dissolvable molecules. Gelation is due to the infinite network in this case. Thus, 'high MW' and 'intermolecular crosslinking' are the two key reasons for the macroscopic gelation (macrogel). Typically, the gelation reaction will be formed via conventional FRP and normal ATRP even under 10-15% yield.

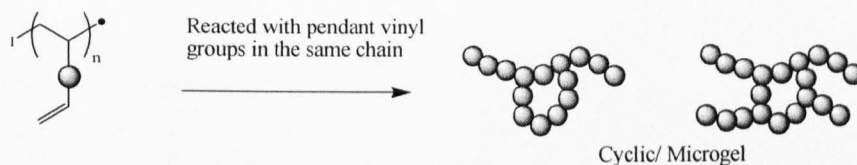
(A) Linear propagation



(B) Branching



(C) Cyclisation/ intramolecular crosslinking



(D) Gelation/ intermolecular crosslinking

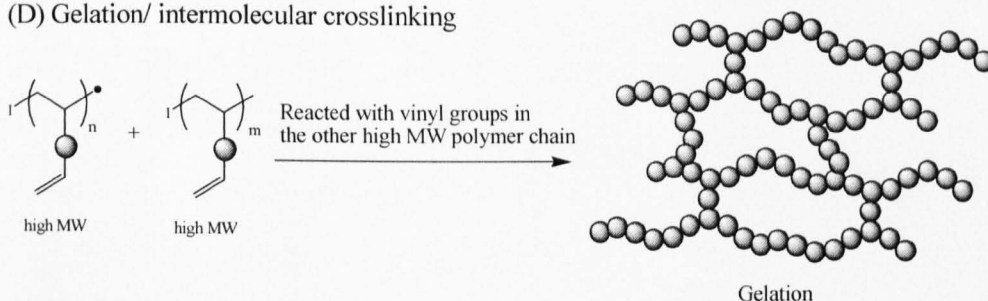


Figure 2.1 The scheme of the four different processes which involved in the homopolymerisation of divinyl monomers.

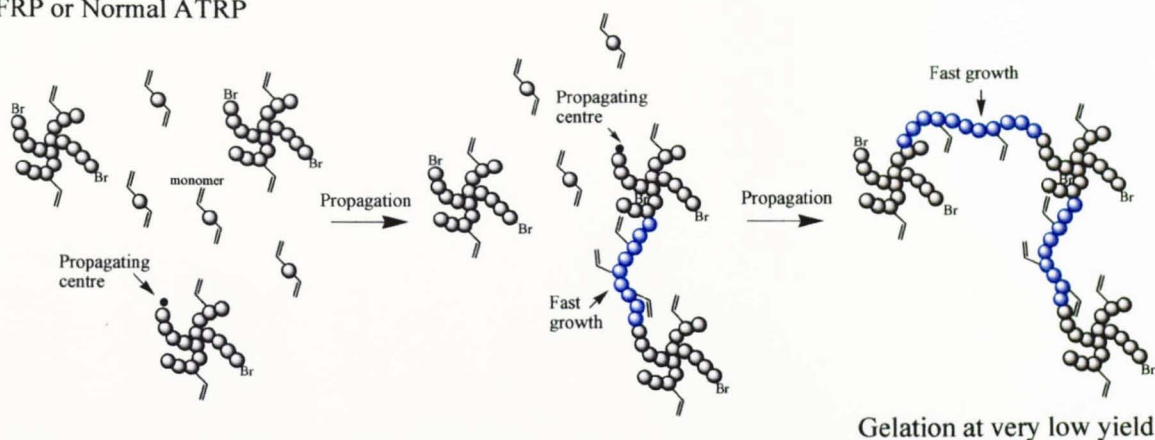
In this thesis, a facile and versatile approach is developed to the formation of highly branched polymer architectures through deactivation enhanced polymerisation of multifunctional vinyl monomer. This strategy overcomes the published limitations, and most importantly, there is no restriction on the concentration of multifunctional vinyl monomer. Indeed, the multifunctional vinyl monomers can even be homopolymerised to form hyperbranched polymer structures rather than cross-linked networks. The key is to find a method for slow growth of each independent and complex hyperbranched molecule

that avoids crosslinking. Wang *et al.* realised that by controlling the competition between chain growth and reversible chain termination via a deactivation enhanced method, hyperbranched polymers can grow effectively. In this strategy, branching is introduced by multifunctional vinyl monomer in a controlled fashion. Also, gelation is prevented, which leads to hyperbranched polymers. The deactivation enhanced process can be achieved by manipulating the equilibrium to increase the deactivation rate and decrease the activation rate. Thus, the deactivation reaction slows down the growth rate of polymer chains. In the case of ATRP, the addition of Cu (II) species to the system slows down propagation.

The different mechanisms of homopolymerisation of divinyl monomer in the concentrated system via conventional free radical polymerisation (FRP), normal ATRP and DE-ATRP are shown in the Figure 2.2. In the FRP reaction, the propagating free radical grows very quickly without control, since hundreds of vinyl groups (large growth range, Figure 2.2) are reacted with the propagating centre (See kinetics simulation, Chapter 1, Table 1.4). Thus, very high MW polymers were produced at the very beginning of reaction (Upper, Figure 2.2). Consequently, these large molecules can easily form intermolecular crosslinking because these species have more pendant vinyl groups and potentially propagating centre. Once the intermolecular cross-links were formed, the whole reaction turned to gel quickly.^{7, 8}

In normal ATRP, the propagation process was controlled by activation-deactivation equilibrium, and only several vinyl groups were reacted with the propagating centre via each cycle. However, this level of control is not good enough to suppress the gelation. Under normal condition, gelation normally occurs at below 10-15% conversion in the homopolymerisation of divinyl monomers via normal ATRP.^{9, 10}

FRP or Normal ATRP



DE-ATRP

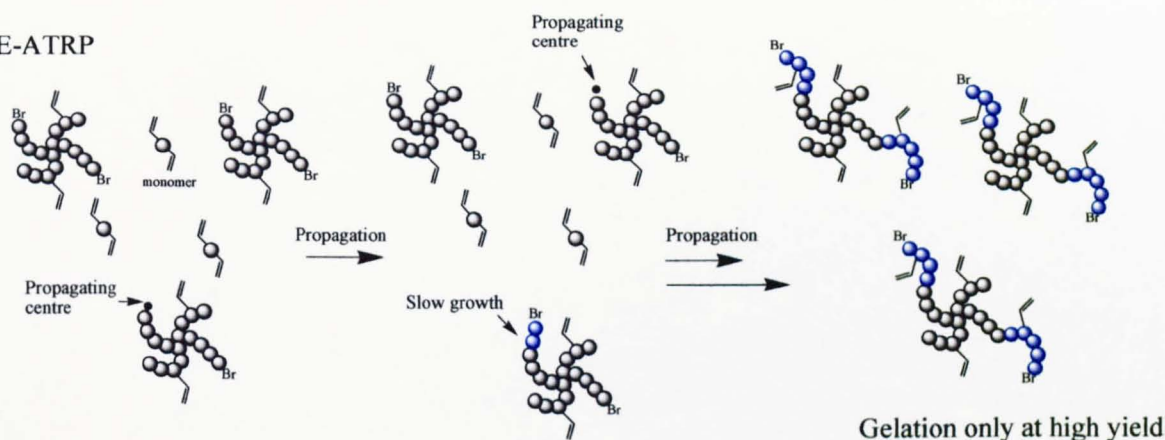


Figure 2.2 Mechanism of deactivation enhanced ATRP (DE-ATRP) to achieve hyperbranched polymer in the homopolymerisation of divinyl monomer. In contrast, the free radical polymerisation (FRP) or normal ATRP reaction will lead to gelation at very low conversion.

In the DE-ATRP reaction, there are two key factors to suppress the gelation in the homopolymerisation of divinyl monomer. Firstly, the DE-ATRP provides much better control over the polymerisation because of the high deactivation rate caused by the added Cu^{II} . In this process, the equilibrium was established between the large numbers of dormant chains and just a few active propagating chains. This situation ensures that only very few vinyl groups are incorporated into the polymer chains during each activation-deactivation cycle (See the kinetics simulation, Table 1.4, Section 1.2.9, Chapter 1). Thereafter, the propagating centre becomes a dormant species quickly and stays for a longer time in the dormant state than normal ATRP. During the dormant period,

the propagating centre cannot grow. Meanwhile, the monomers can easily diffuse into the branched polymer chain during the very long dormant period in DE-ATRP. This results in the probability of reaction of different vinyl species (*eg.* in monomer, same polymer chain or other polymer chain) being statistically determined by their local concentrations at propagating centre. In the DE-ATRP, the number of monomer added is limited to a very few units during each cycle (Figure 2.2). Thus, if one considers a given propagating centre, the deactivation enhanced process increases the probability for monomer consumption and intramolecular crosslinking. In contrast, the intermolecular cross-linking is suppressed, since the local concentration of pendant vinyl groups belonging to other macromolecules is negligible when compared with the concentration of monomer or pendant vinyl groups in the same chain (Bottom, Figure 2.2). Secondly, the molecular weight of polymer increases with monomer conversion due to slow growth. Therefore, high molecular weight polymers form only at the higher conversion region of the reaction. In conclusion, the possibility of intermolecular crosslinking is increased with the conversion of monomers in DE-ATRP. Therefore, the hypothesis is that DE-ATRP cannot eliminate gelation, but can postpone it such that it will not occur until high monomer conversion.

Furthermore, the different gelation processes between FRP, normal ATRP and DE-ATRP in the concentrated system are shown in Figure 2.3. In the FRP and normal ATRP, the reaction gels at very low conversion due to fast propagation. On the other hand, the polymers prepared by DE-ATRP indicate the remarkable differences from the gel produced via FRP or normal ATRP (Figure 2.3). At low conversion, short polymer chains or oligomers are formed due to the relatively high monomer concentration at the beginning of the reaction. Also, the branched polymers are formed by the branching reaction between the linear chains (Figure 2.4). At moderate conversion, the molecular weight of branched polymers is increased via linear propagation. Meanwhile, the pendant vinyl groups in the same polymer chains are consumed via intramolecular cyclisation reactions (Figure 2.4). Thus, the number of branching points increases significantly during the reaction. Finally, the large macromolecules will form a gel via intermolecular

cross-linkings at high yield (around 60% yields), since the concentration of polymer chains is relatively high and the contribution of intermolecular crosslinking becomes significant at the high yield (Figure 2.4).

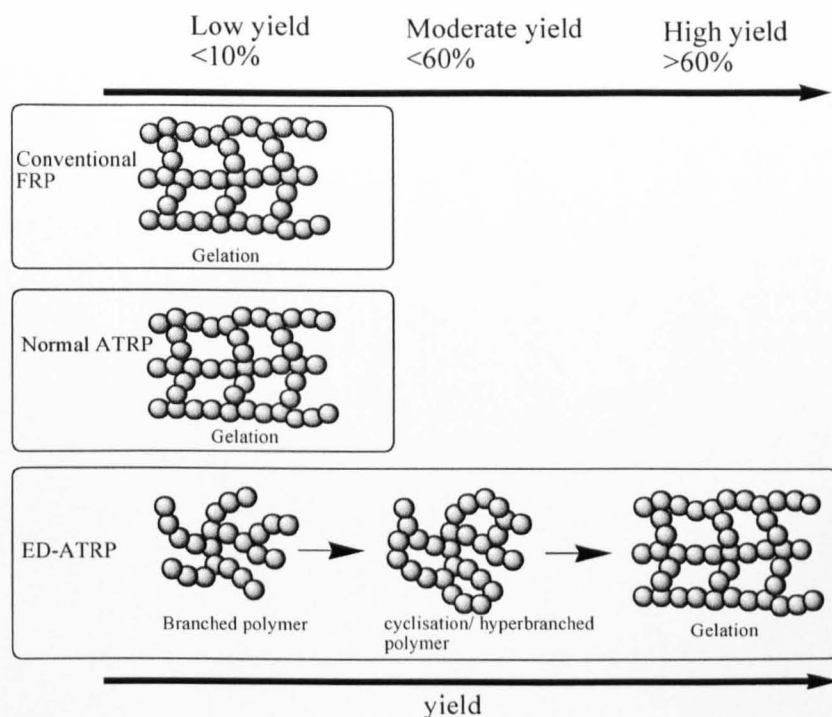
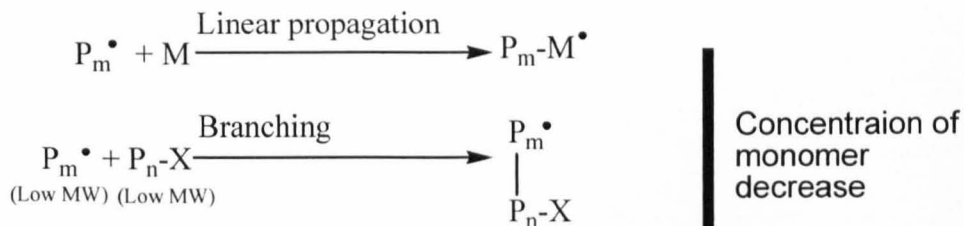
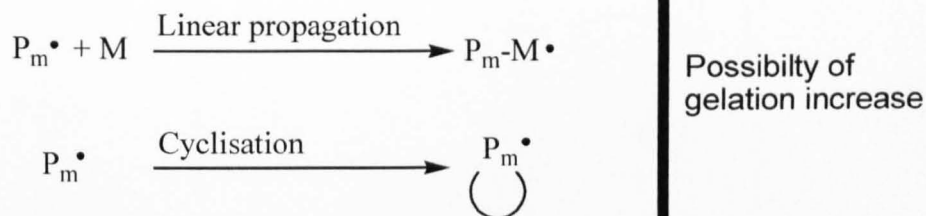


Figure 2.3 Different gelation processes of the homopolymerisation of divinyl monomer between FRP, normal ATRP and deactivation enhanced ATRP (DE-ATRP). In the latter case, gelation does occur, but is postponed until high yield is achieved (*i.e.* >60%)

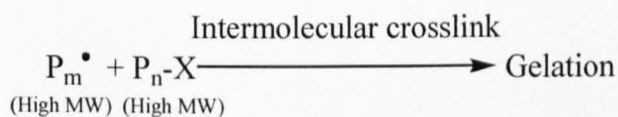
Low conversion



Moderate conversion



High conversion



M=monomer
P=polymer chain
X=halogen

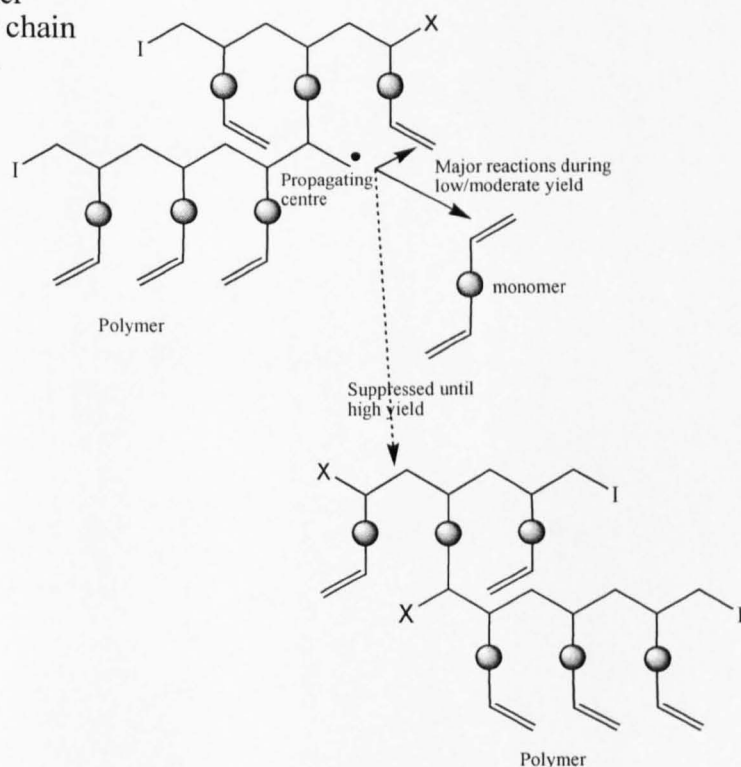


Figure 2.4 Scheme of the contributing reactions at different conversion in the homopolymerisation of divinyl monomer via DE-ATRP.

The differences between FRP (in concentrated and diluted system) and DE-ATRP are summarised in Table 2.1. In the concentrated FRP system, the macroscopic gelation occurs at low conversion due to the high molecular weight and uncontrolled intermolecular cross-linkings. In the diluted FRP system, the macroscopic gelation is suppressed, since the intermolecular cross-linking is suppressed by dilution condition. In the DE-ATRP system, the macrogel is suppressed by the low molecular weight and kinetically controlled intermolecular crosslinking until high monomer conversion.

Table 2.1 The different gelation process between FRP (in concentrated and diluted system) and DE-ATRP route. The macroscopic gelation is controlled by molecular weight and intermolecular crosslinking in polymerisation.

Method	Molecular weight	Intermolecular crosslinking	polymer architecture	
			low conversion	high conversion
FRP (concentrated)	High at beginning of reaction	uncontrolled	Gelation	
FRP (diluted)	High at beginning of reaction	suppressed by dilution	Microgel	Microgel
DE-ATRP (concentrated)	Low at beginning, increased with conversion	suppressed by kinetics	Hyperbranched or Microgel	Gelation

2.1.3 Deactivation Enhanced Strategy in Other Controlled/Living Polymerisations

Thus, the recognition that kinetic effects are an important factor in free radical polymerisation provided an important conceptual breakthrough. The idea now is to test in this theory and to see if deactivation enhanced strategy can influence the onset of gelation. The key to suppress the intermolecular crosslinking by kinetics control is not decreasing the total polymerisation rate (R_p) but the number of growth units per activation-deactivation cycle (kinetic chain length in ATRP). In DE-ATRP, the kinetic chain length ($v_{ED-ATRP}$) is proportional to the constant of propagation (k_p) and concentration of monomer ($[M]$), and inversely proportional to constant of deactivation (k_{deact}) and concentration of Cu^{II} ($[Cu^{II}]$) (Eq. 2.1, also see Eq. 1.30, Chapter 1).

$$v_{ED-ATRP} = \frac{R_p}{R_{deact}} = \frac{k_p[M][P^*]}{k_{deact}[P^*][Cu^{II}]} = \frac{k_p[M]}{k_{deact}[Cu^{II}]} \quad (\text{Eq. 2.1})$$

Furthermore, the deactivation enhanced strategy can be applied to other controlled/living polymerisations. For example, the kinetic chain length in RAFT (v_{RAFT} , Eq. 2.2) is proportional to the constant of propagation (k_p) and concentration of monomer ($[M]$), and inversely proportional to constant of chain transfer (k_{cs}) and concentration of RAFT agent ($[RAFT]$). Thus, the intermolecular cross-linking could be suppressed by choosing RAFT agent with higher chain transfer constant or adding excess RAFT agent initially.

$$v_{RAFT} = \frac{R_p}{R_{chain\ transfer}} = \frac{k_p[M][P^*]}{k_{cs}[P^*][RAFT]} = \frac{k_p[M]}{k_{cs}[RAFT]} \quad (\text{Eq. 2.2})$$

The scheme (Figure 2.5) outlines the homopolymerisation of divinyl monomer via DE-ATRP route. First, the vinyl monomer (A) is selected with a catalyst system (B) where I^\bullet is capable of initiating the polymerisation of vinyl monomer (e.g., by means of radical, cationic, group transfer, or ligated anionic polymerisation) to produce a multi-vinyl macromonomer chain (C). Catalyst (X) can establish an equilibrium

between the active macromonomer chain (C) and dormant macromonomer chain (D). The dormant species (D) can be converted to the active species (C) by thermal, photochemical or chemical stimulation. In this way, all of the growing macromolecules are subject to a rapid equilibrium between active and dormant states; a reversible activation (deactivation) equilibrium. Unlike normal propagations whereby monomers are sequentially added into a polymer chain, here, the active species (C) can undergo two different mechanisms of propagation: either linear chain growth (E) by simple addition of monomer to the existing chain, or formation of branched polymer chains by addition of multi vinyl macromonomer into the growing chain (F). The crucial problem is that in both cases, the deactivation enhanced strategy allows very short and controlled growth of the polymer chains during each cycle. As a result, cross-linking reactions are suppressed efficiently. At low monomer conversion rates, statistics dictate the formation of predominantly polymer chains with moderate branching. However, at higher monomer conversion rates, highly branched structures are formed due to the increased participation of multi-vinyl macromonomers in the reaction. Hence, at high monomer conversion the reaction is driven towards the formation of highly branched species (Figure 2.5).

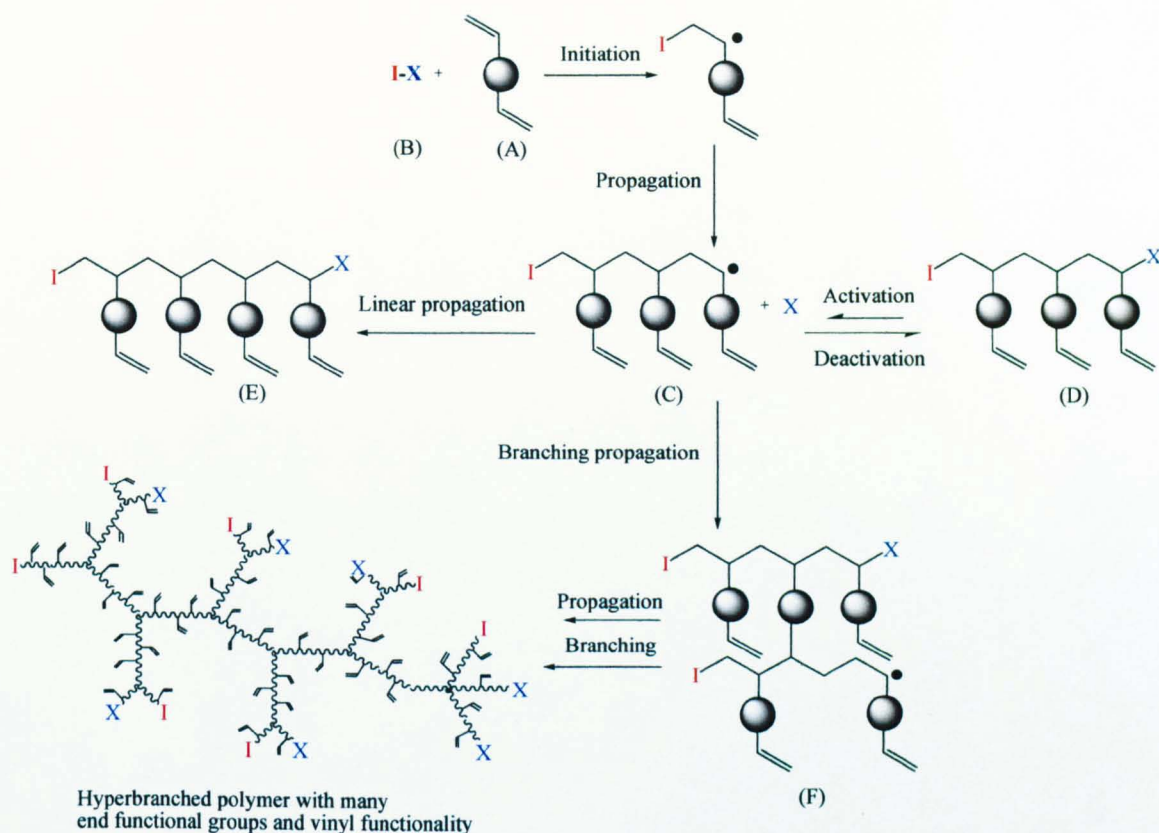


Figure 2.5 Strategy for reversible activation (or deactivation) controlled hyperbranched polymerisation process (I=initiator, X=halogen).

The work in this chapter will show the DE-ATRP strategy by synthesising highly branched poly(DVB) and poly(EGDMA) with a multiplicity of reactive functionalities such as vinyl and halogen functional groups. The only key restriction on the process to prevent the manufacture of insoluble gels is that the overall conversion of monomer to polymer is limited to less than 60%.

2.2 Experimental

2.2.1 Materials

DVB and EGDMA monomer (Aldrich) were purified by passing through a column of activated basic alumina (ACROS) and purged with high-purity nitrogen for 1 hour prior to use. Initiator stock solution was prepared from methyl 2-bromopropionate or methyl 2-chloropropionate (Aldrich) with 2-butanone (99.5+%, HPLC grade, Aldrich). The

concentration of the methyl 2-bromopropionate or methyl 2-chloropropionate was 0.815 mol L⁻¹. The initiator solution and was degassed by high-purity nitrogen. 2, 2'-bipyridine (Bpy, Aldrich), copper (I) bromide (98%, Aldrich), copper (II) bromide (98%, Aldrich), copper (I) chloride (98%, Aldrich) and copper (II) chloride (99%, Lancaster) were used as received. Nitrogen was bubbled through the solutions in order to eliminate molecular oxygen. Liquids were transferred under nitrogen by means of septa and syringes or stainless steel capillaries.

Divinylbenzene is produced from the catalytic dehydrogenation of diethylbenzene resulting in a mixture of ethylvinylbenzene (EVB) and DVB isomers. Thus, it should be considered that 19% complementary ethylvinylbenzene is included in these DVB products from the manufacturer instruction (Table 2.2).

Table 2.2 The contents of isomer in the DVB monomer provided by manufacturer (Sigma-Aldrich).

	EVB	DVB
mole ratio	19%	81%
(%)	para-EVB: meta-EVB= 1:2.3	para-EVB: meta-EVB= 1:2.3

Moreover, the mole ratio of EVB was determined by the ¹H NMR spectroscopy (Figure 2.8) and Eq. 2.3. It was confirmed that 18% mole ratio of EVB were included in the DVB monomer. These contents of mono-vinyl monomers (EVB) will be considered in the calculation of branching ratio.

$$\begin{aligned}
 \text{EVB mole ratio (\%)} &= \frac{\text{EVB}}{\text{DVB} + \text{EVB}} \\
 &= \frac{\text{Integrals of } e/2}{\frac{\text{Integrals of } c - (\text{Integrals of } e/2)}{2} + (\text{Integrals of } e/2)} \times 100\% \\
 &= 18\% \qquad \qquad \qquad (\text{Eq. 2.3})
 \end{aligned}$$

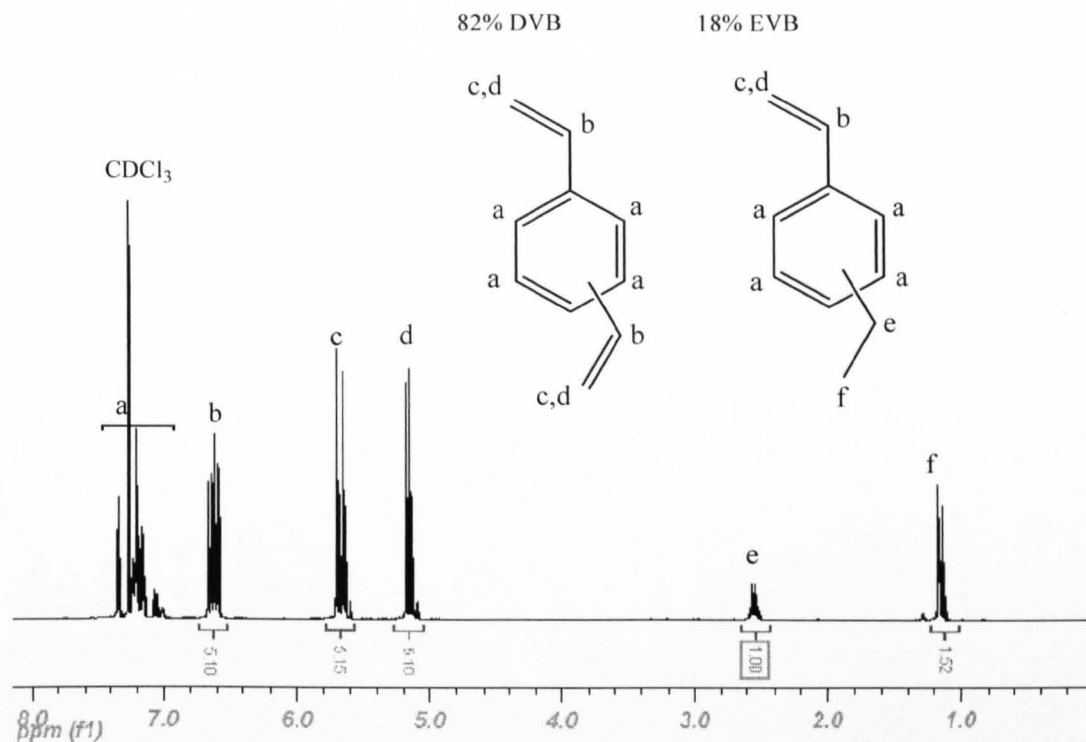


Figure 2.6 ^1H NMR spectroscopy of the divinylbenzene monomer in CDCl_3 at 300 MHz.

2.2.2 Polymerisation Procedure

Homopolymerisation of DVB

Known amounts of CuBr , CuBr_2 and 2,2'-bipyridine (Bpy) were added to a round bottom flask fitted with a three-way stopcock connected to either a nitrogen line or a vacuum pump. Oxygen was removed by repeated vacuum-nitrogen cycles. Once filled with nitrogen, the flask was filled with known amounts of degassed DVB and toluene. After stirred for one hour at room temperature, a known amount of methyl 2-bromopropionate was added, and the polymerisation was conducted at the desired temperature. Followed with polymerisation under stirring at the chosen reaction temperature (typically $90\text{ }^\circ\text{C}$) for the desired reaction time, the solution was diluted with THF and precipitated into a large excess of methanol. After separated by filtration, the polymer was dried under reduced pressure at $30\text{ }^\circ\text{C}$ and weighed in order to calculate the monomer conversion.

An example for the deactivation enhanced ATRP of DVB in toluene (Entry 4, Table 2.3).

CuBr (354 mg, 2.46×10^{-3} mol), CuBr₂ (183 mg, 8.19×10^{-4} mol) and 2,2'-bipyridine (1.03 g, 6.57×10^{-3} mol) were added to a round bottom flask fitted with a three-way stopcock connected to either a nitrogen line or a vacuum pump. Oxygen was removed by repeated vacuum-nitrogen cycles. Once filled with nitrogen, the flask was filled with degassed DVB (50 ml, 0.351 mol) and toluene (50 ml). After stirring for one hour at room temperature, 7.6 ml of 0.815 mol/L methyl 2-bromopropionate/butanone solution was added (6.16×10^{-3} mol), and the polymerisation was conducted at the 90 °C. The samples were taken at 4, 6, 10, 18 and 28 hours. Finally, the polymer solution gelled at 30 hours. The polymer sample was diluted with THF and precipitated into a large excess of methanol. Finally, the polymer product was characterised by ¹H NMR, ¹³C NMR, GPC-MALLS, DLS and viscometer.

An example for the deactivation enhanced ATRP of DVB in cyclohexanone (Table 2.8).

The reproducibility data show the gel points of DVB in toluene are variable even at the same condition, since the solubility of copper/Bpy complex is poor in non-polar solvent. Thus, an alternative cyclohexanone system was developed to overcome this disadvantage. An example for the deactivation enhanced ATRP of polyDVB in cyclohexanone was conducted as below (Table 2.8). CuBr (354 mg, 2.46×10^{-3} mol), CuBr₂ (183 mg, 8.19×10^{-4} mol) and 2,2'-bipyridine (1.03 g, 6.57×10^{-3} mol) were added to a round bottom flask fitted with a three-way stopcock connected to either a nitrogen line or a vacuum pump. Oxygen was removed by repeated vacuum-nitrogen cycles. Once filled with nitrogen, the flask was filled with degassed DVB (50 ml, 0.351 mol) and cyclohexanone (50 ml). After stirring for one hour at room temperature, 7.6 ml of 0.815 mol/L methyl 2-bromopropionate/butanone solution was added (6.16×10^{-3} mol) into reaction, and the polymerisation was conducted at the 60 °C. The samples were taken at 4, 8, 16, 24, 32, 40, 48 and 56 hours. Finally, the polymer solution gelled at 57 hours. The polymer sample was diluted with THF and

precipitated into a large excess of methanol. Then, the polymer product was characterised by ^1H NMR, GPC-MALLS and viscometer.

Homopolymerisation of EGDMA

Known amounts of CuCl / CuCl_2 and Bpy were added to a round bottom flask fitted with a three-way stopcock, which was connected to either a nitrogen line or a vacuum pump. Oxygen was removed by repeated vacuum-nitrogen cycles. Once filled with nitrogen, the flask was charged with known amounts of degassed EGDMA and THF, and stirred at room temperature for one hour. Then, a known amount of methyl 2-chloropropionate was added, and the polymerisation was conducted at the desired temperature under stirring. After the desired polymerisation reaction time, the solution was diluted with THF and precipitated into a large excess of hexane. After separation by filtration, the polymer was dried under reduced pressure at 30 °C and weighed to calculate the yield.

An example for the deactivation enhanced ATRP of EGDMA in THF (Entry 5, Table 2.10).

CuCl (89 mg, 9.03×10^{-4} mol), CuCl_2 (41 mg, 3×10^{-4} mol) and 2,2'-bipyridine (376 mg, 2.4×10^{-3} mol) were added to a round bottom flask fitted with a three-way stopcock connected to either a nitrogen line or a vacuum pump. Oxygen was removed by repeated vacuum-nitrogen cycles. Once filled with nitrogen, the flask was filled with degassed EGDMA (50 ml, 0.24 mol) and THF (146 ml). After stirring for one hour at room temperature, 6 ml of 0.815 mol/L methyl 2-chloropropionate/butanone solution was added (4.8×10^{-3} mol), and the polymerisation was conducted at the 60 °C. The samples were taken at 2, 3.8, 10.5, 21.5 and 29 hours. Finally, the polymer solution gelled at 30.5 hours. The polymer sample was diluted with THF and precipitated into a large excess of cold hexane. Then, the polymer product was then be characterised by ^1H NMR, DLS and GPC-MALLS.

2.2.3 Characterisation of Hyperbranched Polymers

Gel Permeation Chromatography (GPC) Characterisation

Number average molecular weight (M_n), weight average molecular weight (M_w) and polydispersity (M_w/M_n) were obtained by Gel Permeation Chromatography (PL-120, Polymer Lab) equipped with an RI detector. The columns (30 cm PLgel Mixed-C, 2 in series) were eluted by THF and calibrated with polystyrene standards. All calibration and analyse were performed at 40 °C and a flow rate of 1 mL/min. All of the products easily dissolve in THF, and pass through 0.2 μ m filter before injection with little or no backpressure observed – demonstrating the absence of gelation.

Multi-angle Laser Light Scattering-Gel Permeation Chromatography (MALLS-GPC)

The instrument package was supplied by Wyatt and comprised the following equipment: (i) a Jones Chromatography 760 series Solvent D-Gasser, (ii) a Waters 515 HPLC pump operating at room temperature, (iii) a Jasco AS-950 autosampler with 50 position sample racks, (iv) a column oven, (v) a set of 30 cm PLgel Mixed-C, 2 in series, and (vi) detector connected in a serial configuration: a multi-angle laser light scattering detector (mini-Dawn) supplied by Wyatt Technology. The Astra software package for Windows was used to process the data from the detector systems to produce the weight average molar mass, radius of gyration and molar mass *versus* elution volume plots.

NMR Analysis of the Polymers

^1H NMR spectroscopy analysis was carried out on a 300 MHz Bruker NMR with MestRecTM (Mestrelab Research SL) processing software. The chemical shifts were referenced to the lock CDCl_3 .

The chemical shift data of poly(DVB) are summarised as follows: δ ppm 0.6-3.2 (backbone CH_2 , a; CH, b), 3.3-3.6 (end backbone CH, h), 4.4 (initiator terminal $-\text{OCH}_3$, g), 4.8-6.0 (vinyl $\text{C}=\text{CH}_2$, c, d), 6.1- 7.25 (CH, e; CH, f), 7.26 (solvent). (See Figure 2.12)

The chemical shift data of poly(EGDMA) are summarised as follows: δ ppm 0.90-1.40 (backbone CH_3), 1.91 (terminal CH_3), 2.18 (backbone CH_2), 4.05-4.43 ($\text{O}-\text{CH}_2\text{CH}_2-\text{O}$), 5.60 (terminal $\text{C}=\text{CH}_2$), 6.12 (terminal $\text{C}=\text{CH}_2$), 7.26 (solvent). From the ^1H NMR spectrum, the ratio of branched EGDMA units was calculated by comparison of the integrals of the peaks for the backbone protons (a,b) and vinyl protons (c,d). (See Figure 2.28)

Quantitative ^{13}C NMR analysis was carried out in a Bruker AV(III)500 at 125.769 MHz for ^{13}C nuclei. The samples were spun at 298K using a Bruker dual $^{13}\text{C}/^1\text{H}$ Cryoprobe with z-gradients. ^{13}C Quantitative NMR is operated with a relaxation delay of 5s and acquisition of 2.6s, so the pulse repetition rate is 7.6s in the analysis. The pulse sequence used is zgig30 and ^{13}C inverse-gated with ^1H decoupling at a 30 degree flip angle. The spectra were recorded by 8192 times of scans with 128 dummy scans to allow equilibration (see Figure 2.14 and Figure 2.30).

Dynamic light scattering (DLS)

The size distribution of linear polystyrene and hyperbranched poly(DVB) were measured by employing dynamic light scattering via Zetasizer nano series (Malvern Instruments Ltd). The polystyrene standard sample is used as received, the molecular weights were 5000, 9800, 21000, 39000, 72200, 151700, 325000 respectively and PDI for each are less than 1.1 (Polymer laboratories). The scattering angle was fixed at 90 degrees, and the measurements were recorded at a constant temperature 20 °C. Each sample was filtrated through a 0.2 μm filter directly into a pre-cleaned quartz cuvette. The sample concentration was maintained at 1 mg/ ml in the case of M_w less than 50,000, and maintained at 0.5 mg/ml in the case of M_w more than 50,000.

2.3 Results and Discussion

2.3.1 Synthesis and Characterisation of Hyperbranched poly(divinylbenzene)

In this section, different reaction conditions were examined for the deactivation enhanced ATRP of divinylbenzene, especially the ratio of Cu(I) to Cu(II), in order to probe the effect on the polymerisation kinetics, branching degree and final gel point.

The polymerisation rate of ATRP is first order with respect to the concentration of monomer ($[M]$) and constant of propagation (k_p), and inversely proportional to Cu (II) concentration ($[Cu(II)]$) (Eq. 2.1) ^{11, 12}. Thus, control over the polymerisation rate should be obtained by manipulating the feed ratio of Cu(I) /Cu(II). An increase in the concentration of Cu (II) relative to Cu (I) pushes the equilibrium towards the deactivated state. As the ratio of propagation to deactivation decreases, fewer monomer units are added to an active centre before being deactivated, resulting in slow growth of polymer chains. From the results, this deactivation enhanced ATRP leads to the preparation of soluble hyperbranched polymers rather than cross-linked gels provided the overall conversion of monomer to polymer is limited to less than 60%.

For polymerisation of DVB in toluene, the absence of Cu (II) species (Entry 1 and 3, Table 2.3) leads to two observable effects on the polymerisation. The first is that under certain conditions more rapid polymerisation was achieved due to the reduced deactivation levels being applied. Second, the systems quickly lead to insoluble gels in all cases. Thus at low conversions in these conventional ATRP reactions the synthesis of hyperbranched species is observed in these systems. The GPC data reported in Table 2.3 refer to these hyperbranched species isolated at these low yield points in the experiments (Entry 1 and 3). However, as the synthesis progresses it is noted that at yields above 20–25% the systems completely gel making further reaction and analysis by GPC

impossible. The highest yield of soluble polymer that can be achieved under these conditions was only *ca.* 20%. Adding Cu (II) enhances the rate of deactivation; the polymerisation rate is significantly decreased and high yields of soluble hyperbranched polymer are obtained with controlled molecular weight (Entry 2, 4 and 5, Table 2.3).

Table 2.3 Homopolymerisations of DVB by deactivation enhanced ATRP. A high ratio of Cu (II)/ Cu (I) slows significantly the reaction rate leading to high yields of hyperbranched polymer without formation of gels. Reaction conditions: [DVB] = 3.51 M, [Cu(I)+Cu(II)]/[Bpy] = 1:2, all polymerisations were conducted under nitrogen in toluene at 90 °C.

Reaction	DVB: [I]: Cu(I) : Cu(II) Feed ratio (mol)	Time	GPC-RI results		Yield ^b (%)
			M _n (g mol ⁻¹)	M _w /M _n	
1	57: 1: 0.5: 0	5 hrs	14,000	8.5	20.7
2	57: 1: 0.5: 0.167	17 hrs	10,500	4.9	49.5
3	57: 1: 0.4: 0	6 hrs	14,200	22.7	21.5
4	57: 1: 0.4: 0.133	28 hrs	13,600	20.2	61.6
5	57: 1: 0.4: 0.2	32 hrs	6,700	3.2	27.1
6	57: 1: 0.25: 0.25	36 hrs	3,900	1.7	16.6
7 ^a	57: 1: 0: 0	5 mins	Gel		

a. Reaction 7 is a normal radical solution polymerisation using azobisisobutyronitrile (AIBN) as initiator.

b. calculated gravimetrically

A kinetic plot (Figure 2.7) shows the evolution of these ATRP controlled reactions. Significantly the kinetics demonstrates that the yields can be pushed to high levels e.g. 61.6% (Entry 4, Table 2.3). However, the addition of too much Cu (II) with respect to Cu (I) over suppresses the polymerisation (Entry 5 and 6, Table 2.3) giving only low yields. Despite the very long reaction time, cross-linking was not observed, a point which is

further emphasised by comparison of entry 3 and 4. The reaction without Cu(II) leads to gels at very low conversion at 6 hours, which compare to the reaction with Cu(II) no gel until 28 hours and high yield. Clearly, cross-linking and gel formation does eventually occur in these systems, but only when the yield beyond 60% (Table 2.3 and Figure 2.7).

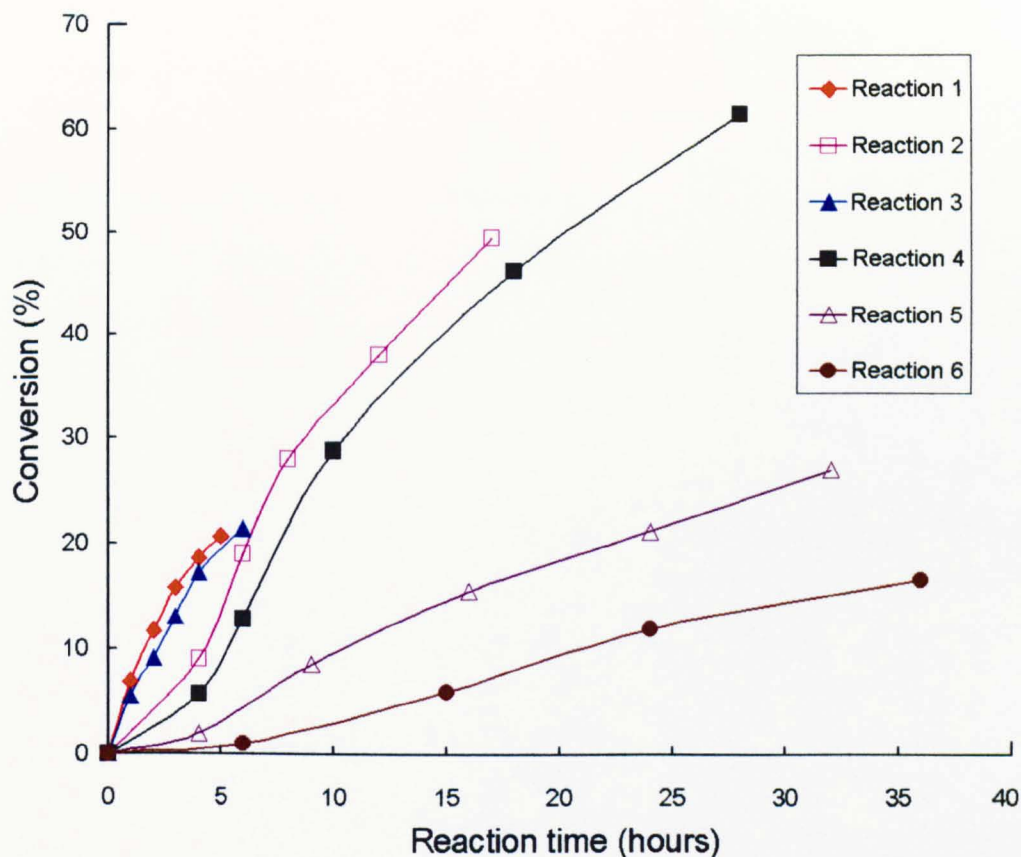


Figure 2.7 The time dependence of monomer conversion during ATRP of DVB (Table 2.2). The reaction of deactivation enhanced ATRP (Entry 4, Table 2.2) revealed that the polymer do not gel until 61% yield at 28 hours.

The molecular weight evolution of the entry 4 was studied in more detail by collecting samples throughout the reaction (Table 2.4). GPC traces (Figure 2.8) obtained by refractive index (RI) and multi-angle laser light scattering (MALLS) detectors clearly show an increase in molecular weight and broadening of polydispersity with reaction time. These data provide sound evidence for formation of hyperbranched poly(DVB). Initially,

statistics dictate the formation of predominantly polymer chains with moderate branching, and the molecular weight distribution should be narrow at low monomer conversion ($PDI_{RI}=1.26$ and $PDI_{MALLS}=1.29$ at 4 hours). As the reaction progresses, both molecular weight and polydispersity increase dramatically because of the increased participation of multi-vinyl macromonomers at high monomer conversion ($PDI_{RI}=20.2$ and $PDI_{MALLS}=6.07$ at 28 hours). This result also indicates why the conversion restriction is important in this synthetic method. At below 60% yield, the balance of reaction is preferred to polymerise with monomer or small molecular due to the steric bulk and molecular mobility effects. However above this conversion threshold, the barriers to large molecules combining significantly reduced thus allowing gel formation to occur.

Table 2.4 Detailed data of hyperbranched DVB samples of reaction 4 collected at different times, Reaction conditions: [DVB] = 3.51 M, [DVB]: [I]: Cu(I):Cu(II) = 57:1:0.4:0.133, [Cu(I)+Cu(II)]/[Bpy] = 1:2, in toluene at 90 °C.

Sample	Reaction time (hrs)	Yield ^a (%)	GPC-RI results			GPC-MALLS results			Degree of branching ^b
			M_n (g mol ⁻¹)	M_w (g mol ⁻¹)	M_w/M_n	M_n (g mol ⁻¹)	M_w (g mol ⁻¹)	M_w/M_n	
4-1	4	2.7	3,000	3,820	1.3	4,496	5,805	1.3	0.16
4-2	6	12.8	4,450	7,130	1.6	6,867	12,830	1.9	0.19
4-3	10	28.8	7,800	30,000	3.9	23,040	126,950	5.5	0.24
4-4	18	36.3	11,400	96,100	8.4	103,600	625,400	6.0	0.27
4-5	28	61.6	13,600	275,900	20.2	885,900	5,373,000	6.1	0.28
4-6	30	65	Gelation						

a. calculated gravimetrically

b. Degree of branching is calculated by the ¹H NMR spectroscopy analysis (see Figure 2.12 and Eq. 2.11)

The data shows that the measured MALLS molecular weight is always higher than the RI results, strongly supporting formation of a hyperbranched architecture¹³. Further, the RI and MALLS data for the sample Entry 5 (Table 2.4 and Figure 2.8) demonstrate a significant issue encountered in the analysis of the materials produced in this programme of work. It is clear from comparison of the GPC and MALLS data that there is a significant difference in the measured M_w and PDIs for the same sample from these differing detector systems¹⁴⁻¹⁶. This is very likely to be due to the highly branched nature of the structures being produced. It is believed that the MALLS data are the more trustworthy and representative of the true M_w of these systems and that the RI system is underestimating the true molecular weights very significantly as a result of three dimensional shapes of the polymers synthesised. Furthermore, the use of GPC column which has operational limits from 2,000 – 2 million Daltons (M_w), has a clear effect upon the data obtained. It is clear from the MALLS data that the material isolated in sample 5 has a significant component above the upper exclusion limit of the system. Thus, it cannot give definitive molecular weight or polydispersity data for this particular sample. It has been included for comparison with the materials sampled at earlier points in the reaction only to demonstrate that the molecular weight of the hyperbranched material is certainly still rising at this point but has not yet become an insoluble gel.

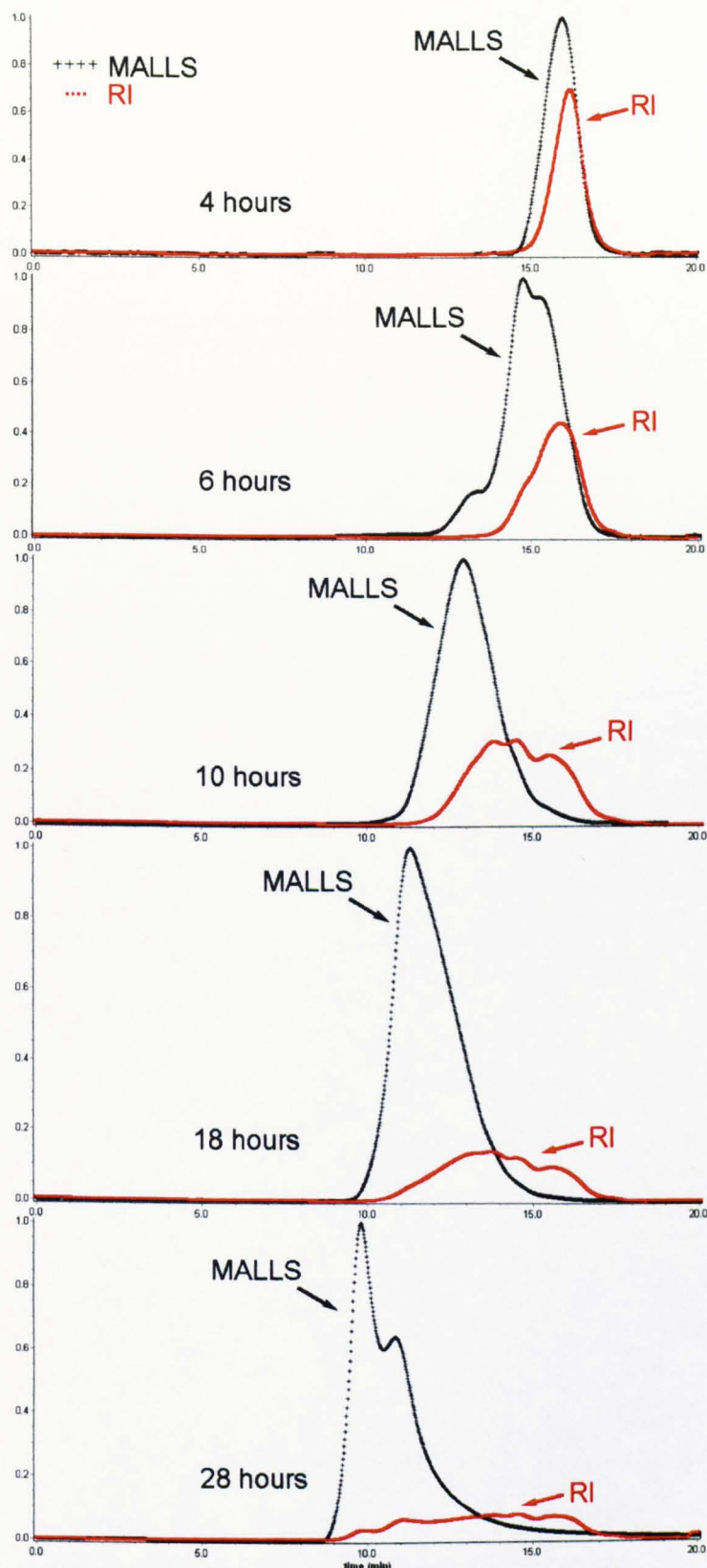


Figure 2.8 MALLS and RI chromatograms for the GPC analysis of poly(DVB) isolated at different reaction times (Table 2.4). The molecular weight and polydispersity clearly show the increase with reaction time, which supports the formation of hyperbranched polymer with controlled chain structure.

The structure of hyperbranched polymer prepared via the homopolymerisation DE-ATRP of divinyl monomers is shown as below (Figure 2.9). A cross-linkage (also referred as branched unit) is formed in the polymer chains via reaction of a pendent vinyl group with a propagating centre. One cross-linkage (or branched unit) consists of two branch points (Figure 2.9). In ATRP, all of the polymer chains should be initiated by the halide alkyl initiator. Thus, there is an initiator fragment at the end of each polymer chain (Figure 2.9). The number of initiator fragments is equal to the number of primary linear chains ($N_{\text{Linear chains}} = N_{\text{Initiators}}$). Statistically, the ratio of the branching units ($N_{\text{Branched units}}$) to the initiators ($N_{\text{Initiators}}$) can generally indicate the structure of highly branched polymer.

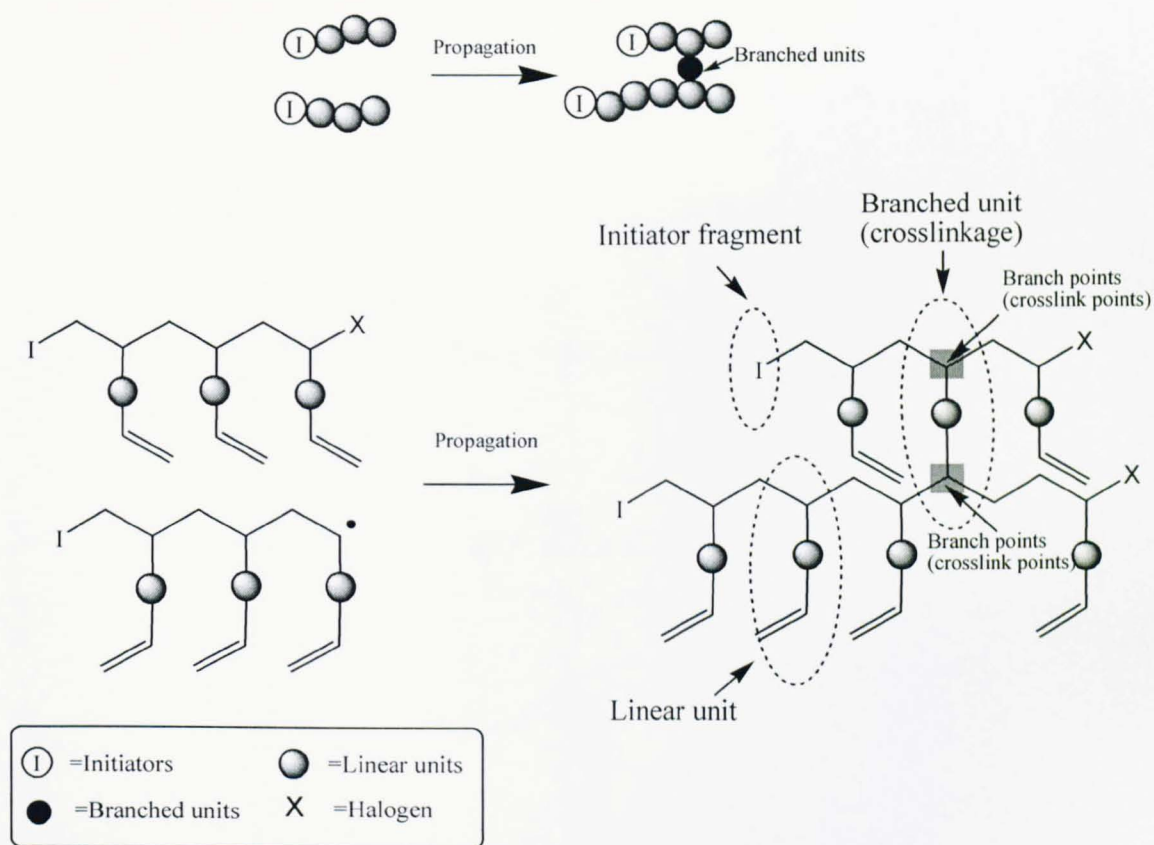


Figure 2.9 The molecular structure in polyDVB. The ratio of branched units to initiators should be below 1 in the ideal hyperbranched polymer. Also, this ratio will be higher than 1 for the cyclic or intramolecular cross-linked polymers.

In ATRP, the branched polymers were formed by the combination of linear polymer chains. From Flory-Stockmayer theory¹⁷⁻²², the critical gelation is one branch point per

primary chain²³. Consequently, Sherrington and Armes have shown that it requires at least (N-1) branched units to form a hyperbranched or cross-linked molecule from N linear chains by divinyl crosslinker.^{2, 5, 24} (Figure 2.10) For the ideal hyperbranched polymer, there is a branched unit between each two linear chains (Figure 2.10 B). Therefore, the number of branching units should be lower than the number of initiators in the ideal hyperbranched polymer (Eq. 2.4).

In ideal hyperbranched polymer:

$$N_{\text{Branching units}} = N_{\text{Linear chains}} - 1$$

$$N_{\text{Linear chains}} = N_{\text{Initiators}} \Rightarrow N_{\text{Branching units}} = N_{\text{Initiators}} - 1$$

$$\text{If } N_{\text{initiators}} \gg 1, N_{\text{Branching units}} \approx N_{\text{Initiators}} \Rightarrow \frac{N_{\text{Branching units}}}{N_{\text{Initiators}}} \leq 1$$

For example, in Figure 2.10 C:

$$N_{\text{Branching units}} = 3, N_{\text{Initiators}} = 4$$

$$\frac{N_{\text{Branching units}}}{N_{\text{Initiators}}} = 0.75 < 1 \quad (\text{Eq. 2.4})$$

Formation of ideal hyperbranched polymer

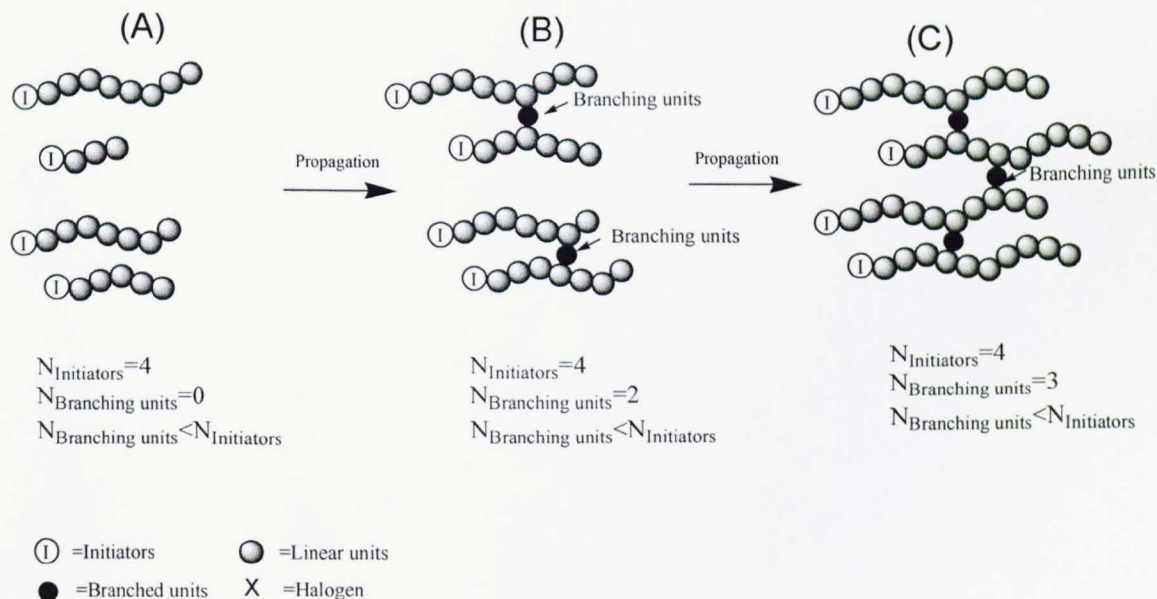


Figure 2.10 Mechanism of an ideal hyperbranched polymer formation via DE-ATRP of divinyl monomer. The ratio of branched units to initiators is lower than 1 in an ideal hyperbranched polymer ($N_{\text{Branching units}} \leq N_{\text{Initiators}}$).

In the cyclic polymer, the branched units between each two linear chains are increased due to the unavoidable intramolecular cross-linkings (Figure 2.11). Therefore, the number of branching units should be higher than the number of primary linear chains. Apparently, the ratio of branching units to initiators should be higher than 1 ($N_{\text{Branching units}}/N_{\text{Initiator}} > 1$) in the cyclic/intramolecular cross-linked polymer (Eq. 2.5). Finally, the cyclisation points can be calculated by Eq. 2.6.

In cyclic/intramolecular cross-linking polymer:

$$\text{All } N_{\text{Branching units}} = N_{\text{Intramolecular crosslinking}} + N_{\text{Intermolecular crosslinking}}$$

$$\text{If } N_{\text{intermolecular crosslinking}} = N_{\text{Linear chains}} - 1 \approx N_{\text{Initiators}}$$

$$N_{\text{Branching units}} = N_{\text{Intramolecular crosslinking}} + N_{\text{Initiators}} \Rightarrow \frac{N_{\text{Branching units}}}{N_{\text{Initiators}}} > 1 \quad (\text{Eq. 2.5})$$

For example, in Figure 2.11 C:

$$N_{\text{Branching units}} = 5, N_{\text{Initiators}} = 4$$

$$\frac{N_{\text{Branching units}}}{N_{\text{Initiators}}} = 1.25 > 1$$

$$N_{\text{Intramolecular crosslinking}} \approx N_{\text{Branching units}} - N_{\text{Initiators}} \quad (\text{Eq. 2.6})$$

Formation of cyclic polymer/ intramolecular crosslinks

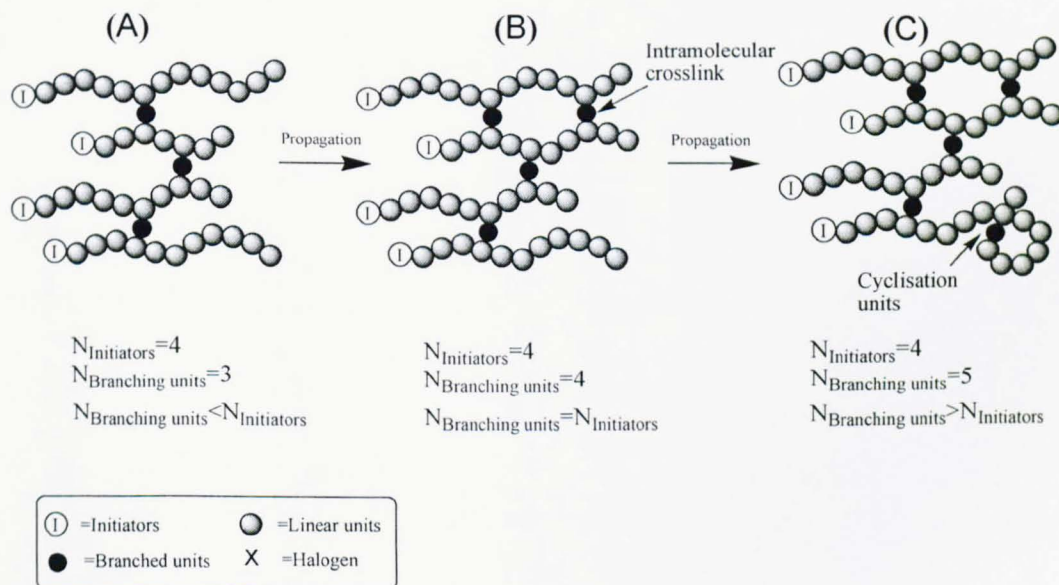


Figure 2.11 Mechanism of the cyclic polymer/intramolecular cross-linkings formation via DE-ATRP of divinyl monomer. The ratio of branched units to initiator is higher than 1 in cyclic polymer due to the unavoidable intramolecular cross-links ($N_{\text{Branching units}} > N_{\text{Initiators}}$).

^1H NMR spectroscopy analysis can confirm the formation of hyperbranched structure for poly(DVB). The presence of a multiplicity of reactive groups (resonance of proton m at 4.5 ppm and c at 3.4 ppm from end functional group, Figure 2.12) and potentially useful vinyl functionalities (resonance of protons h and i from vinyl group at 5-6 ppm, Figure 2.12) is clearly revealed in the ^1H NMR spectra.

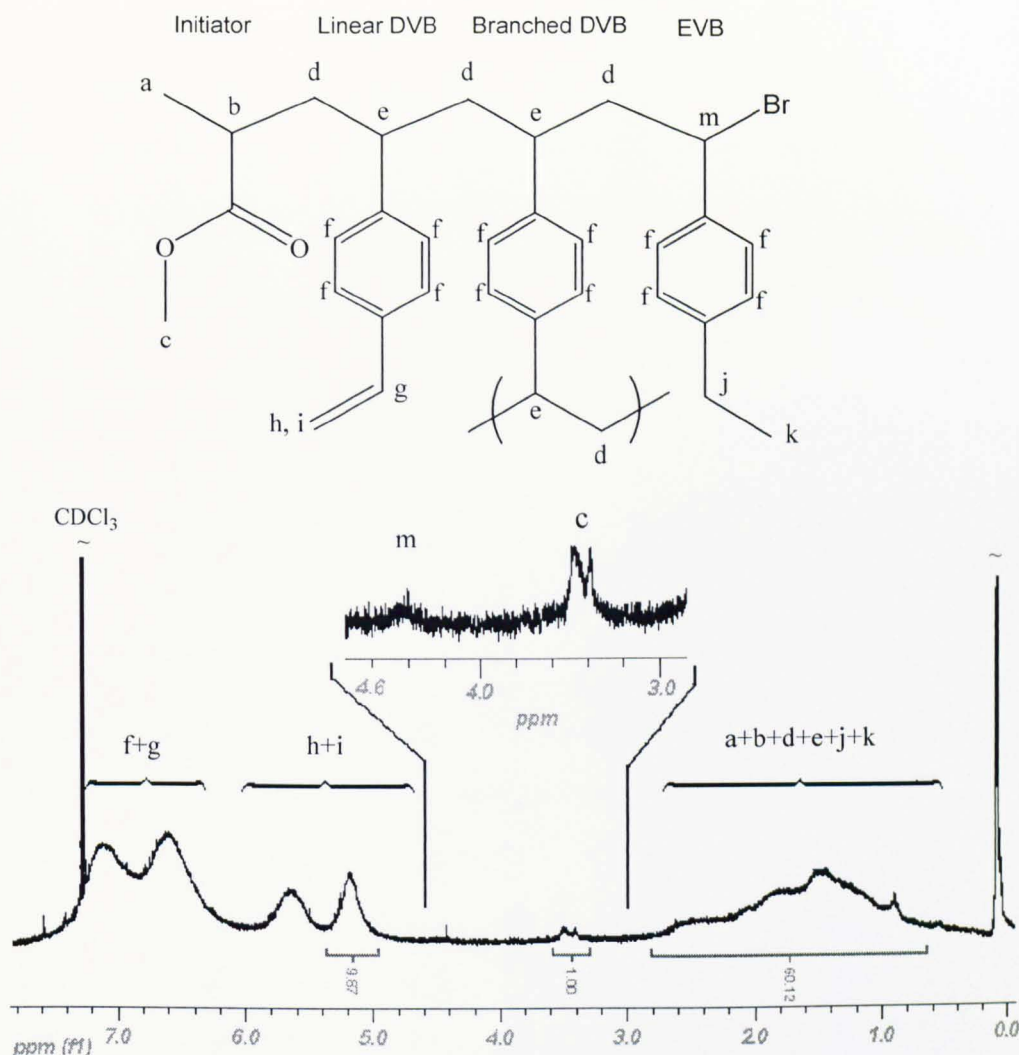


Figure 2.12 ^1H NMR spectrum of hyperbranched poly(DVB) (Entry 5, Table 3.2). Comparison of backbone (d, e) and vinyl (h, i) enables determination of branching ratio. The resonances of protons h, i, c and m show clear presence of vinyl functionalities and terminal functional groups.

Moreover, comparison of the integrals of the backbone and vinyl protons allows an approximation of the ratio of different units in the polyDVB (Eq. 2.7 to Eq. 2.10). First, the resonance of proton c represents the three protons ($-\text{O}-\text{CH}_3$) in initiator (Eq. 2.7).

Second, the resonance of proton h or i represents one proton ($=CH_2$) in a linear DVB unit (Eq. 2.8). It is assumed that the comonomers (DVB and EVB) incorporated in polymer as in the monomer mixture. This assumption has been confirmed by the previous research.²⁵ Therefore, the ratio of EVB to DVB in polymer is 0.22 (0.18/0.82) based on the above assumption (Eq. 2.9). Furthermore, the influence of the *meta*-DVB and *para*-DVB was excluded in the calculation. Thus, the pure *para*-DVB or *meta*-DVB should be used for the further kinetics study in the future (See section 5.2.1, Chapter 5).

Initiator=W, Linear DVB=X, Branched DVB=Y, EVB=Z

Integrals of c= 3W (Eq. 2.7)

Integrals of h= X (Eq. 2.8)

Z= (X+Y)×18/82= 0.22(X+Y) (Eq. 2.9)

Integrals of (0.8-2.6 ppm)=(a and b in initiator)+ (d and e in linear and branched DVB)
+ (j and k in EVB)
=4W+3X+6Y+5Z
=4W+3X+6Y+5×0.22(X+Y)
=4W+4.1X+7.1Y (Eq. 2.10)

The ratio of initiator, linear DVB, branched DVB and EVB units in the polyDVB can be calculated from the above equations. Consequently, the degree of branching (DB_{Frey} , see Eq. 1.36, Chapter 1) can be calculated from Eq. 2.11. Moreover, the cyclisation ratio was defined as the ratio of the cyclisation units to all the units (Eq. 2.12), which the intramolecular crosslinking units were calculated by the Eq. 2.5. It should be noticed that characterisation of the topological structure of hyperbranched polymer by NMR spectroscopy analysis is essentially statistical. The results only represent the macroscopic topology of the overall polymer chains.

$$DB_{Frey} = \frac{2 \times \sum \text{dendritic units}}{2 \times \sum \text{dendritic units} + \sum \text{linear units}} = \frac{2 \times \text{branched DVB units}}{2 \times \text{branched DVB units} + \text{initiator} + \text{linear DVB units} + \text{EVB units}} \quad (\text{Eq. 2.11})$$

$$\text{Cyclisation ratio} = \frac{\text{Intramolecular crosslinking units}}{\text{All units}} = \frac{\text{Branching DVB units-Initiator}}{\text{initiator+linear DVB units+branched DVB units+EVB units}} \quad (\text{Eq.2.12})$$

Here, an example of the calculation for the different unit ratios in the polyDVB (sample 5, Table 2.5 and Figure 2.12) is given as below (Eq. 2.13-Eq. 2.16). The degrees of branching and cyclisation ratio were calculated by Eq. 2.17 and Eq. 2.18, respectively.

$$\text{Initiator}=\text{W}, \text{Linear DVB}=\text{X}, \text{Branched DVB}=\text{Y}, \text{EVB}=\text{Z}$$

$$3\text{W}=1 \quad (\text{Eq. 2.13})$$

$$\text{X}=9.87 \quad (\text{Eq. 2.14})$$

$$\text{Z}=0.22(\text{X}+\text{Y}) \quad (\text{Eq. 2.15})$$

$$4\text{W}+4.1\text{X}+7.1\text{Y}=60.12 \quad (\text{Eq. 2.16})$$

$$\text{W}:\text{X}:\text{Y}:\text{Z}=\text{Initiator: linear DVB: branched DVB: EVB}=1:30:7.5:8.25$$

$$\text{DB}_{\text{fre}} = \frac{2 \times 7.5}{1+30+2 \times 7.5+8.25} = 0.28 \quad (\text{Eq. 2.17})$$

$$\text{Cyclisation ratio} = \frac{7.5-1}{1+30+7.5+8.25} = 0.14 \quad (\text{Eq. 2.18})$$

From the ^1H NMR spectroscopy analysis, the DE-ATRP method produces a high degree of branching in the range of 0.16 to 0.28. For reaction 4 (Entry 1-5, Table 2.5) NMR data can be used to follow the steady increase of the degree of branching as monomer conversion increases (Table 2.5). The polymer product achieves a DB of 0.28 at high conversion (Entry 5, Table 2.5). The molar fraction of branched DVB determined from ^1H NMR spectroscopy analysis was higher than the molar fraction of initiator incorporated in poly(DVB). Ideally, the molar fraction of the branched DVB should be almost equal to initiator in the ideal hyperbranched polymer, since every branch point is formed by two polymer chains combining (see Figure 2.10). This discrepancy may be due to cyclisation by intramolecular combination which has already been reported.²⁶ Consequently, the data indicates that the polyDVB can be considered as hyperbranched polymer below around 12% yield since the ratio of branched units to initiator is lower than 1 (N_{Branched}

units/ $N_{\text{Initiators}} < 1$, white zone, Figure 2.13). Moreover, the ratio of branched units to primary linear chain increases significantly with conversion due to the cyclisation reaction or intramolecular cross-linkings. Apparently, the intramolecular crosslinking occurs when the ratio of branched units to primary linear chains ($N_{\text{Br}}/N_{\text{I}}$) exceeds 1. The ratio of branched DVB to initiator increases to 7.5 before gelation. It indicates that there are average 6.5 cyclisation points in each primary linear chain. Therefore, the polyDVB in the range from 12% to 61.6% yield is essentially a cyclic or intramolecular cross-linked polymer ($N_{\text{Branched units}}/N_{\text{Initiators}} > 1$, grey zone, Figure 2.13).

Table 2.5 The ratio of the different units in the polyDVB sample by ^1H NMR spectroscopy analysis.

Sample	Yield ^a (%)	Initiator: EVB ^b	Linear DVB: Branched DVB:	Degree of branching ^c	Cyclisation ratio ^d
4-1	2.7		1: 4.7: 0.6: 0.6	0.16	-
4-2	12.8		1: 5: 0.9: 1.3	0.19	-
4-3	28.8		1: 14.3: 3.1: 3.8	0.24	0.095
4-4	36.3		1: 21: 5.1: 5.7	0.27	0.125
4-5	61.6		1: 30: 7.5: 8.25	0.28	0.14

a. calculated gravimetrically

b. The ratio of different units in the polymer is calculated from the Eq. 2.7-Eq. 2.10.

c. Degree of branching is calculated from the Eq. 2.11.

d. Cyclisation ratio is calculated from the Eq. 2.12. There are no cyclisation ratio values for the sample 4-1 and 4-2 since the ratio of branched DVB is lower than the initiator ratio in these two samples.

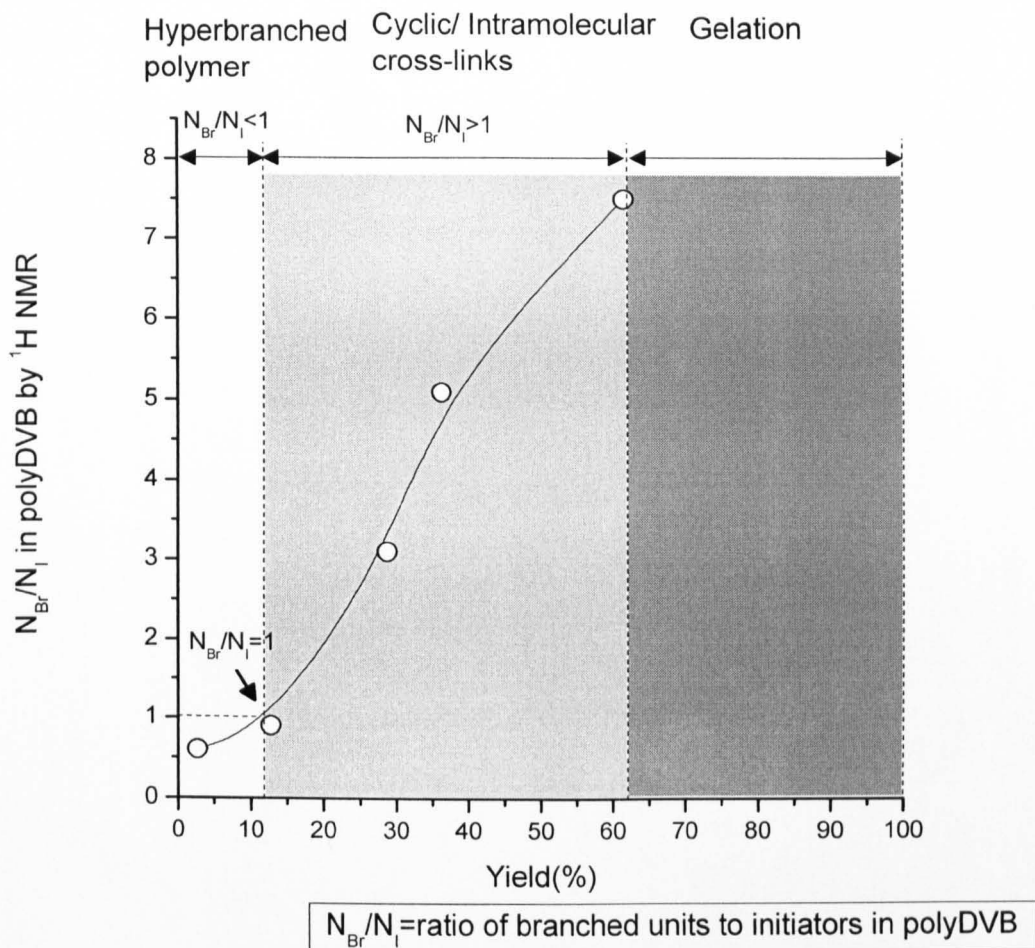


Figure 2.13 The scheme of ratio of branched DVB units to initiator (N_{Br}/N_I) in polyDVB by ^1H NMR spectroscopy analysis *versus* polymer yields. Statistically, it indicates that the polyDVB is general hyperbranched structure below 12% yield ($N_{Br}/N_I \leq 1$). In the range from 12% to 61.6% yield, the intramolecular cross-linkings are formed in polyDVB ($N_{Br}/N_I > 1$).

The ^{13}C NMR spectroscopy analysis was shown in Figure 2.14 along with the resonance assignments which are in agreement with data from literature^{25, 27, 28}. The resonances from backbones (resonances of carbons a, b and c at 38-50 ppm), benzyl ring (resonances of carbons d at 125-130 ppm and g at 145 ppm), initiator fragment (resonances of carbon m at 177 ppm) and vinyl groups (resonance of carbon e at 136 ppm and f at 114 ppm) are presented in the spectra. The spectrum also shows the resonances assigned to the methylene and methyl carbons (resonance of carbon h at 29 ppm and i at 14 ppm) of the ethyl groups from EVB units. Thus, the different ratio of units in the polyDVB can be calculated by Eq. 2.19. Consequently, the degree of branching and cyclisation ratio can be confirmed from previous equation (Eq. 2.11 and Eq. 2.12). However, achieving the

detailed molecular structural characterisation (eg. characterisation of intermolecular and intramolecular crosslinking) of polyDVB by ^{13}C NMR spectroscopy has proved enormously difficult^{25, 27}. Not only because of their highly branched nature, but also because of the complex comonomer mixtures and the presence of intramolecular cyclisation in the reaction.

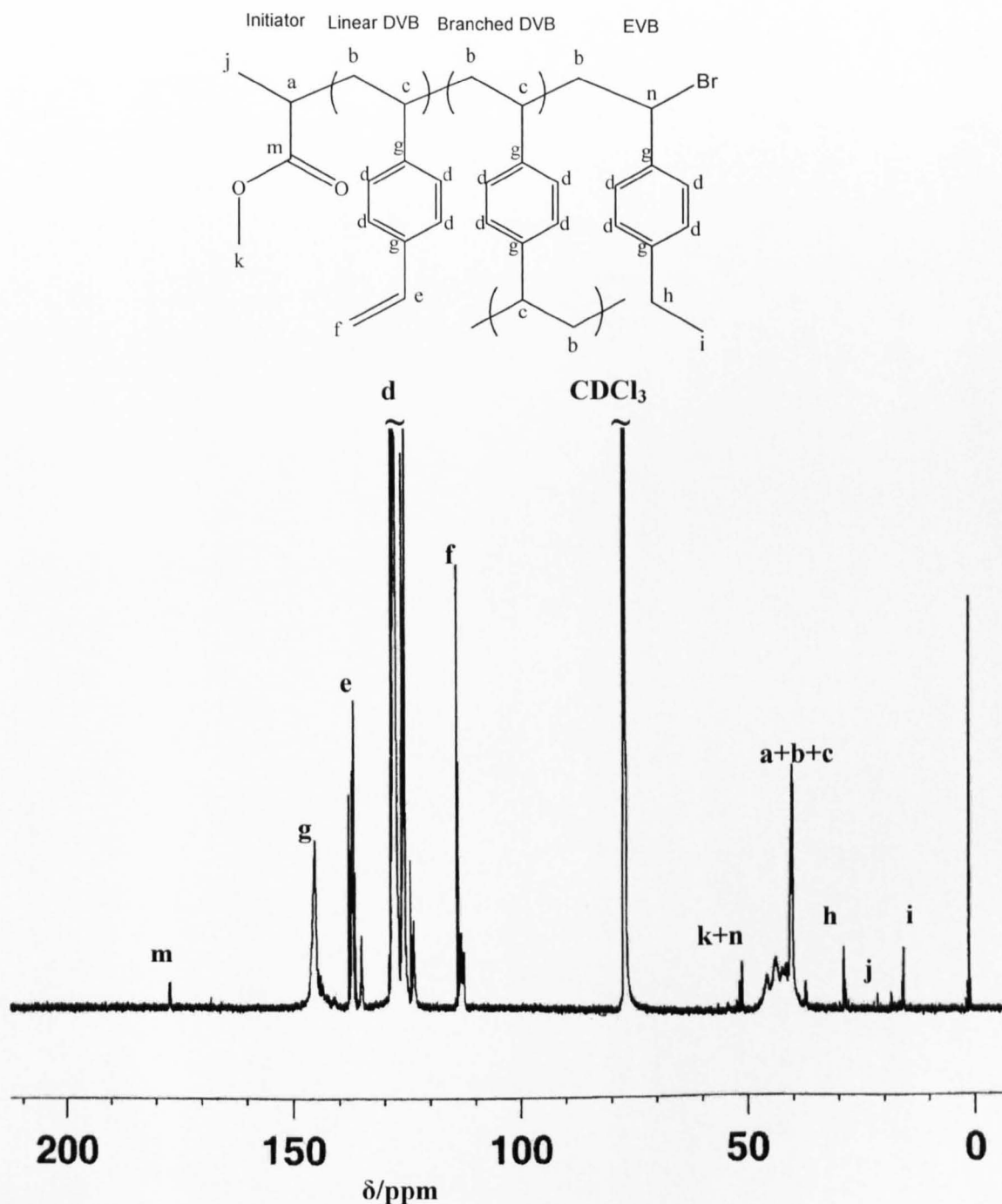


Figure 2.14 ^{13}C NMR spectroscopy spectra of the polyDVB sample in CDCl_3 (sample 5, Table 2.3) at 125 MHz, number of scans=8192.

Initiator=integrals of m

Linear DVB=integrals of f

Branched DVB= $\frac{\text{integrals of d}}{4}$ - integrals of f - integrals of h

EVB=integrals of h

(Eq. 2.19)

The structural analysis of polyDVB by ^{13}C NMR spectroscopy are summarised in Table 2.6. Generally, the ^{13}C NMR agrees the results from ^1H NMR analysis. The DB and cyclisation increase with the polymer yields. It shows that the polyDVB is general hyperbranched structure below 16% yield from ^{13}C NMR spectroscopy analysis (Figure 2.15, $N_{\text{Br}}/N_{\text{I}} \leq 1$). In the range from 16% to 61.6% yield, highly intramolecular cross-linkings are formed in polyDVB ($N_{\text{Br}}/N_{\text{I}} > 1$). However, the ^{13}C NMR analysis indicates the lower DB and cyclisation ratio in the polyDVB samples. There are two reasons for the different results between ^1H and ^{13}C NMR. Firstly, it assumed that the reactivity ratio of DVB is the same as EVB for the calculation of ^1H NMR analysis which may not absolutely accurate. Secondly, the error of integration can be caused by the poor resolution of ^{13}C NMR. Thus, the various conditions of ^{13}C NMR for the pure polyDVB (eg. prepared by pure *para*-DVB or *meta*-DVB monomer) should be studied in the future (see section 5.2.1, Chapter 5).

Table 2.6 The ratio of the different units in the polyDVB sample from ^1H NMR and ^{13}C NMR spectroscopy analysis.

Sample	Yield ^a (%)	^1H NMR			^{13}C NMR		
		Initiator:L-DVB: B-DVB: EVB ^b	DB ^c	Cyclisation ratio ^d	Initiator:L-DVB: B-DVB: EVB ^c	DB ^c	Cyclisation ratio ^d
4-1	2.7	1: 4.7: 0.6: 0.6	0.16	-	1:2.3: 0.2: 0.8	0.09	-
4-2	12.8	1: 5: 0.9: 1.3	0.19	-	1:4 : 0.6: 1.7	0.15	-
4-3	28.8	1: 14.3: 3.1: 3.8	0.24	0.095	1:11: 1.8: 5.1	0.17	0.04
4-4	36.3	1: 21: 5.1: 5.7	0.27	0.125	1:17.4: 2.7: 6	0.18	0.06
4-5	61.6	1: 30: 7.5: 8.3	0.28	0.14	1:27 : 5.6: 9	0.23	0.11

a. calculated gravimetrically

- b. The ratio of different units in the polymer is calculated from the Eq. 2.7-Eq. 2.10 by ^1H NMR spectroscopy analysis. L-DVB= linear DVB unit, B-DVB= Branched DVB unit.
- c. Degree of branching is calculated from the Eq. 2.11.
- d. Cyclisation ratio is calculated from the Eq. 2.12. There are no cyclisation ratio values for the sample 4-1 and 4-2, since the ratio of branched DVB is lower than the initiator ratio in these two samples.
- e. The ratio of different units in the polymer is calculated from the Eq. 2.19 by ^{13}C NMR spectroscopy analysis.

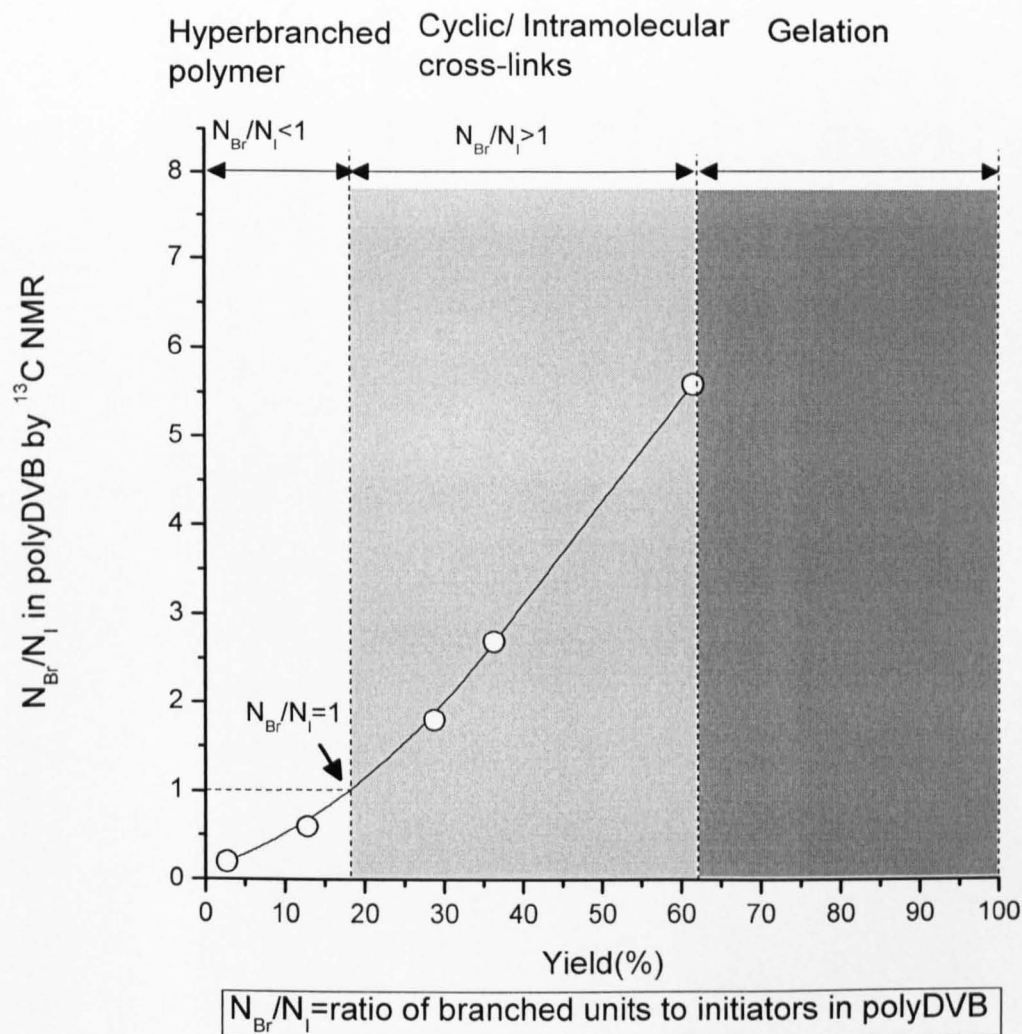


Figure 2.15 The scheme of ratio of branched DVB units to initiator (N_{Br}/N_I) in polyDVB by ^{13}C NMR spectroscopy analysis *versus* polymer yields. Statistically, it indicates that the polyDVB is general hyperbranched structure below 12% yield ($N_{Br}/N_I \leq 1$). In the range from 12% to 61.6% yield, the intramolecular cross-linkings are formed in polyDVB ($N_{Br}/N_I > 1$).

The structural characterisation of hyperbranched polyDVB by NMR spectroscopy is insufficient to define the polymer topology. A complete characterisation requires the use of particular properties of polymers, for example, dynamic radius and viscosity in solution. GPC-MALLS can determine the molar mass and root mean square (RMS) radius for the polymer fractions eluting from the GPC separation. Then information about the polymer chain structure can be gained from the relationship between the molar mass and size. This study of the GPC elution behaviour of the branched macromolecules was carried out as part of an extensive study of the application of GPC-MALLS for the characterisation of branched polymers. In the following part, the role of architecture and branched density on the solution properties and rheology of linear, hyperbranched and microgel polymers will be investigated. To correlate the properties of hyperbranched polymers, hyperbranched polyDVB with different molecular weight and branched ratios are synthesised. Specifically, the size of the molecular structures and their topology will be characterised by using a combination of GPC, viscometer, MALLS and dynamic light scattering (DLS).

Hyperbranched poly(DVB) exhibits interesting solution properties. To further support the formation of the high branched structure in the polyDVB, the viscosity behaviour of the polymers was studied. The relationship between intrinsic viscosity and the molecular weight allows to judge the topology of the polymers in solution by Mark-Houwink-Sakurada (MHS) equation (Eq. 2.20)^{29, 30}, where $[\eta]$ is intrinsic viscosity, K is a constant for different polymers, M is the experiment average molecular weight (viscosity) and α is a constant which relates to the stiffness of the polymer chain. For example, if $\alpha=0$, the polymers are hard spheres; if $\alpha=1$, the polymers are semi-coils. The increasing in the degree of branching is accompanied by the decrease of the exponent in the dependence of the intrinsic viscosity on molar mass.

Mark-Houwink-Sakurada equation: $[\eta] = KM^\alpha$

$$\log[\eta] = \log K + \alpha \log M \quad (\text{Eq. 2.20})$$

A classic Mark-Houwink-Sakurada (MHS) plot (Figure 2.16) shows that the intrinsic viscosity $[\eta]$ of poly(DVB) is much lower than that of linear polystyrene having an

equivalent molecular weight. In addition, the slope of $\log [\eta]$ versus $\log M_r$ is much lower (MHS exponent $\alpha = 0.70$ for linear PS *versus* 0.20 for the hyperbranched polyDVB (Entry 1-5, Table 2.5), demonstrating a significantly decreased level of interaction between solvent and polymer as is typically encountered in densely branched macromolecules.^{3, 31}

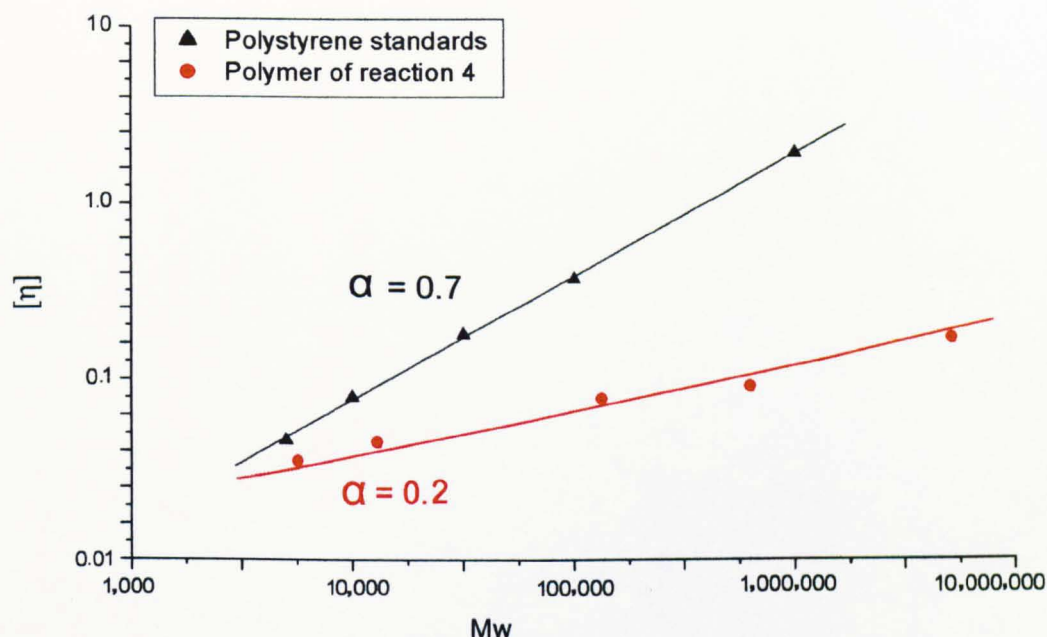


Figure 2.16 Plot of intrinsic viscosity *versus* molecular weight for hyperbranched poly(DVB) and linear poly(styrene) standards. The intrinsic viscosities $[\eta]$ of the hyperbranched poly(DVB) are much lower than those of linear poly(styrene). MHS exponent $\alpha = 0.70$ for poly(styrene) *versus* 0.20 for the hyperbranched poly(DVB) (Entry 1-5, Table 2.5).

Finally, the changes of molecular size observed in the DLS data (Figure 2.17) provide excellent evidence of hyperbranched poly(DVB). Firstly, the molecular size of poly(DVB) is much smaller than that of the equivalent molecular weight linear polystyrene because of their dense structure. Secondly, in the mixture of methanol and THF, poly(DVB) displays much smaller molecular sizes as the addition of the poorer solvating solvent is increased when compared to the effect on linear PS. These data also confirm the hyperbranched

nature, as the molecules clearly have much reduced levels of freedom to interact with differing solvents compared to the corresponding linear materials.

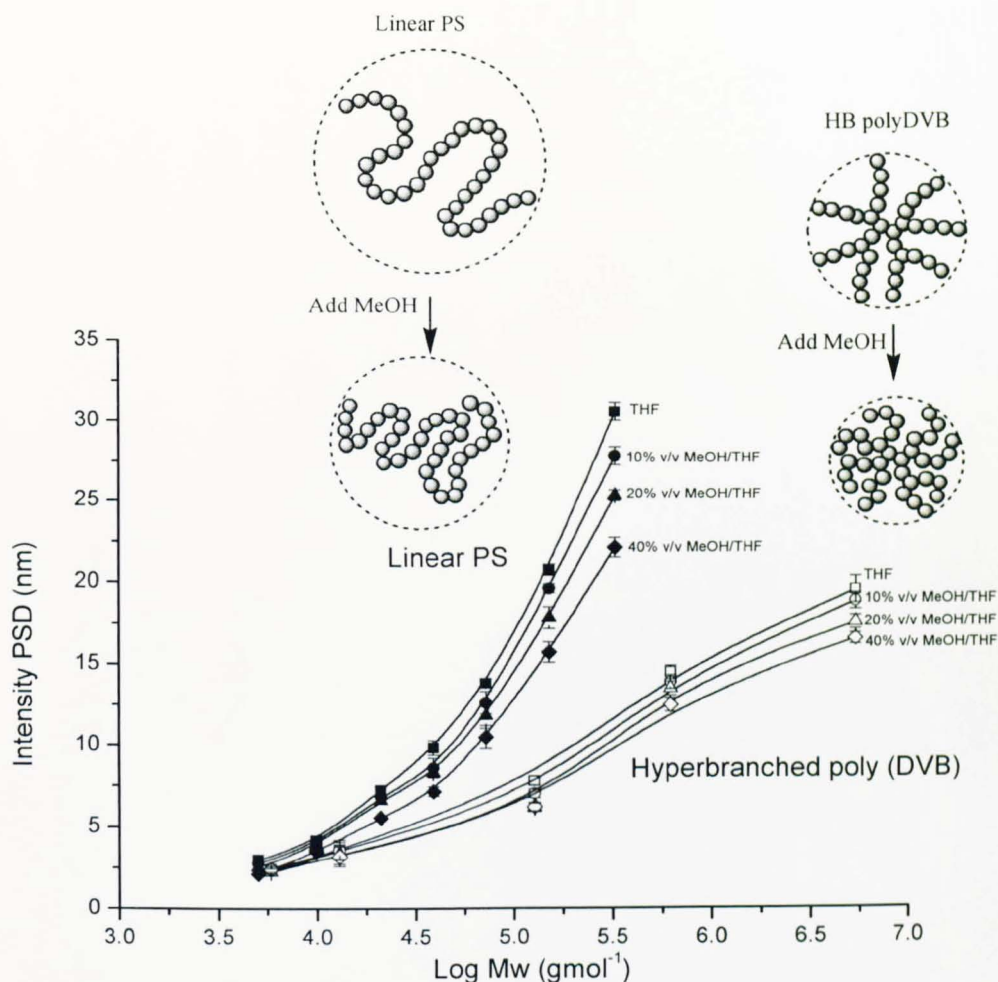


Figure 2.17 Plot of DLS data showing particle (molecular) size distribution versus Log Mw for linear poly(styrene) and hyperbranched Poly(DVB) in THF and a series of complex solvent mixtures with methanol. The molecular weights of the polystyrene samples are 5000, 9800, 21000, 39000, 72200, 151700, 325000 respectively. The poly(DVB) samples are those from entries 1-5 in Table 2.4.

Clearly, to completely eliminate the possibility of microgel formation, it would be necessary to specifically synthesise such microgels for comparison. There is only one published example of such a comparison³² and these authors report that comparisons are not trivial. The root mean square (RMS) radius (r_g^2)^{1/2} (also called the radius of gyration) describes the size of a macromolecular particle in a solution, regardless of its shape or structure. It is important to note that RMS radius is not identical to the geometrical radius

for the species. Figure 2.18 presents the plot of RMS vs. weight-average molecular weight for linear PS, PS microgel and hyperbranched poly(DVB) species obtained from GPC-MALLS analysis.

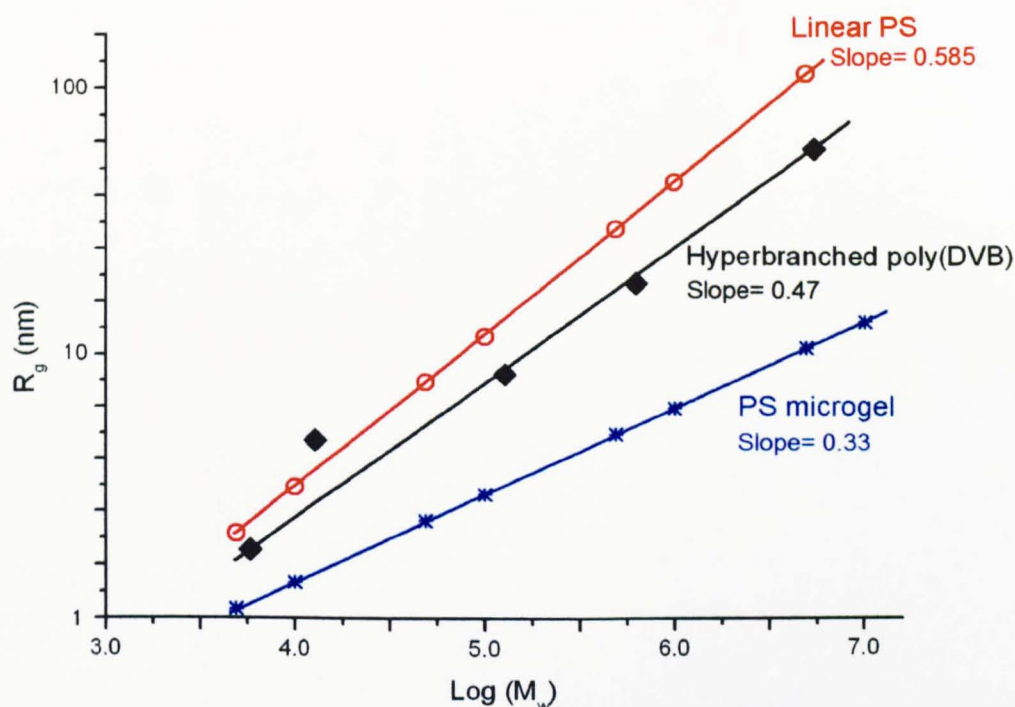


Figure 2.18 Plot of the gyration radius *versus* Log M_w . Comparison of the size of hyperbranched poly(DVB) to those obtained from published linear polystyrene (Eq. 2.24) and polystyrene microgels (Eq. 2.25). The gyration radius of hyperbranched poly(DVB) is demonstrated to be quite different from both of linear PS and microgel PS.

The $(r_g^2)^{1/2}$ values for the hyperbranched poly(DVB) samples were obtained directly from the GPC-MALLS data whilst the corresponding data points presented for the linear polystyrene and microgel examples were obtained from literature data^{13, 33} and calculation from equations (Eq. 2.21)¹³ and (Eq. 2.22)³³, respectively. It should be noted that the accuracy of the first two poly(DVB) samples is not high because of there is a lower limit to the GPC-MALLS data of approximately 10 nm.

$$\text{Linear PS } \langle r_g^2 \rangle^{1/2} = 0.014 \times M_w^{0.585} \quad (\text{Eq. 2.21})$$

$$\text{PS microgel } \langle r_g^2 \rangle^{1/2} = 0.065 \times M_w^{0.333} \quad (\text{Eq. 2.22})$$

The results clearly show the radius of gyration from poly(DVB) is quite different from that of the linear PS and PS microgel (Figure 2.18). Thus indicating that the species synthesised in this study are in fact hyperbranched, because their physical characteristics match neither that of linear or microgel materials.

Furthermore, the data demonstrate that the molecular sizes of the branched macromolecules are smaller than those of the linear polymer of a corresponding molecular weight (Figure 2.19). Thus, as GPC elution volume depends on the R_h (hydrodynamic radius) of polymer, the molecular weight of the branched polymers detected at a particular elution volume should be much higher than these of the linear polymer at that volume. The comparison of the molecular weight against elution volume plots of poly(DVB) and linear PS sample should reveal differences in the behaviour of the molecular structures, indicating different levels of branching. The plot demonstrates that the M_w from poly(DVB) materials are indeed different from those of the linear equivalents at same elution volume. Thus, this result confirms the differences in the structure type and supporting the conclusion that the polymers synthesised are more highly branched because the plots lie significantly above the one for linear PS^{24,25}.

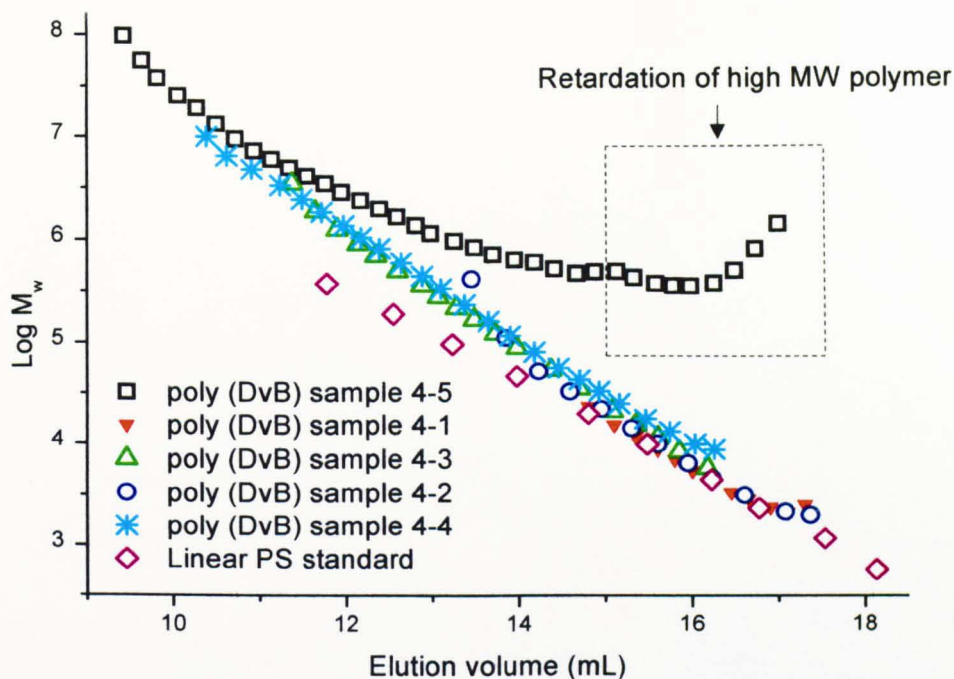


Figure 2.19 Plot of the Log of M_w versus elution volume for the poly(DvB) (Entries 1-5, Table 2.4) and linear PS samples. These data confirm that the poly(DvB) samples are highly branched as high conversions are approached since the plots lie significantly above that of the linear PS.

Last but not least, it shows the large branched molecules with high M_w eluted together with normally eluting smaller molecules at the region of high elution volumes (15 ml to 17 ml, square highlight part, Figure 2.19), which resulted in the M_w vs. elution curve upward in the plot. This is due to the retardation of large highly branched molecules during GPC separation. The MALLS system have different sensitivities to the presence of high molar mass fractions (the RMS radius z average being more sensitive), so the elution time *versus* the molar mass plot shifts upward at regions of lower molar mass. Furthermore, the THF is a good solvent for PS lead the possibility of retardation by adsorption in the cross-linked PS column packing is low. These data suggest the entanglement of large highly branched molecules in the column packing may explain the retardation (Figure 2.20).¹³

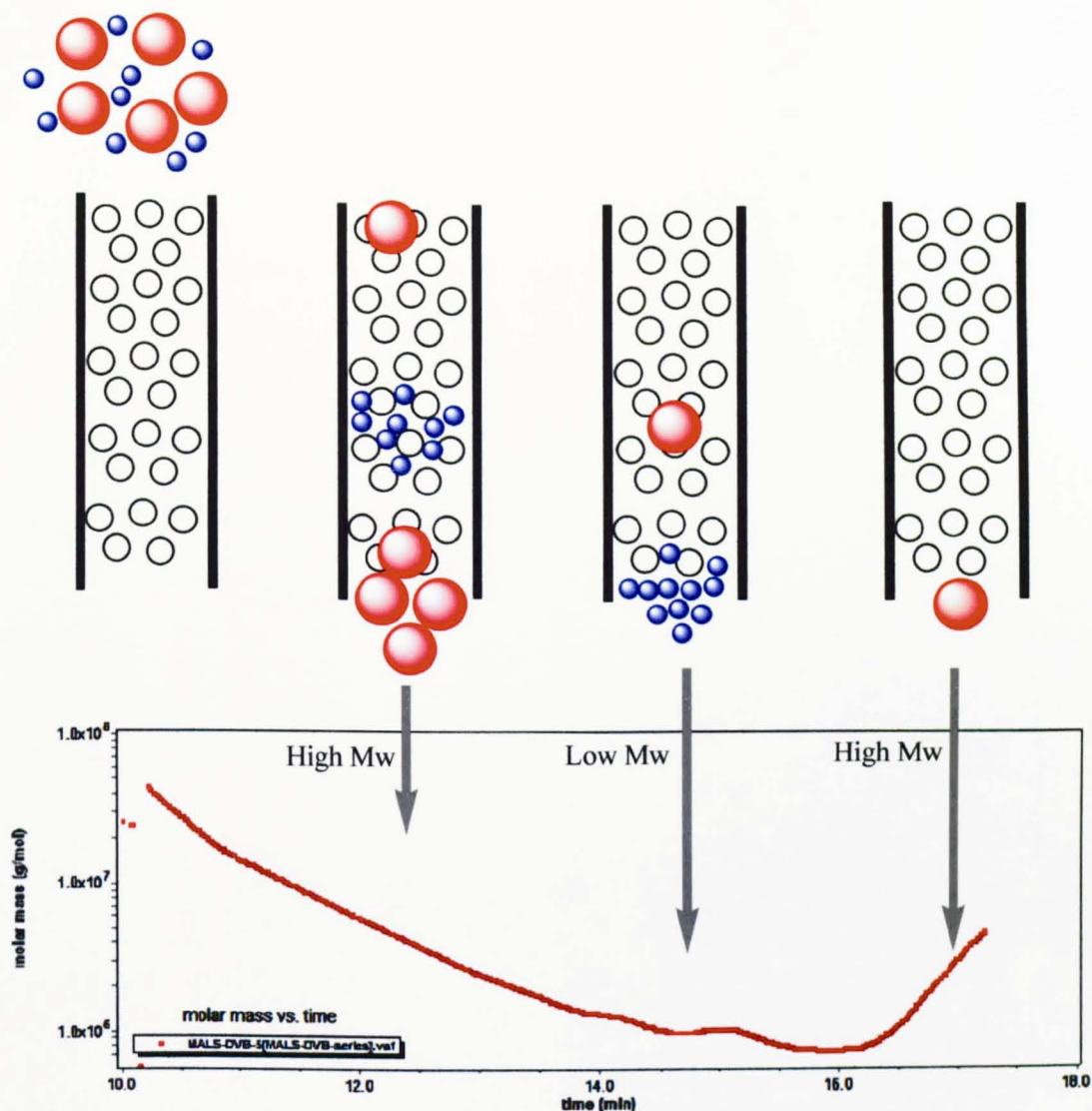


Figure 2.20 Scheme of the retardation of large highly branched molecules during GPC separation. The sample is taken from hyperbranched poly(DVB) (Entry 5, Table 2.4).

The typical GPC system which used for the characterisation was shown in Figure 2.21. First, samples are dissolved in an appropriate solvent ($c \approx 3$ mg/mL). Organic solvent such as tetrahydrofuran (THF) is chosen for GPC. Second, an isocratic pump offers continuous flow of the mobile phase through the whole system (flow rate = 1 mL/min). A solvent degasser is employed to eliminate the bubbles or gases in the solvent. Third, after the sample is injected into the system by autosampler (injection volume = 10 μ L), the sample solution is passed through the guard column and two PLgel Mixed-C columns in series

with porous packing. The polymer molecules are separated by size. Last, the sample elutes are monitored by a detector and the results is collected by data processing software. For the analysis purpose, the polymer eluent was collected after separated by GPC columns at the waste reservoir during every minute. The collected polymer solution samples should indicate the true elution time in the second times GPC running. However, the second time GPC results cannot give any valid results, since the polymer solution was diluted from 3 mg/mL to 1.5×10^{-6} mg/mL by the pure THF solvent during the first time GPC running. The concentration of the diluted polymer solution (1.5×10^{-6} mg/mL) was too low for both of RI and MALLS detection.

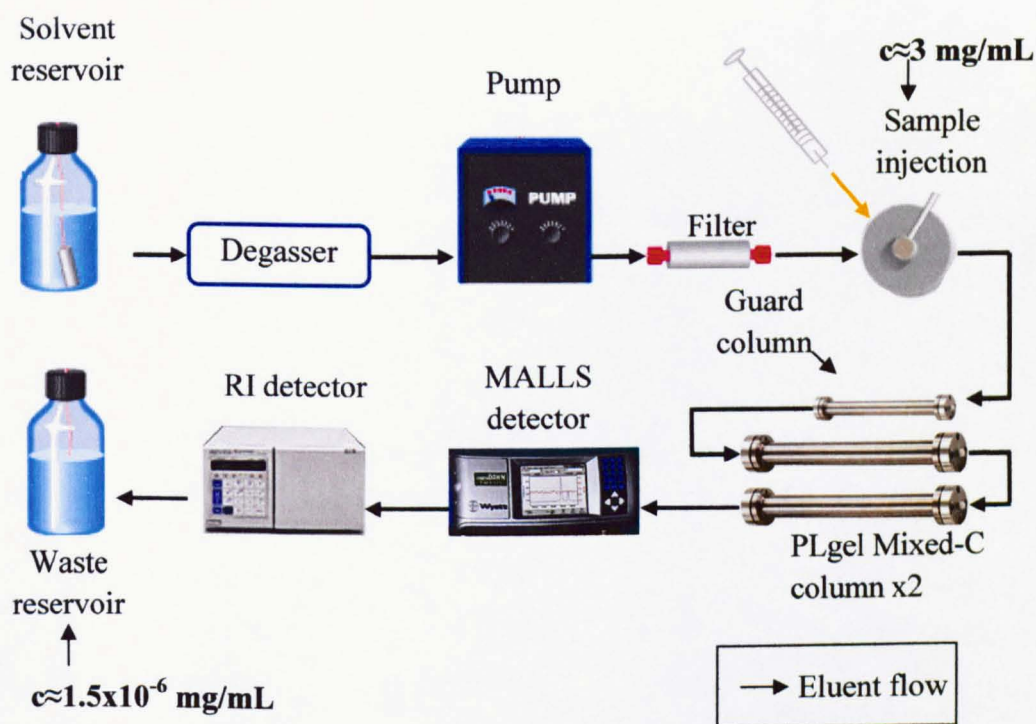


Figure 2.21 A schematic flow diagram showing the setup of the GPC system. The flow of the eluent is displayed. The pump, sampler, columns and detector are all integrated in a single unit (PL-GPC 120, PolymerlabTM).

The large branched molecule may consist of several parts that may behave as separate molecules, penetrating into the column packing and having the effect of anchoring the entire molecule (Figure 2.22). This suggests that the retardation takes place inside the

column pores. More regular linear molecules have less abnormal behaviour, because more regular structures have lower possibility of entangling in the column packing^{15, 16}. GPC–MALLS separated and characterised highly branched samples only in the high molar mass part of their molar mass distribution, but the GPC separation failed in the region of lower molar masses because of delayed elution of the large branched molecules. Therefore, the characterisation of highly branched samples can be improved by their separation into several fractions by either GPC or precipitation fractionation and subsequent GPC–MALLS analysis of particular fractions. Some other methods were employed to reduce this problem, *e.g.*, changing the solvent, the stuffing material of GPC column or adding salts to the eluent. However, these methods are often useless from previous research report³⁴. Recently, a new solution has been found for the separation of highly branched polymers using a column free method, which called asymmetric flow field flow fractionation¹⁵. This technique separates the macromolecules according to their size in a channel with a membrane using the forces of an eluent cross-flow.

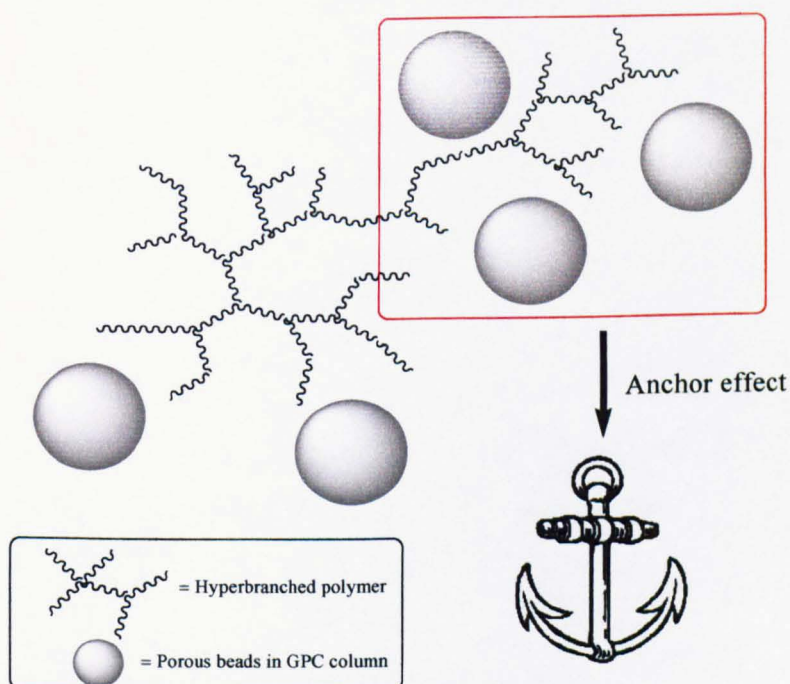


Figure 2.22 The entanglement of large highly branched molecules in the column packing due to the anchor effect.

Despite of the high yield without crosslinking, the preparation of DVB in toluene system has exposed some disadvantages. The most significant disadvantage of this reaction is the unstable result brought by the poor solubility of copper complex in toluene. The reproducibility data of the homopolymerisation reaction in toluene is listed in Table 2.7. The reproducibility data shows the gel points vary even under the same condition due to the inhomogeneous system. The poor solubility of the copper-ligand complex in toluene leads the reaction system to inhomogeneous. The inhomogeneous solution causes the gel appearing at different time. Thus, the gel point and kinetics of this reaction are not very stable.

Table 2.7 Reproducibility data of hyperbranched DVB samples in toluene system.
Reaction conditions: [DVB] = 3.51 M, DVB:I:Cu(I): Cu(II): Bpy = 57:1:0.4:0.133: 1.07, in toluene at 90 °C. The reproducibility data shows the gel points vary even at the same condition due to the inhomogeneous system.

Reaction	Reaction time (hrs)	Yield ^a (%)	GPC-RI results		
			M _n (g mol ⁻¹)	M _w (g mol ⁻¹)	M _w /M _n
A	28	61.6	13,600	275,900	20.2
B	16	48.7	14,010	119,550	8.53
C	10	51.5	14,260	324,120	22.7
D	20	46.3	13,950	206,270	14.8
E	17	39.9	11,460	96,180	8.4

a. Calculated gravimetrically

An alternative cyclohexanone system was developed to overcome this disadvantage. The well solubility of copper complex in cyclohexanone makes the reaction solution staying in homogeneous phase. The cross-linking between large molecules occur early can be avoided in homogeneous solution, making this reaction becomes stable and reproducible.

The reaction conducted in cyclohexanone is listed below (Table 2.8). This reaction is repeated at the same condition as reaction 4 of the toluene system (Entry 4, Table 2.3). The ratio of Cu(I) to Cu(II) was kept at 3 to 1. Furthermore, another different condition is the temperature, which decreases to 60 °C due to the homogeneous system. The lower reaction temperature can also help to control the system due to the decreasing of the polymerisation rate. In the cyclohexanone system, the reaction gels at around 64% yields (Entry 5, Table 2.8). The reaction time increased from 30 hours (toluene system) to 57 hours (Figure 2.23). It can be concluded that the reaction in cyclohexanone system exhibits a much slower polymerisation rate compared to the same reaction in toluene under different solvent and temperature. Furthermore, the degree of branching of polyDVB in cyclohexanone is similar as the reaction conducted in toluene, which achieved 0.26 at 64% conversion.

Table 2.8 Detailed data of hyperbranched DVB samples in cyclohexanone system at different times. Reaction conditions: [DVB]=3.51 M, [DVB]:[I]:[Cu(I)]:[Cu(II)]:[Bpy] = 57:1:0.4:0.133: 1.07, in cyclohexanone at 60 °C.

Sample	Reaction time (hrs)	Yield ^a (%)	GPC-RI results			GPC-MALLS results			DB ^b
			M _n	M _w	M _w /M _n	M _n	M _w	M _w /M _n	
			(g mol ⁻¹)	(g mol ⁻¹)		(g mol ⁻¹)	(g mol ⁻¹)		
1	4	1	1,560	1,970	1.26	2,710	3,500	1.29	0.11
2	16	15	2,270	3,180	1.4	3,610	4,950	1.37	0.17
3	24	21	2,550	3,700	1.45	4,357	6,100	1.4	0.19
4	40	37	4,700	9,290	1.98	9,430	16,230	1.72	0.23
5	56	64	14,690	326,700	22.3	124,960	712,300	5.7	0.26
6	57	Gelation							

a. Calculated gravimetrically

b. Degree of branching was calculated by ¹H NMR spectroscopy analysis (Eq. 2.13).

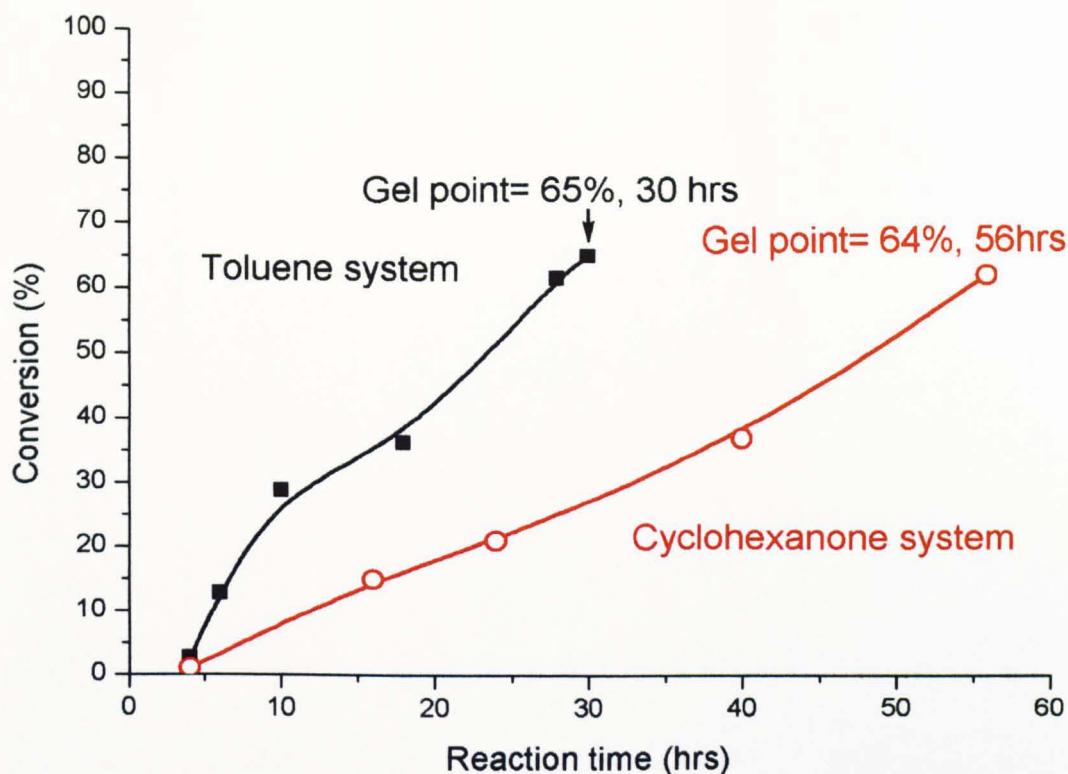


Figure 2.23 The comparison of time dependence of monomer conversion of DVB in toluene and cyclohexanone (Table 2.8). The reaction in cyclohexanone shows a slower reaction rate due to the change of solvent and temperature. Reaction conditions: [DVB] = 3.51 M, DVB:I:Cu(I): Cu(II) = 57:1:0.4:0.133.

Except for the longer reaction time, the other feature of the cyclohexanone system is the lower molecular weight at the same conversion rate. The inhomogeneous solution of toluene causes the combination of macromolecules and results in an extremely high molecular weight. For example, the M_w of polyDVB syntheses in toluene reaches 126,900 g/mol at 28% conversion (Figure 2.24), while the M_w of polyDVB prepared in cyclohexanone is only 10,080 g/mol at the same yield. Furthermore, at around 61% yield, the M_w of polyDVB prepared in toluene is 5.4 million Daltons, compared to only 712,000 Daltons (M_w by MALLS) in cyclohexanone (Entry 5, Table 2.8). The lower M_w in cyclohexanone system demonstrates a better control over reaction owing to depressing the combination between large polymer chains.

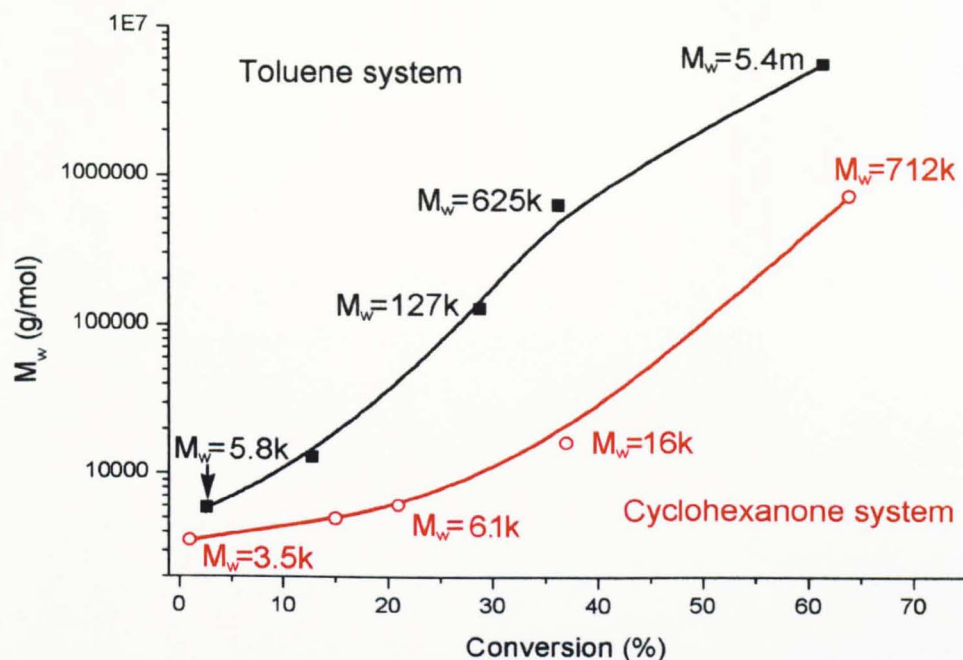


Figure 2.24 Comparison of molecular weight of polyDVB prepared in toluene and cyclohexanone system. The M_w is determined by MALLS detector. The reaction in cyclohexanone displays lower the M_w due to the homogeneous system.

Unlike the unstable toluene system, the homopolymerisation of poly(DVB) in cyclohexanone system represents very good reproducibility (Table 2.9). As mentioned before, the good solubility of copper complex in cyclohexanone enhanced the homogeneous nature of the polymerisation. Thus, the homogeneous reaction system allows for a much more stable polymerisation rate.

Table 2.9 Reproducibility data of hyperbranched DVB samples at same condition in cyclohexanone system. Reaction conditions: [DVB] = 3.51 M, [DVB]:[I]:[Cu(I)]:[Cu(II)]: [Bpy] = 57:1:0.4:0.133: 1.07, in cyclohexanone at 60 °C. The data shows the reproducibility is much better than toluene system due to the homogeneous solution.

Reaction	Reaction time (hrs)	Yield ^a (%)	GPC-MALLS results		
			M_n	M_w	M_w/M_n
			(g mol ⁻¹)	(g mol ⁻¹)	
A	56	64	14,690	326,700	22.3
B	54	61.3	13,850	267,200	19.3
C	52	61.7	15,590	293,500	18.8

a. calculated gravimetrically

2.3.2 Synthesis and Characterisation of Hyperbranched poly(EGDMA)

In this part, the investigation is focused on the polymerisation of EGDMA which is a methyl methacrylate related monomer. The mechanism of homopolymerisation of hyperbranched poly(EGDMA) is illustrated in Figure 2.25 via the deactivation enhanced ATRP. First, initiator (2) is activated by Cu (I) complex, yielding a new radical. Since the Cu (I)/Cu(II) ratio and concentration are chosen specifically for short chain propagation, the new propagating centre only propagates a few times with EGDMA (1) to form a short chain (3) with many pendent vinyl groups. Second, this short chain radical is subsequently deactivated to form a halogen terminated oligomeric macromonomer (4) through halogen transfer catalysed by Cu(II). This macromonomer (4) is reinitiated by the Cu(I) complex leading to the same propagation process and halogen transfer. If macromonomer (4) is incorporated into the chain, it forms a branching point (5). Finally, every macromonomer incorporated generates a branching point, which gives rise to a highly branched structure (6) with many halogen and vinyl end functional groups.

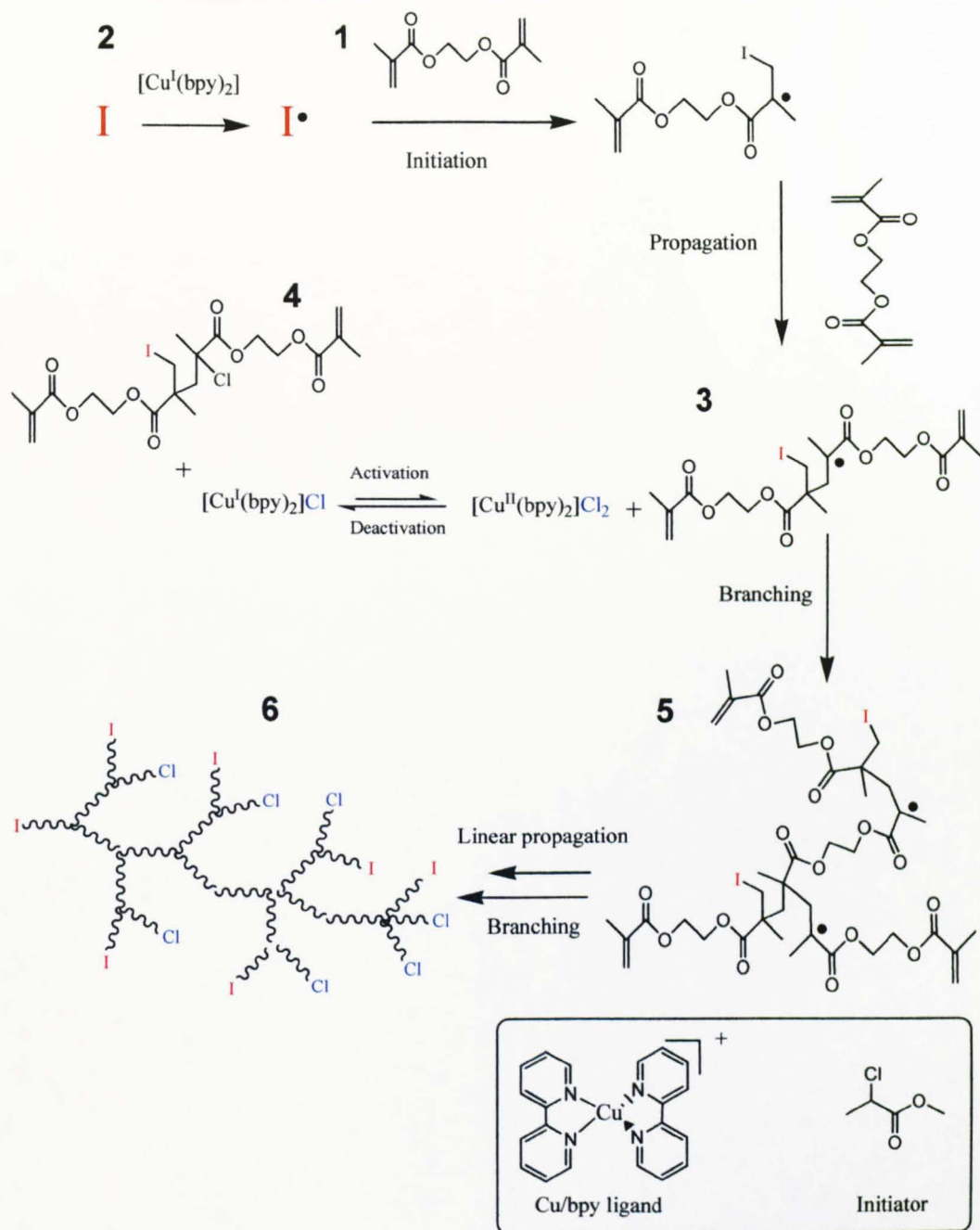


Figure 2.25 Mechanism for homopolymerisation of EGDMA via DE-ATRP.

A series of EGDMA polymerisations were conducted under different reaction conditions (Table 2.10). As the reactivity of methacrylate monomers is generally higher than styrenic monomers with the ATRP system used in this study, it was decided to investigate changing two conditions to further slow down the polymerisation. Firstly, the 2-methyl chloropropionate and $\text{CuCl}/\text{CuCl}_2$ are used instead of bromide initiator and catalyst

applied in polymerisation of poly(DVB). Secondly, the monomer concentration was decreased to 1.22 mol/L in this system to reduce the polymerisation rate. Under normal ATRP conditions (Entries 1 and 2, Table 2.10) gels formed within 3 hours due to the rapid polymerisation rate. To prevent crosslinking, the reactions were modified to slow the polymerisation rate by adding Cu(II). A significant improvement was achieved (Entries 3 and 4, Table 2.10). To add further control, the total amount of copper catalyst was reduced relative to initiator, *i.e.* $[I]/[Cu(I)+Cu(II)]$ from 2.5/ 1 to 4/1 (Entry 5, Table 2.10), the strong polar solvent 2-butanone was replaced by less polar THF and a slightly lower temperature was adopted. Under these conditions, the growth of polymer chains was greatly decreased. Thus, the cross-linking was suppressed leading to higher yields of soluble hyperbranched polymer. The most significant result (Entry 5, Table 2.10) was the attainment of a high yield, 63% after 29 hours polymerisation (Figure 2.26). Beyond this point gelation began to occur, and extending to higher yield is a future targets. By contrast, under normal free radical polymerisation conditions, a gel is formed almost instantly^{35, 36}. The results give further solid evidence to prove the success in poly(EGDMA).

Table 2.10 Homopolymerisations of EGDMA by DE-ATRP.^a Note, A high ratio of Cu (II)/ Cu (I) slows significantly the reaction rate leading to high yields of hyperbranched polymer without formation of gels.

Entry	[EGDMA]:[I]:[Cu(I)]:[Cu(II)] (mol ratio)	Solvent	Temp (°C)	Time (hour)	$M_n \times 10^{-4}$ ($gmol^{-1}$)	PDI	Yield ^c
1	50:1:1:0	Butanone	60	3	-	-	gel
2	50:1:0.5:0	Butanone	60	5	-	-	gel
3	50:1:0.18:0.03	Butanone	65	7	4.4	3.1	38%
4	100:1:0.3:0.1	Butanone	65	15	4.8	3.5	48%
5	50:1:0.188:0.063	THF	60	29	15.0	4.1	63%
6 ^b	100:1:0:0	THF	60	0.15			gel

^a. For all reactions: [EGDMA] = 1.22 M, $[Cu(I)+Cu(II)]/[Bpy] = 1:2$

^b. AIBN was used as the initiator in reaction 6, a normal radical solution polymerisation.

^c. Calculated gravimetrically

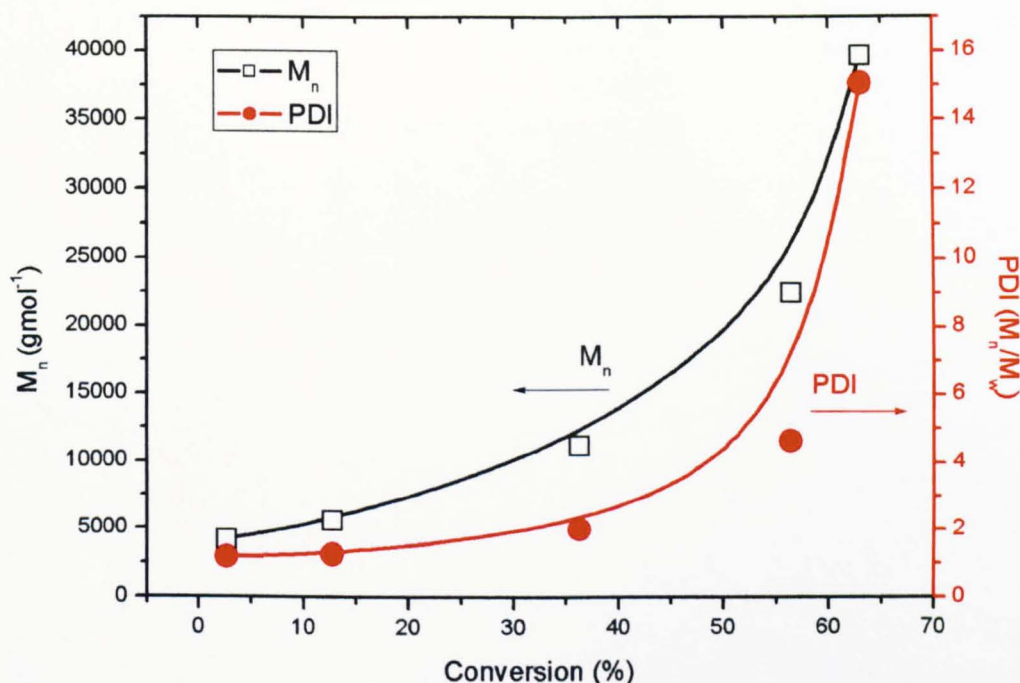


Figure 2.26 Plot of the M_n and molecular weight distribution of poly(EGDMA) (M_n (□) and PDI (●) by RI detector) versus monomer conversion for the deactivation enhanced ATRP of EGDMA. Reaction conditions: [EGDMA]=1.22 M, [EGDMA]:[I]:[Cu(I)]:[Cu(II)]=50:1:0.188:0.063, [Cu(I)+Cu(II)]/[bpy] =1:2, T= 60 oC. (Entry 5 in Table 2.10)

Monitoring of the polymerisation process using GPC equipped with both RI and MALLS detectors clearly demonstrates the influence on the polymerisation of the reversible activation (or deactivation) controlled hyperbranched polymerisation mechanism (Figure 2.27 and Table 2.11). The molecular weight of the polymers increases with monomer conversion, demonstrating a living polymerisation process. The molecular weight distribution broadens with increasing monomer conversion, as is commonly observed in the synthesis of hyperbranched polymers. However, it is worth noting that in the initial stages of the polymerisation process, the molecular weight of the polymer increases with monomer conversion, but they retain narrow polydispersity. This is because at low monomer conversion the propagation mainly leads to linear polymer chains with a low level of branching (See Entry 1 in Table 2.11). As the reaction proceeds with

multi-functional monomer, the molecular weight of polymer increases much faster than normally expected for ATRP (Entries 2-5 in Table 2.11). This is because at later stages of polymerisation, significant levels of the monomer and lower molecular weight oligomers have been consumed and the reactions tend towards branching rather than linear growth. Furthermore the reaction again demonstrated a monomer conversion ceiling of approximately 60% as in the poly(DVB) case, indicating that at this point the molar fraction, steric bulk and molecular mobility effects that are inhibiting gelation are reduced to a point that gel formation begins to take place. The data shows that the measured MALLS molecular weight is always higher than the RI results (Figure 2.27 and Table 2.11), which also strongly support formation of a hyperbranched architecture¹³. At this point it must be stressed that, as with the DVB case, the GPC and MALLS data for sample number 5 have been included (Table 2.11 and Figure 2.27) for comparison with the materials sampled at earlier points in the reaction only to demonstrate that the molecular weight of the hyperbranched material is still rising at this point but has not yet become an insoluble gel. Again the MALLS data are predicting that sample 5 has a significant component of its molecular weight distribution above the upper exclusion limit of the system (upper limit of M_w is 2 million Dalton) and thus cannot be treated as giving definitive molecular weight nor polydispersity data.

Table 2.11 Hyperbranched poly(EGDMA) samples collected at different reaction times for the reaction 5 in Table 2.10.^a

Sample	Reaction time (hours)	Yield (%) ^b	GPC-RI results			GPC-MALLS results			Degree of branching ^c
			M _n (g mol ⁻¹)	M _w (g mol ⁻¹)	PDI	M _n (g mol ⁻¹)	M _w (g mol ⁻¹)	PDI	
5-1	2.0	3.0	4,100	4,800	1.16	4,370	5,100	1.17	0.375
5-2	3.8	13.1	5,500	7,000	1.25	6,915	9,710	1.40	0.44
5-3	10.5	36.5	9,480	13,900	1.46	12,210	21,890	1.79	0.40
5-4	21.5	55.4	20,430	43,300	1.69	33,530	72,030	2.15	0.51
5-5	29.0	63.0	150,080	607,320	4.05	861,300	3,244,000	3.78	0.50
5-6	30.5	66.0	Gelation						

^a. Reaction conditions: [EGDMA] = 1.22 M, [EGDMA]:[I]:[Cu(I)]:[Cu(II)] = 50:1:0.188:0.063, [Cu(I)+Cu(II)]/[Bpy] = 1:2, T = 60 °C.

^b. Calculated gravimetrically

^c. Determined by ¹H NMR spectroscopy analysis (See Figure 2.28 and Eq. 2.23-Eq. 2.25).

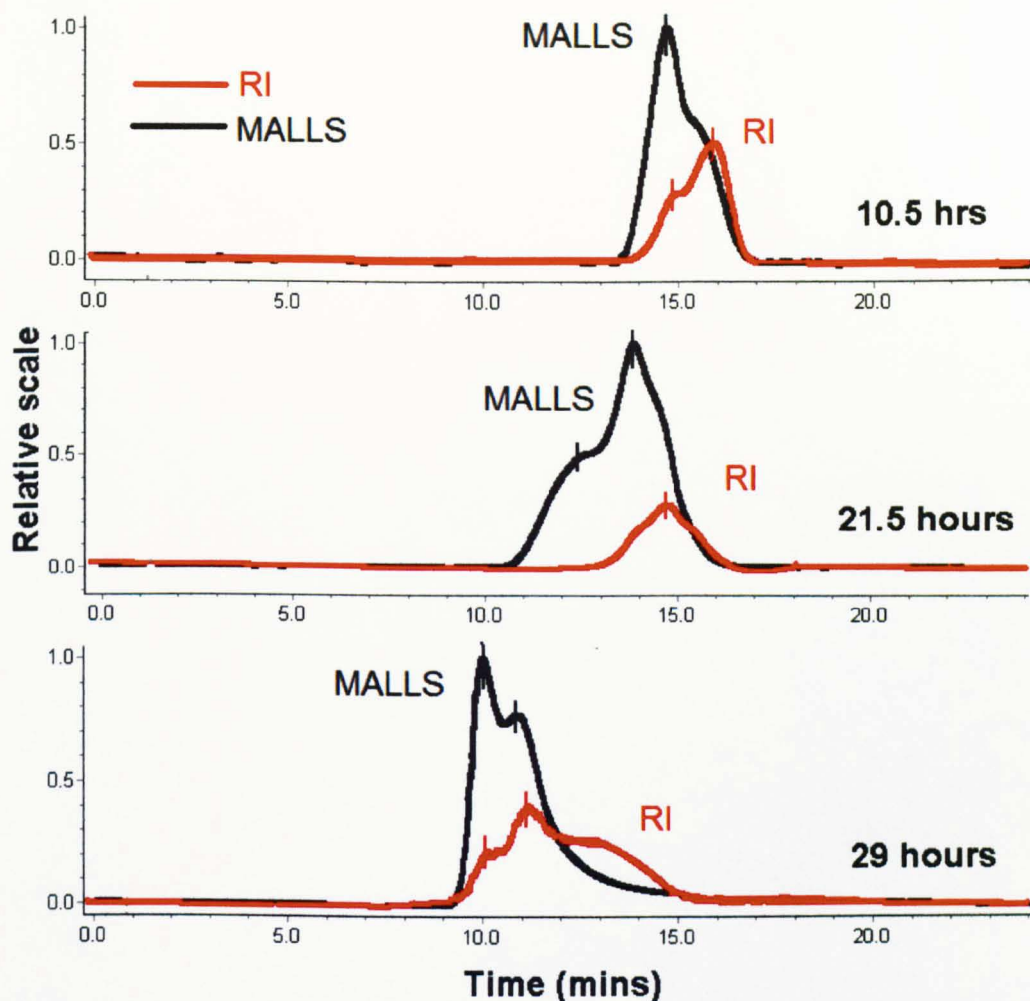


Figure 2.27 MALLS and RI chromatograms of GPC analysis for poly(EGDMA) samples (Entries 3 to 5 in Table 2.11). Note, the evolution of molecular weight and molecular weight distribution with reaction time showing the formation of hyperbranched polymer.

The hyperbranched structure of poly(EGDMA) was also confirmed by ^1H NMR (Figure 2.28). The presence of a multiplicity of reactive groups (resonance of protons g at 3.7 ppm from initiator fragment), EGDMA units (resonance of proton c at 4.0-4.6 ppm) and potentially useful vinyl functionalities (resonance of protons e and f from vinyl group at 5.6 and 6.2 ppm) are clearly revealed in the ^1H NMR spectra. Furthermore, the ratio between the branched EGDMA to the linear EGDMA is calculated as shown in Eq. 2.23-Eq.2.25.

Initiator=Integrals of g/3 (Eq. 2.23)

Linear EGDMA=Integrals of e (Eq. 2.24)

Branched EGDMA=(Integrals of c/4)- linear EGDMA
 =(Integrals of c/4)- Integrals of e (Eq. 2.25)

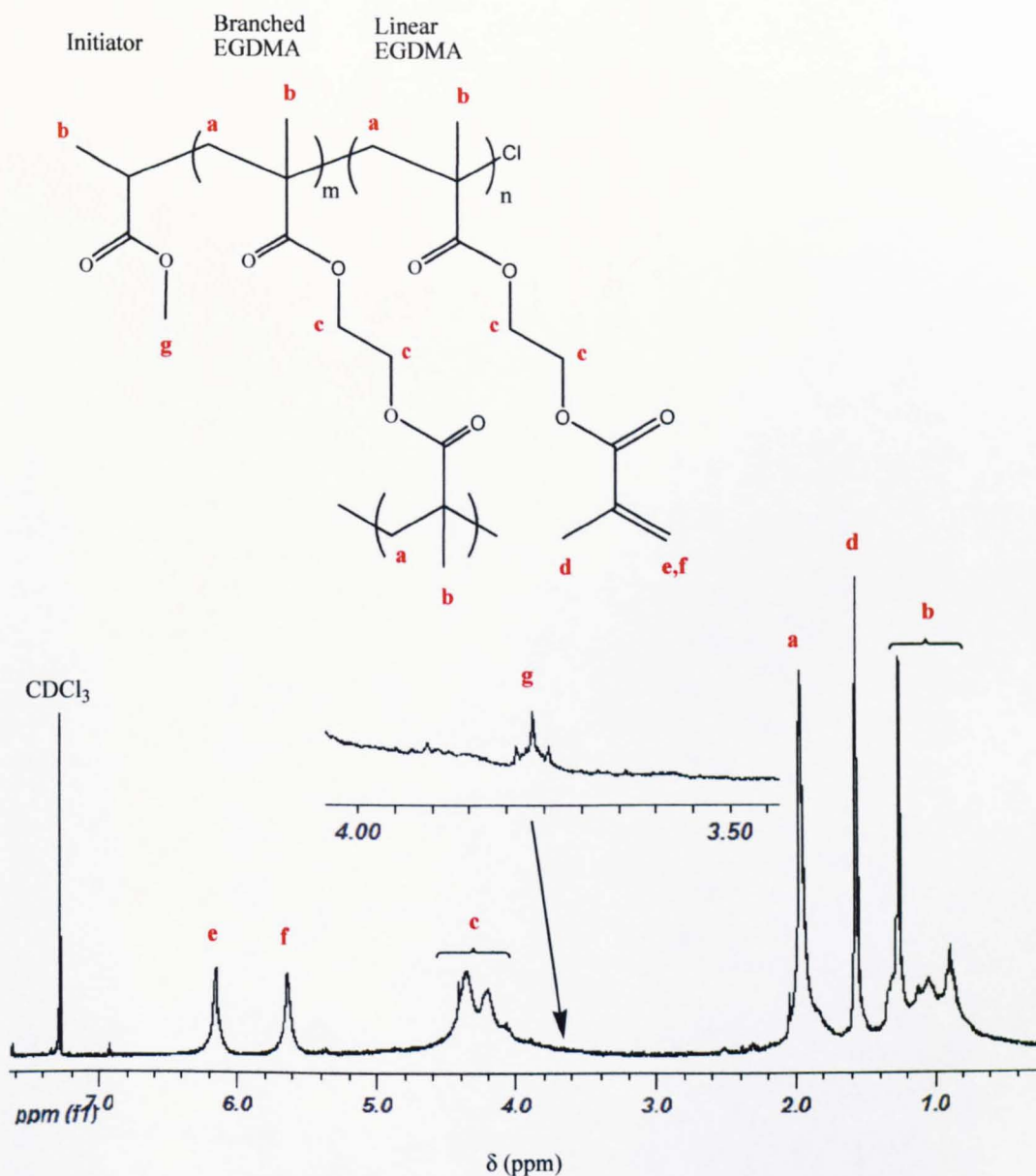


Figure 2.28 ¹H NMR spectrum of poly(EGDMA) in CDCl₃ at 300 MHz (entry 5, Table 2.11). The significant concentration of peaks e and f relative to peak c demonstrate a high branch ratio for the poly(EGDMA). Clearly, there is potential for hyperbranched polymers which contain high levels of vinyl groups to cross-link during further polymerisation. However, this is not thought to be the case here because the samples are completely soluble in the solvent of choice (THF or CDCl₃).

Table 2.12 The ratio of the different units in the polyEGDMA sample by ^1H NMR spectroscopy analysis.

Sample	Yield ^a (%)	Initiator: Linear EGDMA: Branched EGDMA ^b	Degree of branching ^c	Cyclisatio n ratio ^d
1	3.0	1: 2 : 0.9	0.38	-
2	13.1	1: 4.1: 2	0.44	0.14
3	36.5	1: 13: 4.7	0.40	0.19
4	55.4	1: 16.5: 9.4	0.51	0.31
5	63.0	1: 20.6: 11	0.50	0.31

a. Calculated gravimetrically.

b. The ratio of different units in the polymer is calculated from the Eq. 2.23-Eq. 2.25.

c. Degree of branching is calculated from the Eq. 2.26.

d. Cyclisation ratio is calculated from the Eq. 2.27. There is no cyclisation ratio for the sample 1 because the ratio of branched DVB is lower than the initiator ratio.

$$\text{DB}_{\text{Frey}} = \frac{2 \times \text{branched EGDMA units}}{2 \times \text{branched EGDMA units} + \text{initiator} + \text{linear EGDMA units}} \quad (\text{Eq.2.26})$$

$$\begin{aligned} \text{Cyclisation ratio} &= \frac{\text{Cyclisation units}}{\text{All units}} \\ &= \frac{\text{branching EGDMA units} - \text{Initiator}}{\text{initiator} + \text{linear EGDMA units} + \text{branched EGDMA units}} \quad (\text{Eq.2.27}) \end{aligned}$$

The degree of branching in polyEGDMA is calculated by the Eq.2.26. The DB of polyEGDMA is calculated to be *ca.* 0.375-0.5 (Entry 1-5 in Table 2.12), which agrees with a hyperbranched structure. Branching ratios of this level, whilst successfully achieving the synthesis of soluble hyperbranched polymers via a one-step free radical polymerisation have never been reported before.^{5, 35} Moreover, the cyclisation ratio can be calculated by the Eq. 2.27. It shows the cyclisation has occurred at lower yield (at 5% yield) than polyDVB (at 11% yield) (Figure 2.29). In addition, the cyclisation ratio of polyEGDMA (0.14-0.31) is higher than polyDVB (0.095-0.14). The ratio of branched units to initiators increased to 11 at the 63% yield (Figure 2.29). The results indicate the cyclisation (or intramolecular crosslinking) reaction is more easily occurred in

polyEGDMA than polyDVB, since the residual vinyl groups are highly reactive in longer and flexible EGDMA monomer molecules.

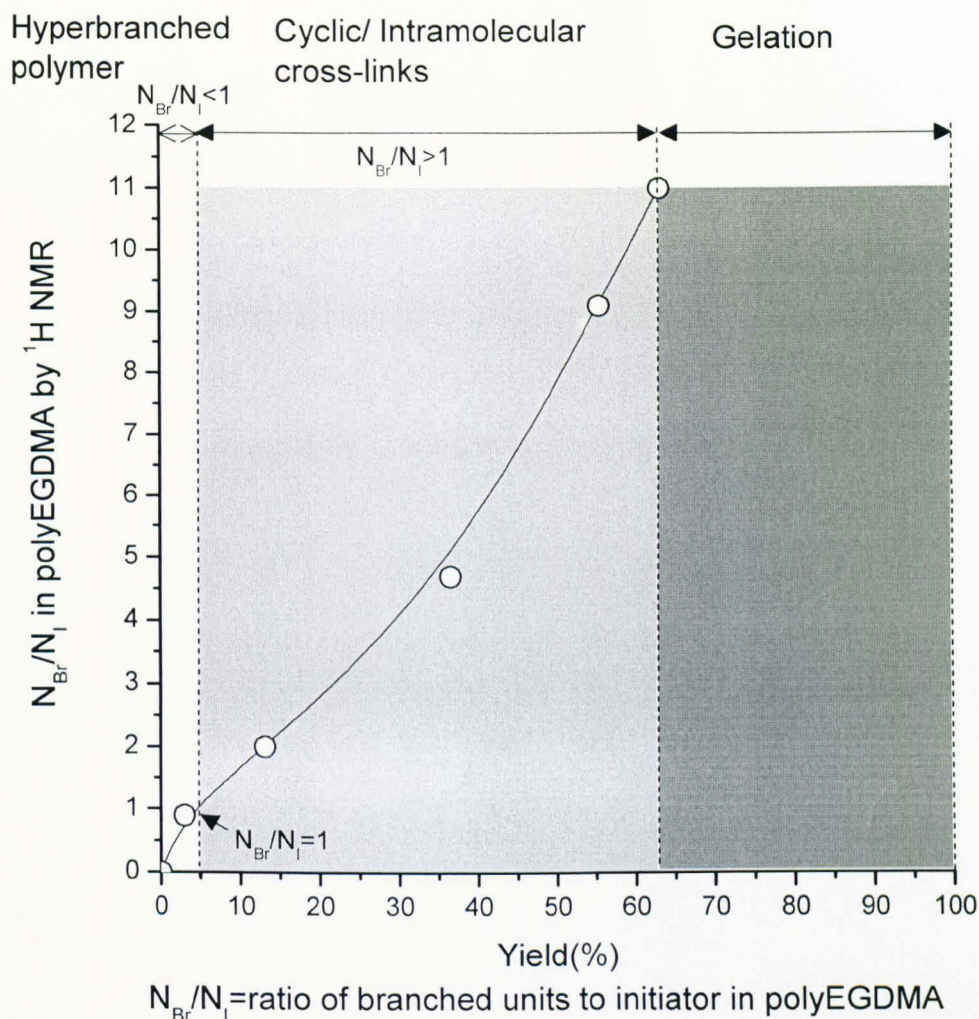


Figure 2.29 The ratio of branched EGDMA units to initiators (N_{Br}/N_I) in polyEGDMA by ^1H NMR spectroscopy analysis *versus* polymer yield. Statistically, it clearly shows the polyEGDMA is hyperbranched structure below 5% yield ($N_{Br}/N_I \leq 1$). In the range from 5% to 63% yield, the intramolecular cross-linkings are formed in polyEGDMA ($N_{Br}/N_I > 1$).

The ^{13}C NMR spectroscopy analysis was shown in Figure 2.30 along with the resonance assignments. The resonances from backbones (resonances of carbon d at 52 ppm), EGDMA units (resonances of carbons g at 60-67 ppm), initiator fragment (resonances of carbon c at 50 ppm) and vinyl groups (resonance of carbon h at 137 ppm and j at 126 ppm) are presented in the spectra. The different ratio of units in the polyDVB can be calculated

by Eq. 2.28. Consequently, the degree of branching and cyclisation ratio can be confirmed from previous equation (Eq. 2.26 and Eq. 2.27).

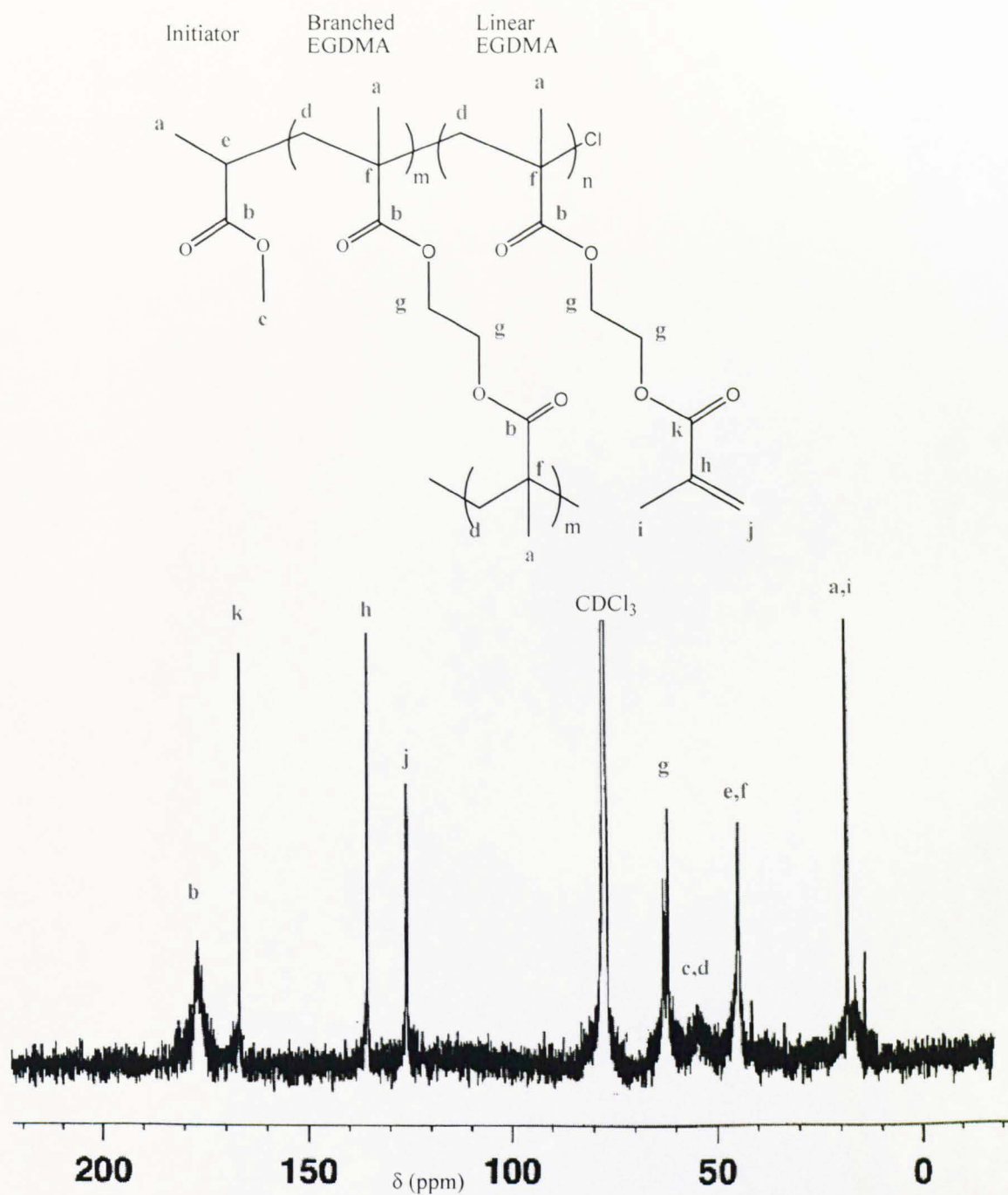


Figure 2.30 ^{13}C NMR spectroscopy spectra of the polyEGDMA sample in CDCl_3 (sample 5, Table 2.11) at 125 MHz, number of scans=8192.

Linear EGDMA=Integrals of j

Branched EGDMA=(Integrals of g/2)- linear EGDMA
 =(Integrals of g/2)- Integrals of j

Initiator=(Integrals of b)- Linear EGDMA- 2×Branched EGDMA
 =(Integrals of b)- (Integrals of j)- 2×[(Integrals of g/2)- Integrals of j]
 =(Integrals of b)- (Integrals of g)+(Integrals of j) (Eq. 2.28)

Furthermore, the ^{13}C NMR spectroscopy result agrees with the previous ^1H NMR spectroscopy study on poly(EGDMA), which noted that branched EGDMA units significantly increases with the yields and led to a highly intramolecular cross-linking structure between 4%-63% yield (Table 2.13 and Figure 2.31).

Table 2.13 The ratio of the different units in the polyEGDMA sample from ^1H NMR and ^{13}C NMR spectroscopy analysis.

Sample	Yield ^a (%)	^1H NMR			^{13}C NMR		
		I:L-EGDMA: B-EGDMA ^b	DB ^c	Cyclisation ratio ^d	I:L-EGDMA: B-EGDMA ^e	DB ^c	Cyclisation ratio ^d
1	3.0	1: 2 : 0.9	0.38	-	1:2.6: 1	0.36	-
2	13.1	1: 4.1: 2	0.44	0.14	1:5.3 : 2.6	0.45	0.18
3	36.5	1: 13: 4.7	0.40	0.19	1:12:6.2	0.49	0.27
4	55.4	1: 16.5: 9.4	0.51	0.31	1:17.4: 12	0.57	0.36
5	63.0	1: 20.6: 11	0.50	0.31	1:18 : 16.1	0.62	0.43

a. calculated gravimetrically

b. The ratio of different units in the polymer is calculated from the Eq. 2.23-Eq. 2.25 by ^1H NMR spectroscopy analysis. I=Initiator, L-EGDMA= Linear EGDMA unit, B-EGDMA= Branched EGDMA unit.

c. Degree of branching is calculated from the Eq. 2.26.

d. Cyclisation ratio is calculated from the Eq. 2.27. There are no cyclisation ratio values for the sample 1, since the ratio of branched EGDMA is lower than the initiator ratio in this sample.

e. The ratio of different units in the polymer is calculated from the Eq. 2.28 by ^{13}C NMR spectroscopy analysis.

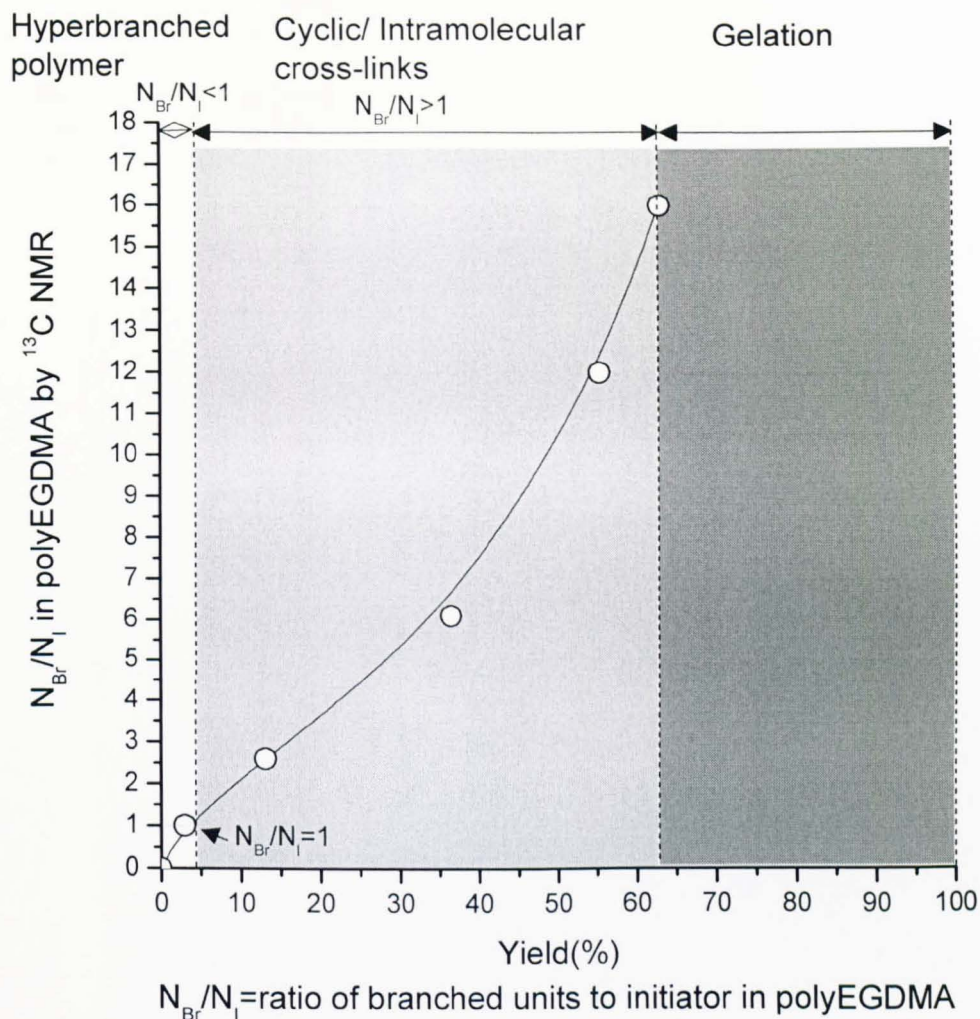


Figure 2.31 The ratio of branched EGDMA units to initiators (N_{Br}/N_I) in polyEGDMA by ^{13}C NMR spectroscopy analysis *versus* polymer yield. Statistically, it clearly shows the polyEGDMA is hyperbranched structure below 4% yield ($N_{Br}/N_I \leq 1$). In the range from 4% to 63% yield, the intramolecular cross-linkings are formed in polyEGDMA ($N_{Br}/N_I > 1$).

The difference in intrinsic viscosity ($[\eta]$) between polyEGDMA and linear PMMA further supports the hyperbranched structure within these polymers. A classical Mark-Houwink-Sakurada (MHS) plot (Figure 2.32) shows that the intrinsic viscosity of poly(EGDMA) is much lower than that of PMMA of similar molecular weight. In addition, the lower slope of $\log [\eta]$ *versus* $\log M_w$ indicates less interaction between solvent and the highly branched polymer^{3, 29, 37}.

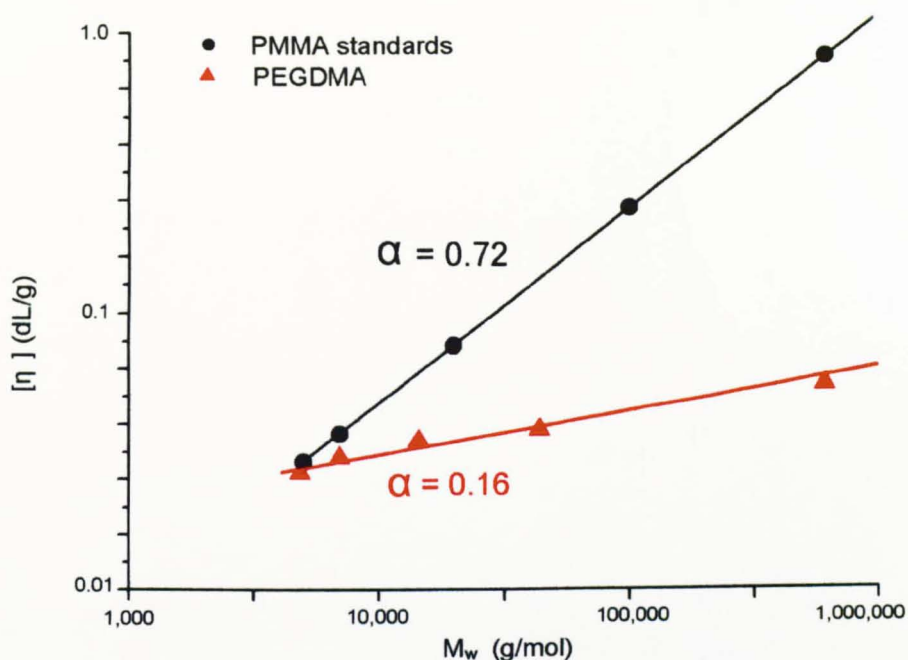


Figure 2.32 Plot of intrinsic viscosity *versus* weight average molecular weight for hyperbranched PEGDMA and linear PMMA. The intrinsic viscosities $[\eta]$ of the hyperbranched poly(EGDMA) are much lower than those of linear PMMA. MHS exponent $\alpha = 0.72$ for PMMA *versus* 0.16 for the hyperbranched poly(EGDMA) (Entry 5, Table 2.10).

2.4 Conclusion

Through deactivation enhanced ATRP, novel hyperbranched poly(DVB) and poly(EGDMA) polymers have been successfully prepared from homopolymerisations of commercially available multi-functional vinyl monomers. Cross-linking or microgel formation was not observed in the polymer provided that the overall monomer conversion is kept below 60%. This figure is far in excess of the yield that can be obtained with such high levels of branching via any other polymerisation mechanisms reported to-date. These new dendritic poly(DVB) and poly(EGDMA) polymers possess highly branched structures with a multiplicity of reactive vinyl and halogen end functional groups, and controlled chain structure. This new strategy for preparation of hyperbranched polymers could open up the field to the polymerisation of a very wide range multifunctional vinyl

monomers or combinations of comonomers in any proportion. This study has demonstrated that this strategy may be applied to ATRP, but could in principle be applied to other vinyl polymerisation mechanisms, *e.g.*, RAFT polymerisation depending on the nature of the initiation system and of the external stimulus that is applied. This new approach could have a major impact on the preparation and application of hyperbranched materials.

2.5 Reference

1. Wichterle, O.; Bartl, P.; Rosenberg, M. *Nature* **1960**, 186, (4723), 494-495.
2. Costello, P. A.; Martin, I. K.; Slark, A. T.; Sherrington, D. C.; Titterton, A. *Polymer* **2002**, 43, (2), 245-254.
3. Guan, Z. *Journal of the American Chemical Society* **2002**, 124, (20), 5616-5617.
4. Sato, T.; Sato, N.; Seno, M.; Hirano, T. *Journal of Polymer Science, Part A-Polymer Chemistry* **2003**, 41, (19), 3038-3047.
5. Isaure, F.; Cormack, P. A. G.; Graham, S.; Sherrington, D. C.; Armes, S. P.; Butun, V. *Chemical Communications* **2004**, (9), 1138-1139.
6. Liu, B. L.; Kazlauciunas, A.; Guthrie, J. T.; Perrier, S. *Macromolecules* **2005**, 38, (6), 2131-2136.
7. Matsumoto, A. *Synthesis and Photosynthesis* **1995**, 123, 41-80.
8. Zhu, S.; Hamielec, A. E. *Macromolecules* **1992**, 25, (20), 5457-5464.
9. Gao, H. F.; Li, W. W.; Matyjaszewski, K. *Macromolecules* **2008**, 41, (7), 2335-2340.
10. Yu, Q.; Zeng, F. Q.; Zhu, S. P. *Macromolecules* **2001**, 34, (6), 1612-1618.
11. Matyjaszewski, K.; Gaynor, S. G.; Muller, A. H. E. *Macromolecules* **1997**, 30, (23), 7034-7041.
12. Patten, T. E.; Xia, J. H.; Abernathy, T.; Matyjaszewski, K. *Science* **1996**, 272, (5263), 866-868.
13. Podzimek, S. *Journal of Applied Polymer Science* **1994**, 54, (1), 91-103.

14. Baudry, R.; Sherrington, D. C. *Macromolecules* **2006**, 39, (16), 5230-5237.
15. Podzimek, S.; Vlcek, T.; Johann, C. *Journal of Applied Polymer Science* **2001**, 81, (7), 1588-1594.
16. Podzimek, S.; Vlcek, T. *Journal of Applied Polymer Science* **2001**, 82, (2), 454-460.
17. Flory, P. J. *Journal of the American Chemical Society* **1941**, 63, 3096-3100.
18. Flory, P. J. *Journal of the American Chemical Society* **1941**, 63, 3091-3096.
19. Flory, P. J. *Journal of the American Chemical Society* **1941**, 63, 3083-3090.
20. Stockmayer, W. H. *Journal of Chemical Physics* **1943**, 11, (2), 45-55.
21. Stockmayer, W. H. *Journal of Chemical Physics* **1944**, 12, (4), 125-131.
22. Stockmayer, W. H.; Jacobson, H. *Journal of Chemical Physics* **1943**, 11, (8), 393-393.
23. Gao, H. F.; Matyjaszewski, K. *Progress in Polymer Science* **2009**, 34, (4), 317-350.
24. Rosselgong, J.; Armes, S. P.; Barton, W. R. S.; Price, D. *Macromolecules* **2010**, 43, (5), 2145-2156.
25. Law, R. V.; Sherrington, D. C.; Snape, C. E. *Macromolecules* **1997**, 30, (10), 2868-2875.
26. Li, Y. T.; Armes, S. P. *Macromolecules* **2005**, 38, (12), 5002-5009.
27. Hubbard, K. L.; Finch, J. A.; Darling, G. D. *Reactive & Functional Polymers* **1998**, 36, (1), 1-16.
28. Periyasamy, M.; Ford, W. T.; McEnroe, F. J. *Journal of Polymer Science Part a-Polymer Chemistry* **1989**, 27, (7), 2357-2366.
29. Mourey, T. H.; Turner, S. R.; Rubinstein, M.; Fréchet, J. M. J.; Hawker, C. J.; Wooley, K. L. *Macromolecules* **1992**, 25, (9), 2401-2406.
30. Zimm, B. H.; Stockmayer, W. H. *Journal of Chemical Physics* **1949**, 17, (12), 1301-1314.
31. Fréchet, J. M. J.; Henmi, M.; Gitsov, I.; Aoshima, S.; Leduc, M. R.; Grubbs, R. B. *Science* **1995**, 269, (5227), 1080-1083.
32. Kharchenko, S. B.; Kannan, R. M. *Macromolecules* **2003**, 36, (2), 407-415.

33. McGrath, K. J.; Roland, C. M.; Antonietti, M. *Macromolecules* **2000**, 33, (22), 8354-8360.
34. Lederer, A.; Voigt, D.; Clausnitzer, C.; Voit, B. *Journal of Chromatography A* **2002**, 976, (1-2), 171-179.
35. Wang, W. X.; Yan, D. Y.; Bratton, D.; Howdle, S. M.; Wang, Q.; Lecomte, P. *Advanced Materials* **2003**, 15, (16), 1348-1352.
36. Jiang, C. F.; Shen, Y. Q.; Zhu, S. P.; Hunkeler, D. *Journal of Polymer Science, Part A-Polymer Chemistry* **2001**, 39, (21), 3780-3788.
37. Hawker, C. J.; Freché, J. M. J.; Grubbs, R. B.; Dao, J. *Journal of the American Chemical Society* **1995**, 117, (43), 10763-10764.

CHAPTER THREE:

HYPERBRANCHED COPOLYMERS

The concept of the deactivation enhanced ATRP (DE-ATRP) was demonstrated in Chapter 2. In this chapter, the preparation of amphiphilic hyperbranched copolymers is demonstrated. Firstly, a novel hyperbranched polymer which contains a large number of hydrophilic blocks, active vinyl groups and halide groups was synthesised by copolymerising 2-(dimethylamino) ethyl methacrylate (DMAEMA) and ethylene glycol dimethacrylate (EGDMA). This synthesis has been successfully carried out through the enhanced deactivation ATRP technique. By controlling the competition between propagation and reversible termination the growth rate of polymer chains is decreased and the gelation reaction is prevented. A variety of reaction conditions were studied, for example, different solvents, monomer concentrations and especially the ratios of Cu(II)/Cu(I). This hyperbranched polymer has been used as a carrier to transfer water-soluble dyes into organic solvents. Secondly, another kind of hyperbranched copolymer was prepared by copolymerisation of poly(dimethylsiloxane mono methacrylate) (PDMSma) and divinylbenzene (DVB) in toluene. In addition, by tracking the relationship between gyration radius (R_g), elution volume and molecular weight, solid evidence for the highly branched structure was obtained. Last but not least, this polymer displayed interesting rheological properties and can be potentially used to thicken silicone oil.

3.1 Introduction

3.1.1 Hyperbranched Copolymers

Amphiphilic polymers are very important in practical applications, ie. emulsifiers, dispersion stabilisers and compatibilisers.^{1, 2} Amphiphilic polymers have the combination of the hydrophilic and hydrophobic properties. Due to their peculiar structures and rheological properties, dendritic polymers have also attracted a great

deal of attention recent years.³⁻¹⁰ Recently, people have also become interested in combining these two kinds of polymers to produce a dendritic and hydrophilic polymer as a gene delivery tool because it could overcome many issues.^{1, 11-14} The properties of dendrimers such as high degree of branching, multifunctional and globular architecture make them become the new scaffolds for drug delivery. The dendritic architecture can provide some advantages for drug delivery applications. First, the dendritic polymer with controlled functionalities can be used to attach different drug groups, for instance, drug molecules, targeting groups or image groups (Figure 3.1).

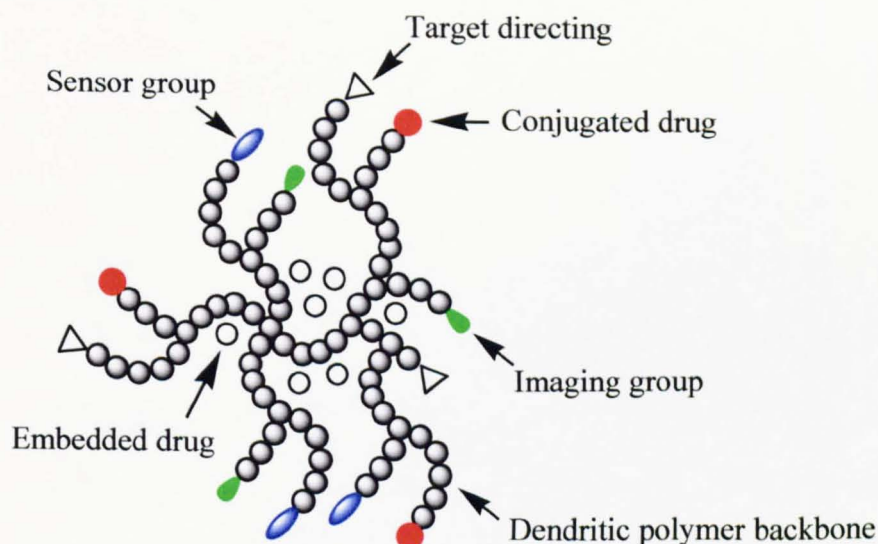


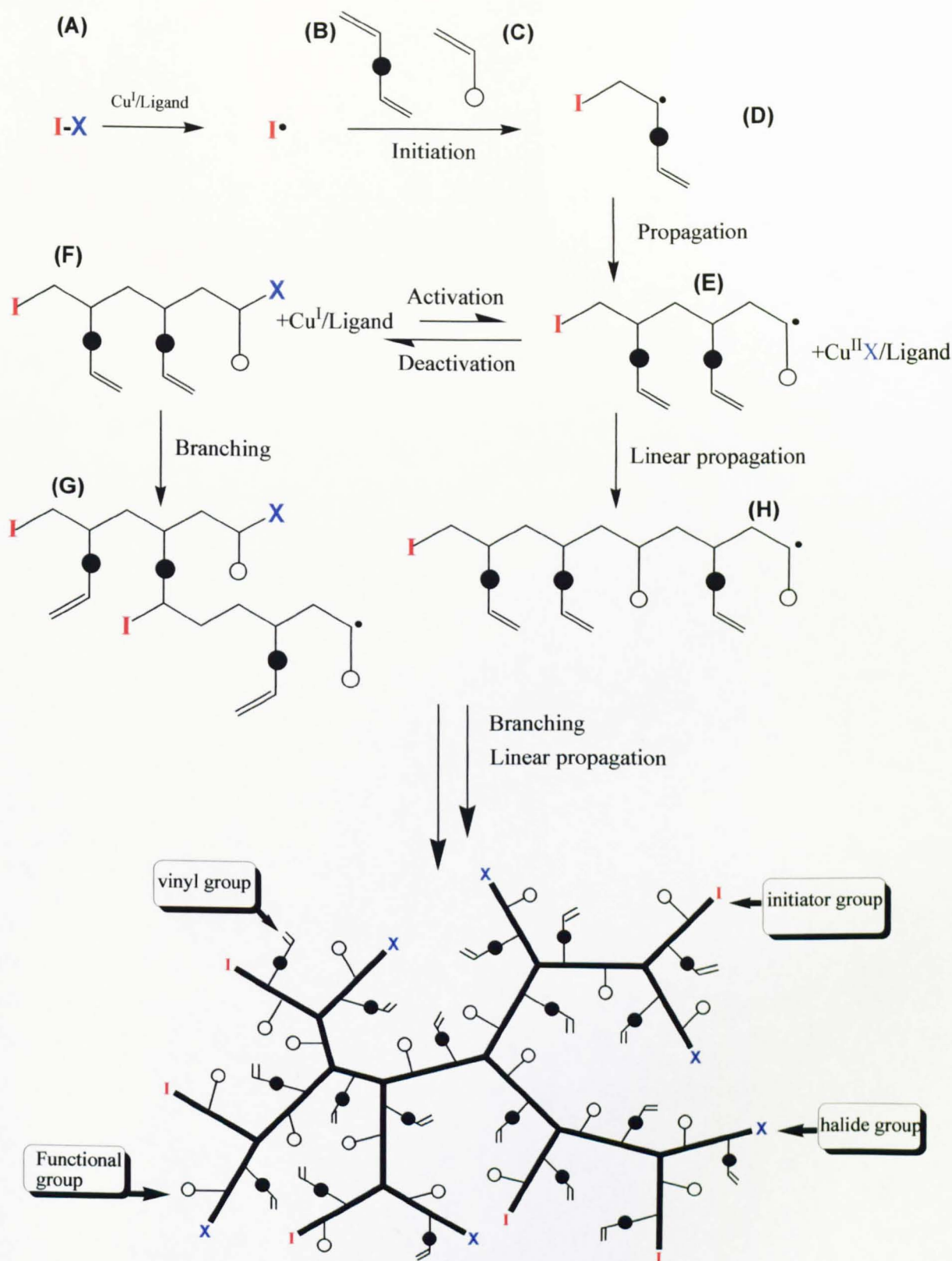
Figure 3.1 Scheme of multi-functional dendritic polymer for drug delivery.

Secondly, the globular shape of dendritic polymer could affect their biological properties which are different with the random coil structure of linear polymers. However, the production of dendrimers requires multistep syntheses with purification after each step, which makes it a costly and time-consuming process.^{15, 16} In contrast, hyperbranched polymers are often far easier to prepare under less strict reaction conditions. The classical approach towards hyperbranched polymers can be dated back to Flory's early description as a special type of polycondensation.¹⁷ This work was carried out on an AB_n monomer where A and B react with each other but not with themselves. In contrast, facile routes for preparing hyperbranched addition polymers

are rare. In 1994, self condensing vinyl polymerisation (SCVP) was first reported by Fréchet.¹⁸ Later, Fréchet and Aoshima first used ‘living cationic’ propagation but extended this to include ‘group transfer’ and ‘living free-radical’ processes. More recently, Matyjaszewski *et al.* have applied the principle of SCVP to atom transfer radical polymerisation (ATRP).^{19, 20} Useful as these routes are, they do require tailored vinyl monomers that are specifically functionalised to allow branching to occur. Beyond that, synthesis of highly branched macromolecules via one-step and one-pot processes has been reported by many scientists. Soluble highly branched polymer was prepared by cobalt-mediated free radical polymerisation as reported by Guan.²¹ Moreover, Sherrington and his co-workers reported a facile route to branched vinyl polymers, employing conventional free radical polymerisation of a vinyl comonomer with a di-functional comonomer in the presence of a free radical transfer agent to inhibit cross-linking and gelation.^{22, 23} Besides using the conventional chain-transfer agent in the synthesis of branched polymers, Sherrington’s and Armes’s groups both applied ATRP and group transfer polymerisation (GTP) to the synthesis of soluble branched polymers.²⁴ Perrier also adopted a similar procedure using reversible addition fragmentation chain transfer (RAFT).²⁵ The limitation of chain transfer methods is that they all require a high ratio of chain transfer agent. Thus, these methods can only yield a polymer with limited branched degree. In 2005, Armes’s group obtained branched polymers by the copolymerisation of EGDMA and DMAEMA using oxyanionic initiation. However, they could not find any vinyl groups in the polymers probably due to highly intra-cyclisation at high conversion.²⁶

In this chapter, a facile and versatile method for synthesis of highly branched dendritic copolymers has been demonstrated. Compared with the hyperbranched homopolymer in Chapter 3, the copolymer has less divinyl monomers but more useful functionalities. The scheme (Figure 3.2) outlines the basic concept: a divinyl monomer (B) and a mono-vinyl monomer (C) is selected with a catalyst system (A), in which I^\bullet is capable of initiating the polymerisation of vinyl monomer to produce multi vinyl macromonomer chain (E) This process is similar to the conventional free-radical

polymerisation. However, catalyst X can establish an equilibrium between the active macromonomer chain (E) and dormant macromonomer chain (F). The dormant species (F) can be converted to the active species (E) by thermal, photochemical, or chemical stimuli. In this way, all of the growing macromolecules are subject to a rapid equilibrium between active and dormant states. Unlike normal propagation where monomers are sequentially added into a polymer chain, in this approach the active species (E) can undergo two different mechanisms of propagation: either linear chain growth (H) by simple addition of monomer to the existing chain, or formation of branched polymer chains (G) by addition of monomer into the growing chain at the side vinyl group. As the concentration of the monomer decreases, the incorporation of oligomers such as (H) and moderate branched polymer (G) becomes statistically more frequent. If one neglects cyclisation, each of the newly formed branched macromolecules will still contain lots of polymerisable vinyl groups that may again be incorporated into other growing chains thereby increasing the number of branching sites and layers. Overall, a hyperbranched polymer with many vinyl groups and functionality is formed as a result of the vinyl polymerisation of linear and subsequently branched fragments.



Hyperbranched polymer with many end functional groups and vinyl functionality

Figure 3.2 The concept for deactivation ATRP hyperbranched copolymerisation process.

3.1.2 Hyperbranched Amphiphilic Copolymers

As described in Chapter 2, the deactivation enhanced concept is once more adapted in this copolymerisation. In the case of ATRP, the rate of polymerisation of divinyl monomer is first order with respect to concentration of monomer, initiator, and Cu (I) complex, and inversely proportional to Cu (II) concentration (Eq. 2.1, Chapter 2). Addition Cu (II) species added to the system can slow down propagation. Thus, control over the polymerisation rate can be obtained by manipulating the feed ratio of Cu (II)/Cu (I).²⁷ At low Cu (II)/Cu(I) ratios, even at very low conversion, the fast propagation rate will be easily form a network and lead to cross-linking. At high Cu(II)/Cu(I) ratio, more Cu(II) units can react initially affording many shorter reactive oligomers and ensuring that most of them are dormant species, since the excess Cu(II) will push the ATRP equilibrium to the deactivation direction.²⁷ Also the shorter propagation period allows the polymer chains to react with monomers and low molecular weight oligomers first. At low conversion, the concentration of monomer is relative much higher than the large molecules. In addition, the mobility and steric hindrance lead the monomers attach to the propagation centre easily. Finally, the polymer chains will react together to create large macromolecules at high conversion. The scheme (Figure 3.3) displays the synthesis of hyperbranched amphiphilic poly(EGDMA-*co*-DMAEMA) copolymer via enhanced deactivation ATRP. As the initiator generates a radical, it will propagate by added EGDMA or DMAEMA. The second vinyl groups have the chance to form a branch point for the polymer. As the polymer chains grow, they will prefer to add small molecules, e.g. monomers or small oligomers, due to not to the fact that only the small molecules easily diffuse onto the propagation site but also their relative higher concentration than large molecules. This prevents the reaction from cross-linking until high conversion. The final polymers will have a high branching degree provided by EGDMA and hydrophilic functionalities provided by DMAEMA.

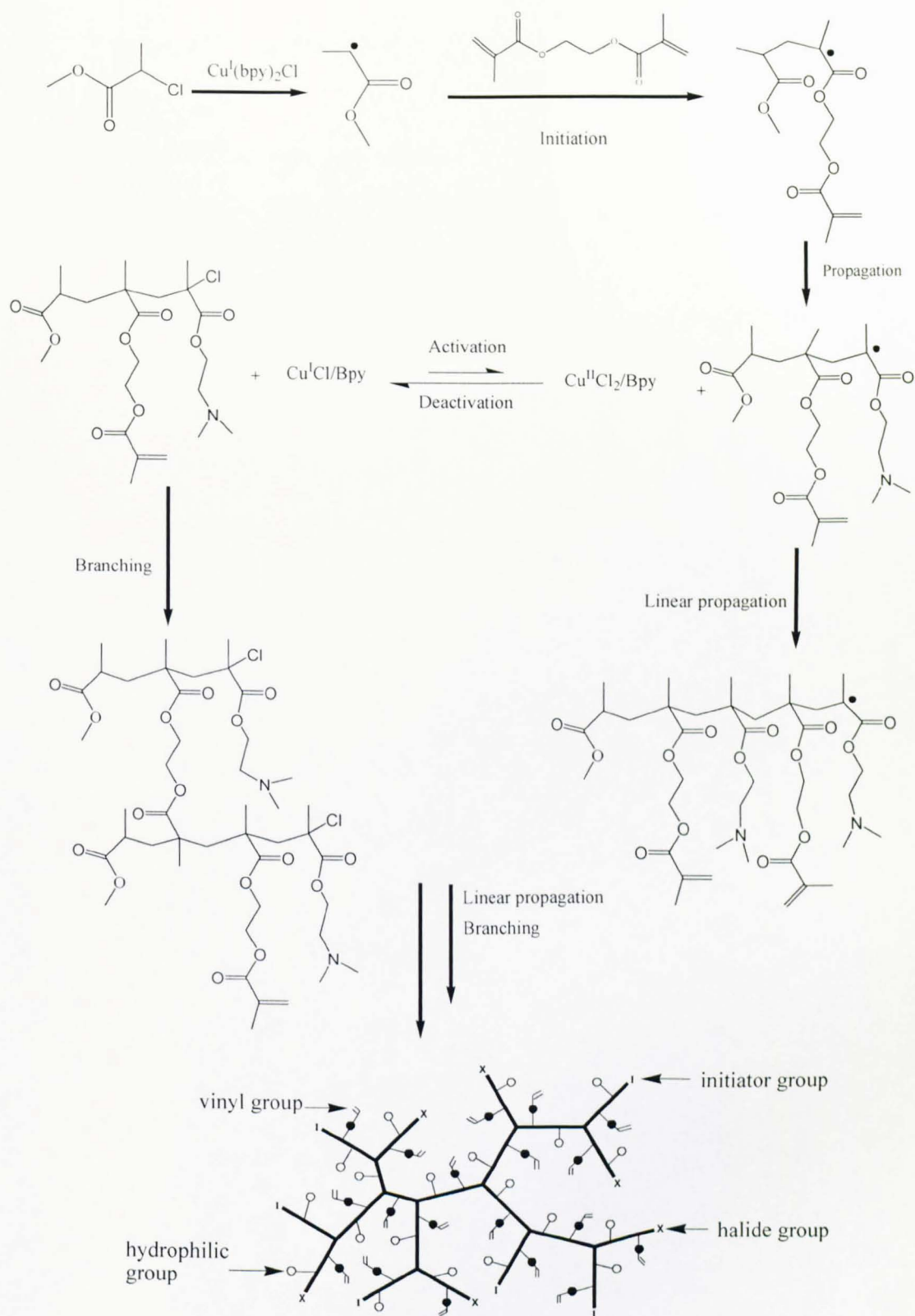


Figure 3.3 Schematic representation of the copolymerisation of EGDMA and DMAEMA via enhanced deactivation ATRP to afford highly branched amphiphilic architecture.

3.1.3 Hyperbranched Siloxane Copolymers

Following the early work in the development of hyperbranched polymers,⁴⁻⁶ the study of hyperbranched siloxy-type polymers is of great interest if one considers the wide-spread usage of linear poly(siloxanes).²⁸ Typically, poly(siloxanes) are known for their unusual properties, for instance, flexibility, low surface energy, very low glass transition temperature and permeability for gas.²⁹ In early studies, hyperbranched polymers can be made by direct coupling of AB_n monomers where n is 2 or greater, and where A and B are complementary reactive groups for coupling. This general strategy has been used for one step synthesis of hyperbranched polycarbosilanes. Due to the feasibility of end-group modification by the facile hydrosilation reaction, the synthesis of hyperbranched siloxy-type polymers with silicone hydride end groups has attracted researchers' attention.³⁰ In this way, siloxy based polymers and their derivatives displayed remarkable properties. For example, they can be used in areas such as catalysis and adhesion agent, or surface active polymers, or even as conducting materials. These applications can be achieved by using a hyperbranched structure which contains a multiplicity of tunable end groups. Furthermore, hyperbranched poly(siloxysilanes) and poly(alkoxysilanes) have been prepared by polyhydrosilation of AB_3 and AB_2 monomers. These polymers contain SiH and alkene functionalities.³¹⁻³³ Despite of the uncontrollable molecular weight, a self-regulating process has been suggested for the growth of these siloxy-type hyperbranched polymers. For example, Möller and his co-workers have reported the polymerisation of an AB_2 monomer to afford a degradable hyperbranched poly(bis-alkoxymethylsilane). This kind of polymer contains a broad molecular weight distribution that does not vary significantly upon addition of more monomer.³¹ It has been suggested that this behaviour is the result of formation of a globular molecule for which further growth is limited by steric hindrance.³⁰

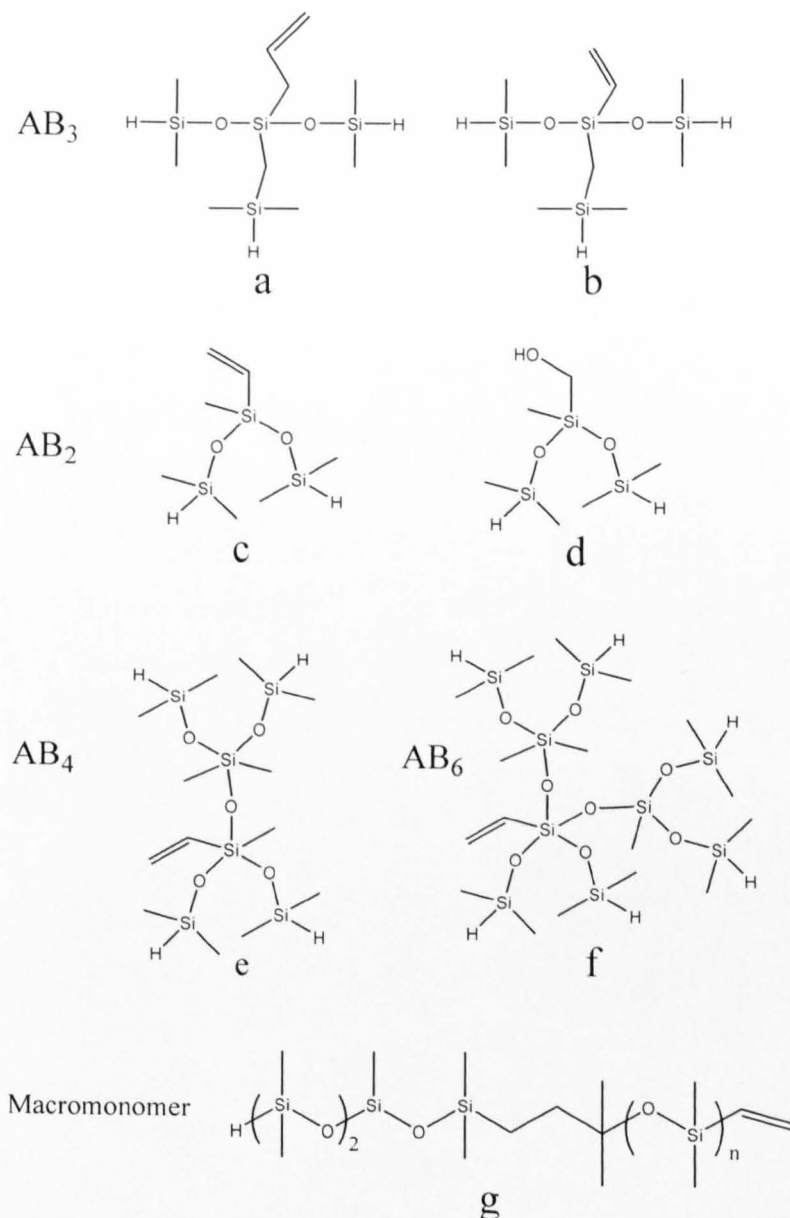


Figure 3.4 Monomers for the preparation of hyperbranched poly(siloxysilanes).

In earlier work, Mathias and his co-workers first reported³³ the preparation of a hyperbranched poly(siloxysilane) by polymerisation of allyltris(dimethylsiloxy)silane (Figure 3.4, a). The initial work found that the hyperbranched polymer had a narrow molecular weight distribution. It is suggested that this was perhaps caused steric inhibition to growth. Later on, reports on analogous systems by the same authors suggested that broader molecular distributions were obtained and the intramolecular cyclisation reaction of the monomer was prevalent in this system. Unfortunately, no

yields were provided in the preliminary communications regarding this work. Rubinsztajn³² has also reported the synthesis of related poly(siloxysilane) polymers. For example, polyhydrosilation of the AB₃ type monomer (Figure 3.4, b) produced the corresponding hyperbranched polymer with a molecular weight of 10,000 g mol⁻¹ and a polydispersity of 1.5. Fréchet *et al.* have reported the preparation of new hyperbranched polysiloxanes from AB₂, AB₄ and AB₆ monomers (Figure 3.4, c-f).³⁴ The advantage in using AB₄ and AB₆ monomers is that with AB₂ monomers, the intramolecular cyclisation reaction was significantly reduced. The preparation of hyperbranched polysiloxanes from macromonomers has also been reported.³⁵ However, all of the above methods have some common disadvantages: the synthetic procedure is complicated and the molecular weight obtained is below 10,000 Daltons.

In the second part of this chapter, a novel copolymerisation will be carried out to prepare hyperbranched siloxane polymer by enhanced deactivation ATRP (Figure 3.5). Generally, the concept of this reaction is similar to the copolymerisation of poly(EGDMA-*co*-DMAEMA). However, there are some differences with the previous reaction. Firstly, the polydimethylsiloxane mono methacrylate (PDMSma) was chosen as a macromonomer. Secondly, 1,1,4,7,10,10-Hexamethyltriethylenetetramine (HMTETA) was chosen for this reaction, since the reactivity of PDMSma is quite low and HMTETA has higher reaction rate than Bpy (see section 1.2.7, Chapter 1). Consequently, a hyperbranched poly(DVB-*co*-PDMSma) can be obtained from this reaction. The long PDMSma chains make the polymer soluble in silicone oil. Moreover, the large number of remain double bonds gave an opportunity for a gelation process to be carried out later.

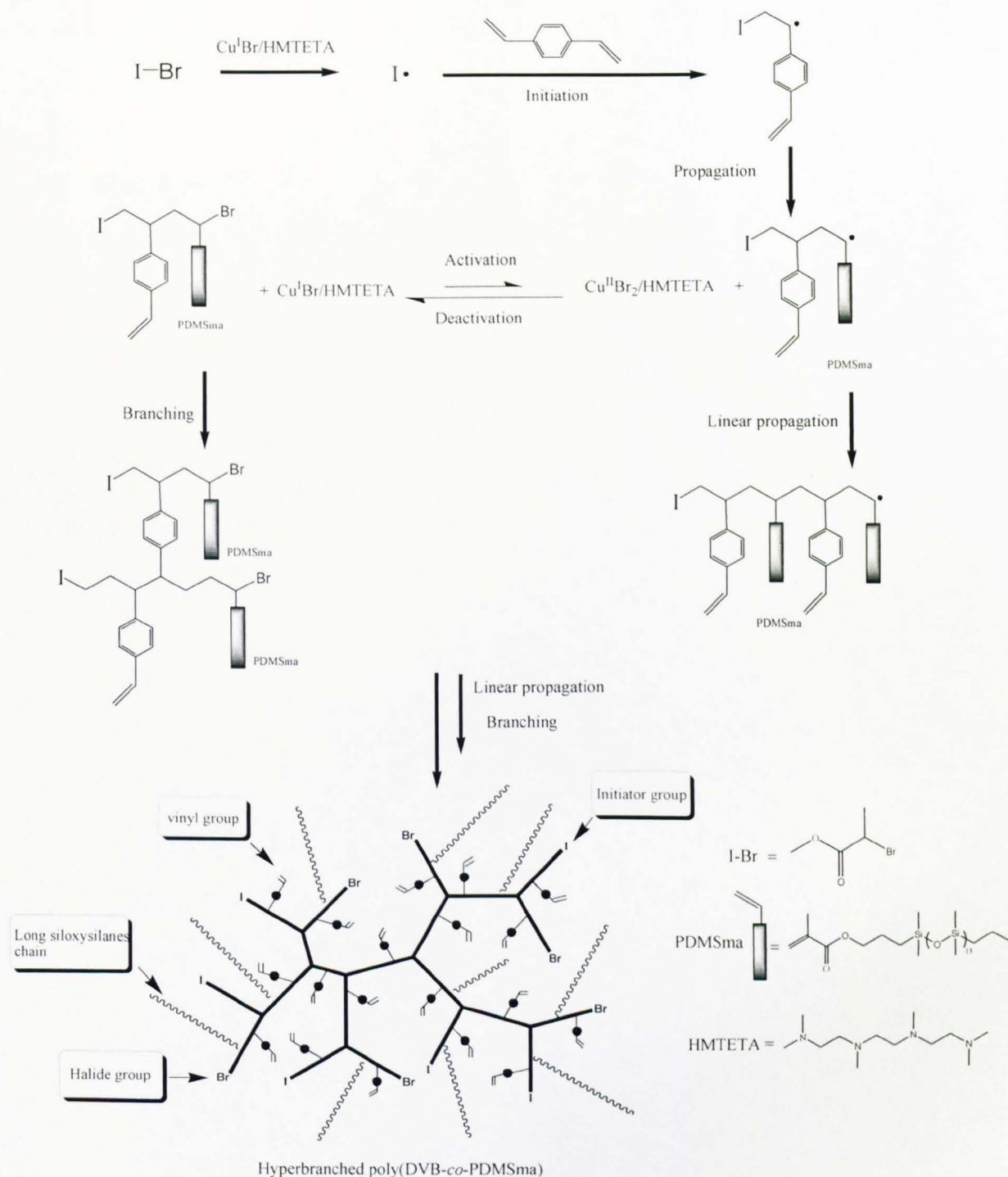


Figure 3.5 Mechanism of synthesis of hyperbranched poly(DVB-co-PDMSma) via enhanced deactivation ATRP.

3.2 Experimental

3.2.1 Materials

EGDMA and DMAEMA monomers (Aldrich) were passed through a column of activated basic alumina (ACROS) and purged with high purity nitrogen for 1 hour prior to use. Initiator stock solution was prepared by dissolving methyl 2-bromopropionate or methyl 2-chloropropionate (Aldrich) in 2-butanone (99.5%, HPLC grade, Aldrich). The concentration of methyl 2-bromopropionate was 0.815 mol L^{-1} and was degassed by high-purity nitrogen. 2, 2'-bipyridine (Bpy, Aldrich), copper(I) chloride (98%, Aldrich) and copper(II) chloride (99%, Lancaster) were used as received. Nitrogen was bubbled through the solutions in order to eliminate molecular oxygen. Liquids were transferred under nitrogen by means of septa and syringes or stainless steel capillaries.

All PDMS_{ma} samples were obtained from Sigma-Aldrich and used without further purification. Methacrylate-PDMS which has a molecular weight of approximately 10,000 g/mol (confirmed by ^1H NMR spectroscopy) was found to have a polydispersity index (PDI) of 1.1, determined by ourselves using gel permeation chromatography (GPC) calibrated with universal calibration. DVB monomer (Aldrich) was purified by passing through a column of activated basic alumina (ACROS) and purged with high-purity nitrogen for 1 hour prior to use. 1,1,4,7,10,10-hexamethyltriethylenetetramine (HMTETA, 97%, Aldrich), copper(I) bromide (98%, Aldrich), copper(II) bromide (98%, Aldrich) were used as received. Nitrogen was bubbled through the solutions in order to eliminate oxygen. Liquids were transferred under nitrogen by means of septa and syringes or stainless steel capillaries.

3.2.2 Polymerisation Procedures

Poly(EGDMA-*co*-DMAEMA)

Known amounts of CuCl, CuCl₂ and Bpy were added to a round bottom flask fitted with a three-way stopcock connected to either a nitrogen line or a vacuum pump. Oxygen was removed by repeated vacuum-nitrogen cycles. Once filled with nitrogen, the flask was filled with known amounts of degassed EGDMA, DMAEMA and THF. After stirring for one hour at room temperature, a known amount of methyl 2-chloropropionate was added and the polymerisation was conducted at the desired temperature. After polymerisation under stirring at 60 °C for the desired reaction time, the solution was diluted with THF and precipitated into a large excess of hexane. After separation by filtration, the polymer was dried under reduced pressure at 30 °C and weighed in order to calculate the monomer conversion. The polymer was characterised by ¹H NMR spectroscopy and MALLS-GPC.

An example for the DE-ATRP of poly(EGDMA-*co*-DMAEMA) in THF (Entry 6, Table 3.3)

CuCl (89 mg, 9.03x10⁻⁴ mol), CuCl₂ (41 mg, 3x10⁻⁴ mol) and 2,2'-bipyridine (376 mg, 2.4x10⁻³ mol) were added to a round bottom flask fitted with a three-way stopcock connected to either a nitrogen line or a vacuum pump. Oxygen was removed by repeated vacuum-nitrogen cycles. Once filled with nitrogen, the flask was filled with degassed EGDMA (23.79 g, 0.12 mol), DMAEMA (18.87 g, 0.12 mol) and THF (75 ml). After stirring for one hour at room temperature, 2.94 ml of 0.815 mol/L methyl 2-chloropropionate/butanone solution was added (2.4x10⁻³ mol), and the polymerisation was conducted at the 60 °C. The samples were taken at 5, 10, 20 and 29 hours, respectively. The polymer solution became a gel at 30 hours. The polymer sample was diluted with THF and precipitated into a large excess of cold hexane. Then, the polymer product can then be characterised by ¹H NMR spectroscopy, DLS and GPC-MALLS.

Poly(DVB-co-PDMSma)

known amounts of CuBr (0.33 equivalent) and CuBr₂ (0.11 equivalent) were added to a round bottom flask fitted with a three-way stopcock connected to either a nitrogen line or a vacuum pump. Oxygen was removed by repeated vacuum-nitrogen cycles. Once filled with nitrogen, the flask was filled with known amounts of degassed DVB, PDMSma, HMTETA (0.44 equivalent) and toluene. A known amount of methyl 2-bromopropionate (1 equivalent) was added, and the polymerisation was conducted at the desired temperature. After polymerisation under stirring at the chosen reaction temperature (typically 90 °C) for the desired reaction time, the solution was diluted with THF and precipitated into a large excess of methanol. After separated by filtration, the polymer was dried under reduced pressure at 30 °C and weighed in order to calculate the monomer conversion.

An example for the DE-ATRP of poly(DVB-co-PDMSma) in toluene (Entry 5, Table 3.12)

CuBr (35.4 mg, 2.46×10^{-4} mol), CuBr₂ (18.3 mg, 8.19×10^{-5} mol) and HMTETA (75.6 mg, 3.28×10^{-4} mol) were added to a round bottom flask fitted with a three-way stopcock connected to either a nitrogen line or a vacuum pump. Oxygen was removed by repeated vacuum-nitrogen cycles. Once filled with nitrogen, the flask was filled with degassed DVB (3.88 g, 2.98×10^{-2} mol), PDMSma (74.5 g, 7.45×10^{-3} mol) and toluene (50 ml). After stirring for one hour at room temperature, 0.91 ml of 0.815 mol/L methyl 2-bromopropionate/butanone solution was added (7.45×10^{-4} mol), and the polymerisation was conducted at the 90 °C. The samples were taken at 6, 12, 24 and 29 hours. Finally, the polymer solution gelled at 30 hours. The polymer sample was diluted with toluene and precipitated into a large excess of cold methanol. Finally, the polymer product can then be characterised by ¹H NMR and GPC-MALLS.

3.2.3 Characterisation Section

Multiangle Laser Light Scattering-Gel Permeation Chromatography (MALLS/ GPC).

Described as in experimental section of Chapter 2.

NMR Analysis of the Polymers

The chemical shift data are summarised as follows:

Poly(EGDMA-*co*-DMAEMA) δ ppm: 0.90-1.40 (backbone CH₃, b), 1.91 (terminal CH₃, d), 2.00 (backbone CH₂, a), 2.20 (N (CH₃)₂, j), 2.60 (NCH₂, i), 4.05-4.43 (OCH₂, h; OCH₂CH₂O, c), 5.60-6.12 (terminal C=CH_eH_f), 7.26 (solvent, s), see Figure 3.13.

Poly(DVB-*co*-PDMSma) δ ppm: 0.08 PDMS (Si(CH₃)₂, l), 0.6 (PDMS Si-CH₂, k), 0.9 (PDMS terminal CH₃, n), 1.3 (PDMS CH₂CH₂, c and backbone CH₃, h), 1.8 (PDMS CH₂, j), 0.8-2.8 (DVB backbone CH₂CH, a,b and PDMS backbone CH₂, g), 3.5 (initiator OCH₃, o), 4.0 (PDMS OCH₂, i) 6.12 (terminal C=CH, e), 5.2 and 5.6 (DVB vinyl CH₂, e, f), 6.0-7.6(DVB benzyl ring CH, c and CH, d), 7.26 (solvent), see Figure 3.28.

Encapsulation of water-soluble dyes

Typically, 10 mL aqueous solution of methyl orange (MO, 3×10^{-5} molL⁻¹) or Congo red (CR, 9×10^{-5} molL⁻¹) was mixed with 10 mL chloroform solution of the amphiphilic hyperbranched polymer (polyEGDMA-*co*-DMAEMA) at different concentration in a glass vial. The mixture was shaken for 24 hours to ensure the two phases were mixed adequately. The bottom layer of chloroform solution was transferred to a 1 cm UV/vis cuvette after the two phases were completely separated, and its UV/vis spectrum was recorded. In all of the experiments, the dye in the aqueous solution was in excess to ensure saturation solution and ensure its encapsulated amount achieving the maximum of the loading capacity (C_{load}). The encapsulated amount of dye per hyperbranched polymer ([MO]/[polymer] or [CR]/

[polymer]) was determined quantitatively. (MO UV/vis: $\lambda_{\max}=460$ nm; CR UV/vis: $\lambda_{\max}=510$ nm) The calibration line of absorbance against dye concentration is shown in Table 3.1 and Figure 3.6:

Table 3.1 The calibration data of dyes for the encapsulation test.

Congo Red		Methyl Orange	
Concentration ($\times 10^{-6}$ molL $^{-1}$)	Absorption (AU)	Concentration ($\times 10^{-6}$ molL $^{-1}$)	Absorption (AU)
3	0.1434	3.5	0.1079
6	0.2839	7.63	0.2558
12	0.5395	16.8	0.4647
24	0.978	22.9	0.7213
Absorption= [CR] $\times 10^6 \times 0.0405 + 0.0246$ Adj. R-square=0.99598		Absorption= [MO] $\times 10^6 \times 0.0302 + 0.00271$ Adj. R-square=0.99027	

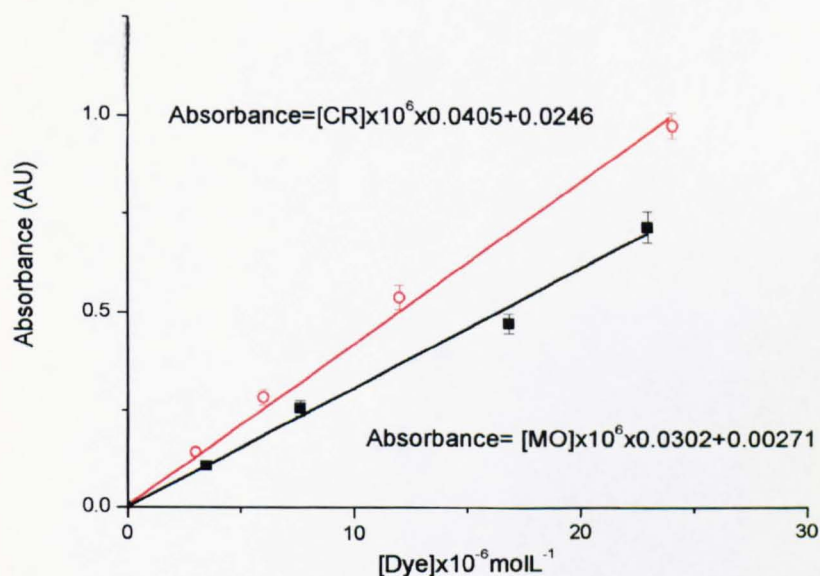


Figure 3.6 Calibration plot for absorbance in UV-vis against concentration of Congo red (upper line) and methyl orange (lower line) in water.

Thus, the relationship of dyes and absorbance by UV-vis can be obtained from the calibration plot. (Eq. 3.1) It worth noticed that the accurate calibration should be obtained in chloroform solution. However, it is impossible to get the calibration data

of dyes in chloroform, since the dyes cannot dissolve in chloroform. Thus, the calibration data in water is always used for the calculation from the previous published research works³⁶⁻³⁸.

Congo red: Absorption= $[CR] \times 10^6 \times 0.0405 + 0.0246$

Methyl orange: Absorption= $[MO] \times 10^6 \times 0.0302 + 0.00271$ (Eq. 3.1)

Here, a detailed example of Congo red encapsulation ability by hyperbranched poly(EGDMA-*co*-DMAEMA) was given (Figure 3.7, Figure 3.8 and Table 3.2). There is not any absorbance from the hyperbranched polymer in the range of 400 nm to 600 nm. After the Congo red encapsulation into chloroform by polymer, the UV-vis shows a series of spectra with different absorbance of Congo red in chloroform (Figure 3.7). The absorbance of dye was increased with polymer concentration in chloroform. For example, the absorbance is 0.114 when the concentration of poly(EGDMA-*co*-DMAEMA) is $0.56 \times 10^{-6} \text{ mol L}^{-1}$ in chloroform (red line, Figure 3.7). The absorbance is 0.3595 when the concentration of polymer is $2.1 \times 10^{-6} \text{ mol L}^{-1}$ (black line, Figure 3.7).

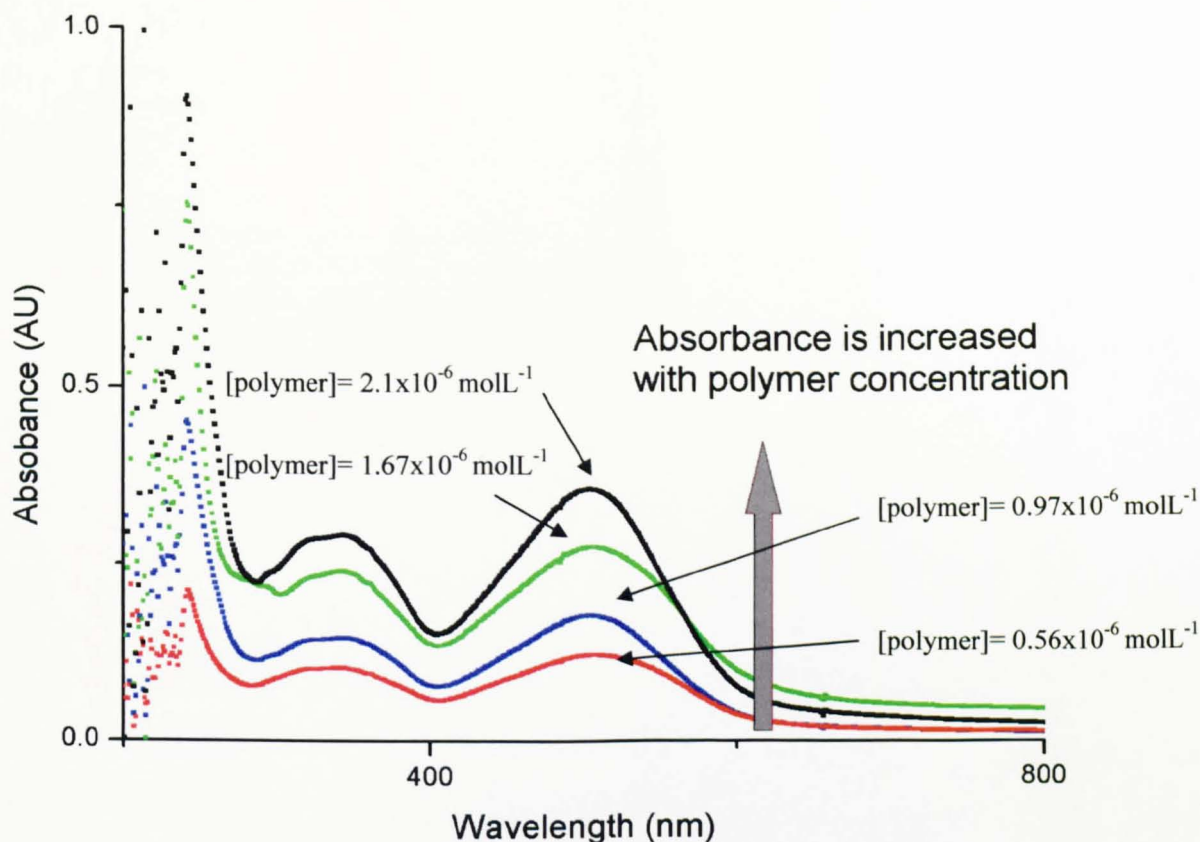


Figure 3.7 Different UV-vis absorbance spectra of Congo red dyes in chloroform which encapsulation by a series concentration of hyperbranched poly(EGDMA-co-DMAEMA). The concentration of hyperbranched polymer in chloroform is $0.56 \times 10^{-6} \text{ molL}^{-1}$ (bottom line), $0.97 \times 10^{-6} \text{ molL}^{-1}$ (second line), $1.67 \times 10^{-6} \text{ molL}^{-1}$ (third line) and $2.1 \times 10^{-6} \text{ molL}^{-1}$ (top line).

Then, the concentration of Congo red encapsulation by polymer in chloroform can be calculated by the calibration equation (Eq. 3.1). All the results were listed in Table 3.2. For example, the concentration of Congo red is 2.21 when absorbance is 0.114 (Entry 1, Table 3.2). Last, a plot of polymer concentration against dye concentration in chloroform was drawn (Figure 3.8). Typically, the encapsulation ability of the hyperbranched polymer is invariable at any concentration. Thus, the dye load amount is expected to proportionally increase with the polymer concentration. Therefore, the slope of the line is the encapsulation ability of Congo red by polymer in Figure 3.8. In the figure, the encapsulation ability is 3.93 indicate each hyperbranched polymer can transfer 3.93 Congo red molecules into chloroform.

Table 2.2 Detailed results for the of Congo red encapsulation ability by hyperbranched poly(EGDMA-*co*-DMAEMA). (see Entry 1, Table 3.9)

Entry	[Polymer] $10^{-6} \text{ molL}^{-1}$	CR Absorbance	[CR] $10^{-6} \text{ molL}^{-1}$	Encapsulation ability [CR]/[Polymer]
1	0.56	0.114	2.21	3.93
2	0.97	0.179	3.82	
3	1.67	0.291	6.58	
4	2.1	0.3595	8.27	

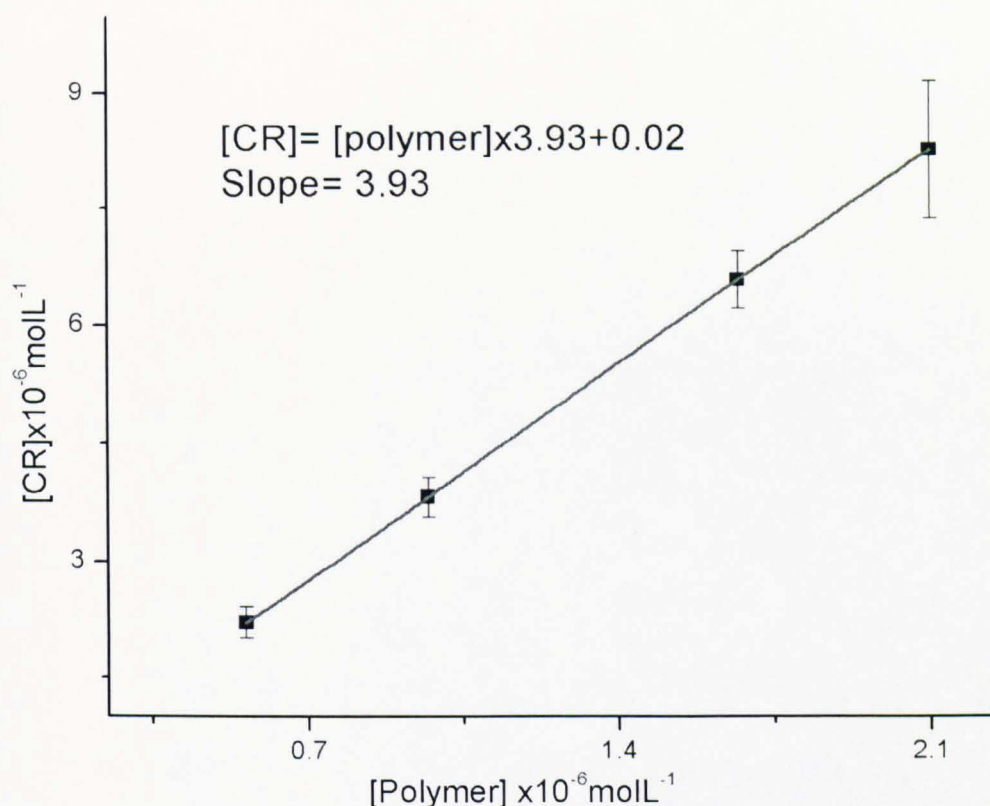


Figure 3.8 Plot of polymer concentration against Congo red concentration in chloroform after encapsulation. The slope of the line is 3.93 which represent each hyperbranched polymer can transfer 3.93 Congo red molecules into chloroform.

Comparison of encapsulation ability of hyperbranched and linear polymer

The hyperbranched poly(EGDMA-*co*-DMAEMA) sample (Entry 1, Table 3.9) was prepared via enhanced deactivation ATRP. The reaction condition is [I]: [EGDMA]: [DMAEMA]: [Cu^I]: [Cu^{II}]: [bpy]= 1:50:50:0.375:0.125:1 in THF at 60 °C. The

sample was taken at 10 hours and precipitated into cold hexane. The weight average molecular weight (M_w) of sample is $5.0 \times 10^4 \text{ g mol}^{-1}$ by GPC-MALLS and the composition was confirmed by ^1H NMR spectroscopy analysis.

The linear poly(MMA-*co*-DMAEMA) sample (Entry 2, Table 3.9) was prepared via normal ATRP (without added excess Cu^{II}). The reaction condition is [I]: [MMA]: [DMAEMA]: [Cu^{I}]:[bpy]= 1:150:150:0.3:0.6 in THF at 60 °C. In practice, CuCl (71.3 mg, 7.2×10^{-4} mol) and 2,2'-Bipyridine (225 mg, 1.44×10^{-3} mol) were added to a round bottom flask fitted with a three-way stopcock connected to either a nitrogen line or a vacuum pump. Oxygen was removed by repeated vacuum-nitrogen cycles. Once filled with nitrogen, the flask was filled with degassed MMA (35.7 g, 0.36 mol), DMAEMA (56.7 g, 0.36 mol) and THF (160 ml). After stirring for one hour at room temperature, 2.94 ml of 0.815 mol/L methyl 2-chloropropionate/Butanone solution was added (2.4×10^{-3} mol), and the polymerisation was conducted at the 60 °C. The sample was taken at 18 hours and precipitated into cold hexane. The molecular weight of linear poly(MMA-*co*-DMAEMA) was $M_w = 4.7 \times 10^4 \text{ g mol}^{-1}$ as determined by GPC-MALLS. The composition of polymer is confirmed by ^1H NMR spectroscopy (Figure 3.9). The resonance f at 3.6 ppm corresponds to the proton of CH_3 group in the MMA unit, and the resonance c at 4.2 ppm corresponds to the proton of $-\text{OCH}_2$ in the DMAEMA unit. The composition of MMA and DMAEMA units was calculated by Eq. 3.2. In this sample, the DMAEMA composition in copolymer is 46% mole ratio:

$$\frac{\text{MMA}}{\text{DMAEMA}} = \frac{(\text{Integrals of peak f})/3}{(\text{Integrals of peak c})/2} \quad (\text{Eq. 3.2})$$

The encapsulation abilities of linear poly(MMA-*co*-DMAEMA) and hyperbranched poly(EGDMA-*co*-DMAEMA) were examined by UV-vis spectroscopy analysis. The encapsulation procedure is conducted as before.

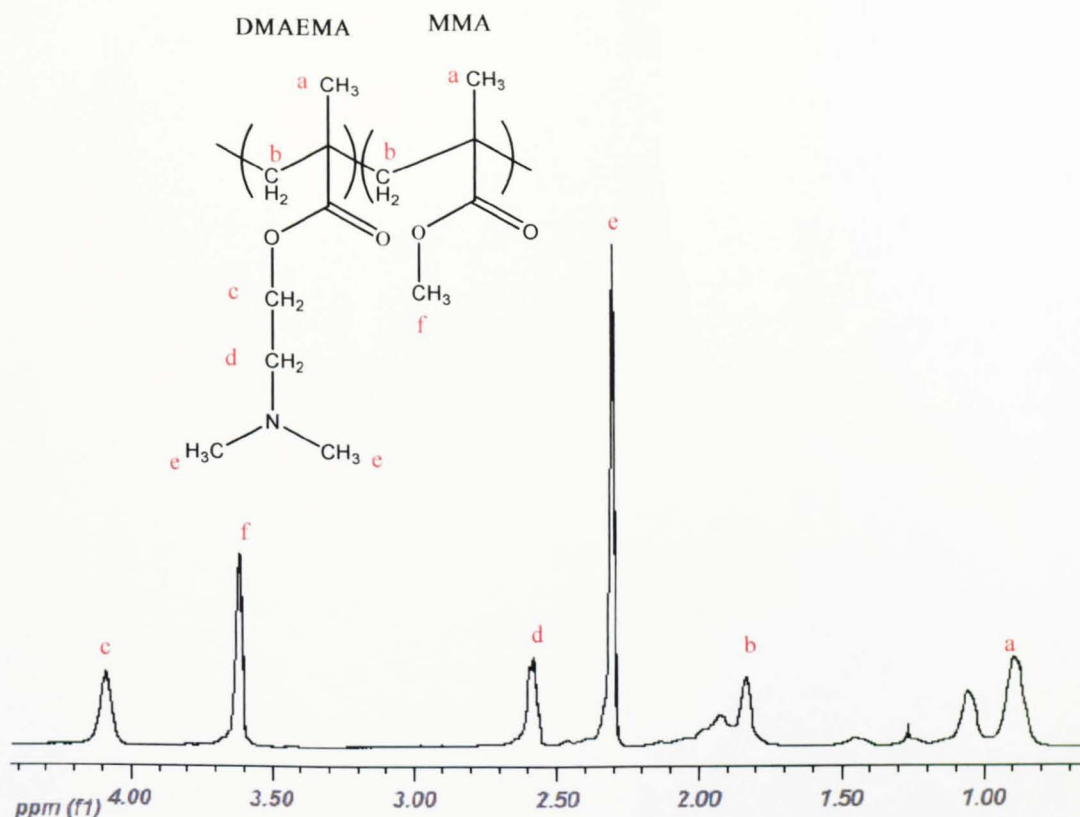


Figure 3.9 ^1H NMR spectroscopy of linear poly(MMA-*co*-DMAEMA) in CDCl_3 . The composition of copolymer can be calculated by the resonance of protons c and f. (See Eq. 3.2)

Effect of molecular weight of hyperbranched polymer on dye transfer ability

The hyperbranched poly(EGDMA-*co*-DMAEMA) sample was prepared via DE-ATRP (Table 3.10). The reaction condition is $[\text{I}]:[\text{EGDMA}]:[\text{DMAEMA}]:[\text{CuI}]:[\text{CuII}]:[\text{bpy}] = 1:50:50:0.375:0.125:1$ in THF at 60°C . The synthesis procedure was conducted as the same as described in above. The sample was taken at 2, 6 and 10 hours and precipitated into cold hexane. The molecular weights (M_w) of three samples are 1.2×10^4 , 3.7×10^4 and $5.0 \times 10^4 \text{ g mol}^{-1}$ as determined by GPC-MALLS, respectively. The three poly(EGDMA-*co*-DMAEMA) samples were taken for Congo red and Methyl orange encapsulation test as described above.

Composition of hyperbranched polymer effect on dye transfer ability

Poly(EGDMA-*co*-DMAEMA) samples of different composition were prepared via DE-ATRP.

The first reaction condition is [I]:[EGDMA]:[DMAEMA]:[CuI]:[CuII]:[bpy]=1:50:50:0.375:0.125:1 in THF at 60 °C (Entry 1, Table 3.11). In practice, CuCl (89 mg, 9.03×10^{-4} mol), CuCl₂ (41 mg, 3×10^{-4} mol) and 2,2'-Bipyridine (376 mg, 2.4×10^{-3} mol) were added to a round bottom flask fitted with a three-way stopcock connected to either a nitrogen line or a vacuum pump. Oxygen was removed by repeated vacuum-nitrogen cycles. Once filled with nitrogen, the flask was filled with degassed EGDMA (23.79 g, 0.12 mol), DMAEMA (18.87 g, 0.12 mol) and THF (75 ml). After stirred for one hour at room temperature, 2.94 ml of 0.815 mol/L methyl 2-chloropropionate/butanone solution was added (2.4×10^{-3} mol), and the polymerisation was conducted at the 60 °C. The sample was taken at 10 hours and precipitated into cold hexane. The M_w of sample was 5.0×10^4 gmol⁻¹ as determined by GPC-MALLS and the composition was confirmed by ¹H NMR spectroscopy analysis.

The second reaction condition is [I]:[EGDMA]:[DMAEMA]:[CuI]:[CuII]:[bpy]=1:25:75:0.375:0.125:1 in THF at 60 °C (Entry 2, Table 3.11). In practice, CuCl (89 mg, 9.03×10^{-4} mol), CuCl₂ (41 mg, 3×10^{-4} mol) and 2,2'-bipyridine (376 mg, 2.4×10^{-3} mol) were added to a round bottom flask fitted with a three-way stopcock connected to either a nitrogen line or a vacuum pump. Oxygen was removed by repeated vacuum-nitrogen cycles. Once filled with nitrogen, the flask was filled with degassed EGDMA (11.88 g, 0.06 mol), DMAEMA (28.3 g, 0.18 mol) and THF (75 ml). After stirring for one hour at room temperature, 2.94 ml of 0.815 mol/L methyl 2-chloropropionate/butanone solution was added (2.4×10^{-3} mol), and the polymerisation was conducted at the 60 °C. The sample was taken at 13 hours and precipitated into cold hexane. The M_w of sample was 4.6×10^4 gmol⁻¹ as determined by GPC-MALLS and the composition was confirmed by ¹H NMR spectroscopy

analysis.

The third reaction condition is [I]:[EGDMA]:[DMAEMA]:[CuI]:[CuII]:[bpy]=1:75:25:0.375:0.125:1 in THF at 60 °C (Entry 3, Table 3.11). In practice, CuI (89 mg, 9.03×10^{-4} mol), CuCl₂ (41 mg, 3×10^{-4} mol) and 2,2'-bipyridine (376 mg, 2.4×10^{-3} mol) were added to a round bottom flask fitted with a three-way stopcock connected to either a nitrogen line or a vacuum pump. Oxygen was removed by repeated vacuum-nitrogen cycles. Once filled with nitrogen, the flask was filled with degassed EGDMA (11.88 g, 0.18 mol), DMAEMA (9.43 g, 0.06 mol) and THF (75 ml). After stirred for one hour at room temperature, 2.94 ml of 0.815 mol/L methyl 2-chloropropionate/butanone solution was added (2.4×10^{-3} mol), and the polymerisation was conducted at the 60 °C. The sample was taken at 8 hours and precipitated into excess cold hexane. The M_w of sample was 5.6×10^4 g mol⁻¹ as determined by GPC-MALLS and the composition was confirmed by ¹H NMR spectroscopy analysis. The three poly(EGDMA-*co*-DMAEMA) samples were taken for Congo red encapsulation test as described above.

Copolymerisation of divinylbenzene (DVB) and polydimethylsiloxane mono methacrylate (PDMSma)

1. Known amounts of CuBr (0.33 equivalent) and CuBr₂ (0.11 equivalent) were added to a round bottom flask fitted with a three-way stopcock connected to either a nitrogen line or a vacuum pump. Oxygen was removed by repeated vacuum-nitrogen cycles.
2. Once filled with nitrogen, the flask was filled with known amounts of degassed DVB, PDMSma, HMTETA (0.44 equivalent) and toluene.
3. A known amount of methyl 2-bromopropionate (1 equivalent) was added, and the polymerisation was conducted at the desired temperature.
4. After polymerisation under stirring at the chosen reaction temperature (typically 90 °C) for the desired reaction time, the solution was diluted with THF and precipitated into a large excess of methanol. After separated by filtration, the

polymer was dried under reduced pressure at 30 °C and weighed to calculate the polymer yield.

An example for the DE-ATRP of poly(DVB-*co*-PDMSma) in toluene was conducted as below (Entry 5, Table 3.12). CuBr (35.4 mg, 2.46×10^{-4} mol), CuBr₂ (18.3 mg, 8.19×10^{-5} mol) and HMTETA (75.6 mg, 3.28×10^{-4} mol) were added to a round bottom flask fitted with a three-way stopcock connected to either a nitrogen line or a vacuum pump. Oxygen was removed by repeated vacuum-nitrogen cycles. Once filled with nitrogen, the flask was filled with degassed DVB (3.88 g, 2.98×10^{-2} mol), PDMSma (74.5 g, 7.45×10^{-3} mol) and toluene (50 ml). After stirred for one hour at room temperature, 0.91 ml of 0.815 mol/L methyl 2-bromopropionate/butanone solution was added (7.45×10^{-4} mol), and the polymerisation was conducted at the 90 °C. The samples were taken at 6, 12, 24 and 29 hours. Finally, the polymer solution gelled at 29.5 hours.

Viscosity Test

The viscosity test was to exam the viscosity of polymer solution at different concentration. The poly(siloxanes) hyperbranched polymer ($M_w = 2.4 \times 10^4$ g mol⁻¹) and linear polyPDMSma ($M_w = 2.0 \times 10^4$ g mol⁻¹) was dissolved in Dow Corning 245 oil across a series of concentrations. The viscosity has been tested under different shear rates (100-1000 [1/s]) by Physica MCR, 301 Rheometer (Anton Paar).

Fast gelling test

5% wt Hyperbranched poly(DVB-*co*-PDMSma) ($M_w = 2.79 \times 10^5$ g mol⁻¹) and 0.5% initiator (AIBN) are added into stearyl ether oil (Arlamol E), silicone oil (Dow Corning 245) or ester oil (Estol 1512). Thereafter, the solution was stirred by magnetic stirrer and heated to 70 °C, the viscosity of oil is increased significantly, even resulting in gel formation over a period of one minute.

3.3 Result and Discussion

3.3.1 Hyperbranched Poly(EGDMA-co-DMAEMA)

Copolymerisation of EGDMA and DMAEMA was conducted in a solution polymerisation system. The below table (Table 3.3) summarises all the results observed. Initially, the copolymerisation experiments were conducted in the polar solvent methanol as a homogeneous reaction system at room temperature (Entry 1, 2 and 4, Table 3.3). In the first three low EGDMA level reactions (5%, 10% and 25% monomer feed ratio of EGDMA), hyperbranched polymer was obtained successfully in methanol (Entry 1, 2 and 4, Table 3.3). However, for the high EGDMA level (50%), the gel point appeared very early by polar solvent methanol (Entry 5, Table 3.3). Therefore, the less polar solvent THF was used to suppress the active free radical concentration because the ATRP conducted in THF is much slower than methanol. Meanwhile, the temperature was increased to 60 °C to make sure the polymerisation can be completed in a proper time range (Entry 6, Table 3.3). As a result, the polymer was obtained at 58% yield and molecular weight up to $7.8 \times 10^4 \text{ g mol}^{-1}$ (Entry 6, Table 3.3). Furthermore, at the same feed ratio of monomer, the ratio of Cu (II) species determined the deactivation rate and final soluble polymer yields (Compare Entry 3 and 4, Entry 6 and 7, Table 3.3). As Cu (II) addition enhances the rate of deactivation, the polymerisation rate was significantly decreased. High yield and controlled molecular weight soluble hyperbranched polymer were obtained (Entry 4 and 6, Table 3.3). Despite of the very long reaction time, cross-linking was not observed even in the concentrated system ($[\text{EGDMA}] = 1.02 \text{ M}$, Entry 6, Table 3.3). Clearly, cross-linking and gel formation eventually occurred in these systems, but only when the conversion was pushed beyond 58%.

Table 3.3 Copolymerisations of EGDMA and DMAEMA by deactivation enhanced ATRP. A high ratio of Cu(II)/Cu(I) slows the significant reaction rate leading to high yields of hyperbranched polymer without formation of gels.^a

Entry	[DMAEMA] : [EGDMA] : [I] : [Cu ^I] : [Cu ^{II}] (mol ratio)	EGDMA (mol/L)	Solvent	T (°C)	Time (h)	GPC-MALLS			Yield ^d
						M _n × 10 ⁻⁴ (g mol ⁻¹)	M _w × 10 ⁻⁴ (g mol ⁻¹)	PDI	
1	47.5 : 2.5 : 1 : 0.375 : 0.125	0.102	MeOH	rt	39.5	2.7	4.2	1.6	69%
2	45 : 5 : 1 : 0.375 : 0.125	0.204	MeOH	rt	20	1.82	7.5	4.7	60%
3	37.5 : 12.5 : 1 : 0.375 : 0.125	0.54	MeOH	rt	9	1.1	3.9	3.5	38%
4	37.5 : 12.5 : 1 : 0.25 : 0.25	0.54	MeOH	rt	14	1.9	3.4	1.8	49%
5	50 : 50 : 1 : 0.375 : 0.125	1.02	MeOH	rt	6	0.5	1.2	2.4	13%
6	50 : 50 : 1 : 0.375 : 0.125	1.02	THF	60	29	6.3	7.8	1.3	58%
7 ^b	50 : 50 : 1 : 0.375 : 0	1.02	THF	60	2			Gel	
8 ^c	50 : 50 : 1	1.02	THF	60	0.5			Gel	

a. In all reactions, [Cu^I+Cu^{II}]/[Bpy] = 1:2.

b. Reaction 7 reacted under normal ATRP polymerisation conditions without addition of CuCl₂.

c. Reaction 8 is a normal radical solution polymerisation used AIBN as initiator.

d. Calculated gravimetrically

More details about reaction 6 of Table 3.3 are given in below table (Table 3.4).

Initially, the molecular weight is increased with conversion, from 3.42×10^4 g mol⁻¹ at 20% yield to 7.8×10^4 g mol⁻¹ at 58% yield. In addition, the polymerisation rate becomes slower at higher yield as the monomer concentration is decreased. For example, the yield is increased to 20% during the first 5 hours and only 9% in the last 9 hours. Furthermore, polydispersity of sample indicates the formation of predominantly linear polymer chains with moderate branching and the molecular weight distribution is narrow at low monomer conversion ($PDI_{MALLS}=1.2$ at 5 hours, Entry 1 in Table 3.4). As the reaction proceeds, both the molecular weight and polydispersity increased due to the combination of multi-vinyl polymers at high conversion

($PDI_{MALLS}=1.42$ at 29 hours, Entry 4 in Table 3.4). However, the system gelled above 60% due to the significant combination of macromolecules at high yield. Furthermore, the GPC traces obtained by refractive index (RI) clearly show increasing molecular weight and broadening polydispersity with reaction time (Figure 3.10 and Figure 3.11). These data provide certain evidence for formation of hyperbranched poly(EGDMA-*co*-DMAEMA).

Table 3.4 Detailed data of hyperbranched poly(EGDMA-*co*-DMAEMA) samples of reaction 6 collected at different times. Reaction conditions: [I]:[EGDMA] :[DMAEMA]:[CuI]:[CuII]= 1:50:50:0.375:0.125, [EGDMA] = 1.02 M, [Cu(I)+Cu(II)]/[Bpy] = 1:2, in THF at 60 °C.

Entry	Reaction time (hrs)	Yield ^a (%)	GPC-MALLS		
			$M_n \times 10^{-4}$ (gmol^{-1})	$M_w \times 10^{-4}$ (gmol^{-1})	PDI
1	5	20	2.99	3.4	1.2
2	10	33	4.1	5.0	1.3
3	20	49	6.1	6.9	1.3
4	29	58	5.5	7.8	1.4
5	30	60	gel		

a. Calculated gravimetrically

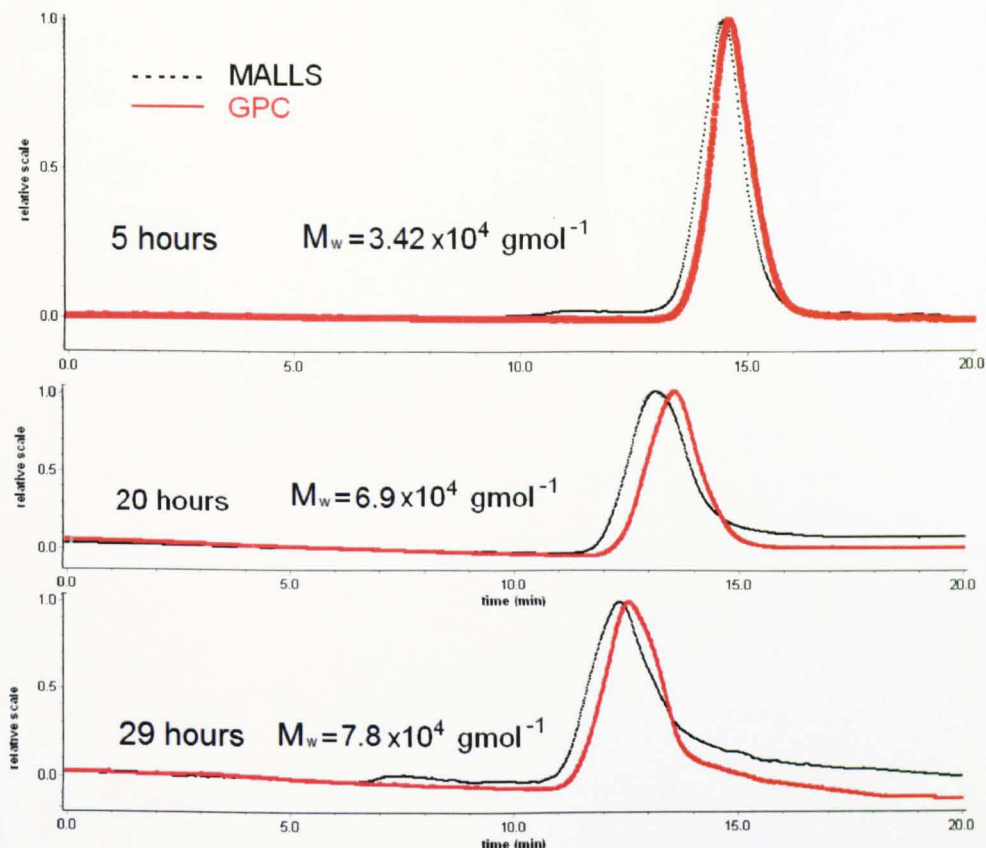


Figure 3.10 GPC analysis of poly(EGDMA-co-DMAEMA) isolated at different reaction times (Entry 6, Table 3.3). The evolution of molecular weight and polydispersity (PDI=1.2, 1.3 and 1.42, respectively) with reaction time clearly show the formation of a hyperbranched polymer.

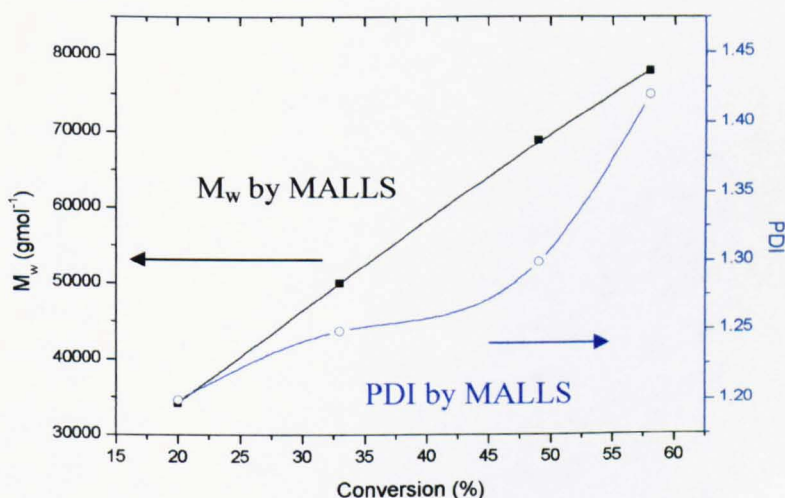


Figure 3.11 The molecular weight and molecular weight distribution of poly(EGDMA-co-DMAEMA) (Entry 1-4, Table 3.4). The plot shows the M_w and PDI versus monomer conversion for the poly(EGDMA-co-DMAEMA). The M_w and PDI data are obtained by GPC-MALLS.

The GPC-MALLS traces also indicates the difference between hyperbranched poly(EGDMA-*co*-DMAEMA) and similar linear polymers (Figure 3.12). For the purpose of comparison, a linear poly(MMA-*co*-DMAEMA) ($M_w=4.7 \times 10^4$ g mol⁻¹, feed ratio of MMA:DMAEMA=1:1) was prepared via normal ATRP which has a similar chemical structure as poly(EGDMA-*co*-DMAEMA). The GPC-MALLS plot clearly indicates that the M_w of hyperbranched poly(EGDMA-*co*-DMAEMA) is much higher than linear ones at the same elution time or hydrodynamic radius. This is because of the architecture hyperbranched polymer is denser than linear ones.

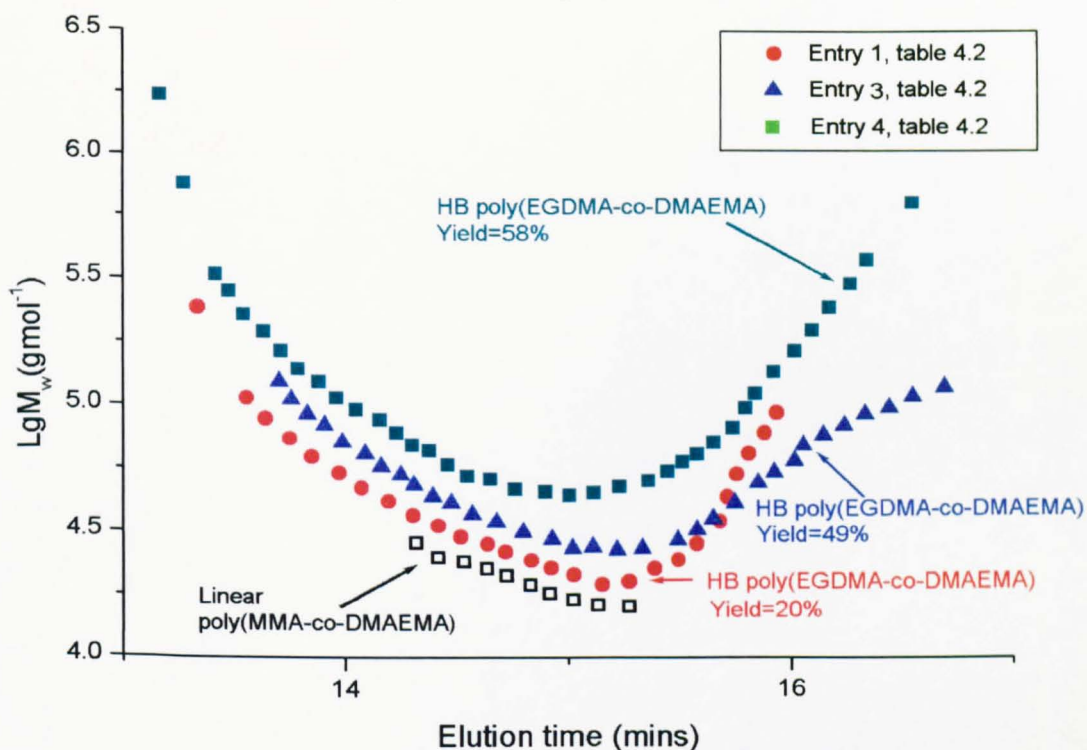


Figure 3.12 Plot of the Log of M_w versus elution volume for the poly(EGDMA-*co*-DMAEMA) (Entry 1, 3 and 4 in Table 3.4) and linear poly(MMA-*co*-DMAEMA) samples by MALLS detector. These data suggest that the polymers in Table 3.4 are highly branched at high conversion since the M_w significantly higher than that of the linear polymer at same elution time.

¹H NMR spectroscopy (Figure 3.13) analysis also confirmed the formation of a hyperbranched structure for poly(EGDMA-*co*-DMAEMA). The presence of hydrophilic groups (resonance of proton j) and vinyl functionalities (resonance of protons e and f) is clearly demonstrated. Moreover, the ratio of hydrophilic groups (DMAEMA units), vinyl groups (linear EGDMA units) and branching points

(branched EGDMA units) was calculated by comparing the resonance of the protons in backbone and vinyl groups (Eq. 3.3). Firstly, the hydrophilic group (DMAEMA units) could be calculated from the integrals of NCH_2 (resonance of proton i). Secondly, the linear EGDMA units could be calculated from the integrals of terminal CH_2 (resonance of protons e and f). Lastly, the branched EGDMA units could be calculated from the integrals of CH_2 (resonance of protons c and h) deducted the part from hydrophilic and vinyl groups.

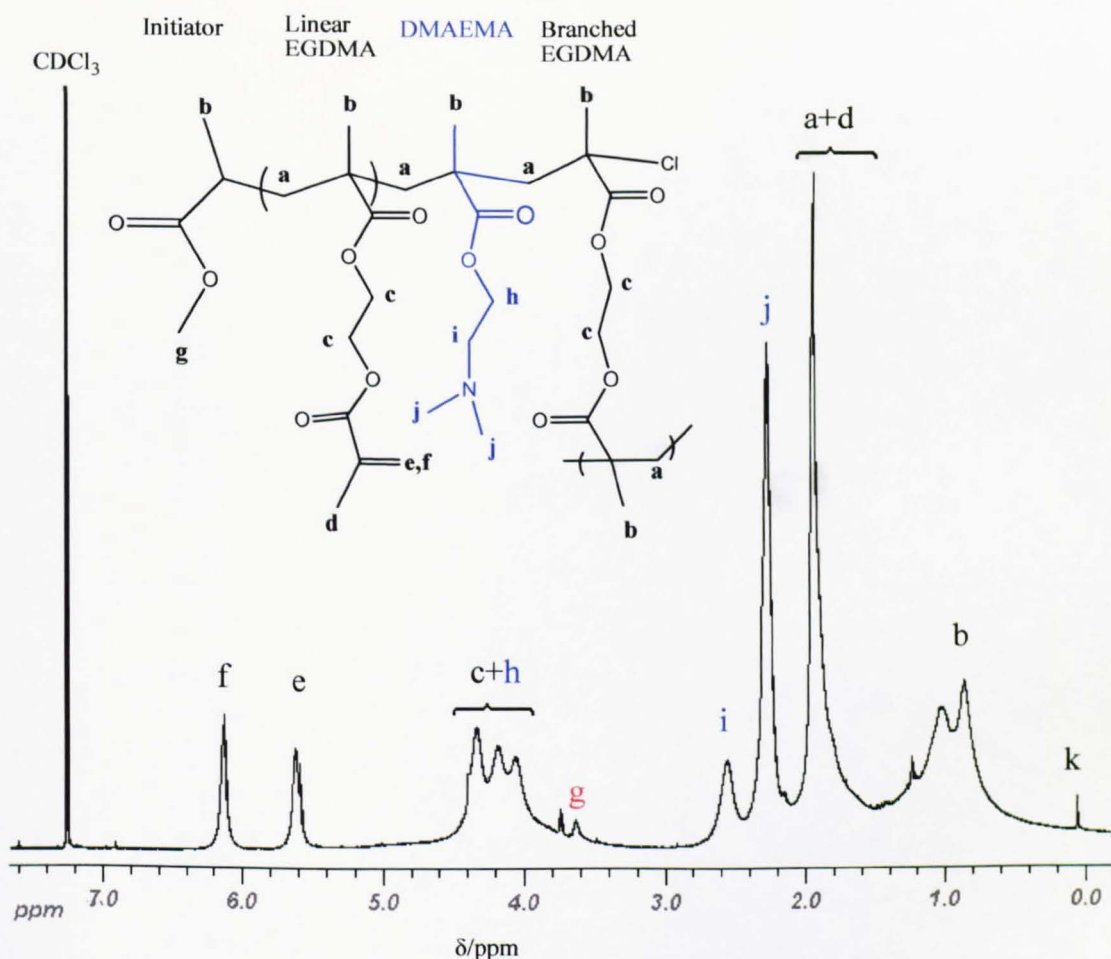


Figure 3.13 ^1H NMR spectrum of hyperbranched poly(EGDMA-co-DMAEMA) in CDCl_3 (Entry 4, Table 3.4) at 300 MHz. In the spectrum, resonance of protons e (~5.6 ppm) and f (~6.2 ppm) present the vinyl groups from the linear EGDMA units. Also, the resonance of proton j (N-CH_3 at 2.3 ppm) and i (N-CH_2 -) indicate the DMAEMA units in copolymer.

Initiator ratio = integrals of g /3

DMAEMA ratio = integrals of i /2

Linear EGDMA ratio = integrals of e

Branched EGDMA ratio = [integrals of (c+ h) - integrals of i]/4 - (integrals of e) (Eq. 3.3)

The results from ^1H NMR spectroscopy analysis were summarised in Table 3.5. The degree of branching (DB, calculated from Eq. 3.5) of poly(EGDMA-*co*-DMAEMA) is in the range of 0.1 to 0.05 (Table 3.5). The polymer product achieves a DB of 0.05 at the 58% yields (Entry 4, Table 3.5). A key feature of the results is the steady decrease of the DB as monomer conversion increases. It indicates that the probability of linear propagation is higher than intra- and inter-molecular crosslinking in this reaction. Moreover, the cyclisation ratio (calculated from Eq. 3.5) is also quite low in the copolymer during whole reaction (from 0.005 to 0.008).

Table 3.5 The ratio of the different units in the poly(EGDMA-*co*-DMAEMA) sample determined by ^1H NMR spectroscopy analysis. Reaction conditions: [I]:[EGDMA] :[DMAEMA]:[CuI]:[CuII]= 1:50:50:0.375:0.125, [EGDMA] = 1.02 M, [Cu(I)+Cu(II)]/[Bpy] = 1:2, in THF at 60 °C.

Sample	Yield ^a (%)	Initiator: Linear EGDMA: Branched EGDMA: DMAEMA ^b	DMAEMA (mole ratio)	Degree of branching ^c	Cyclisation ratio ^d
1	20	1: 10.7 : 1.1 : 8.1	39%	0.1	0.005
2	33	1: 15.7 : 1.4 : 12.1	40%	0.09	0.01
3	49	1: 25.5 : 1.45: 19.3	41%	0.06	0.01
4	58 ↓	1: 34 : 1.51: 25.2	41% ↓	0.05 ↓	0.008

a. Calculated gravimetrically.

b. The ratio of different units in the polymer is calculated from the Eq. 3.3.

c. Degree of branching is calculated from the Eq. 3.4.

d. Cyclisation ratio is calculated from the Eq. 3.5.

$$DB_{\text{Frey}} = \frac{2 \times \text{branched EGDMA units}}{2 \times \text{branched EGDMA units} + \text{initiator} + \text{linear EGDMA units} + \text{DMAEMA units}} \quad (\text{Eq. 3.4})$$

$$\begin{aligned} \text{Cyclisation ratio} &= \frac{\text{Cyclisation units}}{\text{All units}} \\ &= \frac{\text{branched EGDMA units} - \text{Initiator}}{\text{initiator} + \text{linear EGDMA} + \text{branched EGDMA} + \text{DMAEMA units}} \quad (\text{Eq. 3.5}) \end{aligned}$$

Consequently, it indicates that the poly(EGDMA-*co*-DMAEMA) can be considered as hyperbranched polymer below 20% yield since the ratio of branched units to initiator is lower than 1 ($N_{\text{Br}}/N_{\text{I}} < 1$, white zone, Figure 3.14). Moreover, the ratio of branched units to primary linear chain was increased with conversion due to the cyclisation reaction or intramolecular cross-linking. Apparently, the intramolecular crosslinking occurs when the ratio of branched units to primary linear chains exceeds 1 ($N_{\text{Br}}/N_{\text{I}} > 1$, grey zone, Figure 3.14). The ratio of branched EGDMA to initiator is 1.5 before gelation (at 58% yields). It indicates that the intramolecular crosslinking is significantly suppressed in the copolymerisation reaction (eg. $N_{\text{Br}}/N_{\text{I}} = 11$ at 63% yield in polyEGDMA, See Table 2.12, Chapter 2). The intramolecular crosslinking is suppressed by two reasons: firstly, the amount of residue vinyl groups is much lower than the homopolymerisation, since only 50% divinyl monomers are used in this copolymerisation; secondly, the intramolecular crosslinking with the residue vinyl groups in the same polymer chain are hindered by the DMAEMA units from the free radical.

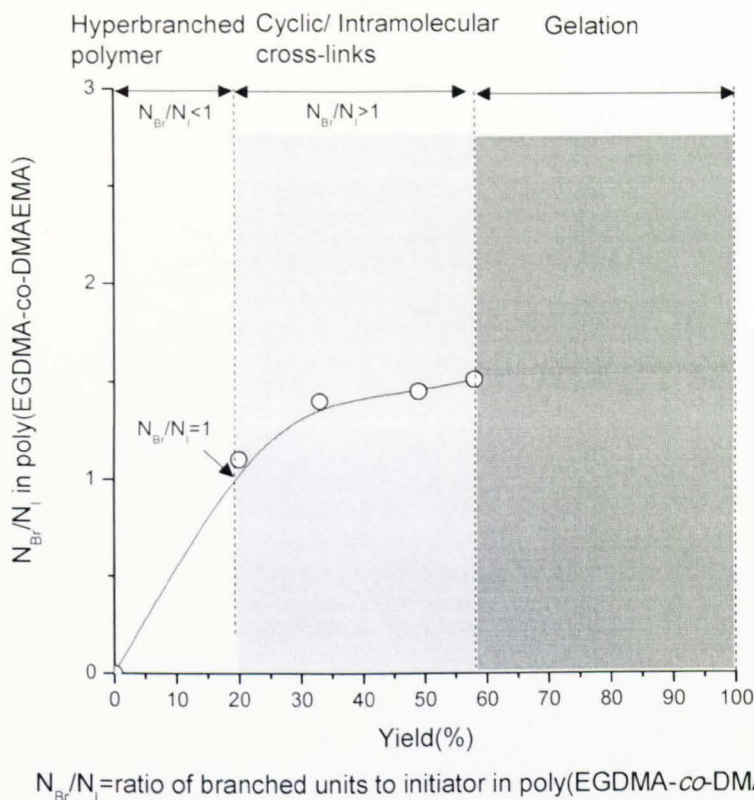


Figure 3.14 The ratio of branched EGDMA units to initiators (N_{Br}/N_I) in poly(EGDMA-co-DMAEMA) versus polymer yield. Statistically, it clearly shows the copolymer is hyperbranched structure below 20% yield ($N_{Br}/N_I \leq 1$). In the range from 20% to 58% yield, the intramolecular cross-linkings are formed in the copolymers ($N_{Br}/N_I > 1$).

From the calculations using ^1H NMR spectroscopy data, the bar chart (Figure 3.15) represents the composition of hyperbranched copolymer in three different feed ratios: DMAEMA:EGDMA=90:10, 75:25, and 50:50 (Table 3.6). It clear shows that the composition of DMAEMA in the resulting polymer is gradually increased with the DMAEMA feed ratio (from 41% to 91%). Furthermore, the ratio of branched units to primary linear chains (N_{Br}/N_I) is increased with the feed ratio of EGDMA (from 0.4 to 1.51).

Table 3.6 The ratio of the different units in the poly(EGDMA-*co*-DMAEMA) sample of different feed ratio determined by ^1H NMR spectroscopy analysis.

Sample	Yield ^a (%)	Feed ratio I:EGDMA:DMAEA	I: Brached EGDMA: Linear EGDMA: DMAEMA ^b	N_{Br}/N_I	DMAEMA (mole ratio)
1 ^c	60	1:5:45	1: 0.4 : 1 : 26.1	0.4	91%
2 ^d	38	1:12.5:37.5	1: 1.1 : 4 : 16	1.1	72%
3 ^e	58	1:50:50	1: 1.51: 34 : 25.2	1.51	41%

a. Calculated gravimetrically.

b. The ratio of different units in the polymer is calculated from the Eq. 3.3.

c. Reaction conditions: $[I]:[EGDMA]:[DMAEMA]:[CuI]:[CuII]:[Bpy] = 1: 5: 45: 0.375:0.125:1$, $[EGDMA] = 0.204\text{ M}$, in methanol at room temperature.

d. Reaction conditions: $[I]: [EGDMA]: [DMAEMA]: [CuI]: [CuII]:[Bpy] = 1:12.5:37.5: 0.375:0.125:1$, $[EGDMA] = 0.54\text{ M}$, in methanol at room temperature.

e. Reaction conditions: $[I]:[EGDMA]:[DMAEMA]:[CuI]:[CuII]:[Bpy] = 1: 50: 50: 0.375:0.125:1$, $[EGDMA] = 1.02\text{ M}$, $[Cu(I)+Cu(II)]/[Bpy] = 1:2$, in THF at $60\text{ }^\circ\text{C}$.

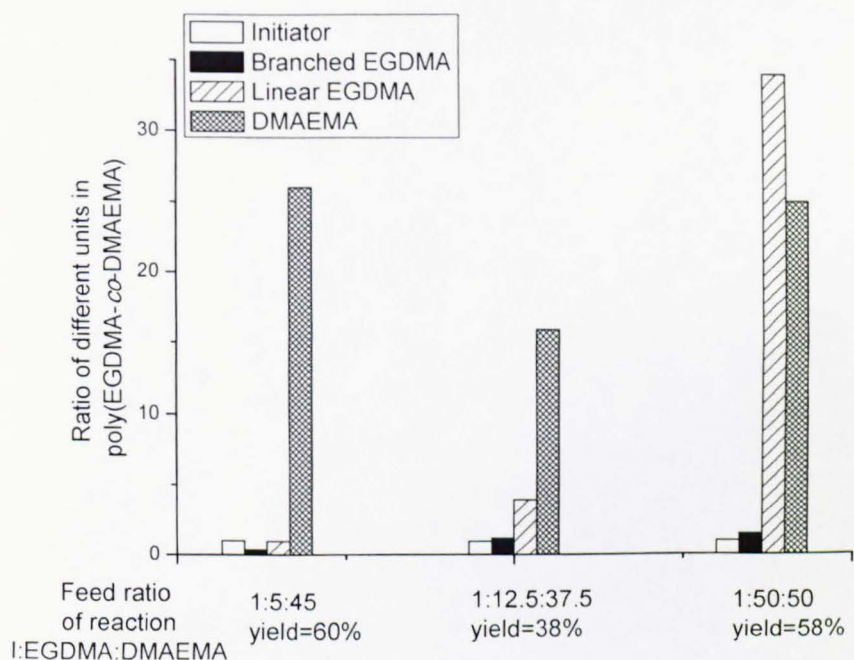


Figure 3.15: The ratio of the different units (hydrophilic group, vinyl groups and branching points) incorporated in the hyperbranched poly(EGDMA-*co*-DMAEMA) at different monomer feed ratios. The bar chart represents the resulting polymers produced from entry 1-3 in Table 3.6, respectively.

In addition, the solubility of poly(EGDMA-*co*-DMAEMA) synthesised from four different feed ratios was examined, respectively. The table below (Table 3.7) summarises the results of the polymer products. These polymers show high solubility in organic solvents, such as chloroform, toluene, THF, acetone, DMF, DMAc and DMSO, which is due to the presence of many non-polar methacrylate linkages in the backbone of the hyperbranched polymer, as well as their globular shape and lack of significant chain entanglement. Moreover, these copolymers could also be partially soluble in polar solvent such as methanol or water. The copolymers made with 95% and 90% DMAEMA feed ratios were partially soluble in the water, because of the high contents of hydrophilic DMAEMA side chains incorporated in the copolymers. Thus, the properties of the hyperbranched polymer is strongly influenced by the numerous terminal groups.⁵ This test shows the unique amphiphilic properties of the hyperbranched poly(EGDMA-*co*-DMAEMA).

Table 3.7 Solubility of poly (EGDMA-*co*-DMAEMA) in different solvent at different monomer feed ratios^a. The polymer is produced from reaction 1, 2, 4, 6 in Table 3.3, respectively.

Reaction	DMAEMA : EGDMA	THF	CHCl ₃	DMF	DMSO	Acetone	MeOH	Water
1	95: 5	++	++	++	++	++	+	+
2	90: 10	++	++	++	++	++	+	+
4	75: 25	++	++	++	++	++	+	-
6	50: 50	++	++	++	++	++	+	-

a. ++ soluble, + partially soluble, - insoluble.

However, the disadvantageous instability of the reaction could be caused by the poor solubility of copper complex in THF. The reproducibility data of this reaction in THF (Table 3.8) show the gel points vary even at the same condition due to the

inhomogeneous system. This phenomenon is quite similar to that of homopolymerisation of poly(DVB) described before (see Chapter 2). Thus, the gel point and kinetics of this reaction are not very stable.

Table 3.8 Reproducibility data of hyperbranched poly(EGDMA-co-DMAEMA) samples in THF system. Reaction conditions: [EGDMA]=1.02 M, [Cu(I)+Cu(II)]/[Bpy]=1:2, in THF at 60 °C. The reproducibility data shows the gel points vary even at the same condition.

Reaction	Reaction time (hrs)	Yield ^a (%)	GPC-MALLS		
			$M_n \times 10^{-4}$ (gmol^{-1})	$M_w \times 10^{-4}$ (gmol^{-1})	M_w/M_n
A	29	58	5.5	7.8	1.42
B	24	50.2	4.7	7.1	1.51
C	15	44	4.3	6.7	1.56

a. Calculated gravimetrically

3.3.2 Encapsulation study

Amphiphilic dendritic polymers consist of both a dendritic polymer as core and an external substituent which has a different solubility from the core. Hyperbranched polymers are attractive as building blocks for the core of such amphiphiles because they possess spherical three-dimensional architecture and numerous functional groups located on the exterior of the molecules.^{1, 39, 40} The different physical properties of dendrimers or hyperbranched polymers in compare to their respective linear analogues have captured considerable attention over the past few years.^{41, 42} The ability to encapsulate guest molecules represents an important property of dendrimers.^{36, 37, 39, 40, 43-48} The encapsulation by dendritic polymers requires as core-shell amphiphilicity and demonstrates the concept of the “unimolecular micelle” or steric densification of the periphery.^{49, 50} The scheme (Figure 3.16) shows the mechanism of dye encapsulation by dendritic polymer. The hydrophilic groups in the polymer act as attractive points and the highly branching structures act

as a ‘dendritic cage’ to help the polymer capture the dyes.⁴⁸ Many hyperbranched polymers prepared by polycondensation method have been published.^{36, 39, 46, 49}

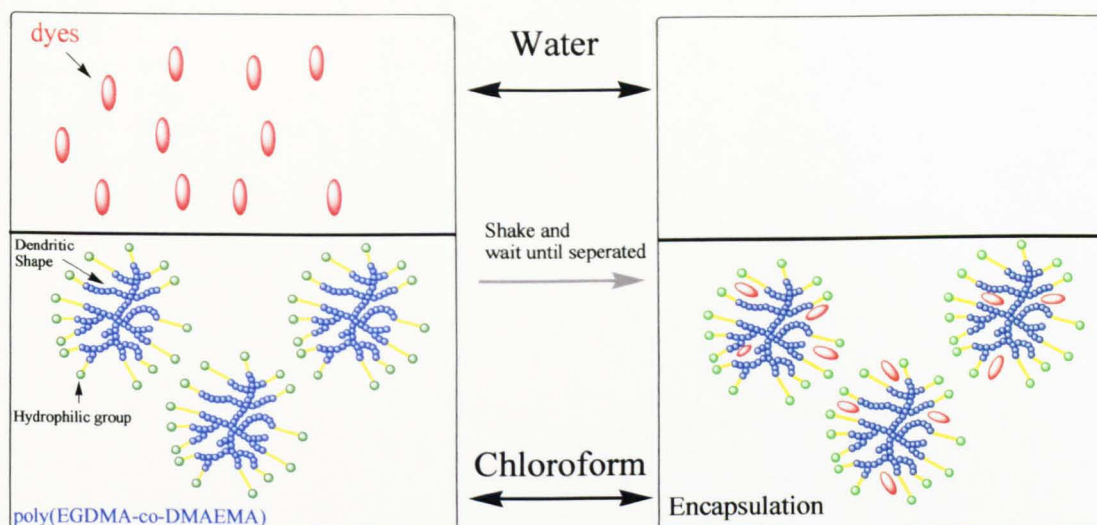


Figure 3.16 Scheme of encapsulation water-soluble dyes and their transfer into organic solvent by amphiphilic dendritic polymer.

However, there is little data on hyperbranched polymers synthesised by one-pot controlled/living polymerisation displaying encapsulation abilities. In order to study the properties of hyperbranched amphiphilic polymers, we examined the encapsulation characteristics for the water-soluble dye Congo red (CR) using the liquid/liquid phase transfer method. Normally, Congo red is difficult to encapsulate because it has a greater extended structure than other dyes including those such as methyl orange, rose bengal or alizarin yellow (Figure 3.17).^{36, 37}

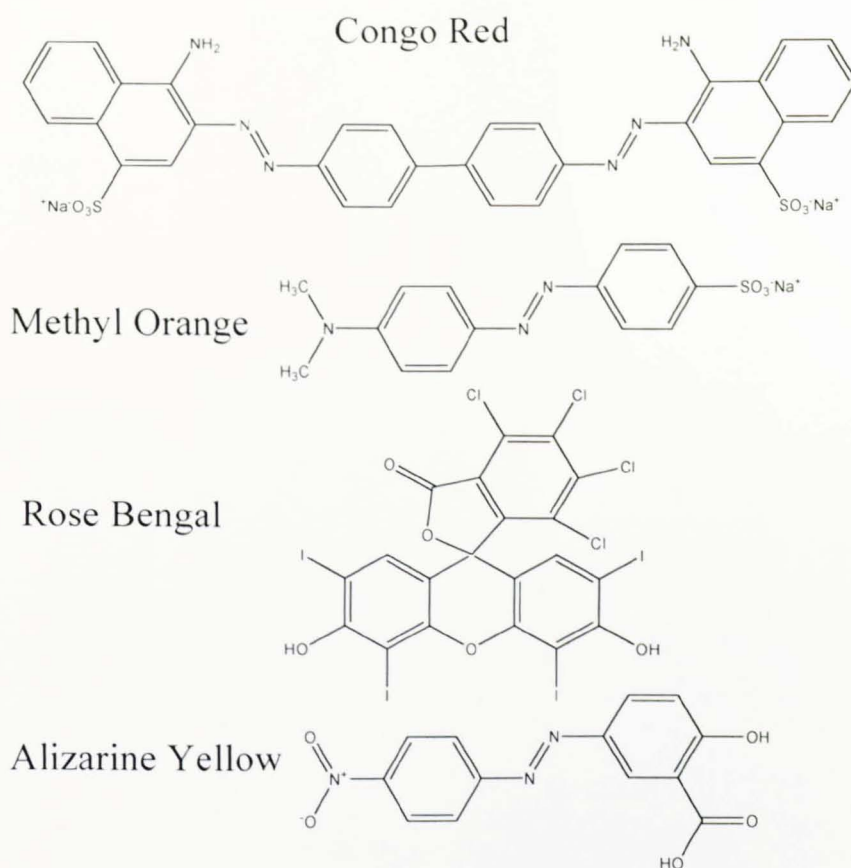


Figure 3.17 Chemical structures of the dyes for encapsulation test.

A previous study indicated that the encapsulation ability of hyperbranched polymer toward these dye molecules should relate to the molecular size of the dye, so the space needed for encapsulating CR was found to be insufficient in the polymer.³⁶ In our experiment, dye aqueous solution was added to chloroform solutions of hyperbranched poly(EGDMA-*co*-DMAEMA), and the mixtures were shaken for 24 hours at room temperature. After removal of any undissolved CR using filter paper, the chloroform phase was apparently coloured (Figure 3.18, upper). By contrast, the same experiment in the absence of hyperbranched polymer showed no colouration. The UV-vis spectra of the chloroform solutions for the CR/poly(EGDMA-*co*-DMAEMA) system show a range of UV-vis absorptions in the region from 200 to 800 nm. The encapsulation ability of poly(EGDMA-*co*-DMAEMA) was also examined using other water-soluble dyes, such as methyl orange (MO), which was also encapsulated readily by the hyperbranched poly(EGDMA-*co*-DMAEMA) (Figure 3.18, bottom).

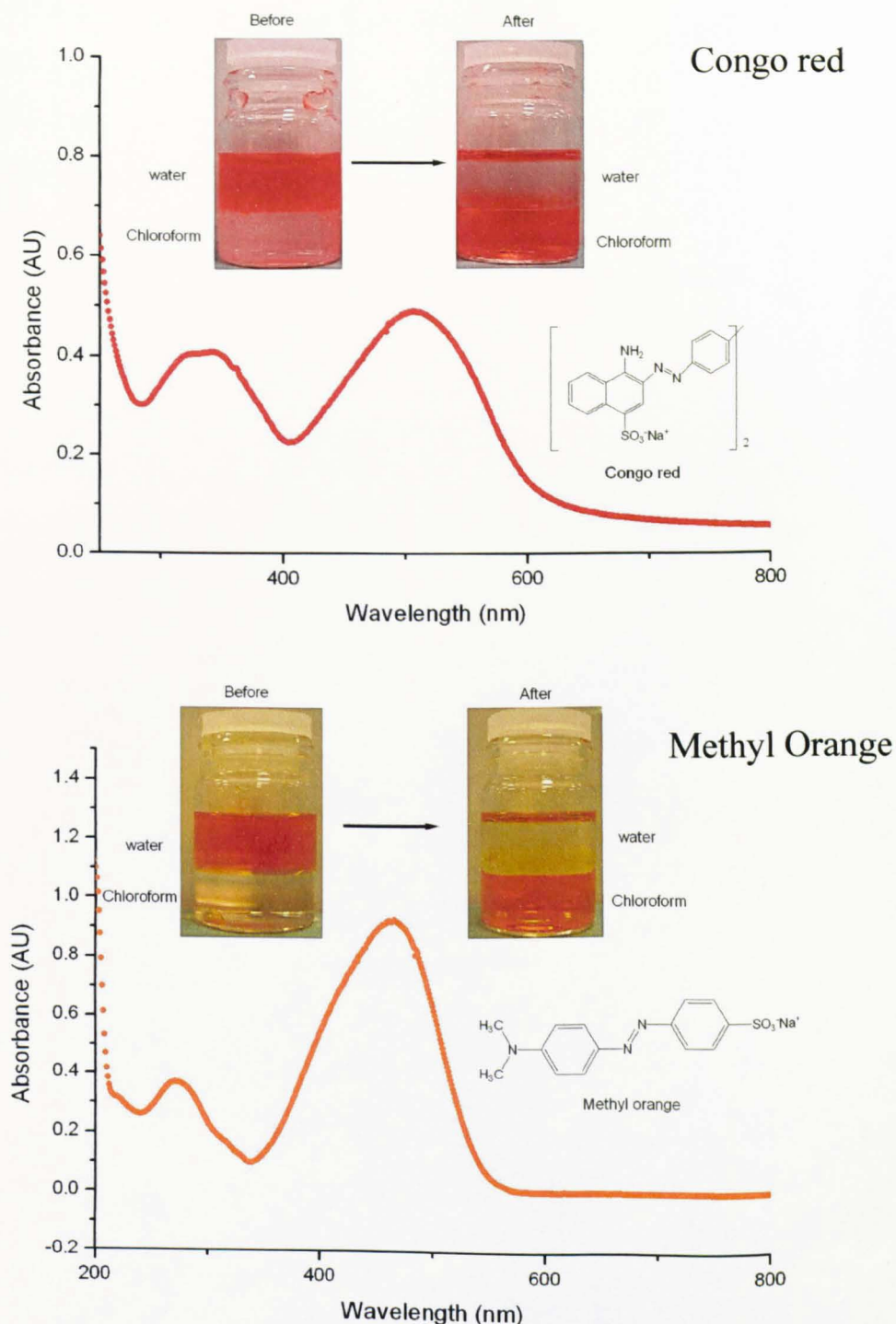


Figure 3.18 UV-vis spectra of CR/poly(EGDMA-co-DMAEMA) system ($M_w=5.0 \times 10^4 \text{ g mol}^{-1}$, $[\text{polymer}]=2.1 \times 10^{-5} \text{ mol L}^{-1}$). The figure clearly shows that the water soluble dye Congo red (upper) and methyl orange (bottom) is encapsulated by hyperbranched poly(EGDMA-co-DMAEMA) and transferred from water (upper layer in vial) into the chloroform layer (bottom layer in vial). In the absence of hyperbranched polymers, no dye transfer was observed.

A comparison of the encapsulation ability between linear and hyperbranched polymers was carried out. The linear poly(MMA-*co*-DMAEMA) has a similar molecular weight (M_w by MALLS = 4.7×10^4 g mol⁻¹) and number of hydrophilic groups (MMA: DMAEMA = 53:47 in polymer, see Figure 3.9 and Eq. 3.2) when compare to hyperbranched ones. With the hyperbranched poly(EGDMA-*co*-DMAEMA) (Entry 1, Table 3.9) and the analogous linear poly(MMA-*co*-DMAEMA) (Entry 2, Table 3.9), a comparison of the encapsulation and phase transfer properties of water-soluble dyes (Congo red and methyl orange) was performed. The dyes transfer into the chloroform phase by the polymers was monitored by UV-vis spectroscopy at different polymer concentrations. The concentrations of the dyes in chloroform were calculated from the calibrated absorbance of prepared dye solution (See Table 3.1, Figure 3.6 and Eq. 3.1). Thus, the dye transfer ability per polymer can be obtained as Eq. 3.6. The detailed experimental and calculation method is list in experimental section.

Dye transfer ability

= amount of dyes transferred by per polymer molecule

$$= \frac{\text{Concentration of dyes transferred to chloroform}}{\text{Concentration of polymer in chloroform}} = \frac{[\text{Dyes}]}{[\text{Polymers}]} \quad (\text{Eq. 3.6})$$

The results (Figure 3.19) demonstrate unambiguously the crucial role of the hyperbranched topology. Hyperbranched poly(EGDMA-*co*-DMAEMA) exhibits the expected CR and MO phase transfer, with saturation concentrations of 3.94 and 1.48 dye molecules per amphiphilic polymer molecule, respectively (Entry 1, Table 3.9). By contrast, the analogous linear poly(MMA-*co*-DMAEMA) showed much lower phase transfer ability for CR and MO of 0.81 and 0.45 dye molecules per polymer (Entry 2, Table 3.9). These data indicate that the hyperbranched polymer has much better encapsulation ability than the linear amphiphilic polymer. Therefore, the highly branched architecture gives a significant advantage for capturing dyes

compared to the random coil linear chains. The branches help the polymers to wrap up the dyes and transfer them into chloroform phase. It is also noteworthy that higher encapsulation values were obtained for CR in comparison to MO. This may be a result of the higher polarity and solubility of CR, despite its bigger size.

Table 3.9 Encapsulation amounts of hydrophilic dyes per amphiphilic hyperbranched poly (EGDMA-*co*-DMAEMA) and linear poly-(MMA-*co*-DMAEMA) molecules.

Entry	Sample	M_w^a (gmol^{-1})	PDI	DMAEMA ^b (%)	Encapsulation ability ([dye] / [polymer]) ^c	
					CR	MO
1	Hyperbranched poly(EGDMA- <i>co</i> -DMAEMA)	5.0×10^1	1.25	40%	3.93	1.48
2	Linear poly(MMA- <i>co</i> -DMAEMA) ^d	4.7×10^1	1.23	46%	0.81	0.45

a. Weight-average molar mass is obtained by MALLS-GPC instrument.

b. DMAEMA unit composition is determined by ^1H NMR spectroscopy analysis.

c. The encapsulation amounts of hydrophilic dye per polymer molecule ([dye]/[polymer]) were determined by quantitative analysis of the UV-vis spectra of the [dye] / [polymer] in chloroform. The calculation details are described in Figure 3.8 and Table 3.2.

d. The linear poly(MMA-*co*-DMAEMA) was synthesised via normal ATRP process. The feed ratio of MMA: DMAEMA is 1:1. Synthesis details are listed in experimental section.

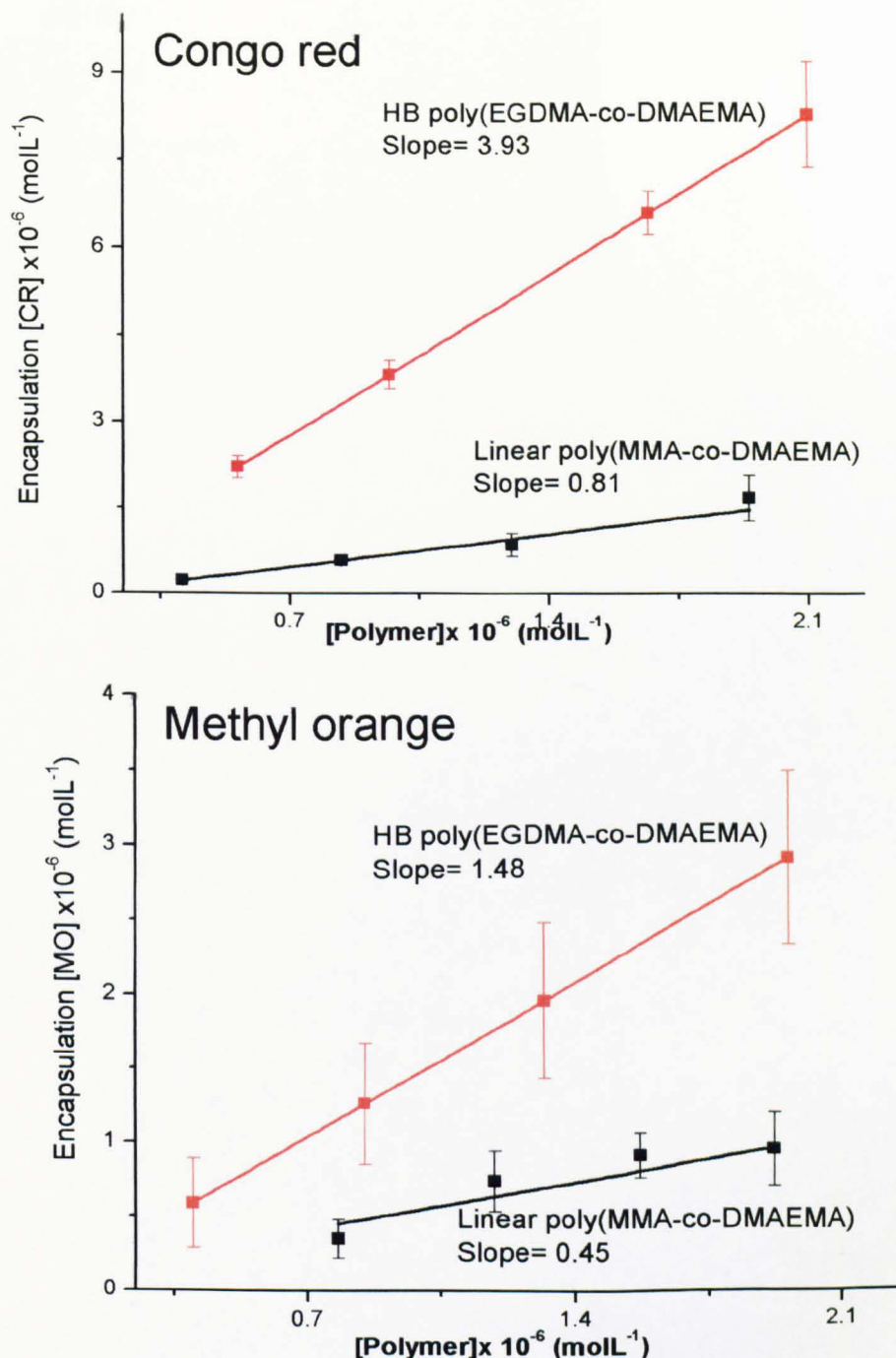


Figure 3.19 Comparison of the encapsulation ability of hyperbranched poly(EGDMA-co-DMAEMA) ($M_w = 5.0 \times 10^4 \text{ g mol}^{-1}$, Entry 1 in Table 3.9) and linear poly(MMA-co-DMAEMA) ($M_w = 4.7 \times 10^4 \text{ g mol}^{-1}$, Entry 2 in Table 3.9). The amounts of the encapsulated dye are determined by UV-vis in chloroform. The figure demonstrates the encapsulation ability of hyperbranched polymer is much better than linear polymers.

In addition, the UV-vis spectrum of water-soluble dye was sensitive to polarity of the environment. Thus, the UV-vis spectra of dyes in water and after encapsulation by hyperbranched poly(EGDMA-*co*-DMAEMA) in chloroform were studied. The comparison was carried out by dye transfer of methyl orange (MO, $3 \times 10^{-5} \text{ mol L}^{-1}$) or Congo red (CR, $9 \times 10^{-5} \text{ mol L}^{-1}$) from aqueous solution into chloroform using poly(EGDMA-*co*-DMAEMA) ($M_w = 5.0 \times 10^4 \text{ g mol}^{-1}$, concentration = $2.1 \times 10^{-6} \text{ mol L}^{-1}$) in a glass vial. Upon encapsulation by hyperbranched poly(EGDMA-*co*-DMAEMA), the UV-vis spectrum of the MO solutions in Figure 3.20 (bottom) exhibited a shift of λ_{max} from 467 nm in water to 424 nm in chloroform. This shift is also confirmed by the colour variation from orange to yellow. This phenomenon suggests the creation of a polar environment in the interior of hyperbranched polymers. The shifts of the peaks in UV-vis are also observed from previous study³⁸. A similar shift in UV-vis absorbance was also obtained by CR although it is much smaller ($\Delta\lambda_{\text{max}} = 6 \text{ nm}$) (Figure 3.20, upper). The previous paper suggests these shifts are the proof that the dyes are surrounded by polymer chains and amphiphilic groups. The significant change of the environment leads to the shift of the absorbance peaks in UV-vis equipment. However, no report has explained the opposite shift from CR and MO in the CHCl_3 after encapsulated.

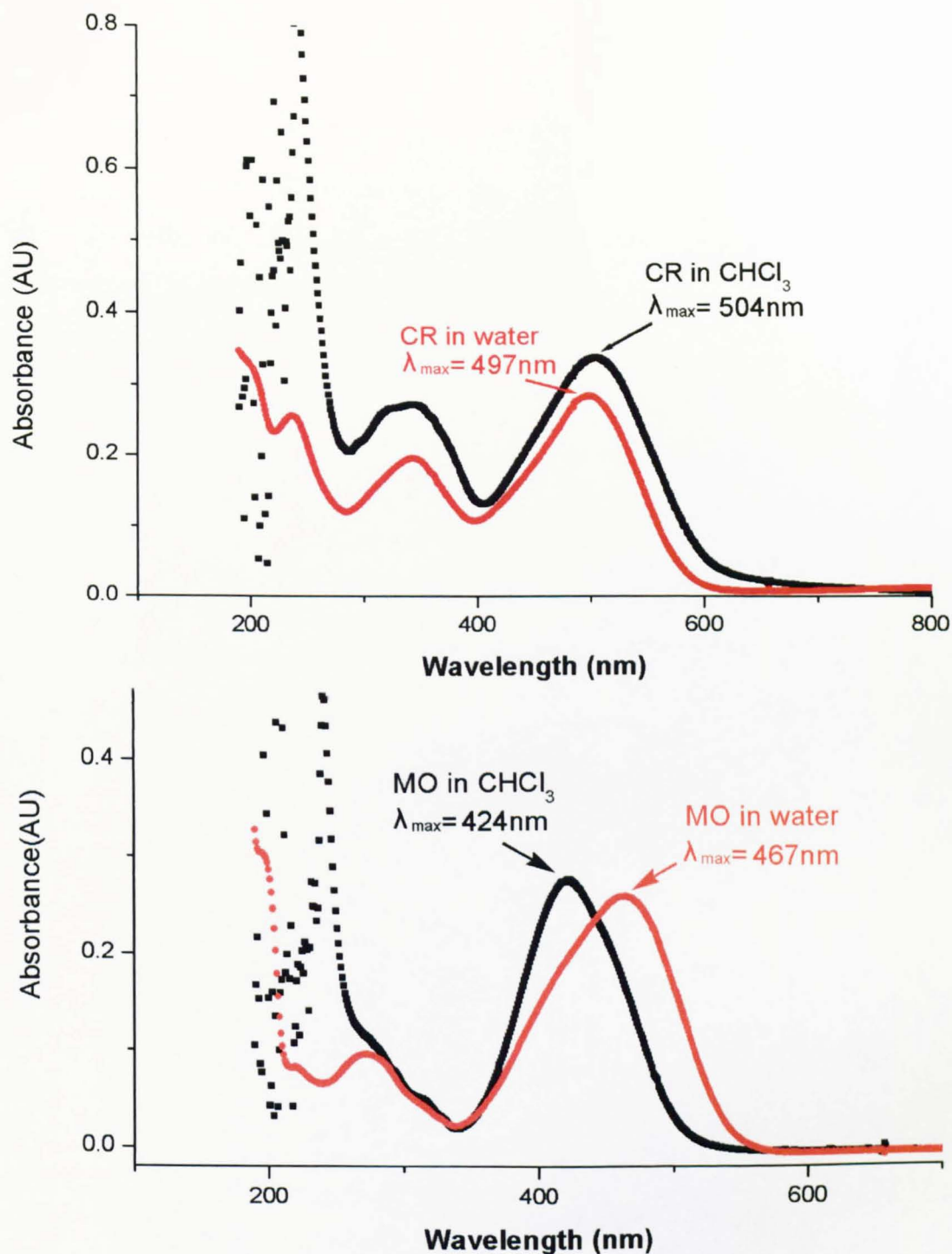


Figure 3.20 The UV-vis spectra of dyes (Congo red and methyl orange) in water and after encapsulation by hyperbranched poly(EGDMA-*co*-DMAEMA) in CHCl₃. The UV-vis spectrum shows a shift of λ_{\max} from 497 nm in water to 504 nm after encapsulated for CR (Upper). Also, a shift of λ_{\max} 467 nm in water to 424 nm in chloroform was exhibited in the case of MO (Bottom).

Furthermore, the effect of molecular weight of hyperbranched poly(EGDMA-DMAEMA) on the dye transfer ability has been studied by UV-vis (Table 3.10 and Figure 3.21). Three different M_w samples of 50:50 feed ratio poly(EGMDA-*co*-DMAEMA) were chosen to perform this test. Both CR and MO cases show that the higher M_w samples transfer more dye from water into organic solvent than lower M_w (Entry 1-3, Table 3.10). The results show at the similar composition, the high molecular weight hyperbranched poly(EGDMA-*co*-DMAEMA) ($M_w=5.0 \times 10^4 \text{ g mol}^{-1}$, Entry 3 in Table 3.10) can transfer 3.93 CR molecules and 1.48 MO molecules into chloroform. In the case of moderate molecular weight samples, the dye transfer ability is decreased to 2.23 for CR and 0.93 for MO respectively ($M_w=3.4 \times 10^4 \text{ g mol}^{-1}$, Entry 2 in Table 3.10). Finally, the low molecular weight poly(EGDMA-*co*-DMAEMA) only can transfer 1.5 CR and 0.6 MO molecules by each polymer ($M_w=1.2 \times 10^4 \text{ g mol}^{-1}$, Entry 1 in Table 3.10). The data prove that the higher molecular weight molecules have better dye transfer ability due to the more hydrophilic groups. Moreover, the longer branch chains and more sufficient space in the large hyperbranched polymer help to grab the dye molecules during the transfer process.

Table 3.10 Dye encapsulation ability of hyperbranched poly(EGDMA-*co*-DMAEMA)_{50:50} samples at different molecular weight. All the samples are synthesised by DE-ATRP (Entry 6, Table 3.3). Reaction conditions: [EGDMA]=1.02 M, [EGDMA]:[DMAEMA]=50:50, [Cu(I)+Cu(II)]/[Bpy]=1:2, in THF at 60 °C. Experimental details are listed in section 2.1.2.2 of Chapter 2.

Entry	$M_w \text{ (g mol}^{-1}\text{)}^a$	PDI	Encapsulation amounts of dye per polymer	
			Congo red	Methyl Orange
1	1.2×10^4	1.21	1.5	0.6
2	3.4×10^4	1.2	2.23	0.93
3	5.0×10^4	1.25	3.93	1.48

a. Weight-average molar mass (M_w) and polydispersity (PDI) is obtained by MALLS-GPC instrument.

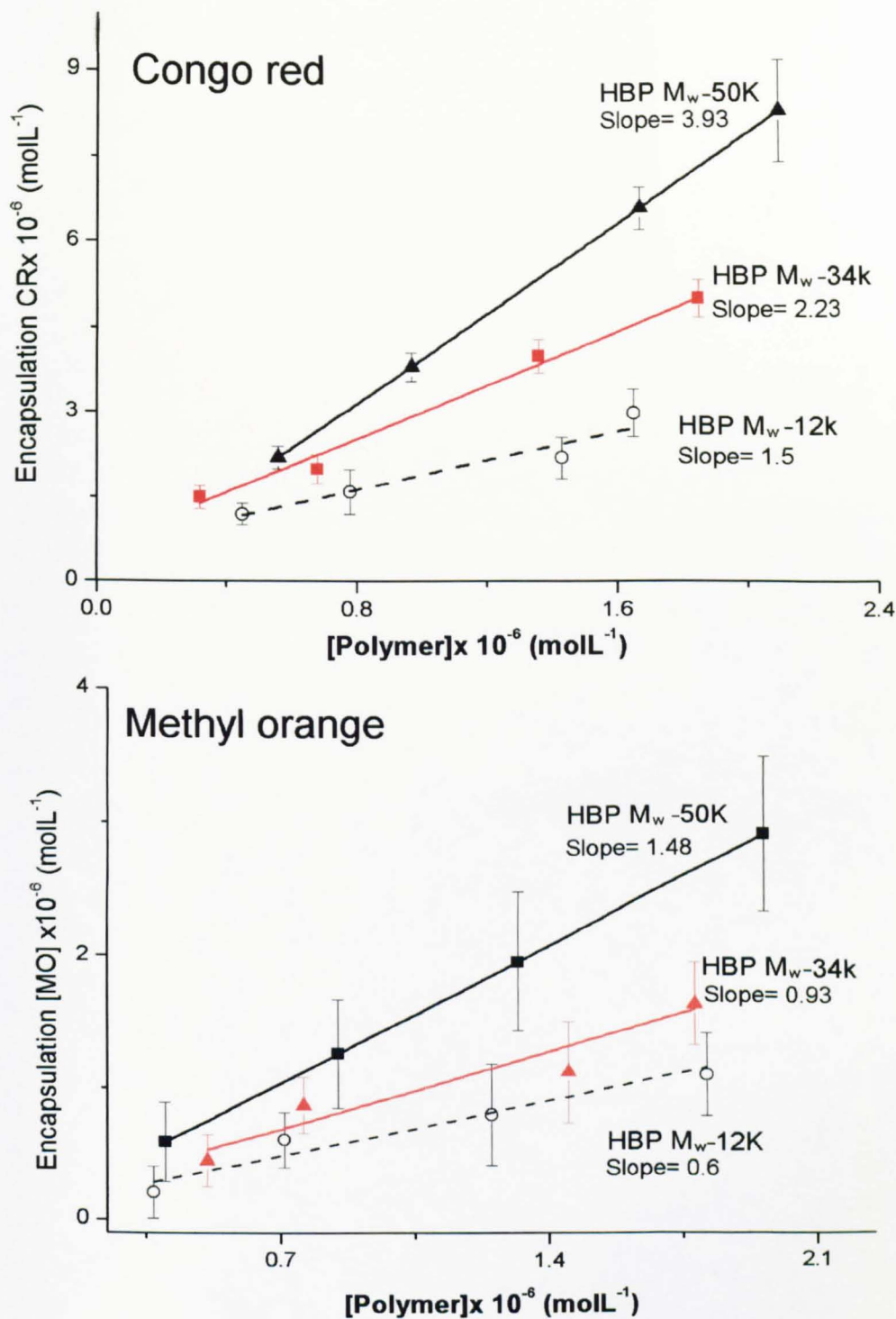


Figure 3.21 Comparison of CR (upper) and MO (bottom) transfer ability from different M_w poly(EGDMA-*co*-DMAEMA) samples. The molecular weights (M_w by MALLS) of poly(EDGMA-*co*-DMAEMA₅₀₋₅₀) are 50k, 34k, and 12k, respectively. The result shows the encapsulation ability of poly(EGDMA-*co*-DMAEMA) is increased with its molecular weight.

To gain insight into the nature of this different encapsulation behaviour, the dye transfer ability of hyperbranched poly(EGDMA-*co*-DMAEMA) with different compositions has also been examined (Table 3.11). Three hyperbranched poly(EGDMA-*co*-DMAEMA) samples were synthesised at similar molecular weight via enhanced deactivation ATRP route. The feed ratios of EGDMA: DMAEMA for the three samples were 50:50, 25:75 and 75:25, respectively.

Table 3.11 Dye encapsulation ability of poly(EGDMA-*co*-DMAEMA) samples with different composition. The samples are synthesised by the DE-ATRP with different feed ratios of EGDMA and DMAEMA. Reaction conditions: [EGDMA]=1.02 M, [Cu(I)+Cu(II)]/[Bpy]=1:2, in THF at 60 °C. The feed ratios of [EGDMA]:[DMAEMA] were 50:50, 25:75, 75:25, respectively. Synthesis details are listed in experimental section.

Entry	Feed ratio of EGDMA:DMAEMA	DMAEMA ^a (%)	M _w ^b (g mol ⁻¹)	DB ^c	Encapsulation ability	
					Congo red	
1	50:50	40%	5.0 x10 ⁴	0.09	3.93	
2	25:75	66%	4.6 x10 ⁴	0.04	3.1	
3	75:25	20%	5.6 x10 ⁴	0.13	1.12	

a. The composition of samples was calculated from ¹H NMR spectroscopy. The calculation method is listed in Eq. 3.3.

b. Molecular weight (M_w) and PDI is obtained by MALLS-GPC instrument.

c. Degree of branching (DB) was calculated from ¹H NMR spectroscopy. The calculation method is listed in Eq. 3.4.

The results indicate the different polymer compositions can also affect the encapsulation loading ability significantly (Table 3.11 and Figure 3.22). At the similar molecular weight, 50% DMAEMA composition polymer (DB=0.09) shows the best transfer ability which is 3.93 CR molecules per polymer (Entry 1, Table 3.11). This means the 50:50 feed ratios is the perfect point for this kind of polymer to transfer the dyes. The polymer with this composition has both of sufficient hydrophilic group and branches. Moreover, the dye transfer ability of 75% DMAEMA feed ratio sample

(Entry 2, Table 3.11) is 3.1 CR dyes per polymer. At this composition, the polymer contains more hydrophilic groups but fewer branches. The more likely linear structure (DB=0.04) of the polymer makes it have poorer transfer ability. Finally, the encapsulation ability of 25% DMAEMA (DB=0.13) is much lower than others which only 1.12 (Entry 3, Table 3.11). The data shows too few hydrophilic groups are also decreasing the encapsulation properties. Thus, molecular encapsulation is clearly a peculiarity of the hyperbranched topology and is related to the amphiphilicity of these polymers. From our study, the feed ratio of 50:50 makes the polymer have the best properties for the dye transfer purposes.

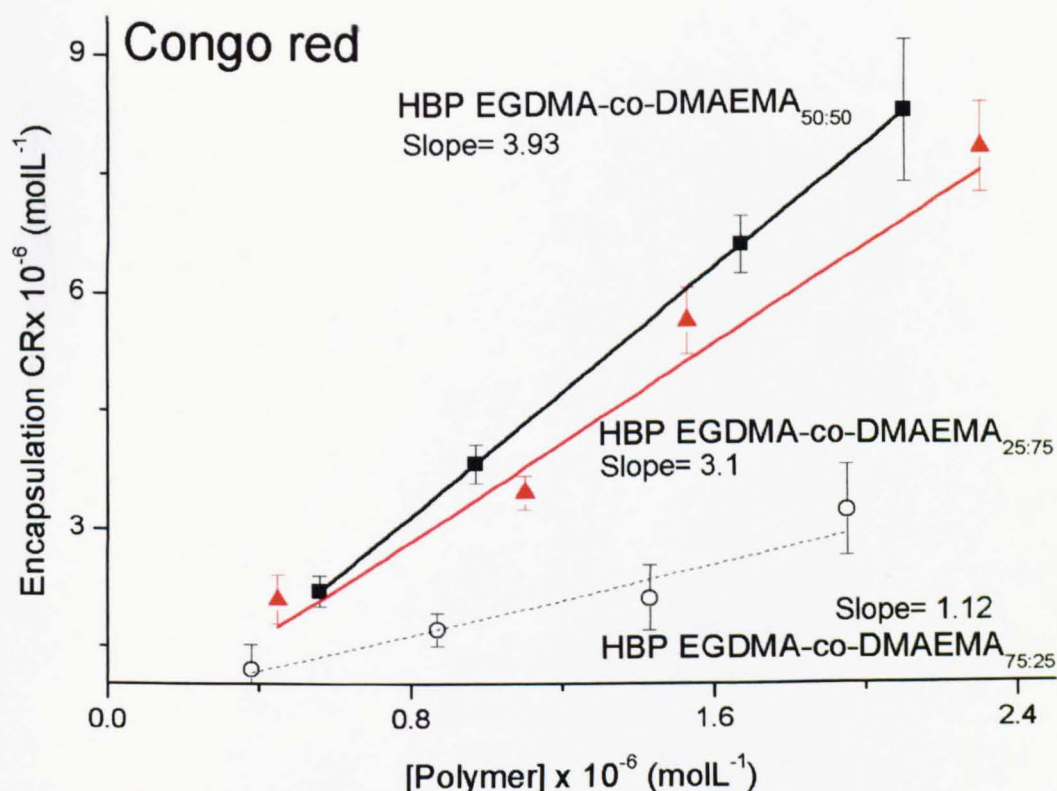


Figure 3.22 Comparison of the dye transfer ability of the hyperbranched poly(EGDMA-co-DMAEMA) with different polymer composition. The samples are prepared to have the similar molecular weight, M_w is 50k, 46k and 56k, respectively. The feed ratios of EGDMA: DMAEMA of the three samples are 50:50, 25:75 and 75:25. The plot shows the hyperbranched poly(EGDMA-co-DMAEMA) has the best encapsulation ability (3.93 CR molecules per polymer) at the feed ratio of 50:50.

3.3.3 Hyperbranched poly(DVB-co-PDMSma)

In this section, the copolymerisations of the divinyl monomer (DVB) and siloxane-type macromonomer ($M_w=1 \times 10^4 \text{ g mol}^{-1}$, PDMSma) were studied via enhanced deactivation ATRP technique. Furthermore, a variety of reaction conditions were studied, for example, the feed ratio of DVB.

For copolymerisation of DVB and PDMSma in toluene, the additional Cu (II) enhances the rate of deactivation. With controlled molecular weight, the polymerisation rate was significantly decreased and high yields of soluble hyperbranched polymer were obtained (Entries 1-5, Table 3.12). In our previous studies, it was found that the ratio of [Initiator]:Cu(I):Cu(II)=1:0.33:0.11 is suitable for enhanced deactivation ATRP system. Adding too much Cu(II) with respect to Cu(I) over suppresses the polymerisation giving only low conversion even after very long reaction times. When the DVB monomer feed ratio increases from 20% (Entry 1, Table 3.12) to 80% (Entry 5, Table 3.12), the polymerisation rate becomes much faster. Despite of the extreme long reaction time, cross-linking was not observed, which is further emphasised by comparison of entries 5, 7 and 9. Clearly, cross-linking and gel formation eventually occurs in these systems, but only when the conversion is pushed up to 65-90%. As a result, the polymerisation of the most highly branched copolymers (feed ratio of DVB is 80%, Entry 5 in Table 3.12) afforded a material of high molecular weight ($M_w=1.77 \times 10^6 \text{ g mol}^{-1}$).

For comparison, the absence of Cu(II) species (Entry 6 and 7, Table 3.12) leads to two observable effects on the polymerisation. Firstly, under certain conditions more rapid polymerisation was achieved due to the absence of enhanced deactivation step. The reaction time was decreased significantly. Secondly, in all cases, the systems quickly lead to insoluble gels within 2 hours. In the typical experimental run under standard ATRP conditions, the polymerisation proceeds in the early stages in a similar manner to those of the equivalent deactivation enhanced examples. Thus, at low conversions

in these conventional ATRP reactions the synthesis of hyperbranched species is observed. However, as the synthesis proceeds it is noted that at yields above 18% the system becomes a gel, making further reaction and analysis by GPC impossible. The highest yield of soluble polymer that can be achieved under these conditions was only *ca.* 10-20%.

Table 3.12 Copolymerisation of DVB and PDMSma via DE-ATRP technique. A high ratio of Cu(II)/Cu(I) slows significantly the reaction rate leading to high yields of hyperbranched polymer without formation of gels. Reaction conditions: $[M]=1.84 \text{ molL}^{-1}$, $[Cu(I)+Cu(II)]/[HMTETA]=1:1$. All polymerisations were conducted under nitrogen in toluene at 90 °C.

Reaction	[I]:DVB:PDMSma: Cu(I) : Cu(II) Feed ratio (mol)	Time (hrs)	GPC-MALLS results		Yield ^c (%)
			M_w (gmol^{-1})	M_w/M_n	
1	1: 10: 40: 0.33: 0.11	140	2.85×10^5	8.5	91
2	1: 12.5: 37.5: 0.33: 0.11	130	3.62×10^5	7.7	90
3	1: 25 :25: 0.3: 0.1	120	4.78×10^5	8.5	90
4	1: 37.5 : 12.5: 0.33: 0.11	50	8.23×10^5	6.2	72
5	1: 40: 10: 0.33: 0.11	29	1.77×10^6	4.9	65
6 ^a	1: 25: 25: 0.3	2	1.2×10^5	6.3	18
7 ^a	1: 40: 10: 0.3	0.5	7.1×10^4	5.4	10
8 ^b	1: 25: 25: 0: 0	<1	Gel		
9 ^b	1: 40: 10: 0: 0	<1	Gel		

a. Reaction 6 and 7 are carried out under normal ATRP polymerisation conditions without excess CuBr_2 .

b. Reaction 8 and 9 are normal free radical polymerisations in solution used AIBN as initiator.

c. Calculated gravimetrically.

Moreover, copolymerisation of DVB and PDMSma via conventional free radical polymerisation (Entry 8 and 9, Table 3.12) clearly shows the fast propagation leading the polymer to cross-link during very short time and below 10% conversion.

Furthermore, the GPC trace and MALLS data for reaction 5 (Entry 5 in Table 3.12) demonstrates a significant issue encountered in the analysis of the materials produced in this programme of work (Table 3.13 and Figure 4.17). By comparing the RI and MALLS data, it clearly shows that there is a significant difference in the measured M_w and PDI for the same sample from these two different detectors. This is likely to be to the result of the highly branched nature of the structures being produced. It is believed that the MALLS data are more trustworthy and representative in the true molecular weight of these systems and that the RI system is underestimating the true molecular weights significantly as a result of shape of the polymers synthesised. It is clear that from the MALLS data that the material isolated in sample 5 (Entry 5, Table 3.13) has a significant component above the upper exclusion limit of the system and thus cannot give definitive molecular weight nor polydispersity data for this particular sample. It was included for comparison with the materials sampled at earlier points in the reaction only to demonstrate that the molecular weight of the hyperbranched material is certainly still rising at this point but the polymer has not yet become an insoluble gel.

Table 3.13 Detailed data of hyperbranched poly(DVB-co-PDMSma) samples of reaction 5 (Entry 5, Table 3.12) collected at different reaction time. Reaction conditions: [M]=1.84 M, [Initiator]:[DVB]:[PDMSma]:[CuI]:Cu[II]=1:40:10:0.33:0.11, [Cu(I)+Cu(II)]/[HMTETA] = 1:1, in toluene at 90 °C.

Entry	Time (hrs)	Yield ^a (%)	MALLS results				Degree of branching ^b
			M _n	M _w	M _w /M _n	RMS	
			(g mol ⁻¹)	(g mol ⁻¹)		(nm)	
1	6	10	2.0 x10 ⁴	2.44 x10 ⁴	1.2	13.3	0.33
2	12	25	5.5 x10 ⁴	9.87 x10 ⁴	1.8	26	0.38
3	24	53	9.1 x10 ⁴	2.79 x10 ⁵	3.1	35.5	0.41
4	29	65	6.3 x10 ⁵	1.77 x10 ⁶	2.8	68	0.38
5	30	67	Gelation				

a. Calculated gravimetrically.

b. The polymer composition is obtained from ¹H NMR spectroscopy data (see Figure 3.28 and Equation 3.7-3.11). B-DVB: the DVB units having reacted both of vinyl groups as a branch point. L-DVB: the DVB units which only polymerised one vinyl groups.

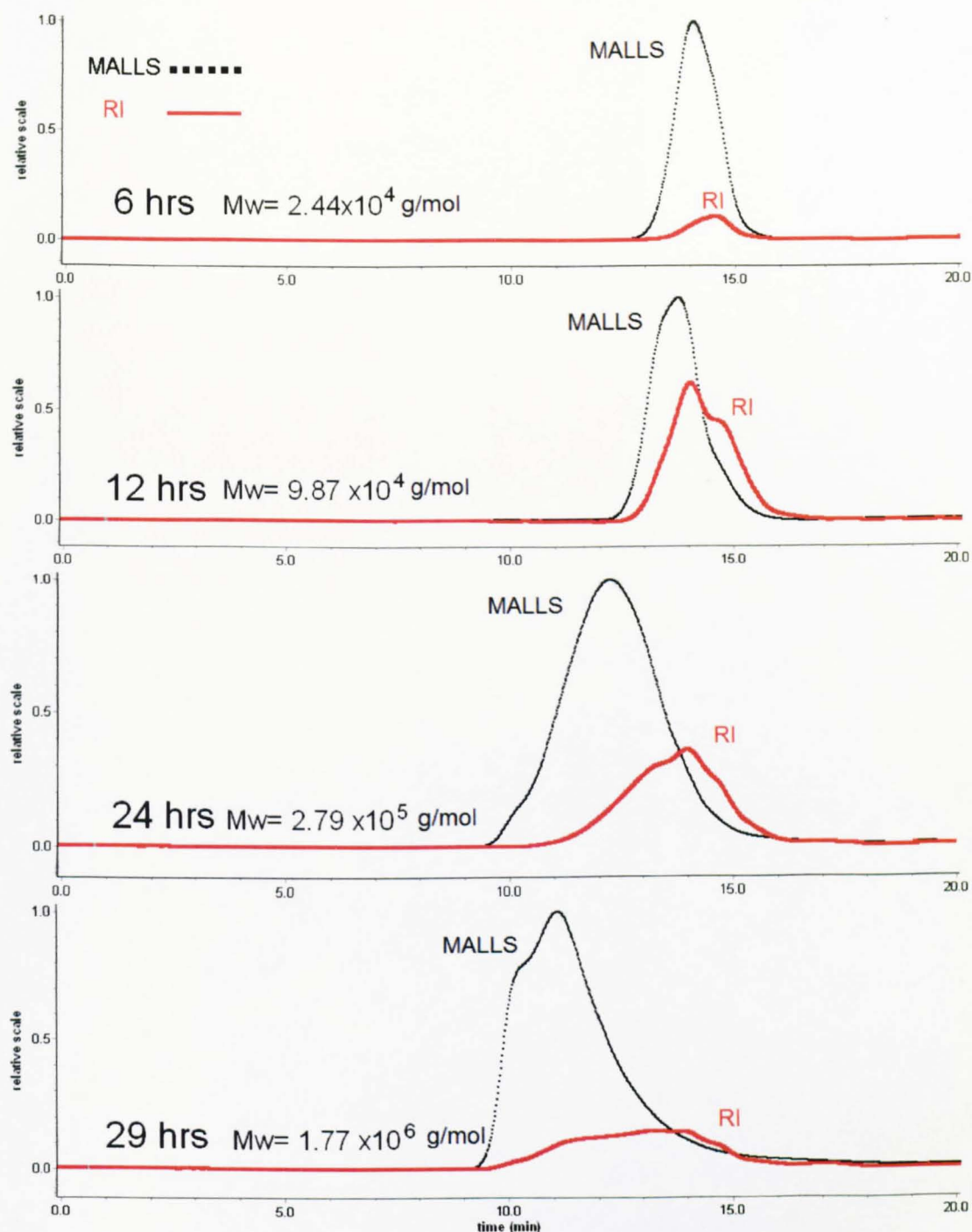


Figure 3.23 MALLS and RI chromatograms for the GPC analysis of poly(DVB-co-PDMSma) isolated at different reaction times (Entry 1 to 4 in Table 3.13). It clearly shows that the weight and polydispersity of polymers are increased with reaction time, which supports the formation of hyperbranched polymer with controlled chain structure.

The log-log plot of RMS *versus* M_w for linear PDMS and our hyperbranched poly(DVB-co-PDMS) species (samples in Table 3.13) is obtained from GPC-MALLS analysis (Figure 3.24). The RMS radius values for the hyperbranched poly(DVB-co-PDMS) and linear PDMS samples were obtained directly from the MALLS detector. The result shows that the exponents ($\alpha=0.39$) of hyperbranched poly(DVB-co-PDMSma) are slightly higher than that value of massive spheres ($\alpha=0.33$). In addition, the slope of linear PDMS samples is 0.52 ($\alpha=0.52$) because of their unperturbed Gaussian chain. This behaviour is in strong agreement to the expected shape for hyperbranched polymers.

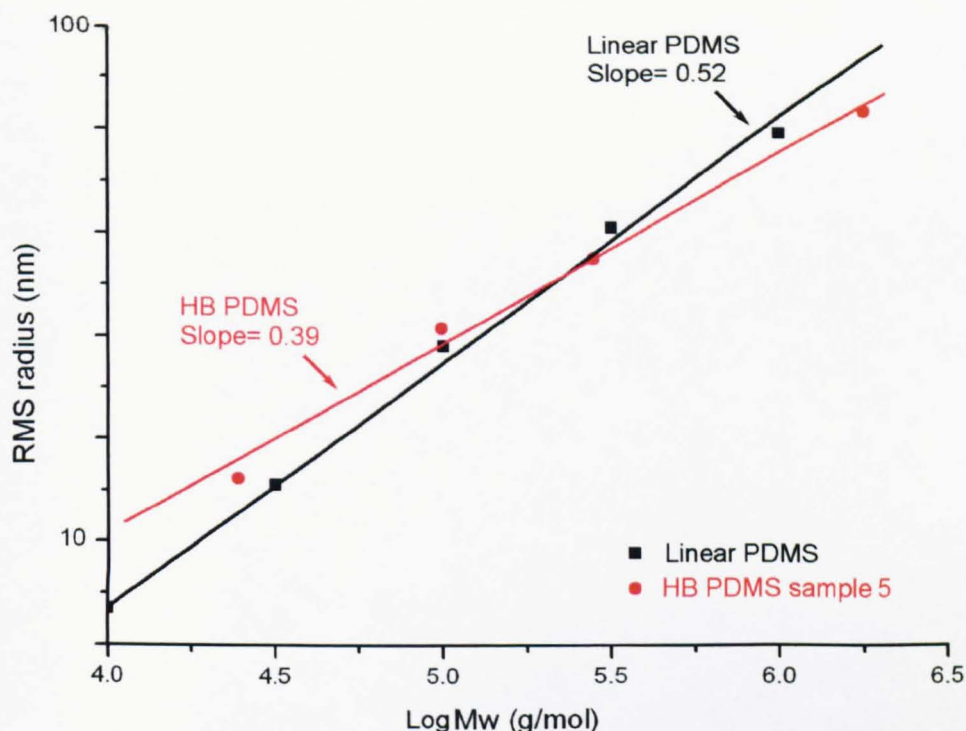


Figure 3.24 Plot of the gyration radius versus Log M_w by MALLS detector. Comparison of the size of hyperbranched poly(DVB-co-PDMSma) to those obtained from published linear PDMSma. The slope of hyperbranched poly(DVB-co-PDMSma) line ($\alpha=0.39$) is demonstrated to be different from the linear PDMSma ($\alpha=0.53$).

More details of RMS radius of hyperbranched poly(DVB-co-PDMSma) samples (Entry 3 and 4 in Table 3.13) were studied by MALLS detector (Figure 3.25). The result shows the gyration radius of linear PDMSma is much higher than that of hyperbranched PDMSma at the same molecular weight. Moreover, the plot indicates that there are some linear PDMS chains in the hyperbranched poly(DVB-co-PDMSma) samples (highlight part, Figure 3.25). These linear chains have very low degree of branching and M_w than other branched chains.

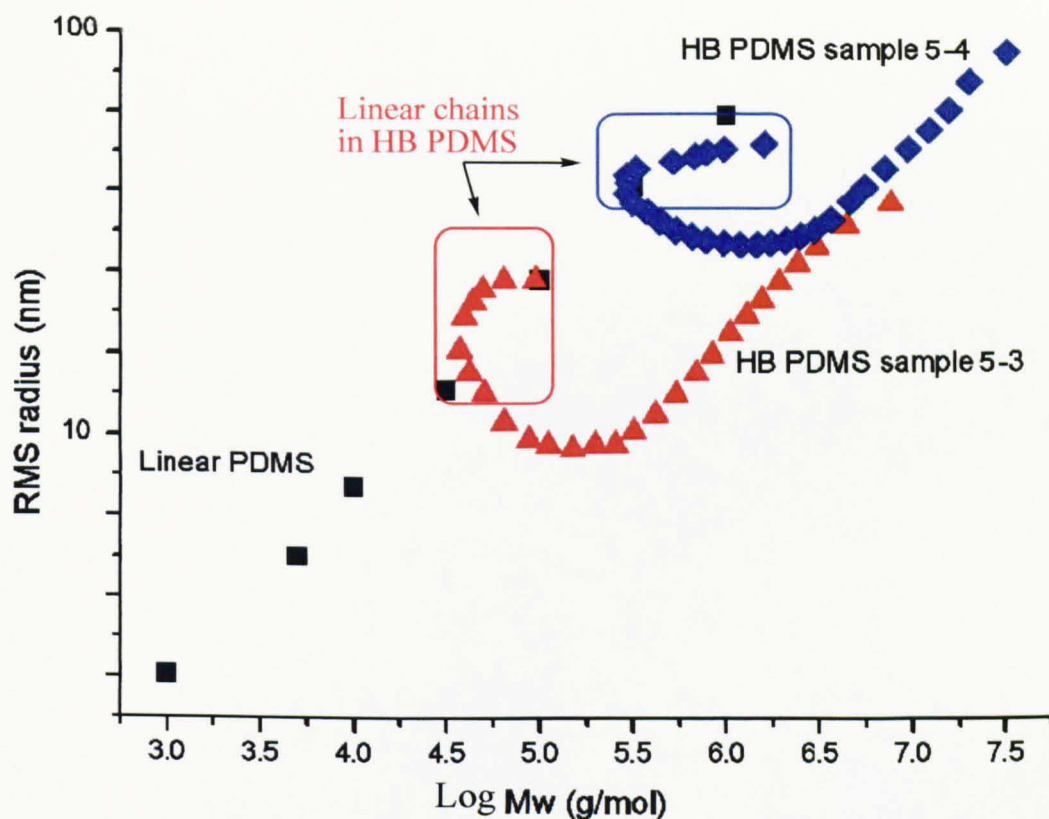


Figure 3.25: The RMS radius *versus* the molar mass plots of linear PDMS and hyperbranched poly(DVB-co-PDMSma) (Entry 3 and 4, Table 3.13).

Furthermore, the data demonstrate that the hydrodynamic radius of the branched macromolecules is smaller than those of the linear polymer of a corresponding molecular weight (Figure 3.26). Thus, as GPC elution volume depends on the R_h of the polymer, the molecular weight of the branched polymers detected at a particular elution volume should be much higher than that of the linear polymer at that volume.

The comparison of the molecular weight against elution volume plots of poly(DVB-co-PDMS) and linear PDMS sample should reveal differences in the behaviour of the molecular structures, indicating different levels of branching. In addition, the result (Figure 3.26) demonstrates that the data from poly(DVB) materials are indeed different from those of the linear equivalents. Thus, it also confirms the differences in the structure type and supports the conclusion that the polymers synthesised are more highly branched because the plots lie significantly above that for linear PDMSma.

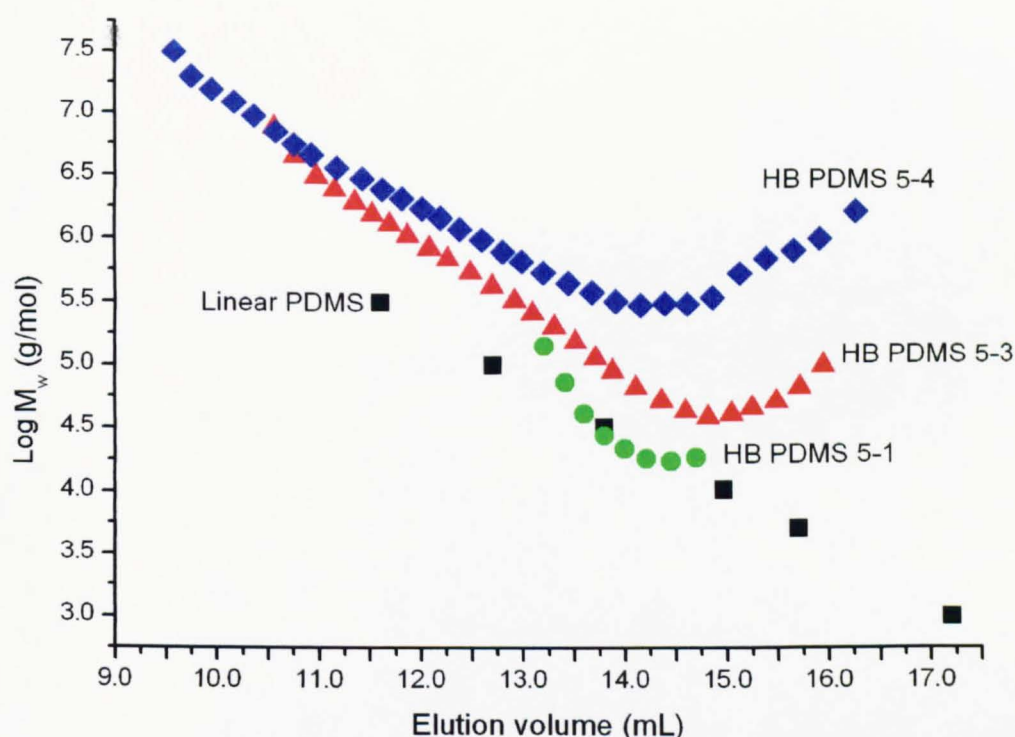


Figure 3.26: Plots of the Log of M_w versus elution volume for the poly(DVB-co-PDMSma) (Entries 1, 3 and 4, Table 3.13) and linear PDMSma samples. These data confirm that the poly(DVB-co-PDMSma) samples are highly branched since the M_w lie significantly above that of the linear sample at same elution volume.

Furthermore, the plot chart (Figure 3.26) shows that the highly branched sample has abnormal GPC elution behaviour. After the normal decreasing of the molar mass with increasing elution volume, the plots curved up in the region of 14-16.5 ml (X axis).

This effect was also observed in the RMS radius versus the elution volume as seen in following figure (Figure 3.27). This effect indicates that there are some large molecules with high molecular weight that was retarded through the GPC column (Anchor effect). This is also observed in other hyperbranched samples (*eg.* polyDVB) and more details have been discussed previously in Chapter 2.

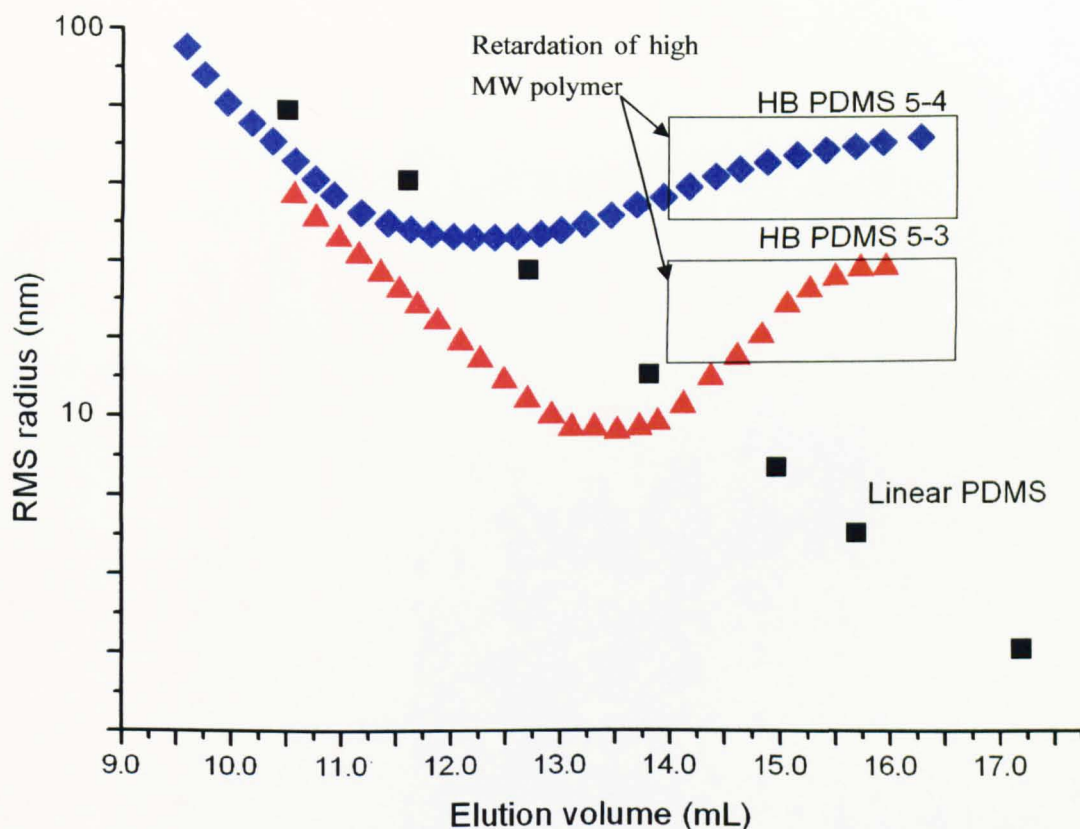


Figure 3.27: The RMS radius *versus* the elution volume plots of linear PDMS_{ma} and hyperbranched poly(DVB-*co*-PDMS_{ma})(Entry 3 and 4, Table 3.13). The plot shows that some large polymer pieces are eluted out in the region of 14-16.5 mL due to the anchor effect.

^1H NMR spectroscopic analysis also confirms the formation of a hyperbranched structure for poly(DVB-*co*-PDMS) (Figure 3.28). The presence of a multiplicity of reactive and potentially useful vinyl functionalities is clearly demonstrated (resonance of protons e and f from vinyl groups, resonance of protons i and k from PDMS_{ma} units and resonance of proton o from initiator groups). Moreover, comparison of the

integrals of the backbone and vinyl protons allows an approximation of the ratio of different units in the poly(DVB-*co*-PDMSma)(Eq. 3.7-3.11). Firstly, the resonance of proton o represents the three protons (-O-CH₃) in initiator (Eq. 3.7). Secondly, the resonance of proton k represents the protons (-CH₂-Si) in PDMSma unit (Eq. 3.8). Thirdly, the resonance of proton e or f represents the proton (=CH₂) in linear DVB unit (Eq. 3.9). Moreover, it assumed that the comonomers (DVB and EVB) incorporated in copolymer as in the monomer mixture. Therefore, the ratio of EVB to DVB in copolymer is 0.22 (0.18/0.82) bases on the above assumption (Eq. 3.10). Lastly, the branched DVB units can be calculated from the resonance of protons c and d in all DVB and EVB units (Eq. 3.11).

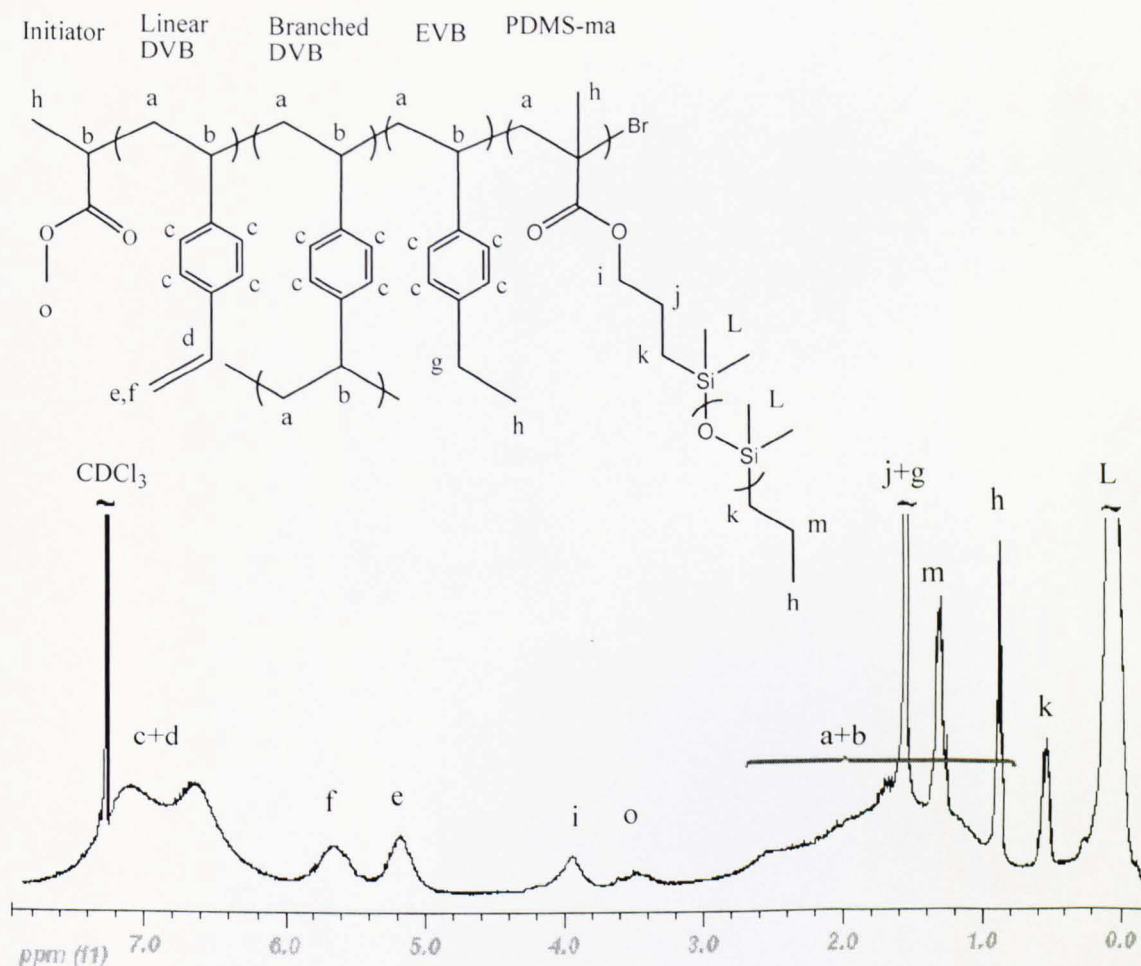


Figure 3.28: ¹H NMR spectrum of hyperbranched poly(DVB-*co*-PDMS) (Entry 4, Table 3.13) in CDCl₃ at 300 MHz. Comparison of benzyl (c) and vinyl (e) enables determination of branching ratio (Eq. 3.7-3.11). Also, resonance of protons e, f and o show clear presence of vinyl functionalities and terminal initiator groups.

$$\text{Initiator ratio: } \frac{\text{integrals of o}}{3} \quad (\text{Eq. 3.7})$$

$$\text{PDMSma ratio: } \frac{\text{integrals of k}}{4} \quad (\text{Eq. 3.8})$$

$$\text{Linear DVB ratio} = \text{integrals of e} \quad (\text{Eq. 3.9})$$

$$\text{EVB ratio} = (\text{Linear DVB} + \text{Branched DVB}) \times 0.22 \quad (\text{Eq. 3.10})$$

$$\text{Branched DVB} \times 4 + \text{Linear DVB} \times 5 + \text{EVB} \times 4 = \text{integrals of (c+d)}$$

$$\text{Branched DVB} \times 4 + (\text{integrals of e}) \times 5 + (\text{integrals of e} + \text{Branched DVB}) \times 0.22 = \text{integrals of (c+d)}$$

$$\text{Branched DVB} = \frac{\text{integrals of (c+d)} - (\text{integrals of e}) \times 5.22}{4.22} \quad (\text{Eq. 3.11})$$

From the NMR analysis, the DE-ATRP method produces a much higher branched ratio (from 0.33 to 0.41) than previous published ones (from 0.05 to 0.15).⁵¹ The equation used to calculate the DB is shown as Eq. 3.12. For the reaction 5, NMR data can be used to follow the steady increase of the degree of branching as monomer conversion increases (Table 3.14), with the final product achieving a ratio of 0.38. Furthermore, the ¹H NMR spectroscopy data shows the DVB has a higher competition rate than PDMSma monomer. The ratio of PDMSma units in copolymer is 0.12 at low yield (Entry 1, Table 3.14) and increases to 0.21 at 65% conversion (Entry 4, Table 3.14). These results indicate that the hyperbranched poly(DVB-co-PDMSma) is potentially a core-shell structure which contains a hyperbranched core and linear PDMS shell. Lastly, the cyclisation ratio (Eq. 3.13) of poly(DVB-co-PDMSma) is in the range from 0.06 to 0.22 is relative higher than the poly(EGDMA-co-DMAEMA). It indicates that the probability of intramolecular crosslinking reaction was not suppressed in this copolymerisation.

Table 3.14 The ratio of the different units in the poly(DVB-*co*-PDMSma) sample determined by ^1H NMR spectroscopy analysis. Reaction conditions: $[\text{I}]:[\text{DVB}]:[\text{PDMSma}]:[\text{CuI}]:[\text{CuII}]:[\text{HMTETA}] = 1:40:10:0.33:0.11:0.44$, $[\text{DVB}] = 1.02 \text{ M}$, in toluene at 90°C .

Sample	Yield ^a (%)	Initiator: Branched DVB: Linear DVB:EVB: PDMSma ^b	PDMSma ratio	Degree of branching ^c	Cyclisation ratio ^d
1	10	1: 1.4: 2.8: 0.9: 0.8	0.12	0.33	0.06
2	25	1: 3.1: 5.4: 1.9: 1.8	0.14	0.38	0.16
3	53	1: 6.7: 10: 3.7: 4	0.16	0.41	0.22
4	65	1: 7.2: 12.8: 4.4: 6.8	0.21	0.38	0.19

a. Calculated gravimetrically.

b. The ratio of different units in the polymer is calculated from the Eq. 3.7-Eq. 3.11.

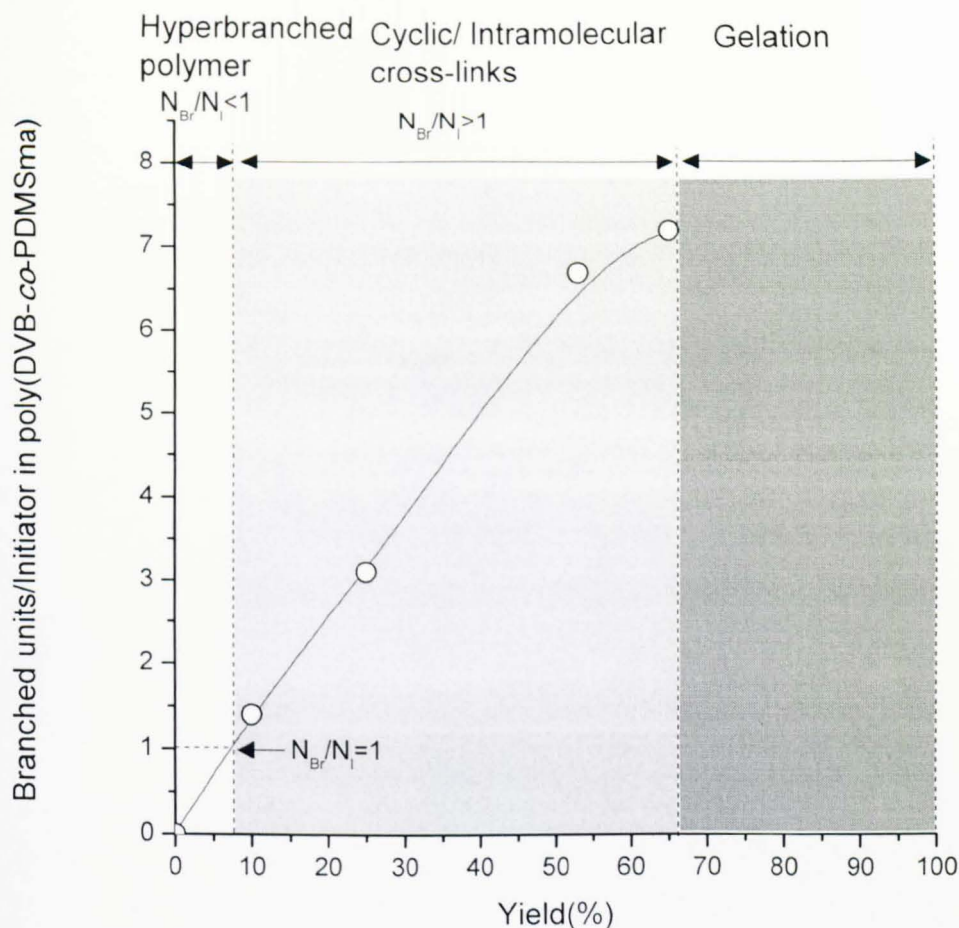
c. Degree of branching is calculated from the Eq. 3.12.

d. Cyclisation ratio is calculated from the Eq. 3.13.

$$\text{DB}_{\text{Frey}} = \frac{2 \times \text{branched DVB}}{2 \times \text{branched DVB} + \text{initiator} + \text{linear DVB} + \text{EVB} + \text{PDMSma}} \quad (\text{Eq. 3.12})$$

$$\begin{aligned} \text{Cyclisation ratio} &= \frac{\text{Cyclisation units}}{\text{All units}} \\ &= \frac{\text{branched DVB-Initiator}}{\text{initiator} + \text{linear DVB} + \text{branched DVB} + \text{EVB} + \text{PDMSma}} \quad (\text{Eq. 3.13}) \end{aligned}$$

Therefore, it shows that the poly(DVB-*co*-PDMSma) can be considerate as hyperbranched polymer below 8% yield since the ratio of branched units to initiator is lower than 1 ($N_{\text{Br}}/N_{\text{I}} < 1$, white zone, Figure 3.29). Moreover, the ratio of branched units to primary linear chain was increased significantly with conversion due to the intramolecular cross-linking. Apparently, the intramolecular crosslinking occurs when the ratio of branched units to primary linear chains ($N_{\text{Br}}/N_{\text{I}}$) exceeds 1. Therefore, the poly(DVB-*co*-PDMSma) in the range from 8% to 65% yield is essential cyclic or intramolecular cross-linked polymer ($N_{\text{Br}}/N_{\text{I}} > 1$, grey zone, Figure 3.29). The ratio of branched DVB to initiator increases to 7.2 before gelation.



N_{Br}/N_I = ratio of branched units to initiator in poly(DVB-co-PDMSma)

Figure 3.29: The scheme of ratio of branched DVB units to initiator (N_{Br}/N_I) in poly(DVB-co-PDMSma) *versus* polymer yield. It indicates that the polyDVB is general hyperbranched structure below 8% yield ($N_{Br}/N_I \leq 1$). In the range from 8% to 65% yield, the intramolecular cross-linkings are formed in poly(DVB-co-PDMSma) ($N_{Br}/N_I > 1$).

The main areas of potential applications for these polymers are connected with the high level of functionality and the globular geometry resulting in relatively low viscosity at high molecular weight. We have compared the viscosity change (Figure 3.30) of silicone oil by adding linear ($M_w = 2.0 \times 10^4 \text{ g mol}^{-1}$) and hyperbranched poly(DVB-co-PDMS) ($M_w = 2.4 \times 10^4 \text{ g mol}^{-1}$, Entry 1 in Table 3.13). More important, the viscosity increase of the oil after adding hyperbranched polymer is not significant but even lower than that after adding linear polymers. This demonstrates a significantly decreased interaction between solvent and polymer because of its densely branched

structure.

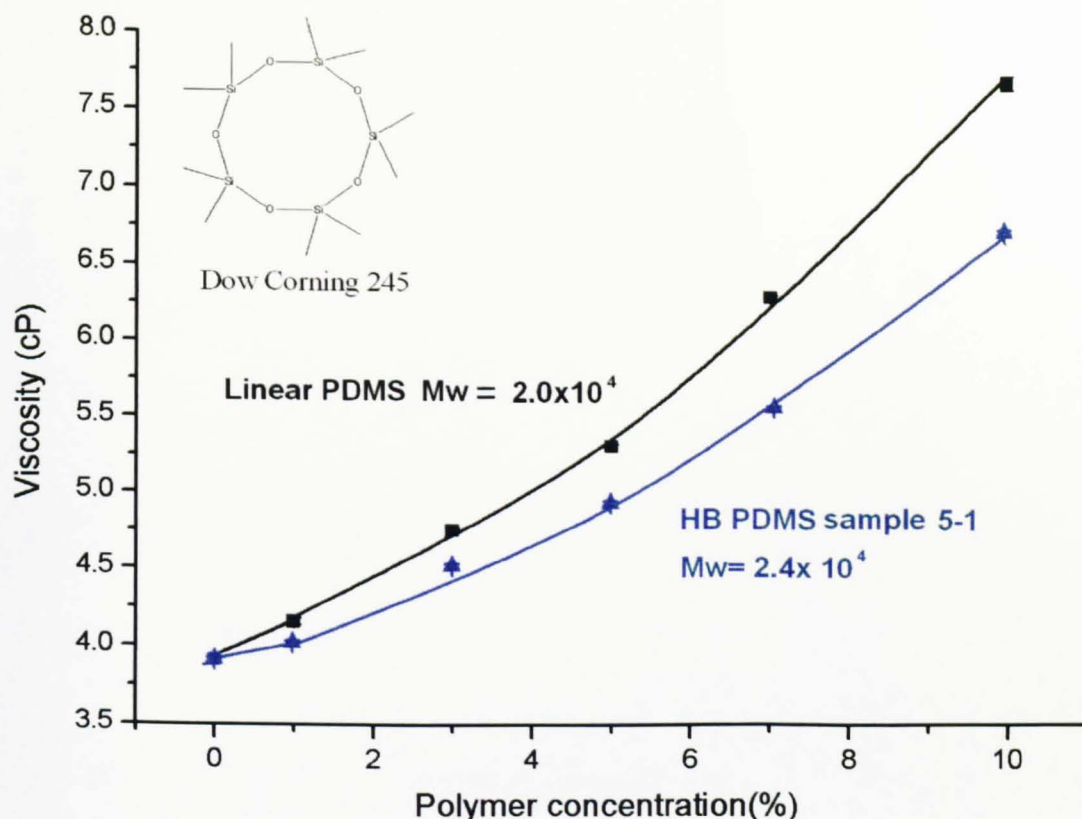


Figure 3.30: Comparison of silicone oil DC 245 thickens by linear PDMSma and hyperbranched PDMSma (Entry 1, Table 3.13). After addition of hyperbranched poly(DVB-co-PDMSma), the viscosity of silicone oil was increased lower than that add linear PDMSma was added.

However, 5% wt concentration poly(DVB-co-PDMSma) ($M_w=2.79 \times 10^5 \text{ g mol}^{-1}$, Entry 3, Table 4.13) and 0.5% initiator (AIBN) were added into the stearyl ether oil (Arlamol E, PPG-15 stearyl ether) (Figure 3.31, A). Then the oil was stirred and heated to 70 °C (Figure 3.31, B and C). The viscosity of oil is increased significantly, even resulting in gel formation over the course of one minute (Figure 3.31, D). This phenomena is because of the residue vinyl group on the branches were initiated by AIBN and forms the crosslink network immediately. Furthermore, the same test is conducted in silicone oil (Dow Corning 245, Figure 3.32) and ester oil (Estol 1512, Figure 3.33).

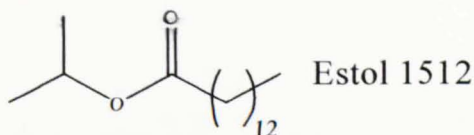
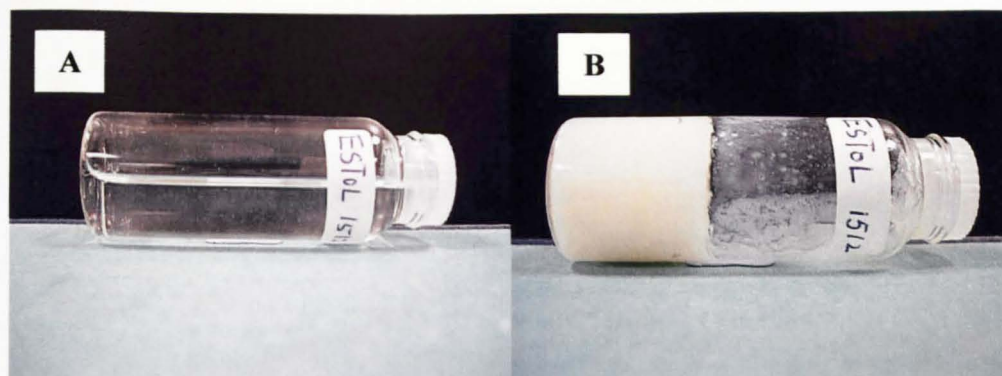


Figure 3.33 (A) original Estol 1512. (B) Estol 1512 oil forms a gel formation immediately after adding 5% w/w poly(DVB-*co*-PDMSma) ($M_w=2.79 \times 10^5 \text{ g mol}^{-1}$, Entry 3, Table 3.13) and 0.5% w/w initiator (AIBN) into it then heating to 70 °C.

Finally, unlike the copolymerisation of EGDMA and DMAEMA reaction, this reaction represents a relatively good reproducibility (Table 3.15). As mentioned before, the low reaction rate of PDMSma slows down the overall reaction rate. Therefore, the slow reaction rate can help to control the system. Thus, the very slow reaction rate makes the polymerisation stay in a much more stable stage.

Table 3.15 Reproducibility data of hyperbranched poly(DVB-*co*-PDMSma) samples at same condition in toluene system. Reaction conditions: $[M]=1.84 \text{ M}$, $[\text{Initiator}]:[\text{DVB}]:[\text{PDMSma}]:[\text{CuI}]:[\text{CuII}]=1:40:10:0.33:0.11$, $[\text{Cu(I)}+\text{Cu(II)}]:[\text{HMTETA}]=1:1$, in toluene at 90 °C.

Reaction	Reaction time (hrs)	Yield (%)	MALLS-GPC results		
			M_n (g mol^{-1})	M_w (g mol^{-1})	PDI
A	29	65	6.3×10^5	1.77×10^6	2.8
B	27.5	63	6.0×10^5	1.52×10^6	2.5

3.4 Conclusion

In conclusion, a novel copolymer which contains hyperbranched structure, hydrophilic blocks, numerous of active vinyl groups and halide groups by copolymerising of DMAEMA and EGDMA has been prepared successfully. DE-ATRP demonstrates a facile route to hyperbranched polymer from multifunctional vinyl monomers. The hyperbranched structure was confirmed by MALLS-GPC and NMR analysis. Furthermore, this hyperbranched amphiphilic shows great encapsulation ability by transfer water-soluble dyes into chloroform. The data shows the hyperbranched structure helps raise the encapsulation ability.

Moreover, a novel hyperbranched poly(DVB-*co*-PDMSma) was prepared via the enhanced deactivation ATRP route. The resulting polymers were characterised by GPC-MALLS and NMR. The GPC-MALLS analysis shows that the hyperbranched poly(DVB-*co*-PDMSma) has high molecular weight and broad polydispersity, which are exactly in agreement with the recognised property of hyperbranched polymers. In addition, by tracking the relationship between the RMS radius, elution volume and molecular weight, it indicates solid evidence for the highly branched structure. It is also apparent that from the ^1H NMR spectroscopic data that active vinyl groups presented in the hyperbranched polymer even at low conversion. Last, the oil thickening test shows the oil viscosity increases less by adding hyperbranched polymer. The silicone oil was transformed to gel after adding poly(DVB-*co*-PDMSma) and initiator.

3.5 Reference

1. Adams, M. L.; Lavasanifar, A.; Kwon, G. S. *Journal of Pharmaceutical Sciences* **2003**, 92, (7), 1343-1355.
2. Alexandridis, P. *Current Opinion in Colloid & Interface Science* **1996**, 1, (4), 490-501.
3. Kim, Y. H. *Journal of Polymer Science, Part A-Polymer Chemistry* **1998**, 36, (11), 1685-1698.
4. Kim, Y. H.; Webster, O. W. *Journal of the American Chemical Society* **1990**, 112, (11), 4592-4593.
5. Fréchet, J. M. J. *Science* **1994**, 263, (5154), 1710-1715.
6. Fréchet, J. M. J.; Hawker, C. J.; Gitsov, I.; Leon, J. W. *Journal of Macromolecular Science-Pure and Applied Chemistry* **1996**, A33, (10), 1399-1425.
7. Hult, A.; Johansson, M.; Malmström, E., Hyperbranched polymers. In *Branched Polymers* 1999; Vol. 143, pp 1-34.
8. Tomalia, D. A.; Brothers, H. M.; Piehler, L. T. *Abstracts of Papers of the American Chemical Society* **1995**, 210, 39-PMSE.
9. Tomalia, D. A.; Fréchet, J. M. J. *Journal of Polymer Science, Part A-Polymer Chemistry* **2002**, 40, (16), 2719-2728.
10. Voit, B. *Journal of Polymer Science, Part A-Polymer Chemistry* **2000**, 38, (14), 2505-2525.
11. Rungsardthong, U.; Deshpande, M.; Bailey, L.; Vamvakaki, M.; Armes, S. P.; Garnett, M. C.; Stolnik, S. *Journal of Controlled Release* **2001**, 73, (2-3), 359-380.
12. van de Wetering, P.; Schuurmans-Nieuwenbroek, N. M. E.; van Steenberg, M. J.; Crommelin, D. J. A.; Hennink, W. E. *Journal of Controlled Release* **2000**, 64, (1-3), 193-203.
13. Bos, G. W.; Trullas-Jimeno, A.; Jiskoot, W.; Crommelin, D. J. A.; Hennink, W. E. *International Journal of Pharmaceutics* **2000**, 211, (1-2), 79-88.
14. van de Wetering, P.; Moret, E. E.; Schuurmans-Nieuwenbroek, N. M. E.; van

- Steenbergen, M. J.; Hennink, W. E. *Bioconjugate Chemistry* **1999**, 10, (4), 589-597.
15. Tomalia, D. A.; Hall, M.; Hedstrand, D. M. *Journal of the American Chemical Society* **1987**, 109, (5), 1601-1603.
16. Tomalia, D. A.; Naylor, A. M.; Goddard, W. A. *Angewandte Chemie-International Edition in English* **1990**, 29, (2), 138-175.
17. Flory, P. J. *Journal of the American Chemical Society* **1952**, 74, (11), 2718-2723.
18. Fréchet, J. M. J.; Henmi, M.; Gitsov, I.; Aoshima, S.; Leduc, M. R.; Grubbs, R. B. *Science* **1995**, 269, (5227), 1080-1083.
19. Matyjaszewski, K.; Gaynor, S. G.; Kulfan, A.; Podwika, M. *Macromolecules* **1997**, 30, (17), 5192-5194.
20. Matyjaszewski, K.; Xia, J. H. *Chemical Reviews* **2001**, 101, (9), 2921-2990.
21. Guan, Z. *Journal of the American Chemical Society* **2002**, 124, (20), 5616-5617.
22. Costello, P. A.; Martin, I. K.; Slark, A. T.; Sherrington, D. C.; Titterton, A. *Polymer* **2002**, 43, (2), 245-254.
23. O'Brien, N.; McKee, A.; Sherrington, D. C.; Slark, A. T.; Titterton, A. *Polymer* **2000**, 41, (15), 6027-6031.
24. Isaure, F.; Cormack, P. A. G.; Graham, S.; Sherrington, D. C.; Armes, S. P.; Butun, V. *Chemical Communications* **2004**, (9), 1138-1139.
25. Liu, B. L.; Kazlauciusas, A.; Guthrie, J. T.; Perrier, S. *Macromolecules* **2005**, 38, (6), 2131-2136.
26. Li, Y. T.; Armes, S. P. *Macromolecules* **2005**, 38, (12), 5002-5009.
27. Matyjaszewski, K.; Nanda, A. K.; Tang, W. *Macromolecules* **2005**, 38, (5), 2015-2018.
28. Bischoff, R.; Cray, S. E. *Progress in Polymer Science* **1999**, 24, (2), 185-219.
29. Jones; Richard, G., *Silicon-containing polymers*. The Royal Society of Chemistry, Cambridge: 1995.
30. Sellinger, A.; Laine, R. M. *Macromolecules* **1996**, 29, (6), 2327-2330.
31. Muzafarov, A. M.; Golly, M.; Möller, M. *Macromolecules* **1995**, 28, (24), 8444-8446.
32. Rubinsztajn, S.; Lewis, L. N.; Stein, J.; Michalczyk, M. J. *Chemical &*

Engineering News **1994**, 72, (17), 4-4.

33. Mathias, L. J.; Carothers, T. W. *Journal of the American Chemical Society* **1991**, 113, (10), 4043-4044.

34. Miravet, J. F.; Fréchet, J. M. J. *Macromolecules* **1998**, 31, (11), 3461-3468.

35. Vasilenko, N. G.; Rebrov, E. A.; Muzafarov, A. M.; Esswein, B.; Striegel, B.; Moller, M. *Macromolecular Chemistry and Physics* **1998**, 199, (5), 889-895.

36. Kitajyo, Y.; Imai, T.; Sakai, Y.; Tamaki, M.; Tani, H.; Takahashi, K.; Narumi, A.; Kaga, H.; Kaneko, N.; Satoh, T.; Kakuchi, T. *Polymer* **2007**, 48, (5), 1237-1244.

37. Kitajyo, Y.; Nawa, Y.; Tamaki, M.; Tani, H.; Takahashi, K.; Kaga, H.; Satoh, T.; Kakuchi, T. *Polymer* **2007**, 48, (16), 4683-4690.

38. Lin, Y.; Liu, X. H.; Dong, Z. M.; Li, B. X.; Chen, X. S.; Li, Y. S. *Biomacromolecules* **2008**, 9, (10), 2629-2636.

39. Chen, S.; Zhang, X. Z.; Cheng, S. X.; Zhuo, R. X.; Gu, Z. W. *Biomacromolecules* **2008**, 9, (10), 2578-2585.

40. Liu, M. J.; Kono, K.; Fréchet, J. M. J. *Journal of Controlled Release* **2000**, 65, (1-2), 121-131.

41. Hawker, C. J.; Chu, F. K. *Macromolecules* **1996**, 29, (12), 4370-4380.

42. Stiriba, S. E.; Kautz, H.; Frey, H. *Journal of the American Chemical Society* **2002**, 124, (33), 9698-9699.

43. Chen, G. H.; Guan, Z. B. *Journal of the American Chemical Society* **2004**, 126, (9), 2662-2663.

44. Chen, Y.; Shen, Z.; Pastor-Perez, L.; Frey, H.; Stiriba, S. E. *Macromolecules* **2005**, 38, (2), 227-229.

45. Esfand, R.; Tomalia, D. A. *Drug Discovery Today* **2001**, 6, (8), 427-436.

46. Gillies, E. R.; Fréchet, J. M. J. *Drug Discovery Today* **2005**, 10, (1), 35-43.

47. Jeong, B.; Bae, Y. H.; Lee, D. S.; Kim, S. W. *Nature* **1997**, 388, (6645), 860-862.

48. Aulenta, F.; Hayes, W.; Rannard, S. *European Polymer Journal* **2003**, 39, (9), 1741-1771.

49. Jansen, J.; de Brabander-van den Berg, E. M. M.; Meijer, E. W. *Science* **1994**, 266, (5188), 1226-1229.

50. Newkome, G. R.; Moorefield, C. N.; Baker, G. R.; Saunders, M. J.; Grossman, S. H. *Angewandte Chemie-International Edition in English* **1991**, 30, (9), 1178-1180.
51. Baudry, R.; Sherrington, D. C. *Macromolecules* **2006**, 39, (4), 1455-1460.

CHAPTER FOUR: CORE-SHELL HYPERBRANCHED POLYMERS

This chapter examines two possible research avenues for further development of core-shell hyperbranched polymers. The first section looks to extend the DE-ATRP method for preparing a core-shell hyperbranched polymer via a two step procedure. This hyperbranched polymer will consist of a hyperbranched polyDVB core and many linear poly(methyl methacrylate) (PMMA) chains as a shell.

In the second section we explore whether it is possible to combine the RAFT polymerisation of methacrylates (*N,N*-dimethylamino-2-ethyl methacrylate, DMAEMA) with the ring-opening polymerisation of cyclic (ϵ -caprolactone) monomers using a hydroxyl functionalised RAFT agent.

4.1 Introduction

4.1.1 Core-shell Star Polymers

Core-shell star polymers are branched polymers consisting of several linear chains linked to a central core. The synthesis of this kind of polymer has been the subject of numerous studies since the discovery of controlled/living polymerisation.¹⁻³ The three methods leading to core-shell architectures are listed as below: 1. Core-first method via multifunctional initiators;⁴⁻⁹ 2. Arm-first method via di-functional monomer;^{10, 11} 3. Coupling method via multifunctional linking agents.¹²⁻¹⁴ (Figure 4.1)

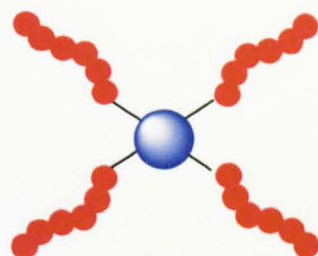
Core-first method



+



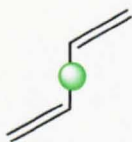
Living polymerisation



Arm-first method

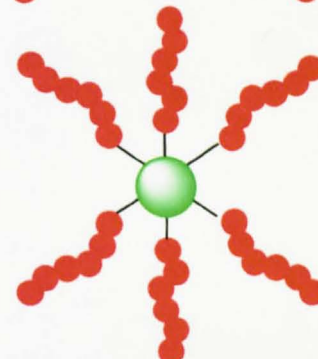


+



Di-functional monomer

Crosslinking



Coupling method



+



Multifunctional linking agent

Coupling

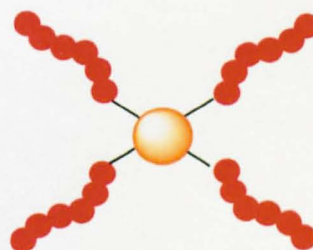
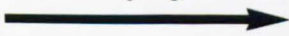


Figure 4.1 Three general routes for the synthesis of star polymers: core-first, arm-first and coupling methods.

In the core-first method, multifunctional initiator compounds are capable of simultaneously initiating the polymerisation of several arms (Figure 4.1).¹⁻³ A multifunctional initiator has the following requirements in order to prepare well defined

star polymers with uniform arms and low molecular weight distribution. All the initiation sites must be equally reactive and the initiation rate is higher than the propagation rate. An important feature of this method is that the arms growing from the core are living and therefore are susceptible to end functionalisation reactions or can be potentially used to initiate the polymerisation of another monomer.

For the arm-first method, the linear arms of the star polymers are synthesised first followed by binding of the arms to form the core, usually by using a divinyl cross-linker (Figure 4.1). For example, a living polymer precursor is used as initiator for the polymerisation of a small amount of a suitable divinyl monomer, such as divinylbenzene (DVB).¹⁵ The number of arms incorporated in the star structure is influenced by many parameters, especially the ratio of divinyl monomer to the arms. The disadvantage is that microgel or tightly cross-linked polymers are formed upon the polymerisation. Furthermore, it is very difficult to predict and control the number of arms.

In the coupling method, the star polymer is synthesised by coupling reactions between linear polymer chains containing a reactive chain end group and a multifunctional coupling agent. For instance, click reactions are used for synthesis of various kinds of star polymer.^{12, 13} The functionality of the linking agent determines the number of the arms of the star polymer, provided that the linking reaction is quantitative. In addition, the living arms can be isolated and characterised independently along with the final star product. Consequently, the functionality of the star can be measured directly and accurately. The disadvantage of the method is that it required a long time for the linking reaction to ensure complete reaction.

In the first section of this chapter, a core-shell polymer (polyDVB_{core}-co-MMA_{shell}) was prepared via two-steps ATRP method. The synthesis strategy is based on the core-first method (Figure 4.2). Firstly, highly branched cores containing multiple initiating sites (2, Figure 4.2) in a statistical distribution will be generated by DE-ATRP of divinyl monomer (1, Figure 4.2). In order to prevent macroscopic gelation or microgel formation, it is essential to enhance the deactivation ATRP by performing the polymerisation with addition of Cu(II). Secondly, initiating sites such as alkyl halide on the core can be used to initiate another monomer such as methyl methacrylate (MMA)

to form a linear shell structure (3, Figure 4.2). Compared to the star polymers synthesised from the traditional core-first method, this new strategy will skip the tedious synthesis of the multifunctional initiator before polymerisation. The structure of the formed star polymer should be similar to the star synthesised by the traditional arm-first method because both of them contain a highly branched core with statistically distributed arms. There is an alternative way to form a cross-linked multifunctional nanogel to use a cross-linker in a diluted solution. However, the less well-controlled polymerisation will increase the core cross-link density and makes it more like a microgel structure.¹⁶

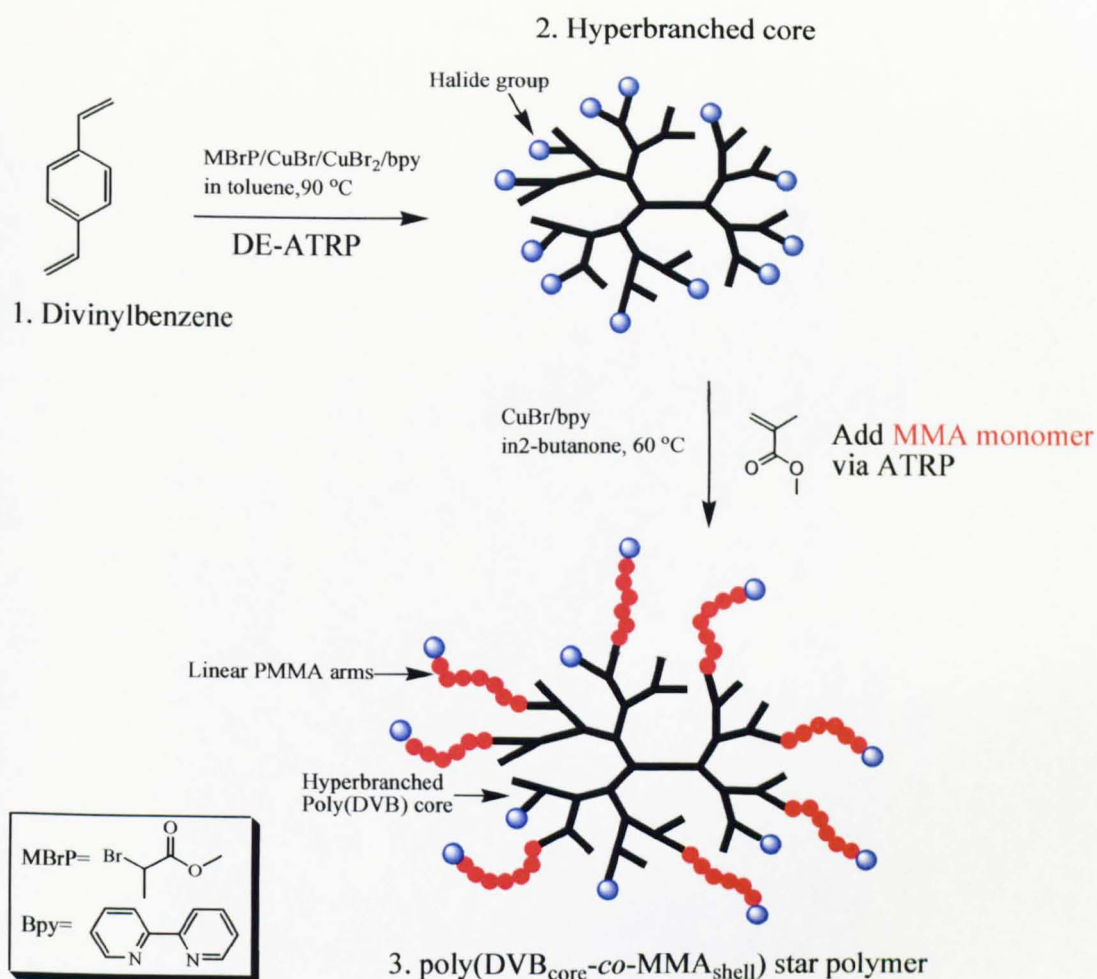


Figure 4.2 Synthesis of core-shell polymer via growth PMMA arms from the hyperbranched poly(DVB) core.

4.1.2 Biodegradable Core-Shell Hyperbranched Materials

For biomedical applications, the choice of polymers is obviously restricted to those that are biocompatible. Thus, biodegradable amphiphilic copolymers are ideal. In recent years, gene delivery, especially using non-viral synthetic vectors based on biodegradable polymers such as poly(ϵ -caprolactone) (PCL) has attracted considerable scientific interest. Polymeric pH-sensitive micelles have been also studied extensively for drug delivery systems with pH-targeting. A remarkable example of pH-sensitive micelles, developed by Müller and co-workers is based on poly(*N*-isopropylacrylamide)-*b*-poly(acrylic acid) (PNIPAM-*b*-PAA).¹⁷ The micellar behaviour of the above amphiphilic block polymer can be studied either directly in solution, in particular with dynamic light scattering (DLS), or in the solid state with atomic force microscopy (AFM) or transmission electron microscopy (TEM). Recently, block copolymers of poly(ϵ -caprolactone) and poly(*N,N*-dimethylamino-2-ethylmethacrylate) (PCL-*b*-PDMAEMA) grafted on cross-linked microspheres have been studied by Stover and co-workers.¹⁸ Furthermore, PCL-*co*-PDMAEMA copolymers have shown amphiphilic behaviour in water.¹⁹ Also, PCL-*b*-PDMAEMA block copolymers have been recently studied by Xu in cisplatin-releasing pH-responsive nanoparticles.²⁰

Dendritic polymers have unique properties because of their highly branched structures and large number of functional end groups²¹⁻²³. Their unique three-dimensional structure also makes them attractive for new applications ranging from drug delivery to nano-building blocks.^{23, 24} The discovery of new mechanisms allowing the polymerisation process to be under control has paved the way to new macromolecular architectures. Recently, 4,4-bioxepanyl-7,7-dione (BOD) has been used as a crosslinker to form a micro-gel or core cross-linked structure.^{25, 26} However, the potential properties and applications are limited by the poor solubility and chain mobility of microgel or core crosslinked structures.

In the second section of this chapter, the aim is to develop a novel method to synthesise the biodegradable core-shell hyperbranched polymer (polyCL-*co*-BOD_{core}-DMAEMA_{shell}). The strategy is based on core-first mechanism. If successful, polymer will consist of a hyperbranched PCL core and pH-sensitive shell. The approach combines controlled ring opening polymerisation (ROP) and reversible addition fragment chain transfer polymerisation (RAFT) (Figure 4.4). Firstly, the hyperbranched

core will prepared via ROP copolymerisation of ϵ -CL and BOD which used as a branched point with initiated by the hydroxyl group on 4,4-azobis(4-cyanovaleric acid) RAFT (ACP-RAFT). The ratio of ACP-RAFT, ϵ -CL and BOD is kept at 1:10:1 to prevent it from cross-linking as reported via the 'Strathclyde method'²⁷⁻²⁹. This process relies on a stannous octoate (SO) catalyst system. SO is the catalyst of choice for lactone polymerisations because of its low cost, low toxicity, and high efficiency. Recently, two types of mechanism about the activity of SO in the polymerisation have been reported. Firstly, the SO serves to activate monomer through coordination with the carbonyl oxygen (directly catalytic mechanism)^{30, 31}. Secondly, the SO acts as co-initiator along with purposely added or adventitious hydroxyl impurities (monomer insertion mechanism). The polymerisation proceeds through an activated stannous alkoxide bond (Figure 4.3)³²⁻³⁷. Most recently, reports have tended to favour the second type mechanisms³².

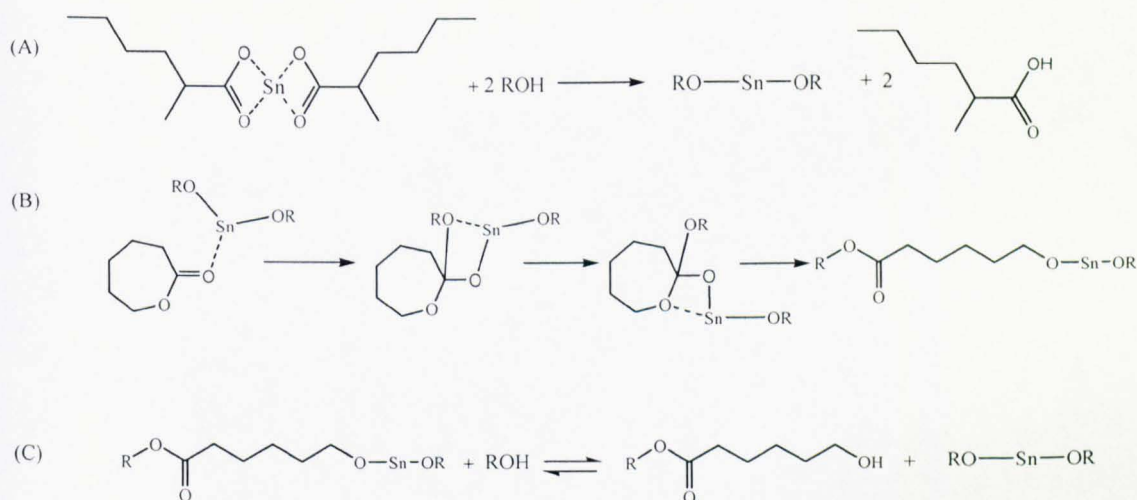


Figure 4.3 Mechanism of initiation in stannous octoate catalysed polymerisation of ϵ -caprolactone. The polymerisation process includes formation of stannous alkoxide species (A), the coordination-insertion propagating process (B) and intermolecular exchange reaction between stannous alkoxide species and initiator (C).

Secondly, the RAFT technique is employed for the controlled polymerisation of vinyl monomer to form a linear shell (Figure 4.4). In this case, the hyperbranched PCL with many RAFT end functionalities is used as a macro-initiator for the RAFT of DMAEMA. Thus, the final polymer will consist of a biodegradable hyperbranched PCL

core and many linear DMAEMA arms. To the best of our knowledge, such amphiphilic hyperbranched copolymers with a pH and temperature sensitive water soluble shell and biodegradable core have never been synthesised via similar route.

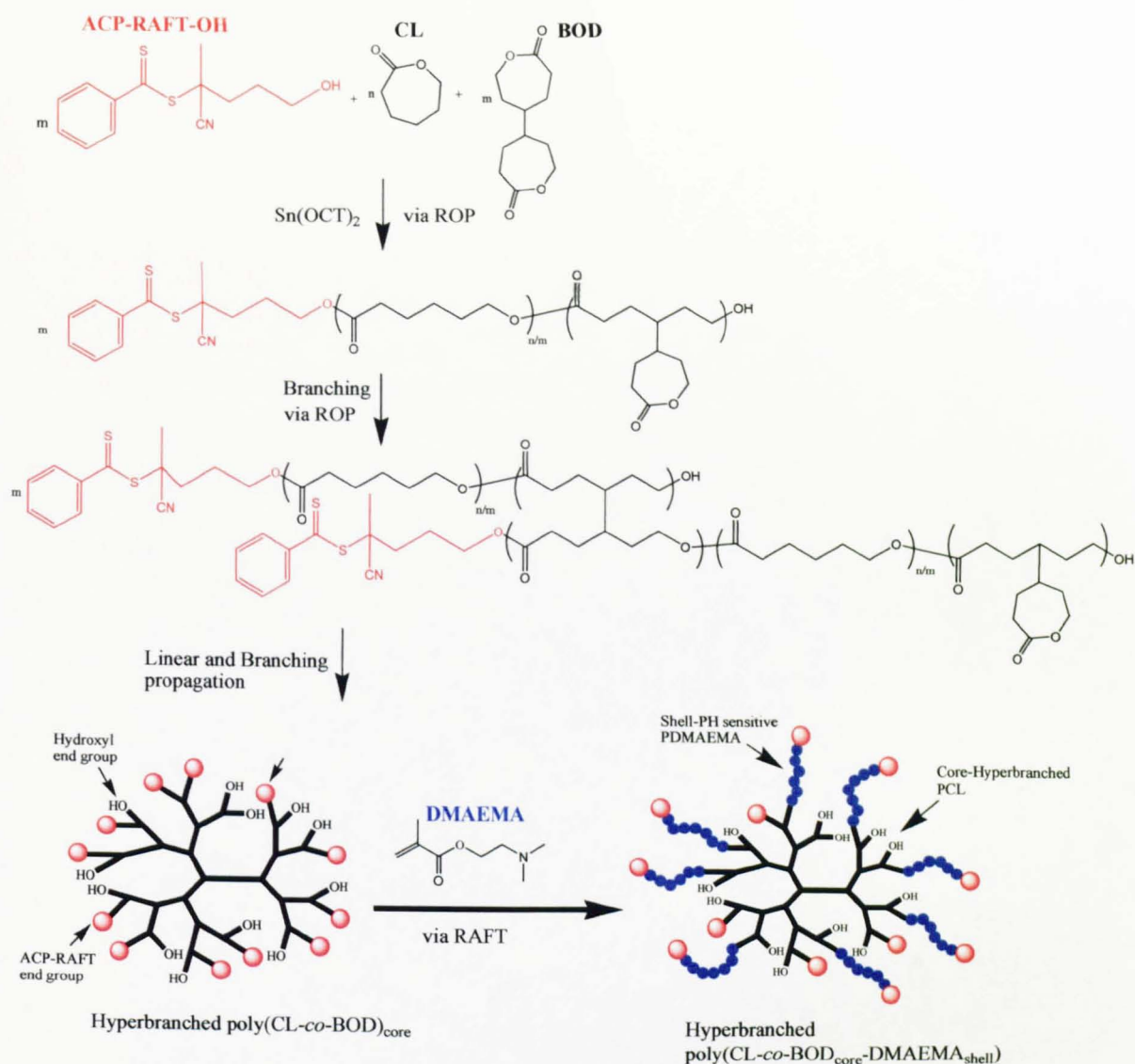


Figure 4.4 Schematic representation of the synthesis route of poly(CL-co-BOD)_{core}-DMAEMA_{shell}. First, the copolymerisation of CL and BOD is conducted via ring-opening polymerisation to afford a highly branched core. In the second stage, the DMAEMA monomer will be added onto this core to form a hyperbranched core-shell polymer via the RAFT method.

4.2 Experimental

Materials

DVB monomer (Aldrich) was purified by passing through a column of activated basic alumina (ACROS) and purging with high-purity nitrogen for 1 hour prior to use. Initiator stock solution was prepared from methyl 2-bromopropionate (Aldrich) with 2-butanone (99.5+%, HPLC grade, Aldrich). The concentration of the methyl 2-bromopropionate or methyl 2-chloropropionate was 0.815 mol L^{-1} , and was degassed by high-purity nitrogen. bpy (Aldrich) copper (I) bromide (98%, Aldrich), copper(II) bromide (98%, Aldrich) were used as received. ϵ -caprolactone (ϵ -CL, from Aldrich, 99%) was dried over calcium hydride (CaH_2) for 48 hours at room temperature and then distilled under reduced pressure before use. Methyl methacrylate (MMA) and *N,N*-dimethylamino-2-ethyl methacrylate (DMAEMA, from Aldrich, 99%) was passed through a column of basic alumina to remove stabilising agents and then stored under a nitrogen atmosphere at room temperature. Toluene and THF (Aldrich, reagent grade) was dried by molecular sieves before use.

Synthesis of hyperbranched poly(DVB) core

Known amounts of CuBr, CuBr₂ and Bpy were added to a round bottom flask fitted with a three-way stopcock connected to either a nitrogen line or a vacuum pump. Oxygen was removed by repeated vacuum-nitrogen cycles. Once filled with nitrogen, the flask was filled with known amounts of degassed DVB and toluene. $[\text{DVB}] = 3.51 \text{ M}$. After stirring for one hour at room temperature, a known amount of methyl 2-bromopropionate was added, the ratio of $[\text{DVB}]:[\text{I}]:\text{Cu(I)}:\text{Cu(II)} = 40:1:0.4:0.133$ and the polymerisation was conducted at 90°C . After polymerisation under stirring at the 90°C for 8 hours, the solution was diluted with THF and precipitated into a large excess of methanol. After separation by filtration, the polymer was dried under reduced pressure at room temperature and weighed in order to calculate the polymer yield gravimetrically.

Synthesis of core-first poly(DVB-co-MMA)

Known amounts of poly(DVB) (0.1 g , $M_w = 7.1 \times 10^4 \text{ g mol}^{-1}$, $1.41 \times 10^{-6} \text{ mol}$), CuBr and Bpy were added to a round bottom flask fitted with a three-way stopcock connected to either a nitrogen line or a vacuum pump. DVB-Br is the potential initiation sites on

polyDVB. From our calculation, there are average 54.1 potential initiation sites on each polyDVB core (see Eq. 4.2 and Eq. 4.3). Thus, the amount of initiation sites on polyDVB (DVB-Br) is 7.63×10^{-5} mol. Oxygen was removed by repeated vacuum-nitrogen cycles. Once filled with nitrogen, the flask was filled with known amounts of degassed MMA (7.64 g, 7.63×10^{-2} mol) and 2-Butanone (270 ml) as $[MMA] = 0.28 \text{ mol L}^{-1}$. $[MMA]/[DVB-Br]/[CuBr]/[bpy] = 1000/1/1/2$ in Butanone. The polymerisation was conducted at 60°C under stirring. After the desired polymerisation reaction time, the solution was diluted with 2-Butanone and precipitated into a large excess of cold hexane. After separated by filtration, the polymer was dried under reduced pressure at 30°C and prepared for characterisation.

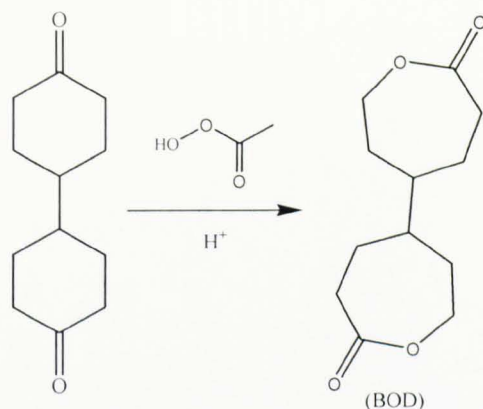
Synthesis of 4,4-azobis(4-cyanovaleric acid) (ACP-RAFT)

Phenyl-magnesium bromide (25 ml, 0.10 M in THF) was placed in a flask containing anhydrous THF (20 ml) and carbon disulfide (4.95 ml, 6.51×10^{-5} mol) was added dropwise. A colour transition from brown to red was observed over the two hour course of the reaction. Using liquid nitrogen traps, the solvent was removed under vacuum to yield a deep red viscous liquid and was washed with chloroform (3x200 ml). An aqueous solution of iodine (10.40 ml, 1.0×10^{-2} mol) was then added dropwise. A colour transition was observed from dark red to pink as the disulfide is precipitated from solution. Excess I_2 was removed using a few crystals of Na_2CO_3 . The mixture is then extracted using methylene chloride, dried using Na_2SO_4 filtered and evaporated to yield a crystalline red solid. The dithio-compound (0.5 g, 1.4×10^{-3} mol) and AIBN (0.255 g, 1.62×10^{-3} mol) in ethyl acetate (120 ml) were placed in a round bottomed flask and degassed. The system was reacted under reflux in a N_2 atmosphere for 16 hours. After such time, the solvent was removed under vacuum and the product was purified on a column, using a solvent mix of ether and hexane (3:7 v/v), collecting the red fraction that was observed due to the pure RAFT compound.

Synthesis of 4,4-bioxepanyl-7,7-dione (BOD)

A solution of urea hydrogen peroxide ($\text{CO}(\text{NH}_2) \cdot \text{H}_2\text{O}_2$) (10.0 g, 106 mmol) in 50 mL of formic acid (99%) was stirred at 23°C for 90 mins. 4,4-Bicyclohexanone (5.0 g, 25.7 mmol) was then slowly added over 5-10 mins and stirred for a further 4 h. Water (200 mL) was added to the mixture followed by extraction with chloroform. The organic fractions were collected, washed with a saturated aqueous sodium bicarbonate solution,

and dried with Na_2SO_4 . The organic fraction was concentrated, and the solvent was removed under reduced pressure to yield a white powder (3.50 g, 60% yield). ^1H NMR (300 MHz, CDCl_3 , see Figure 4.20), chemical shift (ppm): 4.34 (R, R) 4.17 (S, R) (t, 2H, $-\text{CH}_2-\text{OOC}-$), 2.73 (R, R) 2.60 (S, R) (t, 2H, $-\text{CH}_2\text{COO}-$), 1.93-1.83 (m, 2H, $-\text{CH}_2\text{CH}_2\text{OOC}-$), 1.70-1.60 (m, 2H, $-\text{CH}_2\text{CH}_2\text{COO}-$), 1.49 (q, 1H, $-\text{CHCH}_2-$).



Synthesis of hyperbranched PCL core

The equipment was first flame-dried, resulting in a clean airtight system. Particular attention was given to the three neck round bottom flask equipped with a rubber septum, three way tap and condenser. The flask was cleaned, dried, and then purged with nitrogen before use as the polymerisation vessel. BOD (475 mg, 2.1×10^{-3} mol), ACP-RAFT (554 mg, 2.1×10^{-3} mol), ϵ -caprolactone (2.42 g, 2.1×10^{-2} mol) was added to 50ml dried toluene as $[\epsilon\text{-Caprolactone}] = 0.42$ M. Stannous octanoate ($\text{Sn}(\text{Oct})_2$) (405 mg, 1×10^{-3} mol) was added to the flask, then flask was heated to 110°C . The chemical ratio is $[\text{ACP-RAFT}]:[\text{BOD}]:[\epsilon\text{-Caprolactone}]:[\text{Sn}(\text{Oct})_2] = 1:1:10:0.5$. After desired reaction time, 10 ml sample was taken under nitrogen protect to avoid oxidation. The polymer was then selectively precipitated in an excess volume of cold methanol, filtrated, and dried under reduced pressure until constant weight. The results of polymer are summarised in Table 4.2.

Synthesis of core-shell $\text{poly}(\text{CL-co-BOD})_{\text{core}}\text{-(DMAEMA)}_{\text{shell}}$ via RAFT

$\text{Poly}(\text{CL-co-BOD})$ (1.5 g, 1×10^{-4} mol) and ACP initiator (7.8 mg, 3.46×10^{-5} mol) were put in a dry round-bottomed flask. Dry DMAEMA (13.6 g, 8.65×10^{-2} mol) and toluene (170 ml) mixture injected into reaction vessel and the system was freeze pump thawed to remove oxygen. From our calculation, there are average 17.3 $[\text{ACP-RAFT}]$ sites on each $\text{poly}(\text{CL-co-BOD})$ core (See Eq. 4.10). Thus, the amount of ACP-RAFT sites in

the reaction is 1.73×10^{-3} mol. The chemical ratio [ACP-RAFT sites]: [DMAEMA]: [ACP initiator] = 1:50:0.2, [DMAEMA] = 0.5 M. Solution was heated to 60 °C and allowed to react for 12 hours. The polymer was precipitated in excess cold hexane and ready for GPC-MALLS. The results of polymer are summarised in Table 4.3.

Degradation of poly(PCL-*co*-BOD)_{core}-(DMAEMA)_{shell} hydrolysable core

Dioxane (18 ml, 2.04×10^{-4} mol), hydrochloric acid (1.5 ml, 30%) and poly(CL-*co*-BOD)_{core}-(DMAEMA)_{shell} were mixed in a flask, the solution was heated to 60 °C and stirred for 24 hours. After neutralisation by NaOH and extraction, it yielded a fine pale yellow powder of poly(DMAEMA).

Atomic force microscopy (AFM)

A MultiMode AFM with a NanoScope V controller (Veeco Instruments) was used. All measurements were conducted in Tapping ModeTM in air or mixed solvent (40% v/v THF/ water). The images were processed by Nano scopeTM software (Veeco Company).

For the measurements in the air, the samples were dissolved in THF at very dilute concentration (10 µg/L) and spread on silica or mica substrate surface by spin coating (1000 rpm). The drive frequency is used as 300 kHz. Two types of AFM probes were used. In the first set of experiments, we used Tap300Al probes (Budget Sensors) with a typical cantilever spring constant of 40 N/m and a typical probe apex curvature radius of 10 nm. In the second set of experiments, DP15/HI'RES/AIBS probes (MikroMasch) were used with a typical cantilever spring constant of 46 N/m and a typical probe apex curvature radius of 1 nm.

For the measurements in the mixed solvent, the samples were dissolved in THF at very dilute concentration (10 µg/L) and spread on a mica substrate surface by spin coating (1000 rpm). After the substrate was dried in air, the mixed solvent (40% v/v THF/ water) was dipped on the surface. The drive frequency is used as 8 kHz. We used NP-S probes (Veeco) with a typical cantilever spring constant of 0.1 N/m and a typical probe apex curvature radius of 10 nm.

4.3 Results and Discussion

4.3.1 Core-Shell Hyperbranched poly(DVB_{core}-co-MMA_{shell})

In this section, hyperbranched poly(DVB_{core}-co-MMA_{shell}) was prepared via a two-steps ATRP route. Table 4.1 summarises the results from the synthesis of poly(DVB-co-MMA) star polymers. At first, DVB was homopolymerised by enhanced deactivation ATRP in toluene at 90 °C, the molar ratio is [DVB]: [I]: Cu(I) : Cu(II)= 40: 1: 0.4: 0.133 similar to that reported previously in Chapter 2 (Table 2.3). The reaction was stopped after 8 hrs at 22% conversion and polyDVB was purified and precipitated in excess cold methanol. It was difficult to control the second shell addition step if the molecular weight of core is too high, because a large number of vinyl groups on the core polymers will be easily cross-linked with other cores during the shell addition step. Thus, the cores with moderate molecular weight were chosen to avoid the intermolecular crosslinking during the shell adding step. In the reaction, the M_w of hyperbranched poly(DVB) is $7.1 \times 10^4 \text{ g mol}^{-1}$ from GPC-MALLS and the branch ratio is 20% calculated from ^1H NMR spectroscopy data (Entry 1, Table 4.1).

The second step of shell growth is the reaction under normal ATRP in dilute butanone solution at 60 °C, with the ratio of [MMA]:[DVB-Br]:[CuBr]:[bpy] = 1000:1:1:2 and [MMA]=0.28 M, where the DVB-Br is the potential initiation site of bromine on polyDVB. Since the feed ratio of [Initiator]:[DVB]=1:40 for the synthesis of polyDVB core. In addition, all of the initiators are propagated at the very beginning of the reaction due to the mechanism of ATRP³. Thus, the ratio of the [initiator]:[DVB] in the polyDVB core is:

$$[\text{Initiator}]: [\text{DVB units}] = 1: 40 \times \text{Conversion}_{\text{DVB}} \quad (\text{Eq. 4.1})$$

For example, the conversion of the polyDVB is 22% at 8 hours in this reaction. Thus, the ratio of [initiator]:[DVB] in the polyDVB core is:

$$[\text{Initiator}]: [\text{DVB units}] = 1: 40 \times 22\% = 1: 8.8$$

Therefore, the number of the DVB units and initiation sites in the polyDVB core were calculated by Eq. 4.2 and Eq. 4.3.

X is number of total DVB units in polyDVB core

$$FW_{\text{DVB}} \times X + FW_{\text{initiator}} \times (1/8.8) \times X = M_w \text{ of polyDVB}$$

$$130.18 \text{ gmol}^{-1} \times X + 167 \text{ gmol}^{-1} \times (1/8.8) \times X = 71000 \text{ gmol}^{-1}$$

$$X = 476 \quad (\text{Eq. 4.2})$$

$$[\text{DVB-Br}] \text{ in each polyDVB core} = 476/8.8 = 54.1 \quad (\text{Eq. 4.3})$$

Table 4.1 Synthesis of poly(DVB-co-MMA) hyperbranched core-shell polymers by using the core-first method.^a

Entry	Time (hrs)	Conversion MMA ^b	L _{arm.} by conversion ^c	GPC-MALLS				L _{arm.} by Mw ^f
				d _n /d _c ^e (mL/g)	M _n (gmol ⁻¹)	M _w (gmol ⁻¹)	PDI	
1 ^d	0	-	-	0.184	2x10 ⁴	7.1x10 ⁴	3.5	-
2	0.5	3%	30	0.142	1.0x10 ⁵	3.6x10 ⁵	3.6	53.4
3	1	3.5%	35	0.14	1.22 x10 ⁵	4.1x10 ⁵	3.4	62.6
4	1.5	4.5%	45	0.138	1.2 x10 ⁵	4.3x10 ⁵	3.7	66.3
5	2	4.7%	47	0.125	1.23 x10 ⁵	4.5x10 ⁵	3.7	69.9
6	10	6.6%	66	0.12	1.74 x10 ⁵	5.9x10 ⁵	3.4	95.8

a. Reaction condition: initial [DVB]/[Initiator]/[CuBr]/[CuBr₂]/[bpy] =40/1.0/0.4/0.133/0.5 in toluene at 90 °C, [DVB]= 3.51 M, reaction is stopped at 8 hours and poly(DVB) is purified for next step. Second reaction [MMA]/[DVB-Br]/[CuBr]/[bpy] =1000/1/1/2 in Butanone at 60 °C, DVB-Br are the potential initiation sites on polyDVB core (See Eq. 4.2 and Eq. 4.3), [MMA]=0.28 M.

b. MMA conversion is calculated by weight.

c. The values of refractive index increment (d_n/d_c) of hyperbranched core-shell polymers were measured in THF at 35 °C by using a refractometer (See Eq. 4.4 and Figure 4.5).

d. This entry shows the data for the polyDVB core.

e. Theoretical average number of MMA per arm calculated from MMA conversion (See Eq. 4.5).

f. Theoretical average number of MMA per arm calculated from poly(DVB-co-MMA) molecular weight. See the example in Eq. 4.6.

After the system starts the core-shell formation, the absolute molecular weights of hyperbranched core-shell molecules increase with MMA conversion, indicating the growth of the polymer shell. The GPC-MALLS data show the molecular weight (M_w by MALLS) increases to $3.6 \times 10^5 \text{ gmol}^{-1}$ after half an hour and finally reaches $5.9 \times 10^5 \text{ gmol}^{-1}$ at 10 hours. (Entry 2 and Entry 6, Table 4.1) However, the polydispersity of the core-shell polymer remains in the region 3.4 to 3.7 which proves that the coupling between core-shell molecules was almost excluded under dilute condition ($[\text{DVB-Br}] = 2.8 \times 10^{-4} \text{ M}$). In principal, the PDI will increase significantly if the macromolecules are combined with others.

Moreover, the differential refractive index (d_n/d_c) of hyperbranched core-shell polymers is required for GPC-MALLS to calculate the molecular weight, where the value is based on the composition of copolymer. d_n/d_c is how much the refractive index of the polymer solution varies for a increment of polymer concentration.

$$\left. \frac{d_n}{d_c} \right|_{c=0} = \lim_{c \rightarrow 0} \left(\frac{n - n_0}{c} \right) \quad (\text{Eq. 4.4})$$

In our study, the d_n/d_c of the core-shell polymers was measured in THF at 35 °C by using a refractometer. The measurement is operated by measure the refractive index of the polymer solution at different concentration. If a plot was drawn use the concentration of solution against RI value, the slope of the points is the value of d_n/d_c . An example was given for the calculation of the d_n/d_c value of core-shell polymer (Entry 2, Table 4.1 and Figure 4.5). The value is 0.184 for poly(DVB) core at beginning (Entry 1, Table 4.1). The core-shell sample (Entry 2, Table 4.1) shows a significant increase in molar mass and this combined with the lower d_n/d_c (0.142) shows that a lower d_n/d_c polymer is being added (ie $d_n/d_c, \text{PMMA} = 0.089$). Furthermore, the d_n/d_c decreases to 0.12 from the sample taken at 10 hours indicating the continuous addition of more MMA into the shell layers (Entry 6, Table 4.1).

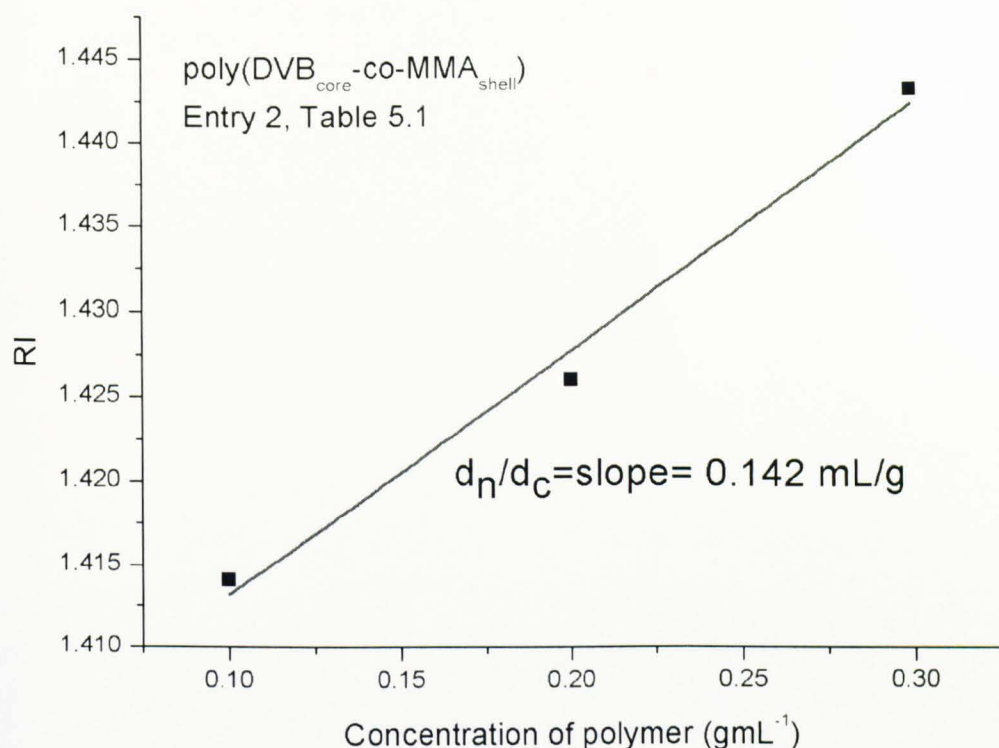


Figure 4.5 The measurement of d_n/d_c value of core-shell polymer in THF (Entry 2, Table 4.1) by refractometer.

An important parameter determining the structure of core-shell polymers is the average length of arms or average number of MMA units per arm. Two methods were used to investigate this value. The first method is based on MMA conversion, as the ratio of [MMA] to [DVB-Br] is 1000, and the number of MMA units per arm can be calculated by:

$$L_{\text{arm, by conversion}} = 1000 \times \text{Conversion}_{\text{MMA}} \quad (\text{Eq. 4.5})$$

For example, for Entry 2 of Table 4.1:

$$L_{\text{arm, by conversion}} = 1000 \times 3\% = 30$$

The other way is based on the increase of the M_w of core-shell by MALLS detector. Therefore, there are on average 54.1 initiation sites on each polyDVB core from this calculation. Moreover, the $L_{\text{arm, by } M_w}$ can be calculated from the increasing of molecular weight divided by molecular weight of MMA units and initiation sites on polyDVB core. For example, for Entry 2 of Table 4.1:

$$\begin{aligned}
L_{\text{arm, by Mw}} &= \frac{M_w \text{ of poly(DVB-co-MMA)} - M_w \text{ of polyDVB core}}{FW_{\text{MMA}} \times (\text{DVB-Br per polyDVB core})} \\
&= \frac{(360000-71000)\text{g mol}^{-1}}{100.12 \text{ g mol}^{-1} \times 54.1} \\
&= 53.4
\end{aligned}
\tag{Eq. 4.6}$$

Both of above two methods indicate there are approximately 30 MMA units per arm at first half an hour, and later it increases to around 60 MMA units per arm at ten hours of reaction (Entry 2 to Entry 6, Table 4.1). However, since the hyperbranched polyDVB core was formed by random coupling of various numbers of primary chains, the molecular weight distribution of polymer chain is broad. Furthermore, obviously there are some initiation sites which cannot initiate the MMA due to steric-hindrance. So the value of arm length calculated was not precise, and the real arm length should be higher than this value.

The Figure 4.6 shows the GPC traces during the synthesis of poly(DVB-co-MMA). The upper one is the trace from RI detector and bottom is from MALLS detector. Both the RI and MALLS traces demonstrate the evolution of core-shell polymers. The reaction starts from polyDVB core (polyDVB curve line, Figure 4.6), then it shifts to left after half an hour (0.5 hour curve, Figure 4.6). There is a shift to later elution that must mean a larger R_h (hydrodynamic radius) and this corresponds to a larger molar mass as well. This means that the PMMA groups must be adding to the outside of the core material as to add inside would not appreciably increase the R_h value. Therefore, it shows the molecular weight is increased with reaction time and conversion under controlled manner.

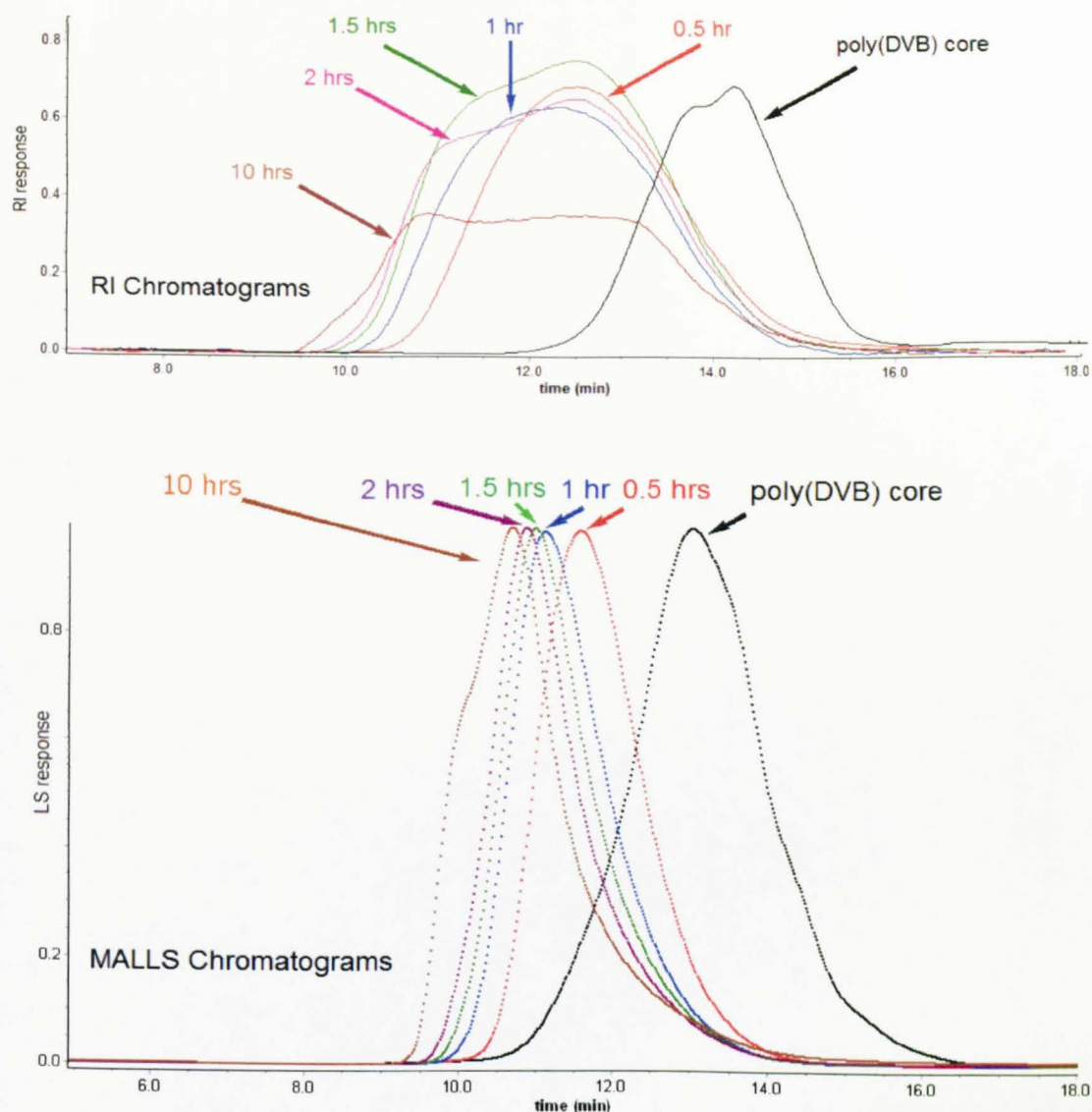


Figure 4.6 The GPC traces during the synthesis of poly(DVB-co-MMA) star polymers. Both of traces from RI detector (upper) and MALLS (bottom) detector show the M_w and R_h of the hyperbranched core-shell polymer grows with time and conversion. Experimental condition: $[MMA]/[DVB-Br]/[CuBr]/[bpy] = 1000/1/1/2$ in Butanone at 60 °C, DVB-Br moieties are the potential initiation sites on polyDVB, $[MMA] = 0.28$ M.

The results from dynamic light scattering (Figure 4.7) show that the size of core-shell polymer in THF is increased with reaction time. It is necessary to note that the size determine by DLS technique is the size of molecules that move in the same manner. In the case of polymer solution, the measured size is not the same as the R_g by MALLS detector. The poly(DVB) core is only 7.8 nm before adding MMA. Obviously, the diameter of molecule keeps increasing after reaction starts, and finally grows to 33.4

nm at 10 hours. This result proves the core-shell grows with MMA monomer under ATRP condition.

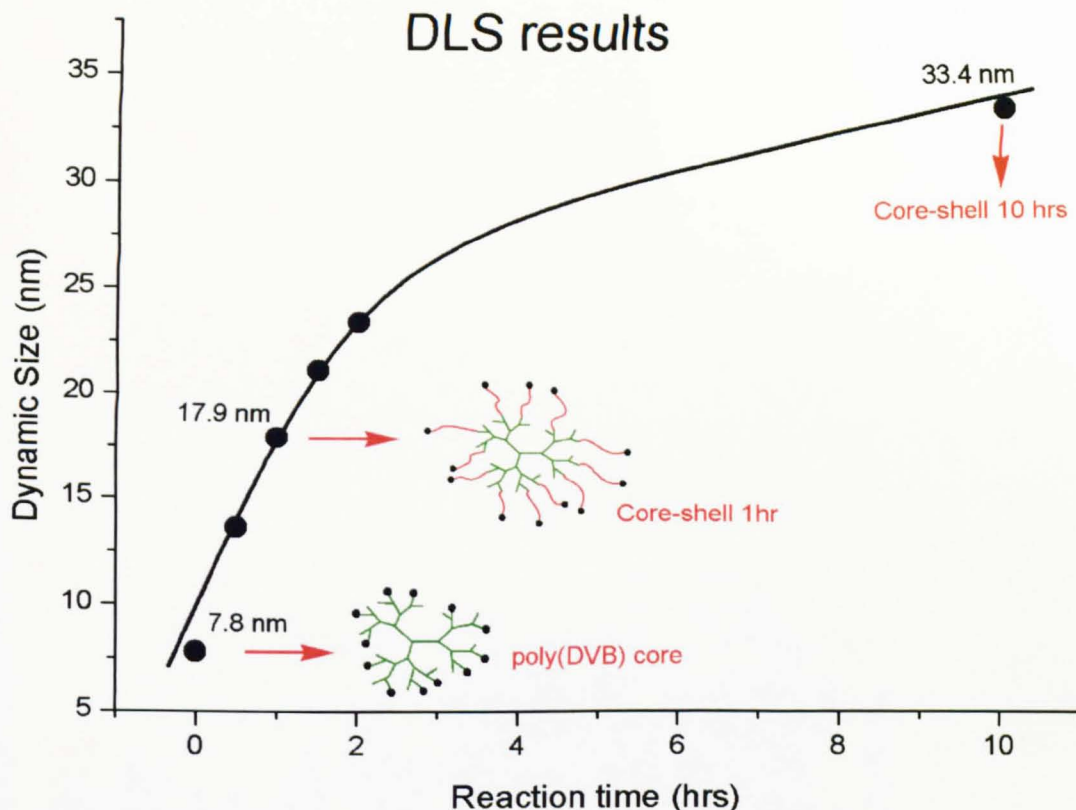


Figure 4.7 The size of core-shell polymer in THF at 25 °C from dynamic light scattering increases with reaction time. The size of core is 7.8 nm at the start of reaction and grows to 33.4 nm after 10 hours.

Furthermore, the star polymers were separated based on hydrodynamic volume, and each slice was analysed by MALLS detector to demonstrate the absolute molecular weight against elution time (Figure 4.8). At a given elution volume (X axis), polymers with higher molecular weight (Y axis) have a more compact structure. In Figure 4.8, the molar mass of the core material (polyDVB core, Figure 4.8) is higher at the same elution point of the core-shell samples (core shell 0.5 hour, Figure 4.8) which again suggests a higher molar mass at the same R_h (hydrodynamic radius). Thus, this further supports the idea that any added molar mass is on the outside of the core. It is also clear that the core-shell polymers have similar structural compactness, because at a given elution volume, all of them have similar molecular weights, which are higher than the values of the linear polyMMA counterpart (linear polyMMA, Figure 4.8). These data show the core-shell polymers have a highly branched core and many radiating arms.

Furthermore, the core-shell polymer is shifted to a more linear-like structure with reaction time due to more and more linear units incorporated into the polymer.

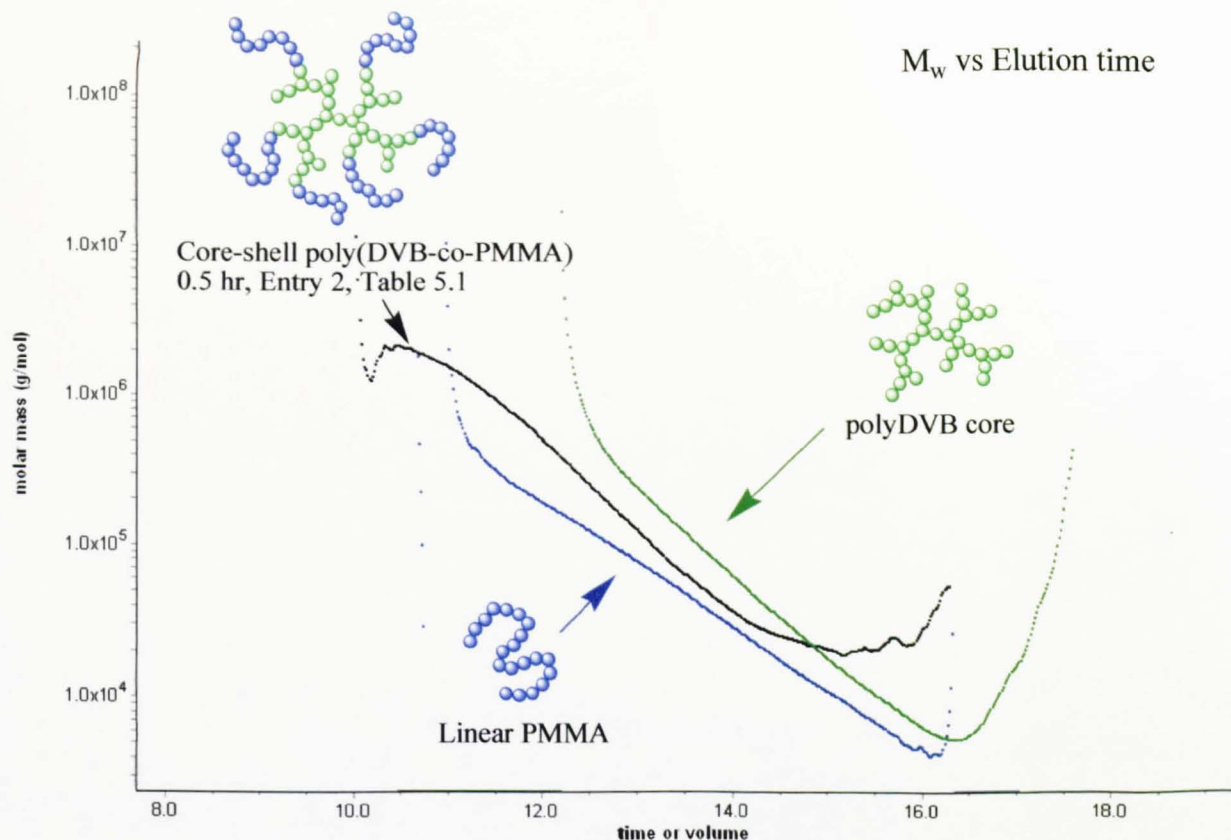


Figure 4.8 Plot of the log of M_w versus elution volume for the poly(DVB) core (Entry 1, Table 4.1), core-shell poly(DVB-co-MMA) (Entry 2, Table 4.1) and linear PMMA samples (prepared by ATRP). The data clearly show the core-shell polymers (core-shell at 0.5 hour) are between of the value of the linear polyMMA and hyperbranched polyDVB counterpart. This result proves that the core-shell polymers have a highly branched core and many radiating arms.

The purified core-shell copolymers were characterised by ^1H NMR spectroscopy (Figure 4.9). The NMR spectrum of core-shell polymer clearly shows the resonance from the protons of the polyMMA arms (resonance of protons f, h and i, Figure 4.9) increase with time during the shell addition reaction. Furthermore, the remained vinyl groups on the polyDVB core (resonance of protons a, b and c, Figure 4.9) slowly decrease during the reaction and disappear after 2 hours. This change is due to the pendant vinyl groups on the core gradually reacting with propagating PMMA units. In this ATRP reaction, the PMMA monomer only can be initiated from bromine group on the polyDVB core as there are not any other initiator group present in the reaction.

Thus, the vinyl groups on the core can only be consumed by the propagating MMA radical centres.

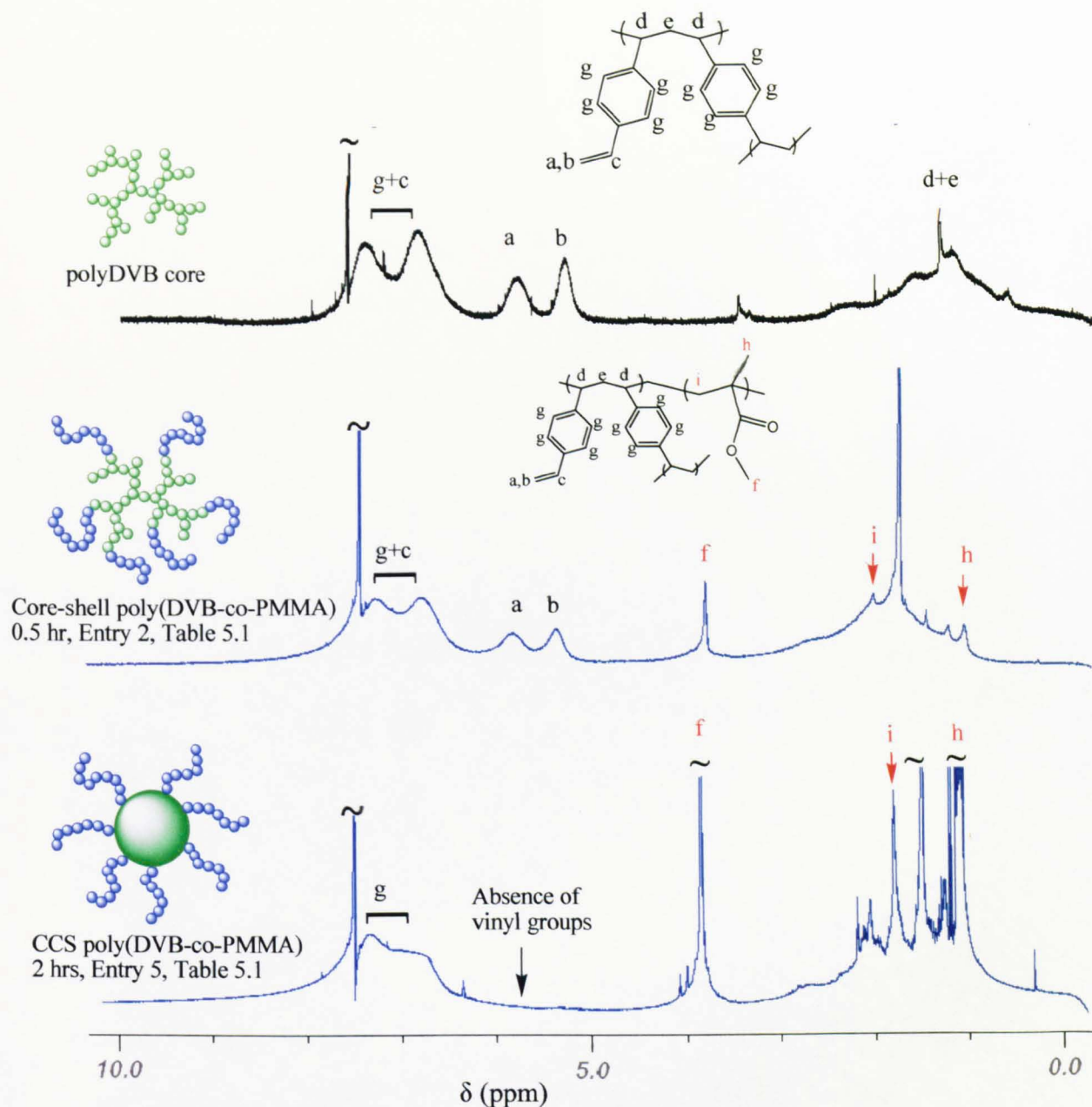
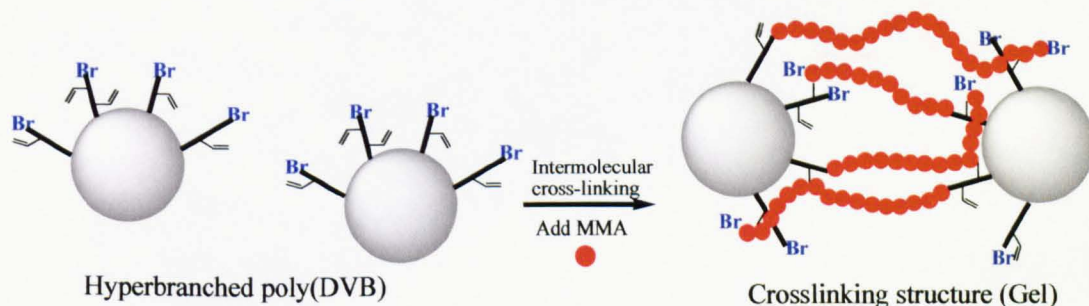


Figure 4.9 ^1H NMR spectra of the poly(DVB) core (Entry 1 of Table 4.1) and purified core-shell poly(DVB-co-MMA) (Entry 2, 3 and 5, Table 4.1) in CDCl_3 . The spectra show the linear PMMA (resonance of protons f, h and i) added on the polymer after the reaction starts. Also, the vinyl groups (resonance of protons a and b) on the cores decrease during the shell addition reaction and disappeared after 2 hours.

There are two possibilities for the consumption of vinyl groups on the poly(DVB) core during the shell addition reaction (Figure 4.10).³⁸ The vinyl groups can react either by intermolecular coupling of growing radicals (Top, Figure 4.10) or in an intramolecular reaction by neighbouring propagating chains (Bottom, Figure 4.10). Typically, the intermolecular cross-linking is dominated in the concentrated system, because the possibilities of two cores coupling are increased with core concentration in solution. On the other hand, the vinyl groups only react with the growing radicals from the same core in the very dilute solution system. In this reaction, the vinyl groups are almost consumed by intramolecular cross-linking because the concentration of poly(DVB) core is very low ($5.22 \times 10^{-6} \text{ mol L}^{-1}$, see experimental section). First, the vinyl groups on the core are decreased during the shell addition step showing that cross-linking is happening (See NMR spectra, Figure 4.9). Furthermore, the polydispersity of the core-shell polymer does not increase (the PDI is kept from 3.4 to 3.7, see Table 4.1) implying that there is no intermolecular cross-linking is not occurring during the reaction. Thus, this results in formation of a cross-linking core-shell structure (CCS) during the shell addition reaction.

1. Intermolecular crosslinking in concentrated system



2. Intramolecular crosslinking in dilute system

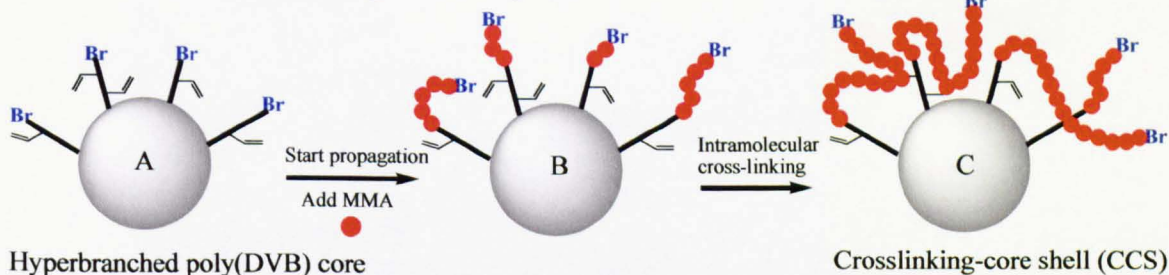


Figure 4.10 Different modes of crosslinking in shell-adding reactions with hyperbranched polyDVB core. The intermolecular cross-linking (1) which occurs in concentrated system will form cross-linking between cores and may lead to gelation. The intramolecular cross-linking (2) which occurs in dilute system forms crosslinking and results in cross-linked core-shell (CCS) structure.

In addition, the composition of core-shell polymer is calculated by comparing the integer of peaks from DVB and MMA in the ^1H NMR spectra (Eq. 4.7). The resonance of proton f represents the three protons (CH_3) in MMA units, and resonance of proton g represents the four protons in benzene ring of DVB units (See NMR spectra, Figure 4.9). Also, because the resonance of proton g is overlap with the peak c (CH= from the vinyl groups). Thus, it need deduced the integrals of resonance of proton c from the region of peak g. Consequently, the integrals of c is equal to the integrals of resonance of proton a or b ($\text{CH}_2=$ from the vinyl groups). The equation for the composition is listed as below:

$$\text{Composition}_{\text{by NMR}} = \frac{\text{MMA}}{\text{DVB}} = \frac{\text{Integral of f/3}}{[(\text{Integral of g+c})-\text{integral of a}]/4} = \frac{7.1}{1} \quad (\text{Eq. 4.7})$$

From the calculation, the ratio MMA: DVB in core-shell polymer is equal to 7.4:1 after 2 hours. This result matches the composition obtained from GPC-MALLS data (Entry 5, Table 4.1) by Eq. 4.8 which is 7.95:1.

$$\begin{aligned} \text{Composition}_{\text{by MALLS-GPC}} &= \frac{\text{MMA}}{\text{DVB}} \\ &= \frac{[\text{M}_w \text{ of poly(DVB-co-MMA)} - \text{M}_w \text{ of polyDVB core}]/ \text{FW}_{\text{MMA}}}{\text{Total DVB units in polyDVB core}} \\ &= \frac{(4.5 \times 10^5 \text{ g mol}^{-1} - 7.1 \times 10^4 \text{ g mol}^{-1})/100.12 \text{ g mol}^{-1}}{476} \\ &= 7.95:1 \end{aligned} \quad (\text{Eq. 4.8})$$

Moreover, the changes of molecular size observed in DLS show evidence of hyperbranched core-shell structure. In good solvents, for example THF, both of the core-shell (open circle, Figure 4.11) and hyperbranched polyDVB (solid square, Figure 4.11) are relaxing and swelling. However, when the poor solvent was dropped in solution, the core-shell poly(DVB-co-MMA) will display much larger molecular contractions compared to the effect on hyperbranched polymers. In Figure 4.11, the molecular size of poly(DVB-co-MMA) ($\text{M}_w=5.9 \times 10^5 \text{ g mol}^{-1}$, Entry 6, Table 4.1) decreases from 33.4 nm to 24 nm when 40% methanol is added into the solution. On the other hand, the polyDVB (prepared via DE-ATRP, entries 1-5 in Table 2.3) at

similar molecular weight ($M_w = 6.25 \times 10^5 \text{ g mol}^{-1}$) is contracted from 14.4 nm to 12.4 nm. This result provides two evidence for the hyperbranched structure of poly(DVB-co-MMA). Firstly, the molecular size of core-shell polymers is higher than hyperbranched ones with same molecular weight. Secondly, the core-shell polymer deswelling is more significant than observed for the hyperbranched samples (see Chapter 2, Figure 2.16).

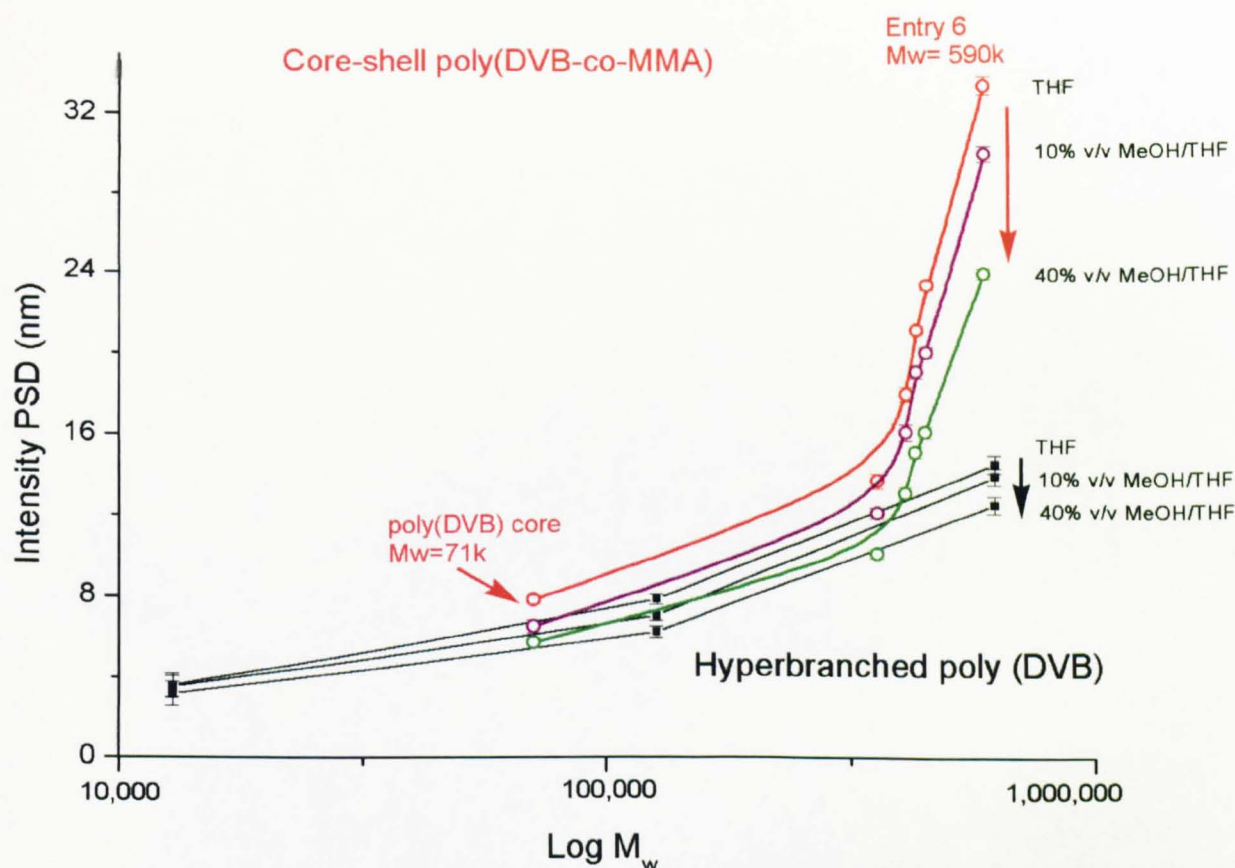


Figure 4.11 Plot of DLS data shows polymer size distribution *versus* $\text{Log } M_w$ for core-shell poly(DVB_{core}-co-MMA_{shell}) (Entry 1-6, Table 4.1) and hyperbranched poly(DVB) in a series of complex THF/methanol solvent mixtures. It clearly indicates that the size of core-shell polymers is higher than hyperbranched ones and the core-shell polymer deswelling is more significant than hyperbranched sample.

By spin coating from sufficiently dilute solution, the core-shell polymer could be deposited on the substrate surface as individual macromolecule.^{38, 39} After the solvent evaporated, the nano-scale particle could be studied in more details using tapping mode AFM. The AFM images can reveal the deposition of core-shell polymer on the

substrate, and the linear arms collapsed around or upon the core forming a ‘fried egg’ shape (Figure 4.12).³⁸

Hyperbranched core-shell polymer

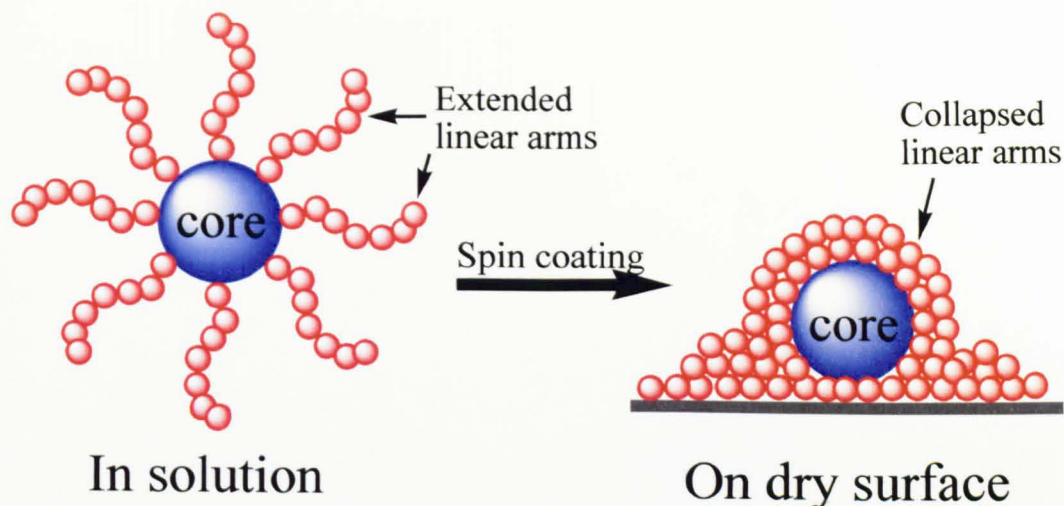


Figure 4.12 The different conformations of hyperbranched core-shell polymer in solution (relaxed conformation) and after deposition on dry substrate (‘fried egg’ shape).

The atomic force microscopy (AFM) images for the poly(DVB) core ($M_w=7.1 \times 10^4$ gmol^{-1} , Entry 1, Table 4.1) are displayed in Figure 4.13. The polymer sample was dissolved in THF and diluted into 10 $\mu\text{g/L}$. Then the diluted solution was dropped on high speed rotation mica substrate. After the THF solvent was evaporated, the substrate was scanned by AFM at room temperature in air. It allows to clearly distinguishing single polymer chains without agglomerating. The AFM can be operated in a number of modes, depending on the application. In the height or topology mode it can give us the basic morphology information of the polymer molecules on the substrate. The topology image of poly(DVB) core (Left, Figure 4.13) shows three features of the core polymer. Firstly, the core polymers are formed as dense and round shape particles on the surface. Secondly, the particle diameters are in the range of 5 to 14 nm. The diameters of the core poly(DVB) are slight higher than the DLS result (7.6 nm, see Figure 4.7) because the polymer is spread on the surface under dry condition. Thirdly, the height of core polymer is limited to 2 nm. In addition, in the amplitude modulation (Right, Figure 4.13), changes in the oscillation amplitude or phase provide the feedback signal for imaging. Thus, changes in the phase of oscillation can be used to discriminate between different types of materials on the surface. The phase image of the poly(DVB) (Right,

Figure 4.13) shows the different materials between core and substrate. The materials of outer and inner part of core polymer are the same from the phase image which also match the result from the height mode.

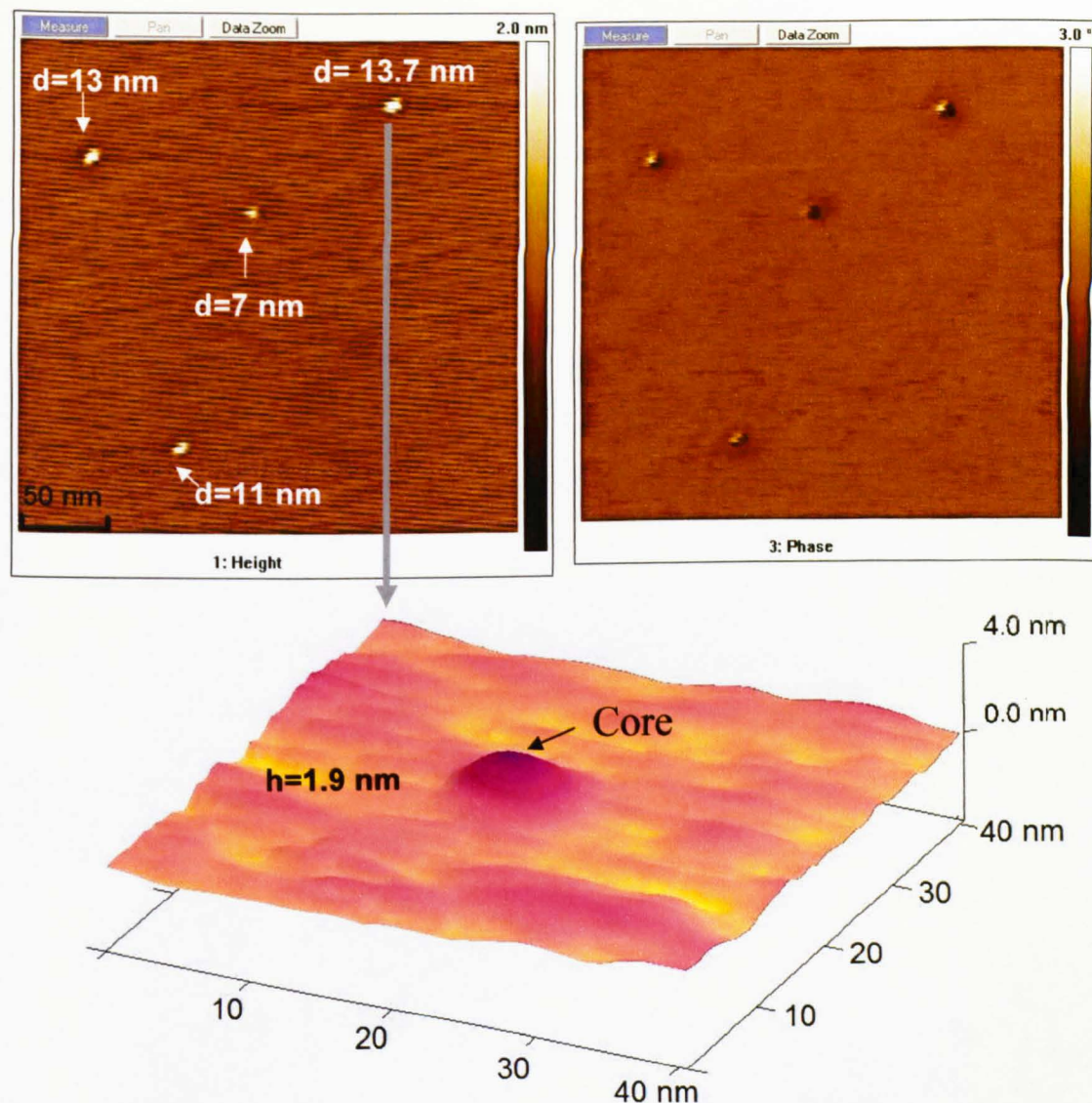


Figure 4.13 AFM topology (left) and phase (right) images for poly(DVB) core ($M_w=7.1 \times 10^4 \text{ g mol}^{-1}$, Entry 1, Table 4.1). The sample was prepared in a diluted solution ($10 \mu\text{g/L}$) in THF and dropped onto mica substrate by spin coating (1000 rpm) to make sure the macromolecules separate from each other. The polymers form round shape particles in the range of 5-14 nm. In the figure, d represents the diameter of molecule; h represents the peak height of molecule.

Furthermore, the core-shell poly(DVB-co-MMA) ($M_w=5.9 \times 10^5 \text{ g mol}^{-1}$, Entry 6, Table 4.1) was examined by AFM under dry conditions. The sample is prepared in dilute solution ($10 \mu\text{g/L}$) and dropped onto mica substrate by spin coating as described. Two

core-shell molecules are displayed in the AFM image (Figure 4.14). The height image (Left, Figure 4.14) of the core-shell polymer shows three different features. Firstly, the core-shell poly(DVB-co-MMA) consists of a prominent core and flat shell arms. Secondly, the diameter of particle is increased to 41.6 nm and 22.4 nm due to the addition of PMMA arms. Last, the height of the core is increased to 2-6 nm. The phase image (Right, Figure 4.14) of the core-shell polymer clearly shows that the material of core part is different from the outer shell part. This is because the outer shell arms are much softer than the intramolecular cross-linked core. It clearly shows the core and collapsed arms formed as 'fried egg' shape in the three dimension reconstruction image (Bottom, Figure 4.14).

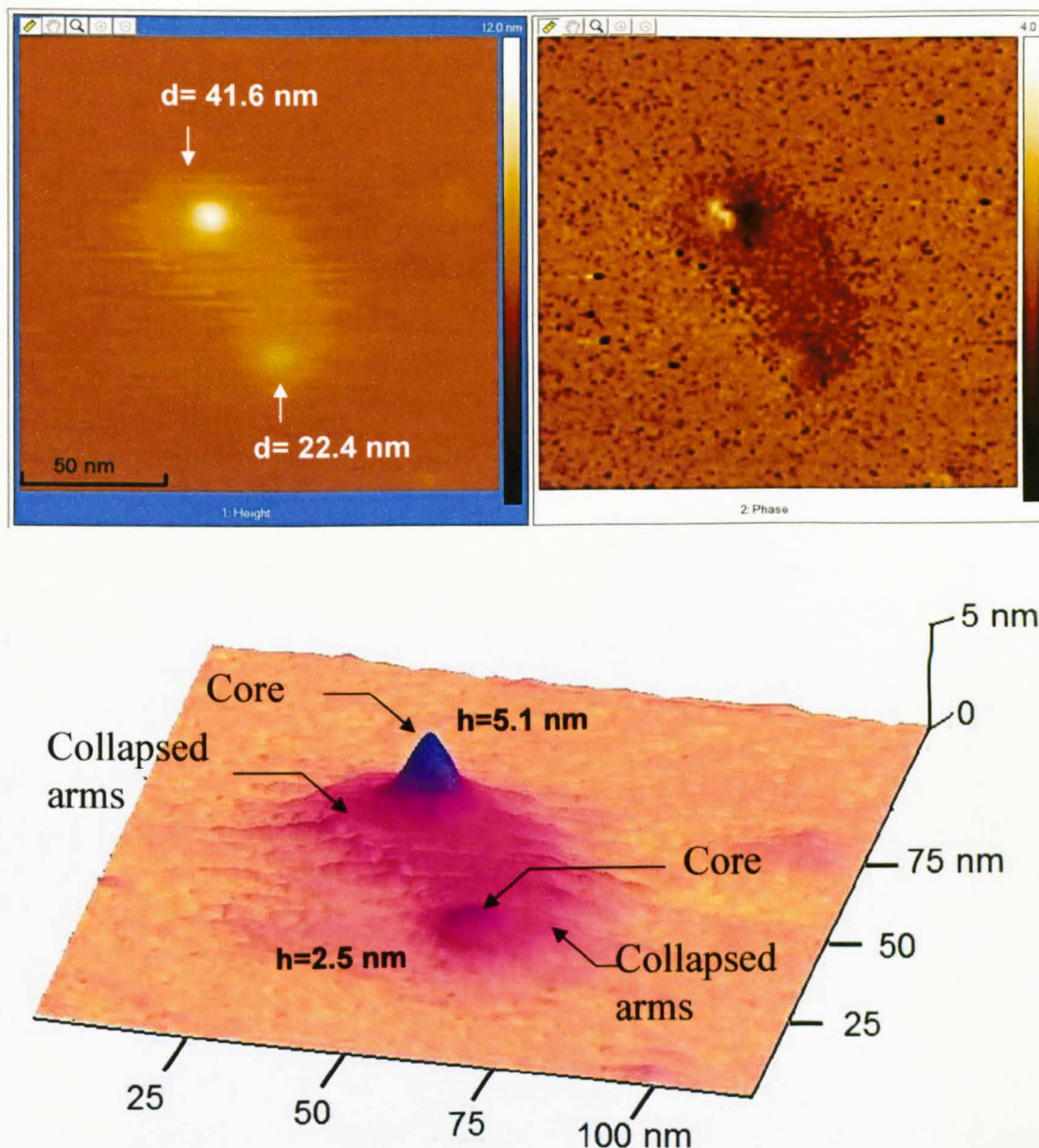


Figure 4.14 AFM topology (left) and phase (right) image for core-shell poly(DVB-co-MMA) ($M_w=5.9 \times 10^5 \text{ g mol}^{-1}$, Entry 6, Table 4.1). The samples are prepared in a dilute solution (10 $\mu\text{g/L}$) in THF and dropped on mica substrate by spin coating (1000 rpm). The PMMA linear arms are collapsed around dense core in a ‘fried egg’ shape. In the figure, d represents the diameter of molecule; h represents the peak height of molecule.

Also, the AFM topology image (Left, Figure 4.15) for core-shell poly(DVB-co-MMA) (Entry 6, Table 4.1) on silica substrate shows the core-shell structure as well. From the enlarged picture (Right, Figure 4.15), it can distinguish the dense core and linear shell

part. This is a solid proof for our hyperbranched core-shell structure. However, the rough silica surface makes it difficult to capture very clear image as mica substrate.

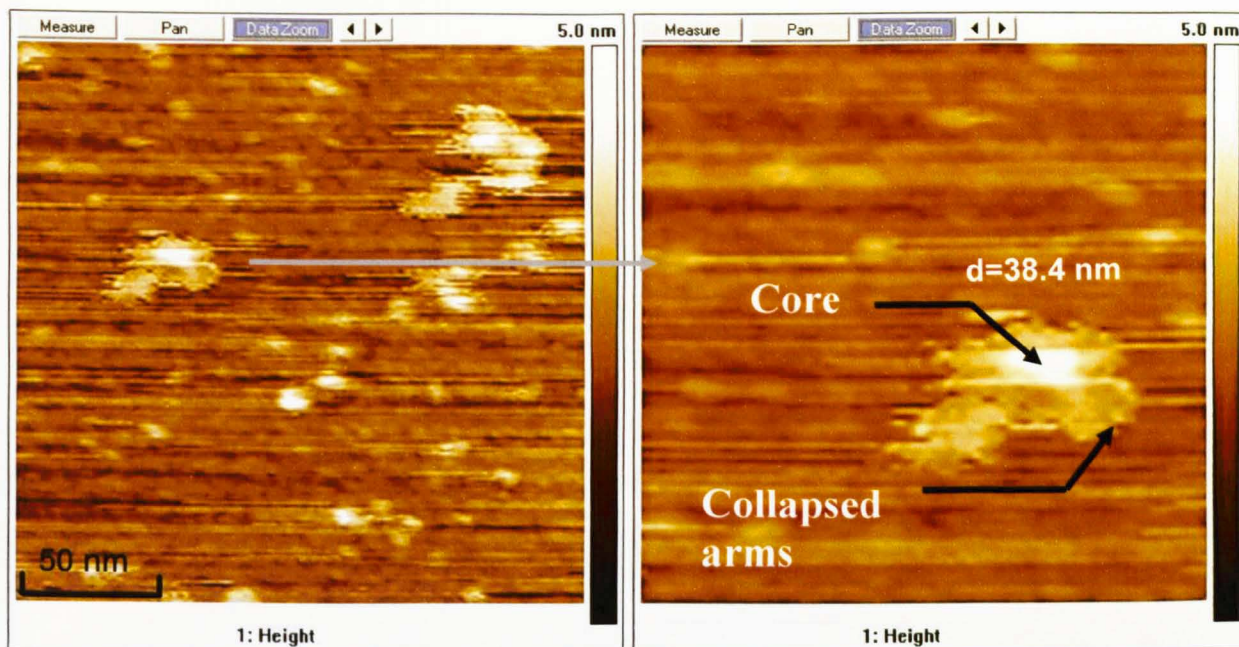


Figure 4.15 AFM topography image for core-shell poly(DVB-*co*-MMA) (Entry 6, Table 4.1). The samples are prepared in a dilute solution (10 $\mu\text{g/L}$) in THF and dropped on silica substrate by spin coating (1000 rpm). The enlarged image (right) clearly shows the core-shell like molecule was formed during the reaction. The core-shell polymer is displayed as a ‘fried egg’ shape on the dry silica substrate.

These were dry, so next the conformation of core-shell on the substrate in solvent was scanned by AFM. Firstly, a very dilute (10 $\mu\text{g/L}$) core-shell THF solution is dropped on mica substrate by spin coating (1000 rpm). After the THF was totally evaporated, mixed solvent (40% v/v THF/water) is dipped on the dry substrate. Then the substrate is scanned by AFM at room temperature using a specific AFM probe and condition (See experimental section). In the mixed solvent, the linear polymer arms are relaxed and extended away from the core. Thus, the shape of core-shell polymer will change from ‘fried egg’ to ‘swollen’ shape after addition of mixed solvent (Figure 4.16).^{38, 40, 41} There are two reasons to scan under mixed solvent rather than pure THF. Firstly, the mobility of polymers is very good in pure THF. Therefore, the polymer molecules are probably will not to attach on the substrate in pure THF and easily removed by the

AFM tip during the scan. Secondly, the evaporation of THF is quite fast which causes very strong noise and signal interference in the images.

Hyperbranched core-shell polymer

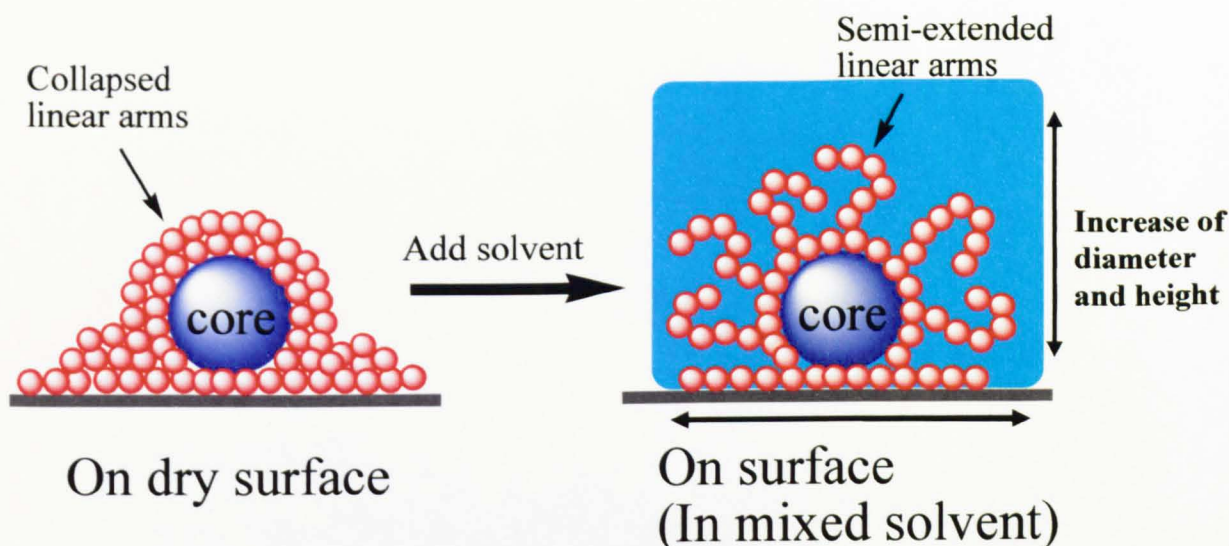


Figure 4.16 The different conformations of core-shell on dry substrate ('fried egg' shape) and after added mixed solvent. In the mixed solvent, the collapsed linear arms of core-shell polymer are swollen. Thus, the core which surrounded by relaxed linear arms becomes invisible in the solvent. In addition, the diameter and height of the core-shell polymers will increase in the mixed solvent.

The morphology of the core-shell polymers in mixed solvent was studied by AFM (Figure 4.17). The height image (Left, Figure 4.17) of core-shell polymer shows several distinguishing features. Firstly, the shape of the core-shell polymer is changed to a large (in the range of 40-80 nm) round shape in the mixed solvent. The linear arms are relaxed around the core in solvent. Secondly, the height of the particles is increase to 7-14 nm which is much larger than the only 5 nm observed on dry substrate previously. This is because the relaxed linear PMMA arms expand the height of the particles. However, the quality of the phase image (Right, Figure 4.17) is not very good because solvent turbulence affects the phase data.⁴²

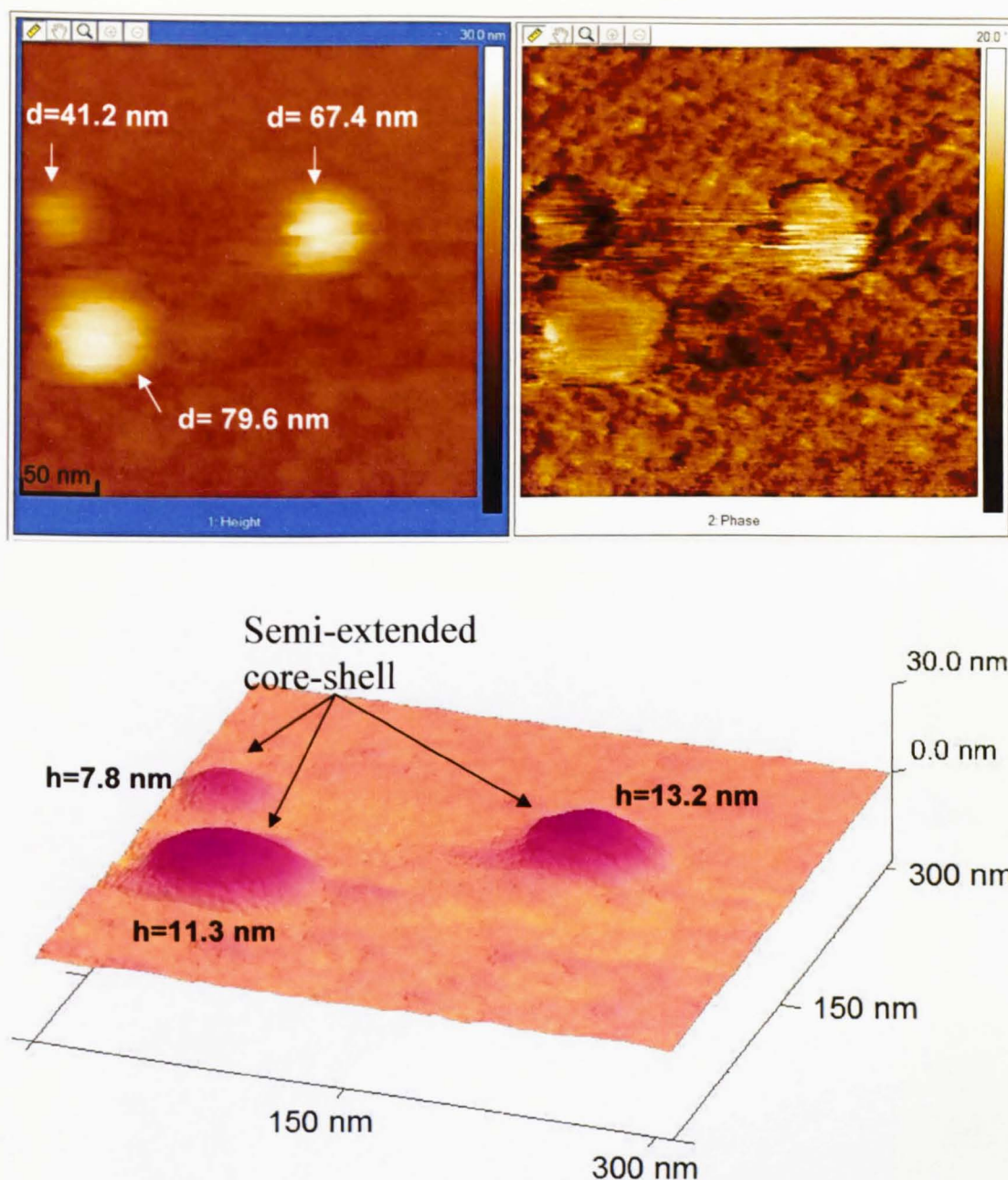


Figure 4.17 AFM topology image (left) and phase image (right) for core-shell poly(DVB-co-MMA) at 10 hours (Entry 6, Table 4.1). The samples are separated by spin coating (1000 rpm) on mica substrate, then the mixed solvent (40% v/v THF/water) was added on the surface. The image shows that the outer linear PMMA arms are relaxed around the core in the mixed solvent and formed as ‘swollen’ shape. The cores are invisible by surrounding of extended linear arms. Also, the height and diameter of molecules are significantly increased in the mixed solvent. In the figure, d represents the diameter of molecule; h represents the peak height of molecule.

4.3.1 Core-Shell Hyperbranched poly(CL-co-BOD)_{core}-DMAEMA_{shell}

In this work, hyperbranched core-shell poly(CL-co-BOD)_{core}-DMAEMA_{shell} polymers were synthesised via a two-step process involving the synthesis of hyperbranched degradable poly(CL-co-BOD) core via ring open polymerisation followed by chain extension of poly(DMAEMA) shell via RAFT. This work was completed by cooperating with the previous researcher in our group, Dr. Kristofer Thurecht. In the first step, ring-opening copolymerisation of ϵ -caprolactone and 4,4-bioxepanyl-7,7-dione (BOD) was performed in the presence of a catalyst (stannous 2-ethylhexanoate) and an initiator (ACP-RAFT) in toluene ([CL]=0.42 M, 110 °C) to produce a hyperbranched poly(CL-co-BOD) core (Table 4.2). After 2 hours, the conversion of ϵ -caprolactone and BOD reaches 40%. The key to avoid formation of microgel or core cross-linked star polymer^{25,26} from the previous study is control of the ratio of initiator site and cross-linker. As described in the 'Strathclyde method'²⁸, if the ratio of [initiator]:[cross-linker] is below 1, it will form a hyperbranched polymer without gel formation. Thus, the ratio of [ACP-RAFT]:[BOD]:[ϵ -Caprolactone] was kept at 1:1:10 which will provide a hyperbranched poly(CL-co-BOD) core. The GPC-MALLS traces are shown in Figure 4.18 for the synthesis of hyperbranched poly(CL-co-BOD).

Table 4.2 Polymerisation data for the synthesis of hyperbranched poly(CL-co-BOD).^a

Entry	Reaction time (hr)	M_n^b (g/mol)	M_w (g/mol)	PDI	Yield ^c
1	1	6.4×10^3	1.13×10^4	1.76	21%
2	2	1.15×10^4	1.5×10^4	1.3	40%

a. Polymerisations were carried out at 110 °C in toluene with initiator (ACP-RAFT), catalyst (stannous 2-ethylhexanoate ($\text{Sn}(\text{Oct})_2$), monomer (ϵ -caprolactone (CL)) and cross-linker (4,4-bioxepanyl-7,7-dione (BOD)). The chemical ratio is [ACP-RAFT]:[BOD]:[ϵ -caprolactone]:[$\text{Sn}(\text{Oct})_2$]= 1:1:10:0.5, [ϵ -CL]=0.42 M

b. M_n , M_w and PDI are determined by gel permeation chromatography equipped with MALLS detector.

c. Yield of ϵ -caprolactone and BOD is calculated by weight.

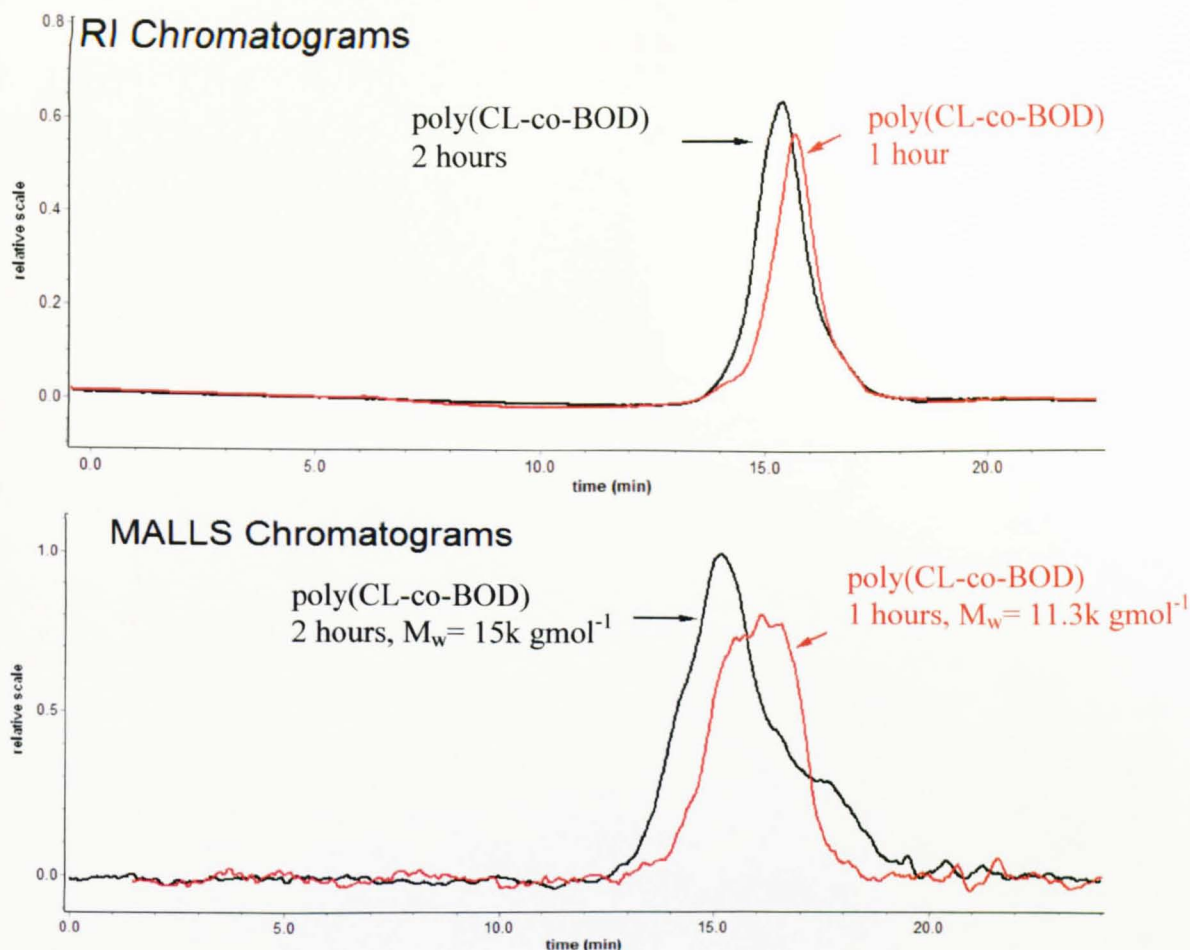


Figure 4.18 RI (top) and MALLS (bottom) traces of for the synthesis of hyperbranched poly(CL-co-BOD). The traces indicate the poly(CL-co-BOD) is formed at 2 hours and $M_w = 15,000$ g/mol.

To distinguish the difference between hyperbranched poly(CL-co-BOD), linear PCL and cross-linked core star(CCS) PCL, the comparison of the molecular weight against elution volume plots could reveal differences in the behaviour of these molecular structures. For this purpose, linear PCL and CCS polymers were prepared following the previous literature²⁵. A plot of the Log of M_w versus elution volume (Figure 4.19) shows the M_w of CCS polymer is much higher than linear ones due to the highly cross-linked structure at the same elution volume. However, the sample of hyperbranched poly(CL-co-BOD) (Entry 1 and 2, Table 4.2) lies between the linear PCL and CCS BOD sample. This figure offers the proof for the hyperbranched structure and the absence of microgels formed in the polymers.

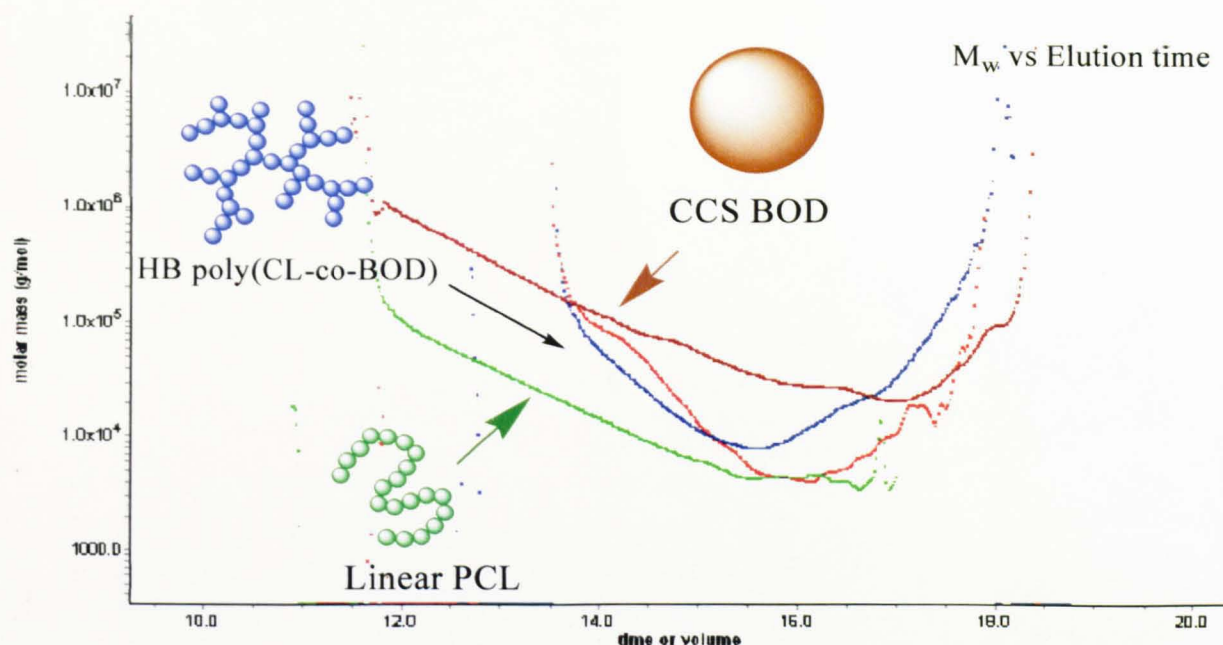


Figure 4.19 Plots of the Log of M_w versus elution volume for the hyperbranched poly(CL-co-BOD) (HB PCL line, Entries 1 and 2, Table 5.2), linear PCL samples (Linear PCL line, prepared by ring open polymerisation) and core cross-linked star PCL (CCS PCL line, prepared as described in literature)²⁵. These data confirm that the hyperbranched samples are highly branched without cross-linking since the plots lie between those of the linear PCL and CCS BOD.

Furthermore, the composition of hyperbranched poly(CL-co-BOD) was confirmed by ^1H NMR spectroscopy analysis (Bottom, Figure 4.20). It clearly shows that the resonances are from ACP-RAFT (resonance of protons 1 and 2), ϵ -caprolactone and BOD units (resonance of protons 3, 4, 5 and 6) in the polymer. In addition, the NMR spectrum shows that there is no resonance from BOD monomer (resonance of proton a at 3.8 and b at 4.4 ppm, Figure 4.20) left in the polymer. It indicates that there are very few pendant BOD rings (lesser than 1%) in the hyperbranched poly(CL-co-BOD) core.

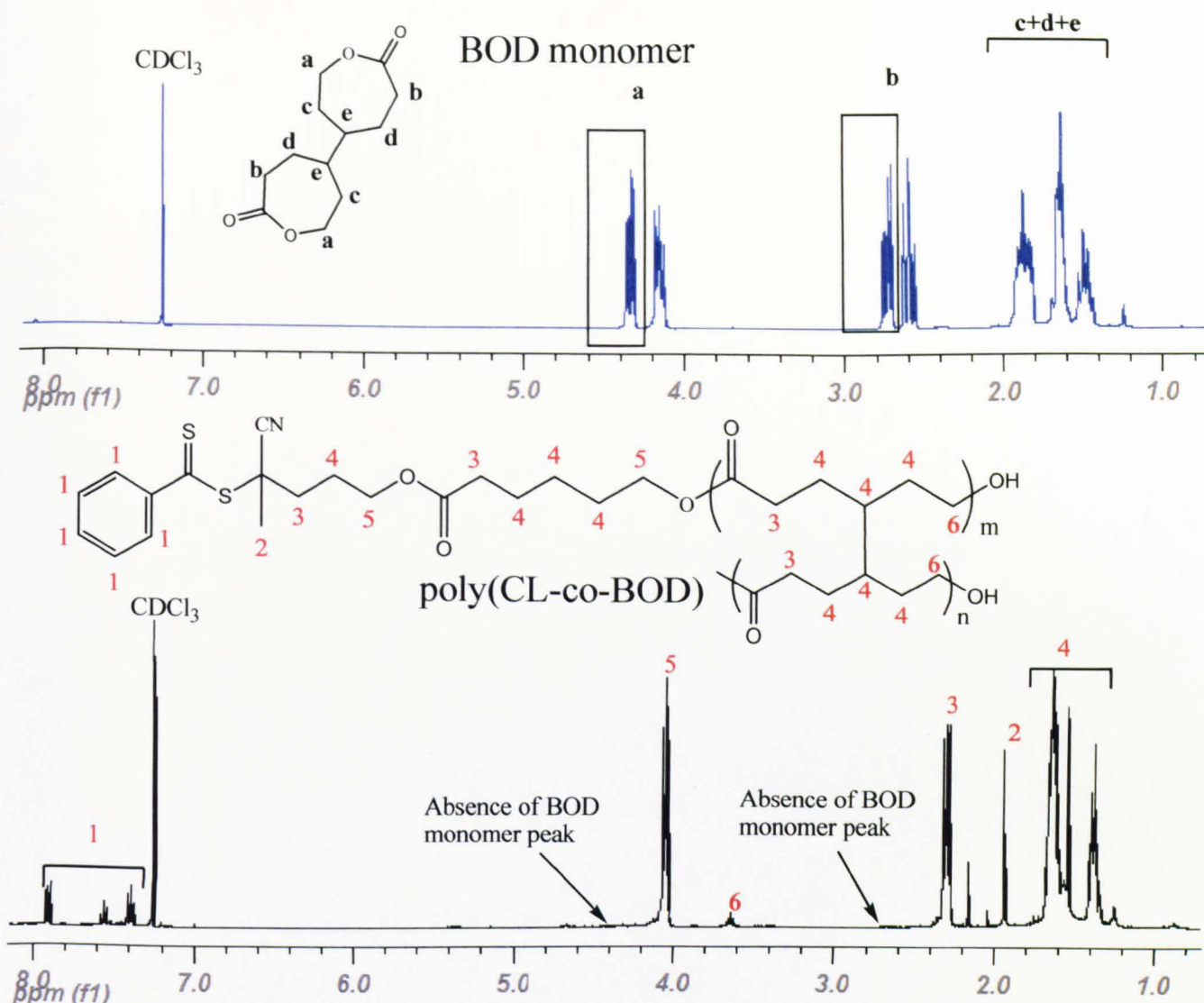


Figure 4.20 ^1H NMR spectrum for BOD monomer (top) and hyperbranched poly(CL-co-BOD)(bottom). It shows the resonances are from ACP-RAFT initiator (resonance of protons 1 and 2) and ϵ -caprolactone units (or BOD units, resonance of protons 3, 4, 5 and 6) in the polymer. Also, the spectrum shows that there are very few (less than 1%) pendant BOD rings (resonance of protons at 3.8 and 4.4 ppm) left in the polymer (Entry 2, Table 4.2).

From the proton NMR spectrum of poly(CL-BOD) (Entry 2, Table 4.2), the RAFT end group was clearly observed in the polymer (peak 1, Figure 4.20). Furthermore, pendant BOD rings were not found in the polymer which matches the mechanism of the 'Strathclyde method'. This means both of the two rings of BOD were opened in polymer. Therefore, the composition of the hyperbranched polymer can be calculated by following equation (Eq. 4.9):

$$\frac{\text{RAFT end group}}{\epsilon\text{-CL} + \text{BOD}} = \frac{(\text{Integrals of peak 1})/5}{(\text{Integrals of peak 5} - \frac{\text{Integrals of peak 1}}{2/5})/2} = 0.19 \quad (\text{Eq. 4.9})$$

The result shows the ratio of RAFT end groups: ϵ -caprolactone plus BOD= 1: 4.3 match the conversion data which indicates the ratio of RAFT end group to ϵ -caprolactone and BOD is approximately 1 to 4. Theoretically, the number of initiators should be equal to the branching points. Thus, the composition of the polymer is RAFT end group: ϵ -caprolactone: BOD= 1: 3.3: 1.

Theoretically, we can calculate the number of ACP-RAFT end groups per polymer by Eq. 4.10. It shows there are on average 17.3 ACP-RAFT end groups in one hyperbranched poly(CL-co-BOD).

Assume number of ACP-RAFT per polymer is X

$$\text{FW}_{\text{ACP-RAFT}} * X + \text{FW}_{\epsilon\text{-CL}} * 3.3 * X + \text{FW}_{\text{BOD}} * X = \text{Mw of poly(CL-co-BOD)}$$

$$264X + 376.9X + 228.4X = 15000$$

$$X = 17.3 \quad (\text{Eq. 4.10})$$

^{13}C NMR is analogous to proton NMR and allows the identification of carbon atoms in molecules (Figure 4.21). Furthermore, DEPT ^{13}C stands for distortionless enhancement by polarisation transfer. It is a very useful method for determining the presence of primary, secondary and tertiary carbon atoms. The DEPT experiment differentiates between CH, CH₂ and CH₃ groups by variation of the selection angle parameter (the tip angle of the final ^1H pulse): 45° angle gives all carbons with attached protons (regardless of number) in phase; 90° angle gives only CH groups, the others being suppressed; 135° angle gives all CH and CH₃ in a phase opposite to CH₂. From the DEPT ^{13}C NMR spectrum of poly(CL-co-BOD) sample (Entry 1, Table 4.2), we can deduce that the ACP-RAFT agent successfully initiated the ϵ -Caprolactone and BOD monomer. First, it shows the carbon of benzyl from RAFT group appears at 125-129 ppm (Figure 4.21, resonance of carbon a). Also, the peaks from ϵ -Caprolactone and BOD were observed in the spectrum (Figure 4.21, resonance of carbons d, e, f and g). However, the full spectrum does not show the resonance of carbon (CH) at the branching points. This is because in the hyperbranched polymer, the internal structure

is so tightly packed due to the highly branched architecture that molecular mobility of the polymer chains is decreased. This matches previous ^1H NMR results and demonstrates that our polymers have a highly branched structure.

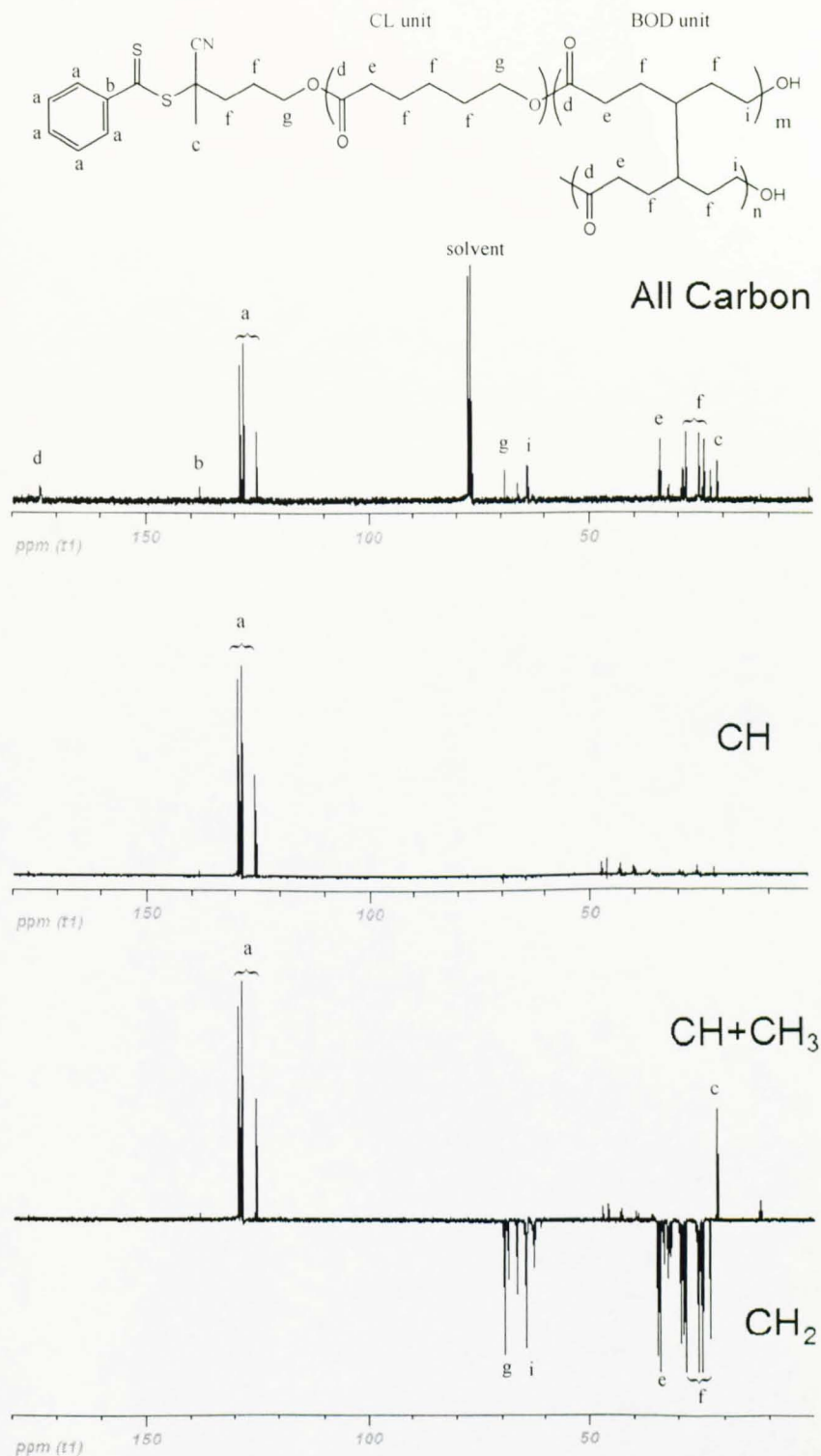


Figure 4.21 DEPT ^{13}C NMR spectra of hyperbranched poly(CL-co-BOD).

The second step to create the core-shell polymer is chain extension at the edge of the hyperbranched core via RAFT. Table 4.3 lists the polymerisation data for this reaction. The core materials were chosen from poly(CL-co-BOD) samples ($M_w = 15,000$ g/mol, Entry 2, Table 4.2). This polymerisation is conducted under typical RAFT conditions in toluene at 60 °C. The ratio of [RAFT sites], initiator and monomer is fed at [ACP-RAFT sites]:[DMAEMA]:[ACP initiator]=1:50:0.2. The percentage of ACP initiator is lower than a normal RAFT reaction to avoid the DMAEMA being polymerised by initiator directly. After 12 hours, the poly(CL-co-BOD)-DMAEMA_n is formed and the M_w is increased to 69,000 g/mol measured by GPC-MALLS (Entry 2, Table 4.3). In addition, the GPC chromatograms (Figure 4.22) show the molecular evolution during this chain extension. Both the RI and MALLS detectors show the polymer peaks being shifted to higher M_w and becoming broader.

Table 4.3 Polymerisation data for the synthesis of core-shell poly(CL-co-BOD)_{core}-(DMAEMA)_{shell} and subsequent hydrolysis.^a

Entry	Reaction time (hr)	M_n^b (g/mol)	M_w (g/mol)	PDI	Conversion DMAEMA ^c	N_{arm}^d	L_{arm}^e
1 ^f _{core}	0	1.15×10^4	1.5×10^4	1.3	0	0	0
2 _{core-shell}	12	3.83×10^4	6.86×10^4	1.79	42%	14.1	24.8
3 ^g _{hydrolysed}		3.1×10^3	3.9×10^3	1.2			

- Reaction is conducted in toluene at 60 °C, with chemical ratio [ACP-RAFT sites]:[DMAEMA]:[ACP initiator]= 1:50:0.2, [DMAEMA]=0.5 M.
- M_n and M_w are calculated by GPC-MALLS and d_n/d_c value for core-shell polymer is measured in THF at 35 °C by using refractometer.
- Conversion of DMAEMA is calculated by weight.
- Number of arms per core-shell polymer is calculated by $N_{arm} = [(M_w \text{ of core-shell polyCL-co-BOD-DMAEMA}_n) - (M_w \text{ of core poly(CL-co-BOD)})] / (M_w \text{ of poly(DMAEMA)}) = (6.86 \times 10^4 - 1.5 \times 10^4) / 3.9 \times 10^3$. See Eq. 4.13.
- Length of poly(DMAEMA) per arm is calculated by $L_{arm} = [M_w \text{ of poly(DMAEMA)}] / (\text{FW of DMAEMA}) = 3.9 \times 10^3 / 157$. See Eq. 4.12.
- This entry is for the poly(CL-co-BOD) core, the same as Entry 2, Table 4.2.
- This entry is the data of poly(DMAEMA) arm from hydrolysed core-shell polymer. Hydrolysis condition: Dioxane (18 ml, 2.04×10^{-4} mol), hydrochloric acid (1.5 ml, 30%) and poly(PCL-co-BOD)_{core}-(DMAEMA)_{shell} were mixed in a flask, and the solution was heated to 60 °C and stirred for 24 hours. After neutralisation and extraction, a fine pale pink powder of poly(DMAEMA) was obtained.

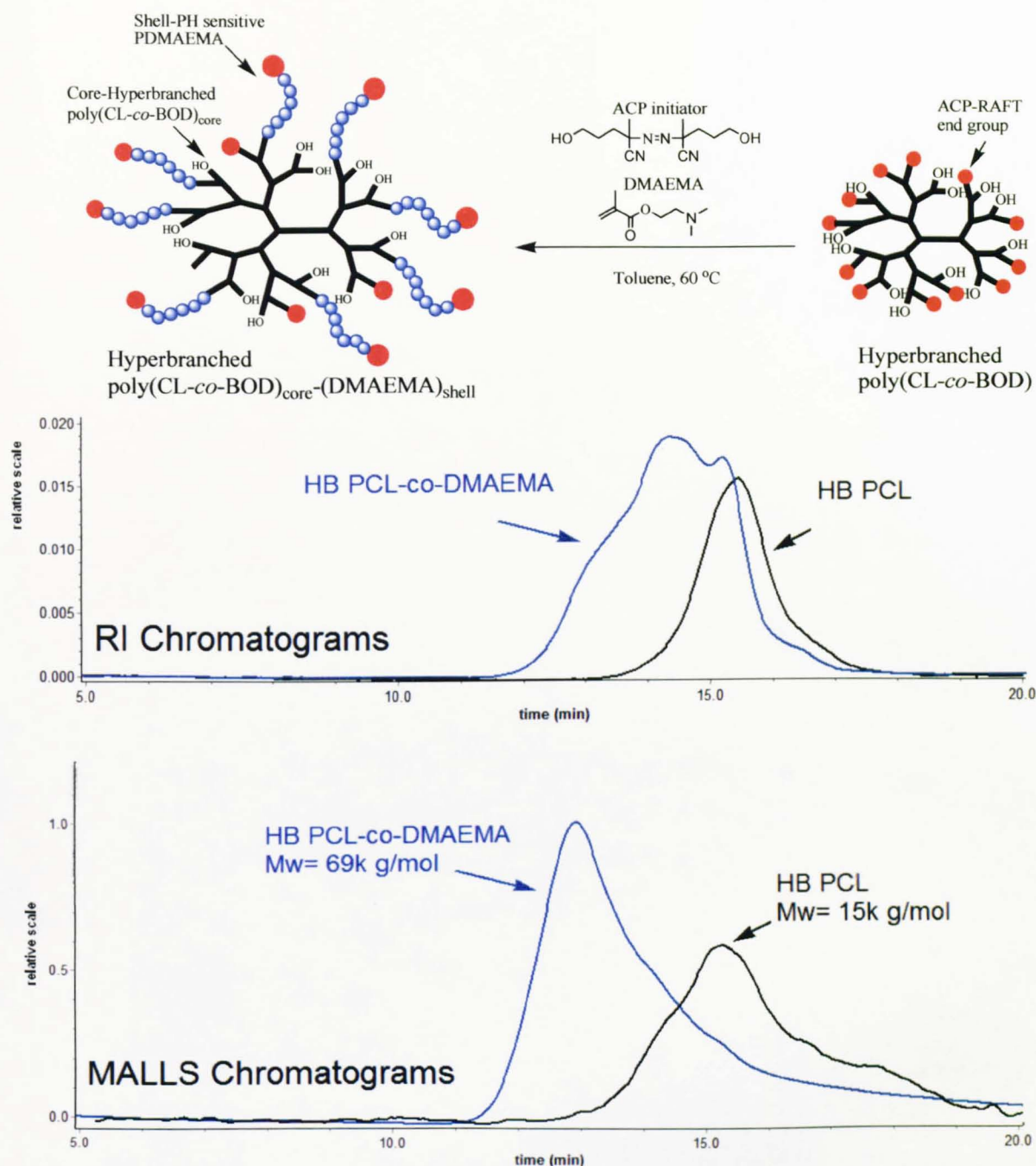


Figure 4.22 RI (top) and MALLS (bottom) traces for chain extension from $\text{poly}(\text{CL-co-BOD})_{\text{core}}$ to $\text{poly}(\text{CL-co-BOD})_{\text{core}}-(\text{DMAEMA})_{\text{shell}}$ by GPC-MALLS. The GPC shows the core-shell polymer was prepared at 12 hours and the M_w is increased from 15,000 to 69,000 g/mol by MALLS detector.

An important parameter for determining the core-shell polymers is the number-average value of the number of arms per molecule (N_{arm}). Since the hyperbranched $\text{poly}(\text{CL-co-BOD})_{\text{core}}$ was formed by random coupling of various numbers of primary chains, the number of actual initiating sites per core is unknown. In order to determine

the value of N_{arm} for star polymers, the length or M_w of PDMAEMA arms are needed. Fortunately, the degradable core of this polymer can allow to release the linear PDMAEMA and to calculate the average arm number per star molecule. The degradability of the PCL core was tested by hydrolysing the poly(CL-co-BOD)_{core}-DMAEMA_{shell} copolymer under acidic conditions. The hydrolysis reaction was stopped after 24 hours by the addition of hexane to precipitate any unhydrolysed polymer. The molecular weight of the unhydrolysed PDMAEMA as determined by GPC-MALLS (Figure 4.23) was 3900 g/mol, which corresponds to the theoretical molecular weight of the PDMAEMA segment 3300 g/mol (Eq. 4.11):

$$\begin{aligned} \text{Theoretical } M_w \text{ of PDMAEMA arms} &= \frac{[\text{DMAEMA}]}{[\text{RAFT}]} \times \text{Conversion} \times F_w(\text{DMAEMA}) \\ &= \frac{50}{1} \times 42\% \times 157.2 \text{ g mol}^{-1} = 3300 \text{ g mol}^{-1} \end{aligned} \quad (\text{Eq. 4.11})$$

Thus, the DMAEMA units per arm can be calculated by the M_w of DMAEMA arms from MALLS data (Eq. 4.12). It means there are 24.8 DMAEMA units on each PDMAEMA arms.

$$\begin{aligned} \text{DMAEMA units per arm} &= \frac{M_w \text{ of PDMAEMA of arm}}{F_w(\text{DMAEMA})} \\ &= \frac{3900 \text{ g mol}^{-1}}{157.2 \text{ g mol}^{-1}} = 24.8 \end{aligned} \quad (\text{Eq. 4.12})$$

Therefore, the averaged arm number per core-shell molecule can be calculated based on the Eq. 4.13:

$$\begin{aligned} \text{Averaged arm numbers of core-shell polymer} &= \frac{(M_w \text{ of core-shell polymer}) - (M_w \text{ of core})}{M_w \text{ of PDMAEMA arm}} \\ N_{\text{arm}} &= \frac{6.86 \times 10^4 - 1.5 \times 10^4}{3900} = 13.7 \end{aligned} \quad (\text{Eq. 4.13})$$

Furthermore, from the above results, the growth percentage of RAFT initiation sites can be worked out by Eq. 4.14, the RAFT end groups on the core is 17.3 which calculated from Eq. 4.10:

$$\begin{aligned}
 \text{Percentages of RAFT end group initiated} &= \frac{\text{Arms number of core-shell}}{\text{RAFT end groups number of core-shell}} \\
 &= \frac{13.7}{17.3} \times 100\% = 79.2\% \quad (\text{Eq. 4.14})
 \end{aligned}$$

This means 79.2 % RAFT end group on the poly(CL-co-BOD) have been activated and propagated DMAEMA units. The remaining 20.8 % of RAFT functionalities are inactive due to the steric-hindrance effect.

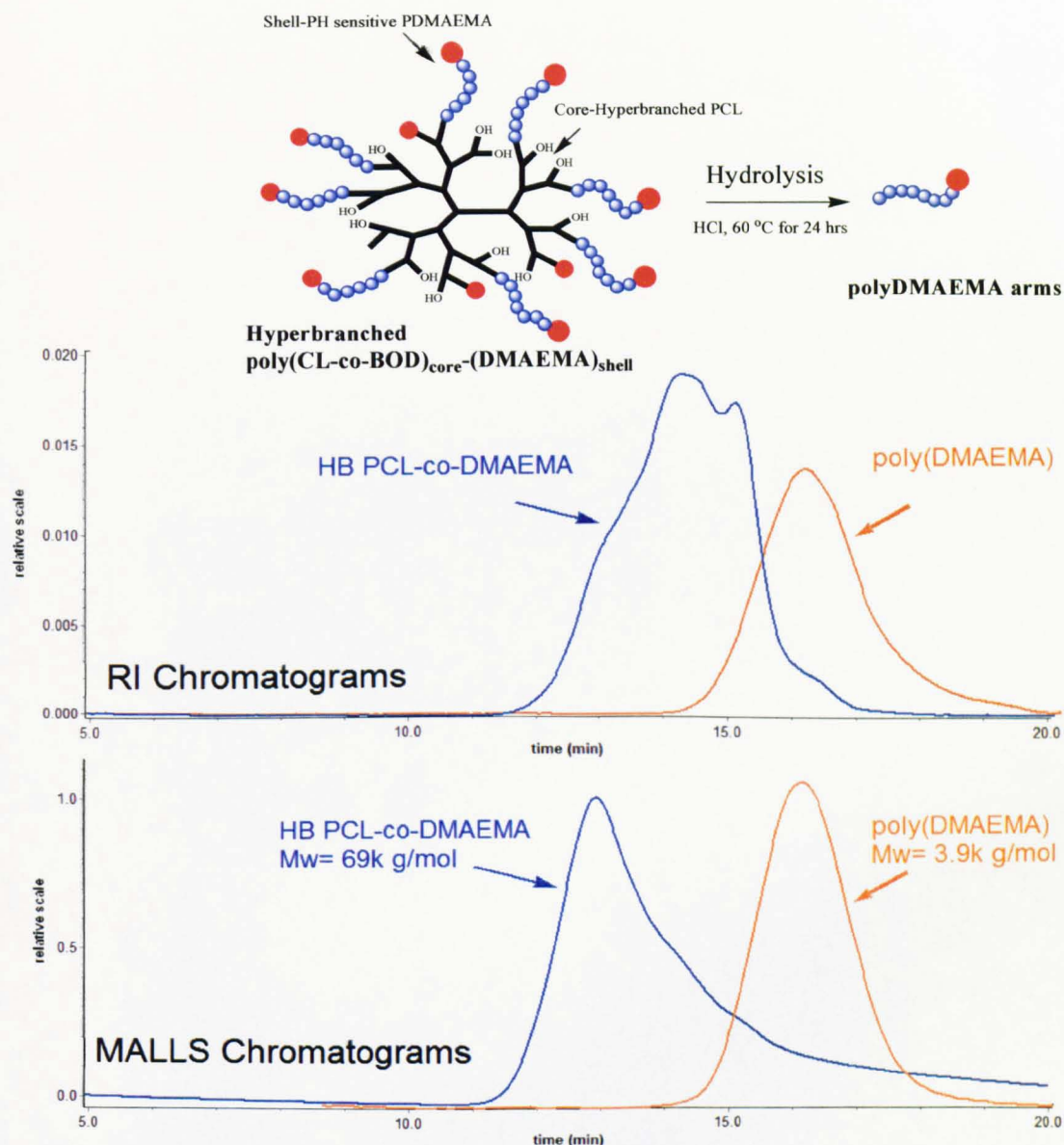


Figure 4.23 RI (top) and MALLS (bottom) traces of gel permeation chromatography equipped with MALLS for hydrolysing of core-shell poly(CL-co-BOD)_{core}-DMAEMA_{shell}. It clearly shows the core-shell polymer is degraded and releases linear PDMAEMA arms. The clean shift to lower molecular weight upon hydrolysis clearly demonstrates that PDMAEMA arms are formed.

The removal of the poly(CL-co-BOD) core from the core-shell polymer after hydrolysis was also confirmed by ^1H spectroscopy NMR analysis. In the spectrum of the core-shell polymer (top spectrum, Figure 4.24), peaks at 1.40 ppm (resonance of proton 8), 1.65 ppm (resonance of proton 11), 2.30 ppm (resonance of proton 7, overlapped with polyDMAEMA) and 4.15 ppm (resonance of proton 9, overlapped with polyDMAEMA)^{43,44} are assigned to the poly(CL-co-BOD) core. It clearly shows that the CH_2 in poly(CL-co-BOD) (resonance of proton 8 at 1.40 and 1.65 ppm) are not present in the spectrum of the hydrolysed polymer (bottom spectrum, Figure 4.24).

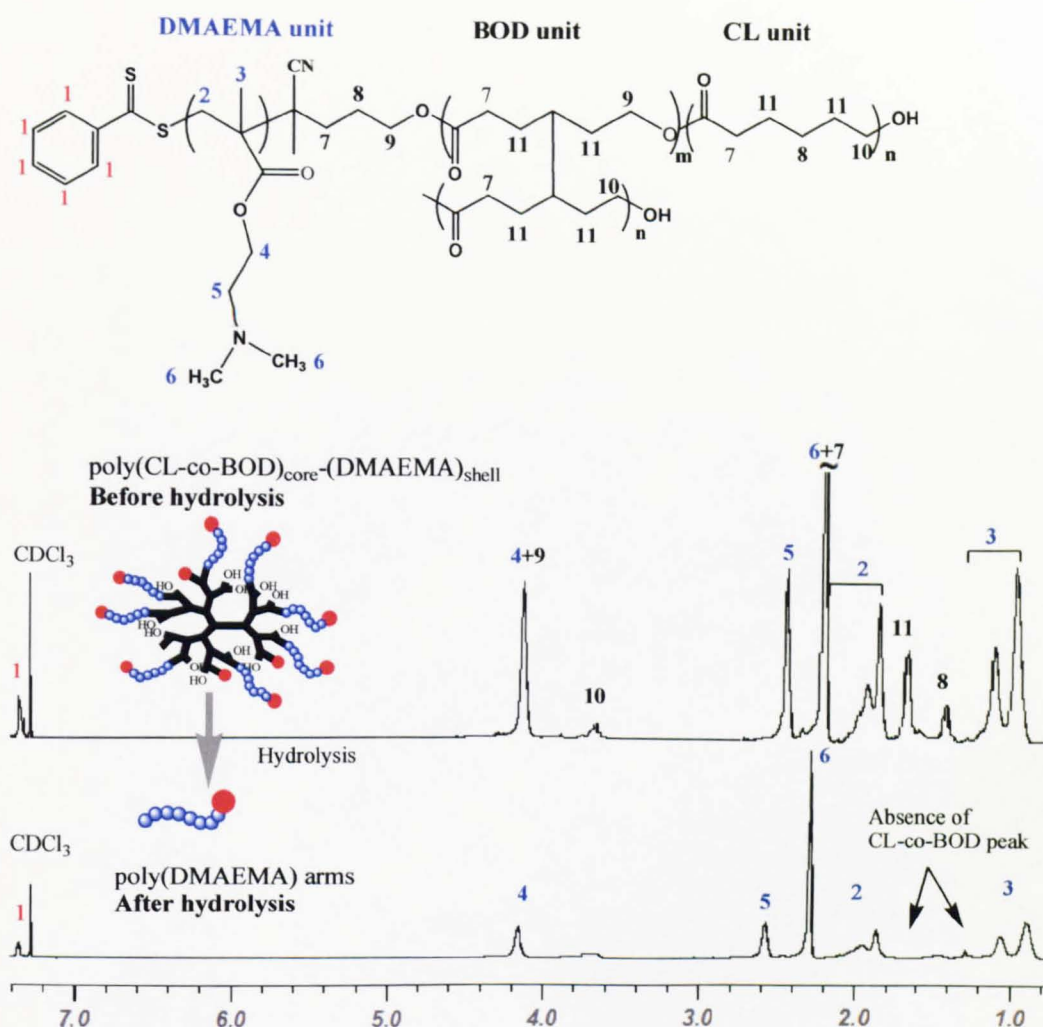


Figure 4.24 ^1H NMR spectra of core-shell poly(CL-co-BOD)_{core}-(DMAEMA)_{shell} (top spectrum) and the remaining linear polymer (PDMAEMA arms, bottom spectrum) after hydrolysis (300 MHz, CDCl_3 , Entry 2 and 3 in Table 4.3). It clearly shows that the resonances are from DMAEMA units (resonances of protons 2, 3 and 5) in the core-shell polymer. Furthermore, the resonances in poly(CL-co-BOD)_{core} (resonances of protons 8 and 11) disappeared after hydrolysis.

NMR spectra provide additional evidence that the composition of poly(CL-co-BOD)_{core}-DMAEMA_{shell} is match the GPC-MALLS result. From previous calculation, the RAFT end group: ϵ -Caprolactone:BOD=1:3.3:1 (Eq. 4.9). In addition, there are average 17.3 RAFT end groups in each poly(CL-co-BOD) core (Eq. 4.10). Thus, there are average 57.1 ϵ -Caprolactone units and 17.3 BOD units in each core. The number of DMAEMA units in each core-shell polymer can be calculated by GPC-MALLS (Eq. 4.15).

$$\begin{aligned} \text{DMAEMA units per core-shell} &= \frac{(M_w \text{ of core-shell polymer}) - (M_w \text{ of core polymer})}{F_w(\text{DMAEMA})} \\ &= \frac{(6.86 \times 10^4 - 1.5 \times 10^4) \text{ g mol}^{-1}}{157.2 \text{ g mol}^{-1}} = 341 \end{aligned} \quad (\text{Eq. 4.15})$$

Thus, the ratio of reacted units in ϵ -Caprolactone units (1 opened ring) and BOD units (2 opened rings) to DMAEMA units is:

$$\begin{aligned} \epsilon\text{-Caprolactone} + \text{BOD} : \text{DMAEMA} &= 57.1 + 17.3 \times 2 : 341 = 91.7 : 341 \\ &= 1 : 3.72 \end{aligned} \quad (\text{Eq. 4.16})$$

Furthermore, the composition of core-shell polymer can be calculated by the NMR spectrum. In the NMR spectrum (Figure 4.24), the peak 3 represents the three protons (CH₃) in DMAEMA units. Also, the peak 11 represents the four protons (-CH₂-CH₂-) in CL and BOD units. Thus, the ratio of opened ring in ϵ -Caprolactone units and BOD units to DMAEMA units can be calculated by Eq. 4.17. The ratio is 1: 4.4 which matched the previous calculation (1: 3.72, Eq. 4.16).

$$\frac{\text{Opened rings in CL and BOD}}{\text{DMAEMA}} = \frac{(\text{Integral of peak 11})/4}{(\text{Integral of peak 3})/3} = \frac{1}{4.4} \quad (\text{Eq. 4.17})$$

4.4 Conclusion

A novel core-shell hyperbranched polymer, poly(DVB_{core}-*co*-MMA_{shell}), was prepared by enhanced deactivation ATRP method via a core-first route. This hyperbranched polymer consists of a hyperbranched polyDVB core and many linear PMMA chains as shell. The unique core-shell structure and properties are confirmed by GPC-MALLS, DLS and AFM. Furthermore, the NMR spectroscopic data obtained indicate the poly(DVB) core of this polymer was slowly cross-linked in the second step which can be potentially used in drug delivery.

The other kind of biodegradable core-shell polymer, poly(CL-*co*-BOD)_{core}-DMAEMA_{shell}, was synthesised by combination of ring open polymerisation and RAFT. This polymer is prepared via a hyperbranched poly(CL-*co*-BOD) core using ACP-RAFT as initiator and followed by chain extension adding PDMAEMA as shell arms. The GPC-MALLS confirmed the evolution of core-shell polymer. Finally, hydrolysis of the poly(CL-*co*-BOD) part of this polymer results in degradation of the core domain and liberation of the non-degradable PDMAEMA arms.

4.5 Reference

1. Hadjichristidis, N.; Iatrou, H.; Pitsikalis, M.; Mays, J. *Progress in Polymer Science* **2006**, 31, (12), 1068-1132.
2. Hadjichristidis, N.; Pitsikalis, M.; Pispas, S.; Iatrou, H. *Chemical Reviews* **2001**, 101, (12), 3747-3792.
3. Matyjaszewski, K.; Xia, J. H. *Chemical Reviews* **2001**, 101, (9), 2921-2990.
4. Angot, S.; Murthy, K. S.; Taton, D.; Gnanou, Y. *Macromolecules* **1998**, 31, (21), 7218-7225.
5. Baek, K. Y.; Kamigaito, M.; Sawamoto, M. *Macromolecules* **2001**, 34, (22), 7629-7635.
6. Eschwey, H.; Hallensl, M.; Burchard, W. *Makromolekulare Chemie-Macromolecular Chemistry and Physics* **1973**, 173, (DEC7), 235-239.
7. Matyjaszewski, K.; Miller, P. J.; Fossum, E.; Nakagawa, Y. *Applied Organometallic Chemistry* **1998**, 12, (10-11), 667-673.
8. Tsitsilianis, C.; Lutz, P.; Graff, S.; Lamps, J. P.; Rempp, P. *Macromolecules* **1991**, 24, (22), 5897-5902.
9. Ueda, J.; Matsuyama, M.; Kamigaito, M.; Sawamoto, M. *Macromolecules* **1998**, 31, (3), 557-562.
10. Gao, H. F.; Ohno, S.; Matyjaszewski, K. *Journal of the American Chemical Society* **2006**, 128, 15111-15113.
11. Xia, J. H.; Zhang, X.; Matyjaszewski, K. *Macromolecules* **1999**, 32, (13), 4482-4484.
12. Altintas, O.; Hizal, G.; Tunca, U. *Journal of Polymer Science, Part A-Polymer Chemistry* **2006**, 44, (19), 5699-5707.
13. Altintas, O.; Yankul, B.; Hizal, G.; Tunca, U. *Journal of Polymer Science Part a-Polymer Chemistry* **2006**, 44, (21), 6458-6465.
14. Whittaker, M. R.; Urbani, C. N.; Monteiro, M. J. *Journal of the American Chemical Society* **2006**, 128, (35), 11360-11361.
15. Worsfold, D. J. *Macromolecules* **1970**, 3, (5), 514-517.
16. Gao, H. F.; Matyjaszewski, K. *Macromolecules* **2008**, 41, (4), 1118-1125.
17. Schilli, C. M.; Zhang, M. F.; Rizzardo, E.; Thang, S. H.; Chong, Y. K.; Edwards, K.; Karlsson, G.; Muller, A. H. E. *Macromolecules* **2004**, 37, (21), 7861-7866.

18. Zheng, G. D.; Stover, H. D. H. *Macromolecules* **2003**, 36, (20), 7439-7445.
19. Mespouille, L.; Degee, P.; Dubois, P. *European Polymer Journal* **2005**, 41, (6), 1187-1195.
20. Wu, D. Q.; Sun, Y. X.; Xu, X. D.; Cheng, S. X.; Zhang, X. Z.; Zhuo, R. X. *Biomacromolecules* **2008**, 9, (4), 1155-1162.
21. Hult, A.; Johansson, M.; Malmström, E., Hyperbranched polymers. In *Branched Polymers II*, 1999; Vol. 143, pp 1-34.
22. Malmström, E.; Hult, A. *Journal of Macromolecular Science-Reviews in Macromolecular Chemistry and Physics* **1997**, C37, (3), 555-579.
23. Trollsås, M.; Kelly, M. A.; Claesson, H.; Siemens, R.; Hedrick, J. L. *Macromolecules* **1999**, 32, (15), 4917-4924.
24. Hedrick, J. L.; Trollsås, M.; Hawker, C. J.; Atthoff, B.; Claesson, H.; Heise, A.; Miller, R. D.; Mecerreyes, D.; Jerome, R.; Dubois, P. *Macromolecules* **1998**, 31, (25), 8691-8705.
25. Wiltshire, J. T.; Qiao, G. G. *Macromolecules* **2006**, 39, (13), 4282-4285.
26. Wiltshire, J. T.; Qiao, G. G. *Macromolecules* **2006**, 39, (26), 9018-9027.
27. Baudry, R.; Sherrington, D. C. *Macromolecules* **2006**, 39, (4), 1455-1460.
28. Isaure, F.; Cormack, P. A. G.; Graham, S.; Sherrington, D. C.; Armes, S. P.; Butun, V. *Chemical Communications* **2004**, (9), 1138-1139.
29. Costello, P. A.; Martin, I. K.; Slark, A. T.; Sherrington, D. C.; Titterton, A. *Polymer* **2002**, 43, (2), 245-254.
30. Schwach, G.; Coudane, J.; Engel, R.; Vert, M. *Journal of Polymer Science Part a-Polymer Chemistry* **1997**, 35, (16), 3431-3440.
31. Du, Y. J.; Lemstra, P. J.; Nijenhuis, A. J.; Vanaert, H. A. M.; Bastiaansen, C. *Macromolecules* **1995**, 28, (7), 2124-2132.
32. Storey, R. F.; Sherman, J. W. *Macromolecules* **2002**, 35, (5), 1504-1512.
33. Kricheldorf, H. R.; Kreiser-Saunders, I.; Stricker, A. *Macromolecules* **2000**, 33, (3), 702-709.
34. Kowalski, A.; Duda, A.; Penczek, S. *Macromolecular Rapid Communications* **1998**, 19, (11), 567-572.
35. Kowalski, A.; Duda, A.; Penczek, S. *Macromolecules* **2000**, 33, (20), 7359-7370.
36. Kowalski, A.; Libiszowski, J.; Duda, A.; Penczek, S. *Macromolecules* **2000**, 33, (6), 1964-1971.
37. Kowalski, A.; Duda, A.; Penczek, S. *Macromolecules* **2000**, 33, (3), 689-695.

38. Pyun, J.; Kowalewski, T.; Matyjaszewski, K. *Macromolecular Rapid Communications* **2003**, 24, (18), 1043-1059.
39. Qin, S. H.; Saget, J.; Pyun, J. R.; Jia, S. J.; Kowalewski, T.; Matyjaszewski, K. *Macromolecules* **2003**, 36, (24), 8969-8977.
40. Pyun, J.; Jia, S. J.; Kowalewski, T.; Matyjaszewski, K. *Macromolecular Chemistry and Physics* **2004**, 205, (4), 411-417.
41. Pyun, J.; Jia, S.; Kowalewski, T.; Patterson, G. D.; Matyjaszewski, K. *Macromolecules* **2003**, 36, (18), 6952-6952.
42. Freure, C.; Chen, G. L.; Horton, J. H. *Surface Science* **1999**, 437, (1-2), 231-238.
43. Zeng, F. Q.; Shen, Y. Q.; Zhu, S. P. *Macromolecular Rapid Communications* **2002**, 23, (18), 1113-1117.
44. Zhang, X.; Xia, J. H.; Matyjaszewski, K. *Macromolecules* **1998**, 31, (15), 5167-5169.

CHAPTER FIVE:

CONCLUSIONS AND FUTURE WORK

5.1 Conclusions

This chapter listed the research results and overall conclusions for the different living polymerisation systems investigated throughout this work. The work includes three main parts: hyperbranched homopolymer by deactivation enhanced ATRP, hyperbranched copolymer by enhanced deactivation ATRP and hyperbranched core-shell polymer via a two step route.

5.1.1 Homopolymerisation of Divinyl Monomers

The deactivation enhanced ATRP was developed and used to prepare hyperbranched polymers. Through this polymerisation, novel hyperbranched poly(DVB) and poly(EGDMA) polymers have been successfully prepared from homopolymerisations of commercially available divinyl monomers. No crosslinking or microgel was observed in the polymer provided that the overall monomer conversion is kept below 60%. This figure being far in excess of the yield that can be obtained with such high levels of branching via any other polymerisation mechanism attempted to-date. These new dendritic poly(DVB) and poly(EGDMA) polymers possess highly branched structures with a multiplicity of reactive vinyl and halogen end functional groups, and controlled chain structure. The GPC-MALLS, DLS and NMR results prove these polymers are hyperbranched structure without microgel. We believe that this new strategy for preparation of hyperbranching polymers could open up the field to the polymerisation of a very wide range multifunctional vinyl monomers or combinations of comonomers in any proportion. This strategy may be applied to ATRP, but could in principle be applied to other vinyl polymerisation mechanisms, *e.g.*, RAFT polymerisation depending on the nature of the initiation system and of the external stimulus that is applied.

5.1.2 Hyperbranched Copolymers

Based on successful development of deactivation enhanced ATRP, a new kind of hyperbranched polymer which contains hyperbranched structure, hydrophilic blocks, plenty of active vinyl groups and halide groups by copolymerising of DMAEMA and EGDMA have been successfully prepared. DE-ATRP demonstrates a facile route to hyperbranched polymer from multifunctional vinyl monomers. The hyperbranched structure is confirmed by MALLS-GPC and NMR results. Furthermore, our hyperbranched amphiphilic molecule shows great encapsulation ability to transfer water-soluble dyes into chloroform. The data show the hyperbranched structure helps raise the encapsulation ability.

Novel hyperbranched poly(siloxysilanes) were prepared via a facile enhanced deactivation ATRP. All the resulting polymers were characterised by GPC-MALLS and NMR. The GPC analysis shows their high molecular weights and a wide polydispersity, which are exactly in agreement with the recognised property of hyperbranched polymer. In addition, by tracking the relationship between RMS radius, elution volume and molecular weight, it shows solid evidence for the highly branched structure. It is also apparent from the ^1H NMR that active vinyl groups are present in the high monomer conversion hyperbranched product, indicating the existence of vinyl end groups. Finally, the viscosity enhancing test shows the oil viscosity increases less by adding hyperbranched polymer.

5.1.3 Hyperbranched Core-Shell Polymers

A novel core-shell hyperbranched polymer poly(DVB-*co*-MMA) was prepared by DE-ATRP method via a core-first route. This hyperbranched polymer consist of a hyperbranched polyDVB core and many linear poly(methyl methacrylate) (PMMA) chains as the shell. The unique core-shell structure and properties are confirmed by GPC-MALLS, DLS and AFM. Furthermore, the NMR data indicate the poly(DVB) core of this polymer is slowly cross-linked in second step which can be potentially be

used in drug delivery.

The other kind of biodegradable core-shell polymer poly(CL-*co*-BOD)_{core}-DMAEMA_{shell} was synthesised by combination of ring open polymerisation and RAFT. This polymer is prepared a hyperbranched poly(CL-*co*-BOD) core used ACP-RAFT as initiator and followed by chain extension added PDMAEMA as shell arms. The GPC-MALLS confirmed the evolution of core-shell polymer. Finally, hydrolysis of the poly(CL-*co*-BOD) part of this polymer resulted in degradation of the core domain and liberation of the non-degradable PDMAEMA arms.

5.2 Future work

5.2.1 More Experimental Works for DE-ATRP

Hyperbranched poly(DVB) has been successfully prepared from DE-ATRP of commercially available divinylbenzene monomers. However, the commercial divinylbenzene monomer is produced from the catalytic dehydrogenation of diethylbenzene resulting in a mixture of ethylvinylbenzene (EVB) and DVB isomers. However, some problems were caused by the EVB isomer, for example, polymer characterisation and kinetics studies. Thus, the pure *para*-DVB or *meta*-DVB should be used for the further kinetics study in the future. The pure *para*-DVB monomer can be prepared from the published method.¹

5.2.2 Kinetic Modeling and Simulation of Deactivation Enhanced Polymerisation

Recently, computational simulation has become one of the major tools in polymer science that helps understanding the molecular structure and dynamics of the polymer chains. It can be applied to study complex gelation processes under various conditions. The gelation in the simulated system depends not only on the parameters used but also

on the applied model. A statistical theory was developed by Flory²⁻⁴ and Stockmayer⁵⁻⁷ (F-S theory) to predict the gel point. In F-S theory, the gel point based on monomer conversion was influenced by the initial molar ratio of cross-linker to initiator, the initiation efficiency, and polydispersity of primary chains. However, the statistical model takes into account only the concentration of involved reagents and cannot consider the kinetic control over the polymerisation. Thus, a new model which including the kinetic parameters should be studied in the future. The new kinetic model can help to better understand and predict the experimental gelation process.

5.2.3 Extension of Deactivation Enhanced Strategy for Other Controlled/Living Polymerisations

As the high deactivation rate can lead the divinyl monomer to form hyperbranched polymer rather than a cross-linked structure, it can extend this mechanism to other living polymerisation, for example the RAFT or NMP process. The deactivation enhanced strategy can be applied to other controlled/living polymerisations. For example, the kinetic chain length in RAFT (v_{RAFT} , Eq. 5.1) is proportional to the constant of propagation (k_p) and concentration of monomer ($[M]$), and inversely proportional to constant of chain transfer (k_{cs}) and concentration of RAFT agent ($[RAFT]$). Thus, the intermolecular crosslinking can be suppressed by choose RAFT agent with higher chain transfer constant or added excess RAFT agent initially.

$$v_{\text{RAFT}} = \frac{R_p}{R_{\text{chain transfer}}} = \frac{k_p[M][P']}{k_{cs}[P'][RAFT]} = \frac{k_p[M]}{k_{cs}[RAFT]} \quad (\text{Eq. 5.1})$$

In NMP reaction, the kinetic chain length in NMP (v_{NMP} , Eq. 5.2) is proportional to the constant of propagation (k_p) and concentration of monomer ($[M]$), and inversely proportional to constant of deactivation (or cross-coupling, k_c) and concentration of persistent radical species ($[Y]$). Thus, the intermolecular crosslinking can be suppressed by choose the reaction with higher k_c or added excess persistent radical

species initially.

$$v_{\text{NMP}} = \frac{R_p}{R_{\text{deactivation}}} = \frac{k_p[M][P^*]}{k_c[P^*][Y]} = \frac{k_p[M]}{k_c[Y]} \quad (\text{Eq. 5.2})$$

Thus, the deactivation enhanced strategy should be extending to RAFT or NMP in the future.

5.2.4 Further Application Tests for Hyperbranched Polymers

Since various hyperbranched polymers were synthesised in this research work and their unique properties have been displayed by GPC-MALLS and DLS. It will be interesting to apply these novel materials to new applications, for example, coatings⁸ or drug delivery.

The hyperbranched homopolymer poly(DVB) and poly(EGDMA) contains many vinyl group in their branches which can be used for further crosslinking. If we dissolve the polymer in solvent (Figure 5.1, A), then spray or spin coat the solution onto substrate (Figure 5.1, B). After that, the substrate was exposed under UV which can lead the vinyl groups in the materials to crosslink (Figure 5.1, C). Finally, the polymer will form a crosslinked film at the surface of substrate which can resist the solvent (Figure 5.1, D).⁸

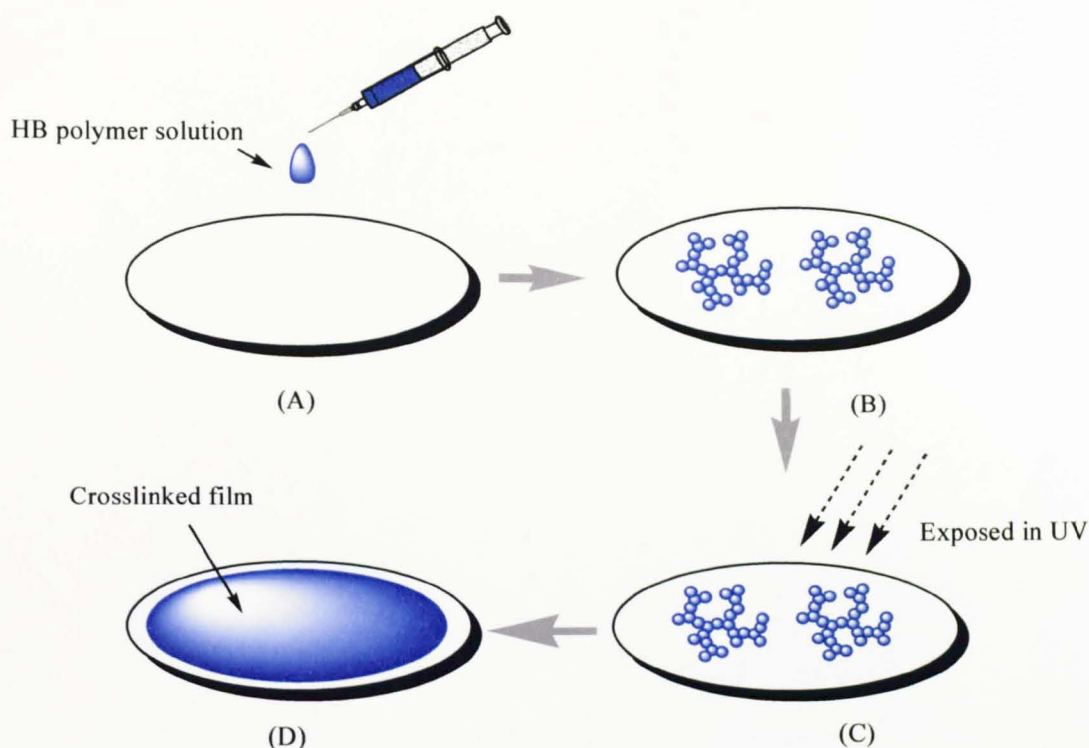


Figure 5.1 Preparation of a cross-linked polymer film on the substrate. The hyperbranched polymer was dropped on the substrate (A). Then the substrate was exposed in UV light (C). The vinyl groups in the hyperbranched polymer will be easily cross-linked with other polymers (D).

Moreover, as we displayed in Chapter 3, the hyperbranched copolymer poly(EGDMA-*co*-DMAEMA) can transfer water-soluble dyes into organic solvent. Thus, the hyperbranched poly(CL-*co*-BOD)_{core}-DMAEMA_{shell} also can be used for drug delivery. The hyperbranched structure can trap the drug in the polymer and bring it into contact with a body. Furthermore, the polymer will slowly hydrolyse *in vivo* and release the drug.

5.2.5 Biodegradable Hyperbranched Core-Shell poly(CL-*co*-BOD)_{core}-DMAEMA_{shell} via Arm-First Route

The hyperbranched core-shell polymer also can be prepared via arm-first route (Figure 5.2). First, the linear polyDMAEMA was prepared by RAFT polymerisation. Then the linear arms could be combined with CL and BOD via ring open polymerisation. The

ACP-RAFT is used in this system as a RAFT agent in first step and initiator in second step. The advantage of this method could be that the linear polyDMAEMA arms can be better controlled under this condition than in core-first method.

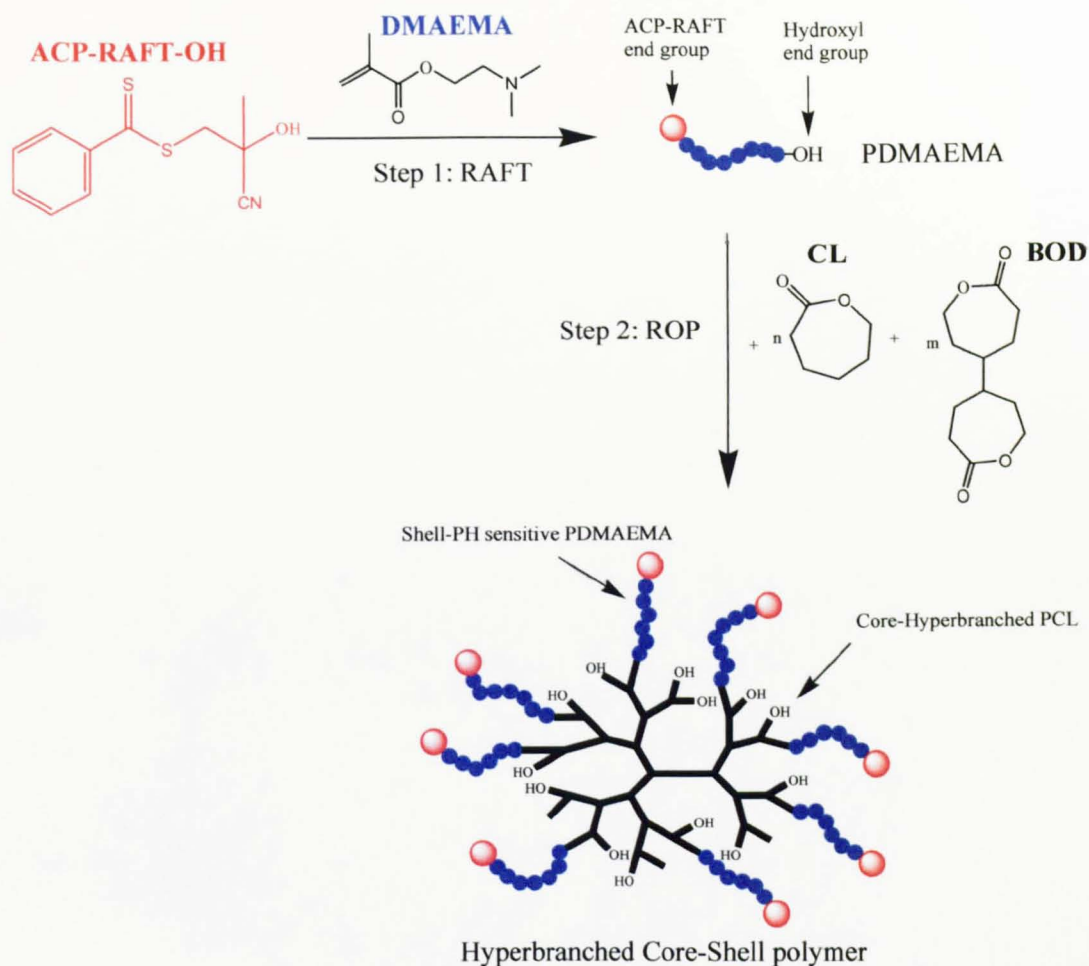


Figure 5.2 Mechanism of synthesis hyperbranched core-shell poly(CL-co-BOD)_{core}-DMAEMA_{shell} via arm-first route.

5.3 Reference

1. Nyhus, A. K.; Hagen, S.; Berge, A. *Journal of Polymer Science , Part A-Polymer Chemistry* **1999**, 37, (16), 3345-3359.
2. Flory, P. J. *Journal of the American Chemical Society* **1941**, 63, 3096-3100.
3. Flory, P. J. *Journal of the American Chemical Society* **1941**, 63, 3091-3096.
4. Flory, P. J. *Journal of the American Chemical Society* **1941**, 63, 3083-3090.
5. Stockmayer, W. H. *Journal of Chemical Physics* **1943**, 11, (2), 45-55.
6. Stockmayer, W. H. *Journal of Chemical Physics* **1944**, 12, (4), 125-131.
7. Stockmayer, W. H.; Jacobson, H. *Journal of Chemical Physics* **1943**, 11, (8), 393-393.
8. Ryu, D. Y.; Shin, K.; Drockenmuller, E.; Hawker, C. J.; Russell, T. P. *Science* **2005**, 308, (5719), 236-239.